WIRELESS INSTRUMENTATION AND METADATA FOR GEOTECHNICAL CENTRIFUGES

by

Yangsoo Lee

A Dissertation Presented to the
FACULTY OF THE GRADUATE SCHOOL
UNIVERSITY OF SOUTHERN CALIFORNIA
In Partial Fulfillment of the
Requirements for the Degree
DOCTOR OF PHILOSOPHY
(CIVIL ENGINEERING)

May 2006

INFORMATION TO USERS

The quality of this reproduction is dependent upon the quality of the copy submitted. Broken or indistinct print, colored or poor quality illustrations and photographs, print bleed-through, substandard margins, and improper alignment can adversely affect reproduction.

In the unlikely event that the author did not send a complete manuscript and there are missing pages, these will be noted. Also, if unauthorized copyright material had to be removed, a note will indicate the deletion.

ProQuest Information and Learning Company
300 North Zeeb Road
P.O. Box 1346
Ann Arbor, MI 48106-1346

Acknowledgements

I would like to express my deepest appreciation and profound gratitude to my academic adviser and dissertation committee chair, Dr. Jean-Pierre Bardet for his guidance, encouragement and helpful suggestions during the course of this research. Without his guidance and support based on experience and deep insight of the subject, I could not have completed the present work.

I would like to extend my sincere gratitude to the other members of the dissertation committee: Dr. Erick Johnson and Dr. John Wilson for their valuable advices.

During the course of my graduate studies at USC, I had great experiences with other excellent colleagues and visiting scholars. It is my pleasure to acknowledge past and present members of the Research Center for Computational Geomechanics (RCCG) with special mention to Dr. Tetsuo Tobita, Dr. Jianping Hu, Dr. Rana Al-fares, Jamal Ramadan, Fang Liu, Amir Zand, and Nazila Mokarram.

Especially, I am passing my warmest regards to Dr. Ben Hushmand of Hushmand Associates, Inc. and John Lee at Stanford University for their discussions and consideration in developing centrifuge modeling.

In addition, I appreciate all the staff in the Civil Engineering Department at the University of Southern California. I would like to send my best regard to Lance Hill, laboratory manager, for his helps and advices for my research.

My family has been a constant source of love, encouragement, and support throughout my graduate studies and my life. I am grateful to my parents and brother for their patience, love, and understanding over the last six years. I also greatly appreciate my father's dedication and encouragement of my research.

I am very grateful for my wife, Sunkyoung Kim for her encouragement, joyfulness, and love she has provided during the Ph.D. period. In addition, special thanks to daughters, Hannah Lee and Euna Lee, to whom I dedicate all my love.

Most of all, I would like to express a heart-felt thanks to the Lord for his unconditional love and companionship - "Do not be anxious about anything, but in everything, by prayer and petition, with thanksgiving, present your requests to God" (Philippians 4:6).

Table of Contents

List of Tables

List of Figures

Abstract

Centrifuges are used in geotechnical earthquake engineering to simulate complicated phenomena such as nonlinear soil-structure interaction and liquefaction induced by earthquakes. Cost efficient alternatives to large scale testing, centrifuge modeling has become widely accepted to analyze experimentally all kinds of geotechnical problems.

This thesis explores the use of wireless technologies to improve data transfer and control remotely data acquisition systems of centrifuges. These improvements greatly reduce electrical noises and increase the high-frequency performance of data acquisition. This thesis also contributes to the introduction of metadata for documenting the experimental results and processes of centrifuge testing.

The first part of the research work consisted of re-assembling the centrifuge of the University of Southern California, modifying the mechanical centrifuge balancing system, replacing outdated parts with more modern ones, and upgrading the hydraulic shaker that simulate in-flight earthquake shakings.

The second part focused on the high-speed wireless instrumentation system that overcomes the limitations imposed by traditional slip ring connections. The new centrifuge system, including renovated mechanical parts and new wireless instrumentation, was tested by carrying out a series of dynamic tests on a laminar box, which simulates the responses of saturate soil deposits to earthquake motions.

The experimental results indicate an overall good performance of the complete centrifuge system.

The third part of the research work deals with the application of novel information technology methods for documenting experimental results as well as experimental processes. Metadata are introduced to describe all experimental steps from the construction of the soil specimen to the final reports. The metadata model, which is proposed for centrifuge modeling, explains the data collected during the experiment through an additional layer of data called "metadata." These metadata, also referred to as data about data, are totally new to centrifuge testing and are likely to become critical for describing increasingly complicated centrifuge experiments. The proposed metadata model, which is applied to generate web reports and computer visualization, leads to powerful ways of exchanging information among researchers.

1 Introduction

1.1 Background of centrifuge modeling and metadata modeling

1.1.1 What is geotechnical centrifuge modeling?

Historically in the 1930s, Bucky (1931) and Pokrovsky (1936) were the first to study full-scale prototypes in geotechnical engineering by using centrifuges and small-scale models. Since then, many geotechnical centrifuges have been built all around the world, and have become valuable research tools for modeling large-scale nonlinear problems where gravity is the primary driving force (e.g., Arulanandan and Scott, 1993; Craig et al., 1988; Kimura et al., 1998; Leung et al., 1994).

A geotechnical centrifuge replaces the earth gravitational force applied to objects by a similar but stronger force. That "centrifugal" force resulting from the centrifuge rotation points away from the rotation center (Schofield, 1981; Schofield, 1988). In most cases, its amplitude is much larger than the earth's gravity. The capacity of a centrifuge for replicating prototypes depends on the strength of its centrifugal force (Taylor, 1995).

Centrifuge modeling has not only contributed to improving our understanding of earthquake-induced phenomena in geotechnical engineering (e.g., liquefaction and land deformation) but has also helped engineers to develop countermeasures for mitigating earthquake devastations (Balakrishnan et al., 1998; Dobry, 1996; Kimura, 1988). Earthquakes are natural disasters that may result in human casualties and cause damages to structures and infrastructures, such as buildings, ports, and bridges.

In 1994, the Northridge earthquake caused widespread damages to freeways and other structures in Los Angeles, California (e.g., Bolin and Stanford, 1998). Centrifuge modeling assisted of computer simulations (e.g., nonlinear finite element analysis) has played an important role in understanding the effects of earthquakes on soil deposits and geotechnical structures (Ko, 1988).

Centrifuge modeling starts from the assumption that centrifuge models and prototypes have identical stress fields (Kutter, 1995; Schofield, 1988). The centrifuge applies an increased gravitational acceleration to physical models. As the centrifuge spins, this force is proportional to the distance from a rotation center to the model (Taylor, 1995). The centrifuge is capable of producing the same geostatic (i.e., self-weight) stress, strength, and stiffness within small-scale models and prototypes, and therefore is a powerful approach to investigate the effects of material nonlinearities in engineering problems (Kutter, 1995).

The similitude relationships between centrifuge models and prototypes are defined using not only physical dimensions (e.g., distance and area) but also physical variables (e.g., viscosity and permeability) (e.g., Ko, 1994; Stewart et al., 1998; Tan and Scott, 1985; Taylor, 1995). The similitude relationships help us interpret the results of centrifuge modeling and understand the effects of stress-dependent nonlinearity in prototypes.

1.1.2 Principal roles of geotechnical centrifuges

Centrifuge modeling plays important roles in geotechnical earthquake engineering especially in the investigation of new phenomena, parametric studies, and validation of computer simulations. Centrifuge modeling is a cost-effective method to investigate of the nonlinear behaviors of full-scale prototype, such as embankments and piles. Centrifuge modeling can be also applied to investigate new phenomena, where depends on gravity (Ko, 1988; Schofield, 1981). For instance, centrifuge modeling is helpful in the research of liquefaction and plate tectonics. Centrifuge modeling also provides benchmark boundary-values problems to verify the results of computer simulations (Byrne et al., 2004; Ko, 1988). Modern designs in geotechnical engineering are based on computer simulations where constitutive equations represent soil properties. However, the computer-based analyses produce results with uncertain accuracy because they have to simplify real engineering problems in order to formulate and solve them. Centrifuge modeling is extremely valuable to compare the results of numerical and centrifuge simulations (e.g., Arulanandan and Scott, 1993; Byrne et al., 2004; Ko, 1988; Popescu and Prevost, 1995).

The centrifugal acceleration is often used as a variable in parametric studies while other parameters remain unchanged. For instance, it is useful to generate data for design charts for specific problems, such as bearing capacity of footings on slopes, and critical parameters in flow processes (Ko, 1988).

1.1.3 Centrifuge comparisons

Table 1 lists the centrifuges that operate around the world as of September 1998 (Kimura et al., 1998). It contains information about the centrifuges, such as nominal radius from center of rotation to tested model, maximum payload (ton), maximum acceleration (g). As shown in Table 1, centrifuges have various sizes and specifications. Large centrifuges, such as the 9-m centrifuge at the University of California, Davis and the 8-m centrifuge at Hong Kong University, have more capacity to simulate larger models. They can use smaller scaling factor, which minimizes the errors caused by exceedingly scaling down the prototypes (Kutter et al., 1994). In addition, larger centrifuges minimize the difference of vertical stress between model and prototype with a longer radius to the model. These stress-field differences are discussed in Chapter 2.

Compared to large centrifuges, small centrifuges present a number of advantages in a research environment. They require less funding, maintenance and labor than larger centrifuges. They can be reconfigured efficiently to approach new types of problems. Their low operational cost allows researchers to perform more tests and to cover more aspects of the problems under investigation.

Table 2 completes Table 1. It compares the characteristics of the centrifuges at the University of Southern California (Uschold and Gruninger), University of California in Davis (UC Davis), Renssalaer Polytechnic Institute (RPI), and University of Colorado in Boulder (UC Boulder).

1.1.4 Application of centrifuge modeling

Figure 1 summarizes the topics, which have been modeled by centrifuges between 1981 and 1998, based on the publications in the American Society of Civil Engineer (ASCE), Canadian Geotechnical Journal, Soil and Foundation, and Geotechnique journals. Centrifuge papers fall into 11 categories as follows:

1. Deep excavation (e.g., Dobry and Abdoun, 2001)
2. Pile and anchors (e.g., Mehle, 1989; Scott et al., 1982)
3. Model preparation and soil properties (e.g., NRC, 1982)
4. Embankments and slopes (e.g., Bardet and Davis, 1998)
5. Earthquake effect (e.g., Rodriguez, 1999)
6. Deep foundation (e.g., Turner et al., 1995)
7. Shallow foundation (e.g., Zeng and Steedman, 1998)
8. Retaining structure (e.g., Richards et al., 1998)
9. Geo-environmental problem (e.g., Savvidou and Culligan, 1998)
10. Ground improvement and earth reinforcement (e.g., Elgamal et al., 2005)
11. Others (e.g., Chari, 1979; Poorooshasb, 1990)

Table 3 lists the topics along with explanations related to Figure 1. For instance, centrifuges modeled the response of pile foundation to earthquake motion and evaluated whether or not the pile foundation withstands a specific degree of earthquake shaking (e.g., Brandenberg et al., 2005). Centrifuges have also modeled other earthquake effects, such as ground deformation (e.g., Balakrishnan and Kutter, 1999; Dobry, 1996; Pilgrim, 1998) and liquefaction (e.g., Dobry, 1989; Kutter, 1988), and have been useful to minimize disasters induced by natural phenomena (e.g., Balakrishnan et al., 1998).

1.1.5 Example of centrifuge modeling

This section illustrates centrifuge modeling (Balakrishnan and Kutter, 1999) by an example of centrifuge test performed at UC Davis. This particular test describes the settlement, sliding, and liquefaction remediation of layered soils.

Major earthquakes such as the 1964 Alaska earthquake (e.g., National Research Council, 1968), 1989 Loma Prieta earthquake (e.g., Bardet and Kapuskar, 1993), and 1995 Hyogoken-Nanbu earthquake (e.g., JGS, 1996) demonstrated the devastating effects of liquefaction on structures such as buildings, bridges, and waterfront structures, which suffered from settlement and lateral spreading. A series of highly instrumented, large-scale centrifuge models were designed to investigate the extent of remediation required to control settlement and lateral sliding of soil deposits at bridge sites.

The centrifuge at UC Davis, shown in Figure 2, has a 9.1m radius from the spindle to the bucket floor. It has a maximum payload of 4500 kg and maximum operating speed of 90 rpm that corresponds to 75 g centrifugal acceleration (Kutter et al., 1994). The slip ring assembly has forty signal rings, twenty video rings, twenty power rings, and two fiber optic rings. The machine is driven by means of a GE 752 1000 HP DC electric motor with SCR motor controller. The servo hydraulic shaker has a capacity to produce a maximum of about 50 tons of shaking force at frequencies up to 200 Hz with a shaking payload of 2,700 kg (CGM, 2005).

As shown in Figure 3, the model was constructed in the model container (1.72 m long, 0.7 m deep and 0.69 m wide) where a stack of six rectangular rings were equipped to allow the soils to deform freely in the horizontal direction. Figure 3 also shows the model configurations of models U50, L80, L80B, and C80. The unimproved soil profile, model U50, simulated a 6.0-m-thick dense sand layer (Dr = 80%) beneath a 9-m-thick medium density sand layer (Dr = 50%), and a sloping surface deposit of over-consolidated clay (Balakrishnan and Kutter, 1999). In model L80, a limited region of the 50% relative density sand layer was densified as Dr = 80%. Model L80B shows the sand was densified to the 80% relative density as in model L80, and an impermeable water barrier, a 19-mm-thick (prototype scale), was placed among different relative densities such as 50% and 80% relative densities. In model C80, the 50% relative density sand layer was completely replaced with 80% relative density sand layer to represent a large extent of remediation. The degree of sand treatment increased in terms of a relative density in the following order: U50,

L80, L80B, and C80. The sand layer was overlain by clay floodplains with a free face at a river channel. The other floodplain has a 9 % slope toward the river (Balakrishnan and Kutter, 1999).

It was clear that the densification of a deep sand deposit (from 50% to 80% relative density) was effective in reducing but not eliminating the effects of liquefaction. Figure 4 shows the settlements on sand surface of different locations among models. Settlements and shear deformations of 80% relative density as in model C80 were smaller by a factor of three than those of 50% relative density sand as in model U50. Figure 5 shows the shear stress-displacement loops at interface in U50 and C80 with Kobe earthquake motion and demonstrated the effect of densification. Larger resistance including many negative shear stress pulses and larger areas endorsed by the stress-displacement loops were shown in the densified model C80.

The centrifuge modeling yielded the following results (Balakrishnan and Kutter, 1999):

- A full-depth ground improvement reduced the settlements and lateral sliding of the sand by about a factor of three.

- The lateral sliding of clay deposit on the surface was not controlled by densification of the sand due to the effects of clay-sand interface,

- Densified zone that was only about 75% of the thickness of the loose sand layer controlled the settlement and sliding of the sand layer (Balakrishnan and Kutter, 1999).

This example illustrates how centrifuge testing constructs the reduced-scale model, customizes the model to examine all possible circumstances in the prototype, and interprets and applies the modeling results to the prototype.

1.2 Background on centrifuge instrumentation

Centrifuge testing involves a lot of electronic instrumentation that are confined within the limited space of a fast moving centrifuge arms subjected to large centrifugal accelerations (Allard, 1983). Until recently, the low-amplitude signals generated by measuring instruments and sensors were amplified within the centrifuge before being transmitted to the laboratory through slip rings connections. These conventional practices systematically degraded data quality and introduced undesirable electric noises (Zornberg et al., 2005). The rapidly evolving field of wireless technologies opened new alternatives to overcome these problems. Wireless methods offered new opportunities to increase the quality and efficiency of data acquisition and transfer systems, and eliminate the troubling noises caused by slip rings and long cables. The advantages and limitations of wireless technologies were a definite research topic that had to be explored in centrifuge modeling.

1.3 Background on data documentation and reporting

Centrifuges yield a large volume of output data, and require a considerable effort to organize and document experimental data, especially when test data have to be shared among researchers (e.g., Bardet et al., 2005; Swift, 2004). Unfortunately, except for a few centrifuge facilities, centrifuge modeling rarely documents experimental results and procedures in detail. In most instances, tests are carried out by isolated investigators at single institutions and partially published in hardcopy papers. These poor experimental practices mean that information is difficult to exchange and test results are difficult to replicate at other centrifuge facilities (e.g., Bardet et al., 2004a; 2004b; 2004c; 2004d; 2004e).

During the construction of the George E. Brown, Jr. **N**etwork for **E**arthquake **E**ngineering **S**imulation (hereafter, called NEES), new ideas emerged to improve the documentation, processing, and archiving of experimental data within collaborative research networks (NSF, 2006). As part of the NEES system integration, new data models were created for documenting the data generation from physical experiments and numerical simulations and extracting relevant information from large data sets (Bardet et al., 2005).

Data modeling is defined as the analysis of data objects and their relationships to other data objects. Recent developments in data modeling originate from information technology. Data modeling is often the first step in database design and object-

oriented programming as the designers first create a conceptual model of how data items relate to each other (Webopedia, 2006).

Capitalizing on the recent advances made in information technology, data modeling was therefore an obvious research topic that deserved to be investigated in details in centrifuge modeling.

1.4 Research objectives

The present research has two main objectives: (1) to apply new wireless technologies to centrifuge modeling and (2) to use advances in information technology to document experimental results.

The first objective is to demonstrate that the wireless control of data acquisition system can simplify instrumentation, reduce electric noises of high-frequency signals, and overall increase the performance of instrumentation and data acquisition (DAQ) system.

The second objective is to develop and test new data models that describe and organize centrifuge data logically and helps to build web reports accessible to all researchers. The data models are intended to be comprehensive, including not only result data, but also testing procedures and equipment.

The road that had to be built to realize these two major objectives lead us to accomplish the following subtasks:

1. Documentation of the USC centrifuge system in terms of mechanical, hydraulic, and electrical components, sensors and instrumentation.

2. Evaluation of centrifuge system after mechanical, hydraulic, and electrical modifications and replacement

3. Testing of centrifuge equipment and instrumentation by performing a liquefaction experiment that investigates the ground deformation caused by excess pore pressure during and after earthquake shaking

1.5 Organization of document

Following the introduction, Chapter 2 reviews the principle of centrifuge modeling and describes the similitude relationships between the centrifuge model and the prototype. The time scale is discussed in the case of multi-physics where both dynamic and water-diffusion events occur simultaneously. The centrifuge modeling of liquefaction phenomenon, caused by earthquake motion, is an example of multi-physics modeling. Here, the earthquake motion is the dynamic event, and soil consolidation after the dissipation of excess pore-pressure is the water diffusion event.

Chapter 3 describes the modified USC centrifuge as well as the new methods of centrifuge operation and calibration associated with the hydraulic pump, accumulators, servo valve controller, and new instrumentation. Chapter 3 covers (1) a general presentation of the USC centrifuge; (2) hydraulic, electric, and mechanical

apparatus; (3) centrifuge instrumentation, transducers and signal conditioners; and (4) calibration results and methods for transducers and signal conditioners.

Chapter 4 illustrates the preceding chapters by describing a complete centrifuge experiment, which investigates the deformations, pore-pressure changes, and accelerations within a saturated soil layer subjected to earthquake shakings. Chapter 4 reviews (1) the model layout; (2) preparation of earthquake motion; (3) model construction with Nevada sand and deaired water; (4) equipment and instrumentation; and (5) test procedures. In addition, Chapter 4 describes the earthquake input motion in the time and frequency domains. It presents the test results in terms of horizontal accelerations, lateral and vertical displacements, and pore-pressure changes at various depths during and after earthquake shaking.

Chapter 5 introduces the data/metadata model and illustrates its application using the centrifuge test of Chapter 4. The test information is organized, stored, and related logically. The data/metadata model is applied for creating a web report and using visualization software. It demonstrates the efficiency of data/metadata modeling for organizing and storing data as well as exchanging information among researchers.

Chapter 6 presents the conclusion.

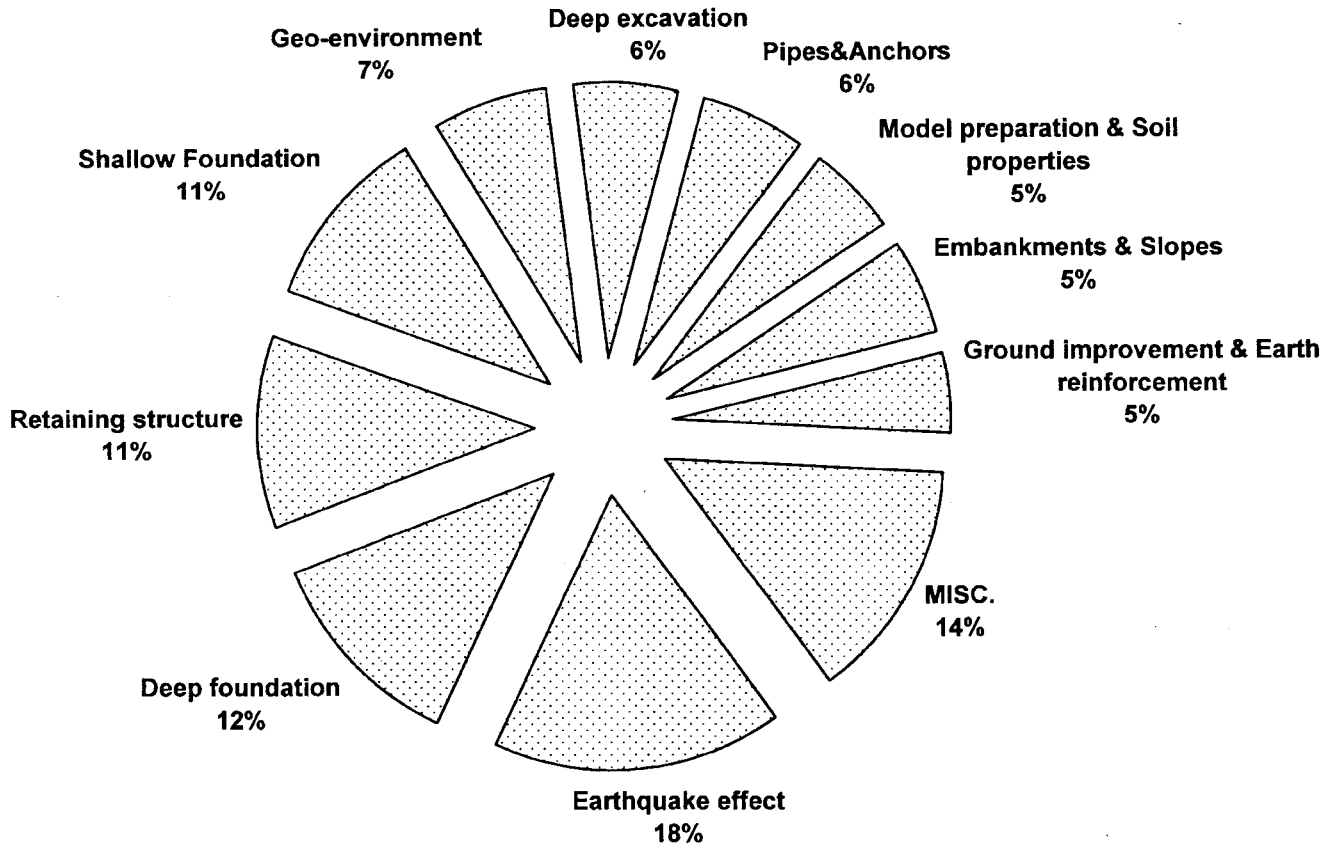

Figure 1-1. Research topics of centrifuge model tests.

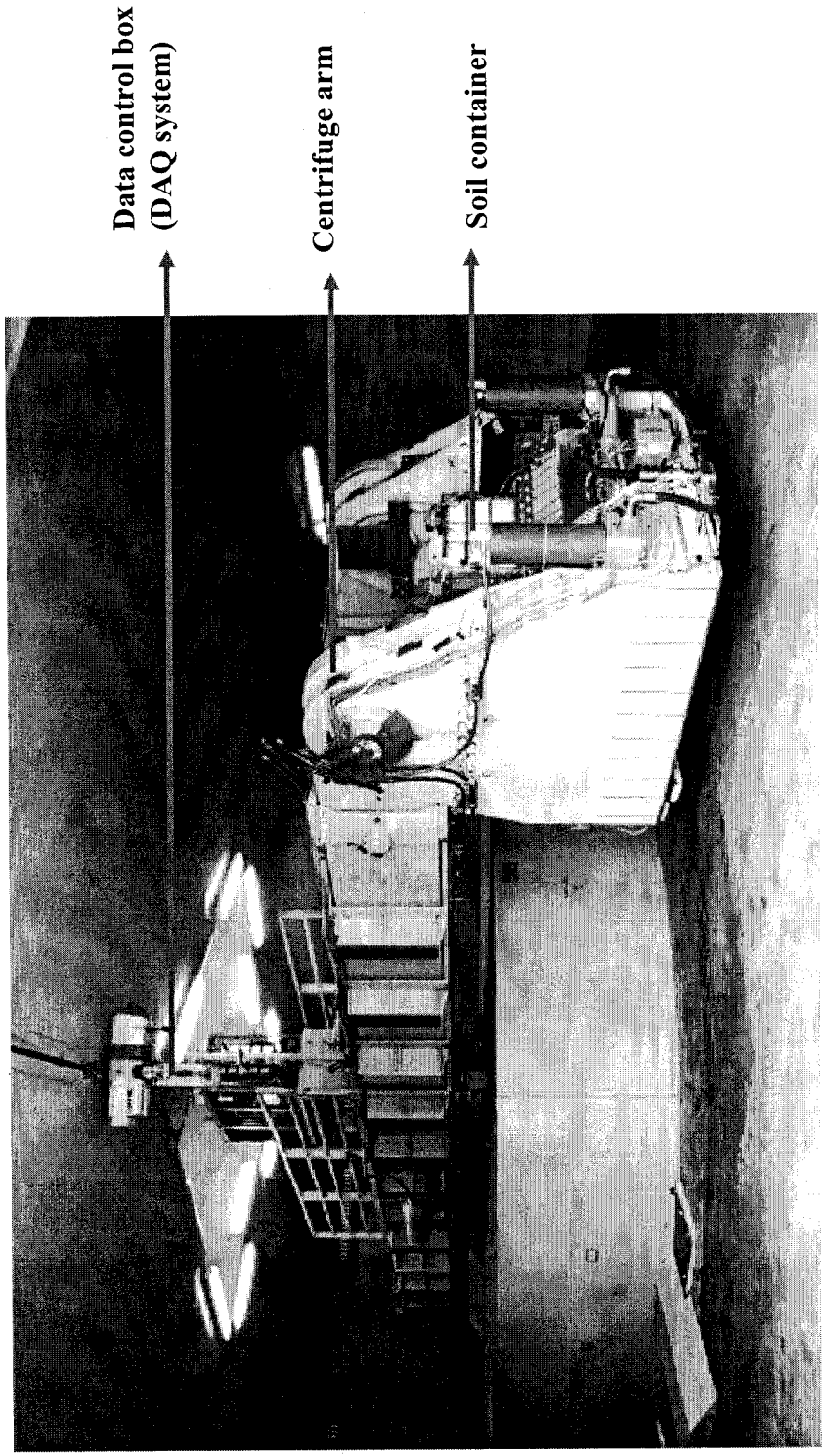

Figure 1-2. 9-m geotechnical centrifuge at UC Davis (Balakrishnan and Kutter, 1999).

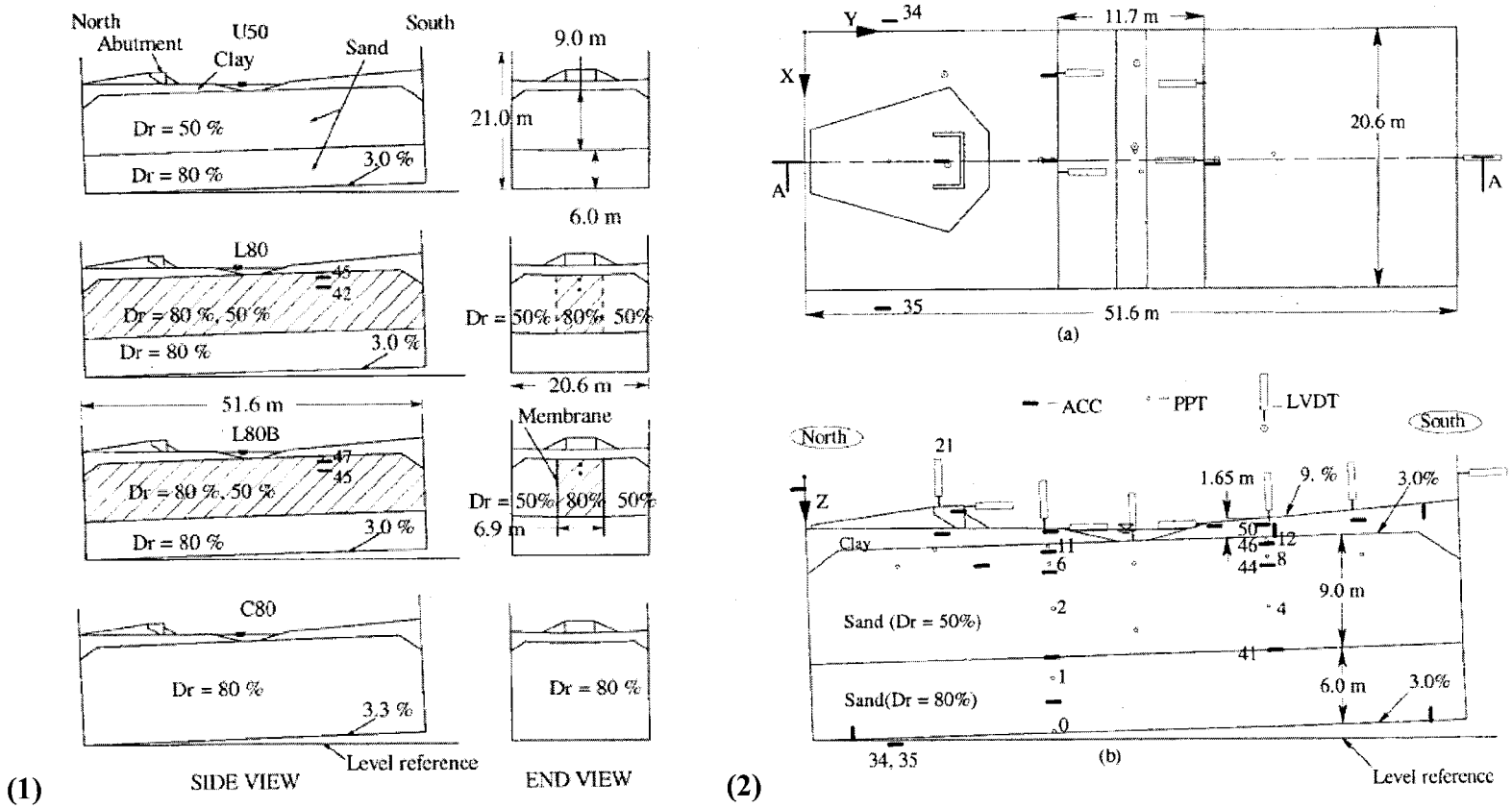

Figure 1-3. (1) Configuration of model layout for different remediation methods and (2) Details of model dimensions and instrument locations of model U50: (a) Plan view; (b) Instrument location on section A-A (Balakrishnan and Kutter, 1999).

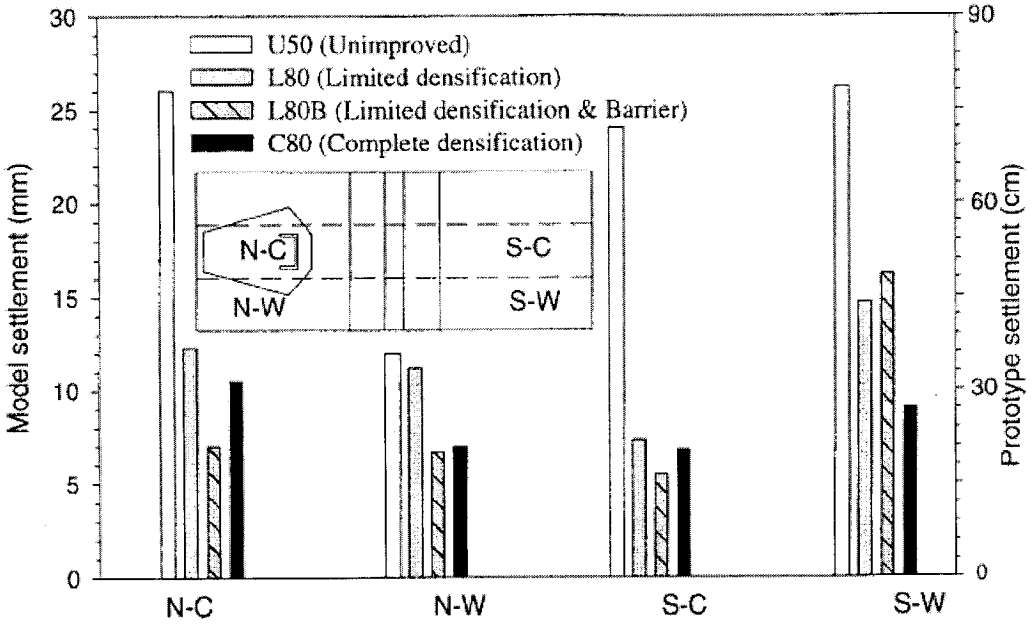

Figure 1-4. Settlement on sand surface for models at different locations (Balakrishnan and Kuter, 1999).

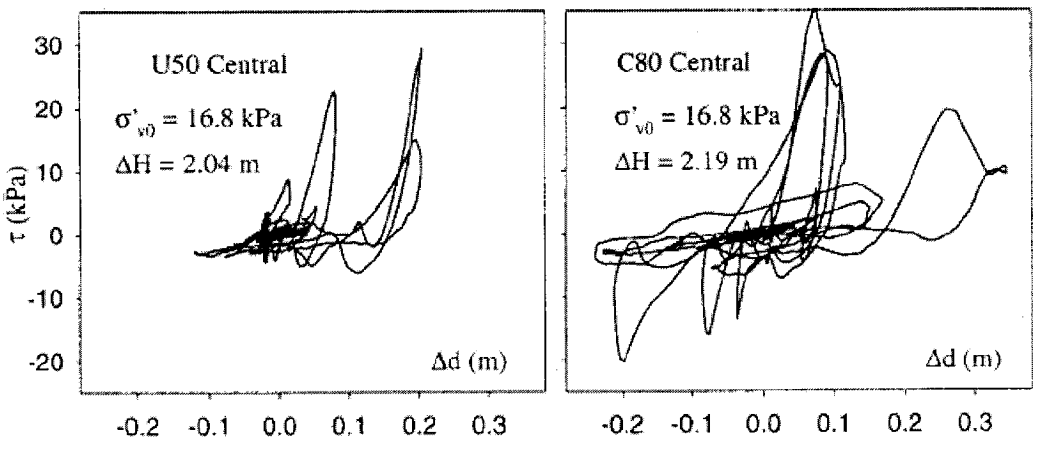

Figure 1-5. Shear stress-displacement loops at interface in U50 and C80 in large Kobe event (Balakrishnan and Kutter, 1999).

Table 1-1. Centrifuges operating in the world (http://www.geotech.cv.titech.ac.jp/~cen-98/Library/MAIN.HTM).

ID	Country	Location	Type	Nominal Radius (m)	Max. Accel.(g)	Max Payload (ton)	Year of First Test	Max. Capacity (g-ton)
1	Australia	Univ. of Western Australia	Beam	1.8	200	0.2	1989	40
2	Brazil	COPPE, Federal Univ.	Beam	0.5	450	0.2	1997	90
3	Canada	C'Core	Beam	5	200	2.2	1993	220
4	Canada	Queen's Univ.	Beam	2.25	120	0.28	1997	33.3
5	Canada	Queen's Univ.	Beam	0.9	60	0.03	1994	1
6	Canada	Univ. of New Brunswick	Beam	1.6	200	0.11	1993	22
7	Denmark	Danish Eng. of Tech.	Beam	2.3	80	1.2	-	96
8	France	CESTA	Beam	10	100	1	1956	100
9	France	L.C.P.C.	Beam	5.5	200	2	1985	200
10	Germany	Ruhr Univ., Bochum	Beam	4.125	250	2	1987	500
11	Germany	Ruhr Univ., Bochum	Beam	1.8	200	0.4	-	40
12	India	India Institute of Tech.	Beam	0.2	300	0.0024	-	0.72
13	Italy	ISMES	Beam	2	600	0.4	-	240
14	Japan	Aichi Institute of Tech.	Beam	1.36	200	0.075	1993	16
15	Japan	Chuo Univ.	Beam	3.05	150	0.66	1988	100
16	Japan	Fisheries Agency	Beam	3	150	0.25	1994	37.5
17	Japan	Hiroshima Univ.	Drum	0.4	447	0.06	1993	26.8
18	Japan	Hokkaido Development Agency	Beam	2.5	200	0.3	1994	60
19	Japan	Japan Defense Agency	Beam	2	100	0.15	-	15
20	Japan	Kajima Co.	Beam	2.63	200	1	1990	100
21	Japan	Kumamoto Univ.	Beam	1.25	250	0.04	1996	10
22	Japan	Kyoto Univ.	Beam	2.5	200	0.12	1988	24
23	Japan	Kyushu Institute of Tech.	Beam	1.27	150	0.18	1998	27
24	Japan	Kyushu Univ.	Beam	0.75	200	0.005	1990	1
25	Japan	Ministry of Agriculture, Forestry and Fisheries	Beam	1.3	200	0.07	-	14
26	Japan	Ministry of Construction	Beam	2	200	0.25	1987	20
27	Japan	Ministry of Construction	Beam	6.6	150	5	1997	400
28	Japan	Ministry of Labor	Beam	2.31	200	0.5	1988	100
29	Japan	Ministry of Transport	Beam	3.8	113	2.769	1980	312
30	Japan	Nagasaki Univ.	Beam	1.5	200	0.06	1997	12

Table 1.1 (Continued).

ID	Country	Location	Type	Nominal Radius (m)	Max. Accel.(g)	Max Payload (ton)	Year of First Test	Max. Capacity (g-ton)
31	Japan	Nippon Koei Co.	Beam	2.6	250	1	1996	100
32	Japan	Nishimatsu Co.	Beam	3.8	150	1.3	1998	200
33	Japan	NNGI	Beam	2.7	200	1	1992	100
34	Japan	Ohita Technical College	Beam	0.8	200	0.04	1996	8
35	Japan	Osaka City Univ.	Beam	2.56	200	0.12	1964	24
36	Japan	Shimizu Co.	Beam	3.35	100	0.75	1991	75
37	Japan	Taisei Co.	Beam	2.65	200	0.4	1990	80
38	Japan	Takenaka Co.	Beam	6.5	200	5	-	500
39	Japan	Tokyo Institute of Tech.	Beam	2.3	230	-	1995	50
40	Japan	Tokyo Institute of Tech.	Beam	1.25	150	0.25	-	38
41	Japan	Toyo Co.	Beam	2.2	250	0.3	1984	-
42	Korea	D.I.C.T.	Beam	2.7	200	1.2	1997	120
43	Netherlands	Delft Geotechnics	Beam	6	400	5.5	1989	-
44	Netherlands	Delft Univ. of Tech.	Beam	1.3	300	0.04	1989	10
45	Netherlands	Delft Univ. of Tech.	Beam	6.4	400	3.5	1988	150
46	P.R.China	Chengdu Science Technology Univ.	Beam	1.5	250	0.1	1991	25
47	P.R.China	China Institute of W.R.H.P.R.	Beam	5.03	300	1.5	1991	450
48	P.R.China	Hehai Univ.	Beam	2	250	0.1	-	25
49	P.R.China	Institute of W.C.H.R.	Beam	4.5	300	1.5	-	450
50	P.R.China	Nanjing Hydraulic Research Institute	Beam	5	200	2	1992	400
51	P.R.China	Nanjing Hydraulic Research Institute	Beam	2.2	250	0.2	-	50
52	P.R.China	Nanjing Hydraulic Research Institute	Beam	1	500	0.01	-	5
53	P.R.China	Nanjing Hydraulic Research Institute	Beam	2.1	250	0.2	1989	50
54	P.R.China	National Central Univ.	Beam	3	200	1	1995	100
55	P.R.China	Shanghai Institute of Railway Technology	Beam	1.55	200	0.1	-	20
56	P.R.China	Tsinghua Univ.	Beam	2.2	250	0.2	1993	50
57	P.R.China	Yangtze River Scientific Research Institute	Beam	3.5	300	-	-	180
58	Portugal	L.N.E.C	Beam	1.8	200	0.4	-	40
59	Russia	Moscow Institute of Railway Eng.	Beam	2.5	322	0.17	1960	-
60	Singapore	National Univ. of Singapore	Beam	1.87	200	0.4	1991	40

Table 1.1 (Continued).

ID	Country	Location	Type	Nominal Radius (m)	Max. Accel.(g)	Max Payload (ton)	Year of First Test	Max. Capacity (g-ton)
61	U.K.	Cambridge Univ.	Beam	4.125	150	1	1973	150
62	U.K.	City Univ.	Beam	1.6	200	0.2	1989	40
63	U.K.	Liverpool Univ.	Beam	1.1	200	0.2	1978	13
64	U.K.	Manchester Univ.	Beam	3.2	130	4.5	1971	600
65	U.K.	UMIST	Beam	1.5	150	0.75	-	100
66	U.S.A.	Air Force Eng. and Service Center	Beam	1.83	100	0.225	-	13
67	U.S.A.	USC-Caltech	Beam	1.02	175	0.1	1974	5
68	U.S.A.	Case Western Research Univ.	Beam	1.37	200	0.182	1997	20
69	U.S.A.	M.I.T.	Beam	1.07	200	0.0681	1985	13.6
70	U.S.A.	New Mexico Eng. Research Institute	Beam	1.8	100	0.227	-	25
71	U.S.A.	Princeton Univ.	Beam	1.3	200	0.076	-	10
72	U.S.A.	Rensselaer Polytech. Institute	Beam	3	200	0.15	1989	150
73	U.S.A.	Sandia Univ.	Beam	7.62	150	1.814	-	300
74	U.S.A.	Sandia Univ.	Beam	2.1	150	0.227	-	15
75	U.S.A.	Univ. of California, Davis	Beam	1	175	0.09	1976	9
76	U.S.A.	Univ. of California, Davis	Beam	9.14	75	4.5	1988	337.5
77	U.S.A.	Univ. of California, Davis	Beam	1	100	0.027	1985	-
78	U.S.A.	Univ. of Colorado, Boulder	Beam	1.5	100	0.15	1981	15
79	U.S.A.	Univ. of Colorado, Boulder	Beam	6	200	2	1988	400
80	U.S.A.	Univ. of Florida	Beam	1	100	0.0227	-	2.5
81	U.S.A.	Univ. of Florida	Beam	2	160	0.0839	-	-
82	U.S.A.	Univ. of Maryland	Beam	1.5	200	0.07	1983	15

Table 1-2. Comparisons of different sized centrifuges.

	USC	UC Davis	RPI	U of Colorado, Boulder
Capacity	10,000 G-Pound (5 G-Ton)	744,000 G-Pound (372 G-Ton)	300,000 G-Pound (150 G-Ton)	800,000 G-Pound (400 G-Ton)
G range	1-175 G	1-75 G	1-200 G	1-200 G
Max payload	200 pounds ($\approx$90.72 kg)	9,920 pounds ($\approx$4,500 kg)	1,500 pounds ($\approx$680.39 kg)	4,000 pounds ($\approx$1,814.37 kg)
Payload Area	18 × 22 $inch^2$ ($\approx$0.46× 0.56 m^2)	78.74 × 78.74 $inch^2$ ($\approx$ 2 × 2 m^2)	39.37 × 39.37 $inch^2$ ($\approx$1 × 1 m^2)	48 × 48 $inch^2$ ($\approx$1.22×1.22 m^2)
Nominal distance to payload (floor bottom)	40 inches ($\approx$1 m)	358 inches ($\approx$ 9 m)	118 inches ($\approx$ 3 m)	216 inches ($\approx$ 5.5 m)

Table 1-3. Topics of centrifuge modeling.

Topics	Example
Earthquake effect	Land deformation induced by earthquake event
Deep foundation	Performance of deep foundation during earthquake shaking
Shallow Foundation	Performance of shallow foundation during earthquake shaking
Retaining structure	Performance of retaining structures during earthquake shaking
Pipes & Anchors	Performance of pipes and anchors during earthquake shaking
Deep excavation	Performance of mat foundation during earthquake shaking
Geo-environment	Effects of contaminated soils
Model preparation & Soil properties	Study of soil mechanics and soil properties
Embankments & Slopes	Analysis of slope stability
Ground improvement & Earth reinforcement	Effects and methods of earth imrpovement
Other	Ocean engineering research

2 Theory of Centrifuge modeling

2.1 Introduction

Centrifuge modeling has been widely used in geotechnical earthquake engineering to solve for engineering problems that harbor complicated stress dependent non-linearities, such as soil-structure interaction and ground deformation (CGM, 2005).

An understanding of the principles of centrifuge modeling is essential to analyze physical phenomena in the centrifuge. The basic idea of centrifuge modeling is that the vertical stresses needs to be identical in both small-scale models and full-scale prototypes, in spite of different dimensions (Schofield, 1988). Hereafter, the terms "model" and prototype refer to small-scale and full-scale objects, respectively. The model stresses are increased by increasing the centrifugal acceleration until they become identical to prototype stresses. Centrifuge modeling attempts to replicate model events comparable to prototype events. The model and prototype events are related by similitude relationships (Taylor, 1995).

This chapter reviews the scale factors of similitude relationships between models and prototypes (e.g., Fuglsang and Ovesen, 1986; Liu et al., 1978; Pokrovsky and Fyodorov, 1975; Roscoe, 1968). These factors are required to convert the model results into the prototype world. The relationships are derived from the two assumptions of centrifuge modeling, i.e., models and prototypes have identical soil density and stress field (Tan and Scott, 1985). The time scales are also reviewed in dynamic and water diffusion events. In this chapter, we will cover the following

topics: (1) Principles of centrifuge modeling, especially stress similarity in model and prototype; (2) Derivation of similitude relationships between model and prototype; (3) Conflict in time scales of multi-physics, where dynamic motion and water diffusion occurs simultaneously; and (4) limitations of centrifuge modeling.

2.2 Principles in centrifuge modeling

Soils have nonlinear mechanical properties that depend on the effective pressure and stress history (CGM, 2005). Centrifuge modeling replicates these nonlinear effects by duplicating within model the gravity forces of full-scale prototypes. The centrifuge applies an increased acceleration force to the models in order to simulate the gravity effect in prototypes (Scott, 1975).

The centrifuge rotation produces an acceleration force, called centrifugal acceleration. The centrifugal acceleration is obtained through the radius r and angular velocity ω during centrifuge flight as shown in Figure 2-1 (Taylor, 1995). The centrifuge increases the "gravitational" acceleration within the physical models until models and prototypes have the same self-weight stress.

The centrifuge models have a free unstressed upper surface; there is no overburden pressure on the upper surface of the model (Taylor, 1995). In addition, the stress increases with the model depth because the gravitational acceleration depends on the radial distance between the center of rotation and the tested model (rotation radius).

The gravitational acceleration is:

$$a_c = \omega^2 \cdot r \tag{2-1}$$

where a_c is centrifugal acceleration; ω is the angular velocity; and r is the radial distance from the center of rotation to the rotating object.

2.3 Similitude relationships of centrifuge modeling

The subsequent sections discuss the fundamental premises and principles to derive similitude rules between models and prototypes through dimensional analysis.

2.3.1 Definition of Similitude in modeling

Centrifuge modeling is generally used to study complex problems where analytical solutions and computer simulations are not reliable (Ko, 1988). Physical modeling provides more practical solutions for complex problems exhibiting strong stress-dependent nonlinearities.

Similitude is a concept used in the testing of engineering models in various fields. In general, a model is said to have similitude with a prototype if they have geometric, kinematic, and dynamic similarities (Wikipedia, 2006). Examples of these similarities include:

- Geometric similarity: the model has the same shape as the prototype but a smaller size.
- Kinematic similarity: the model and prototype have similar velocity fields.

- Dynamic similarity: the ratios of all forces acting on soil particles and boundary surfaces are constant in model and prototype.

The similarities between model and prototype can be verified by means of several analyses including dimensional analysis and governing equations (e.g., Fuglsang and Ovesen, 1986). Dimensional analysis expresses the physical system in terms of a few independent variables and as many dimensionless parameters as necessary. The values of the dimensionless parameters are held identical for models and prototype (Wikipedia, 2006). Fuglsang and Ovesen (1986) reviewed how dimensional analysis defines the similitude relationships; they demonstrated experimental evidence to prove the similarities between models and prototypes.

2.3.2 Similitude laws in geotechnical modeling

Centrifuge modeling attempts to reproduce the same soil behaviors (i.e., soil strength and stiffness) in models and prototypes (Schofield, 1988). To this effect, centrifuges recreate (1) the In-situ stress changes with depth; and (2) the soil behavior as a function of stress level and stress history (Taylor, 1995).

The scale factor N between the accelerations in models and prototypes is determined using the centrifugal acceleration a_c (Equation 2-1). It is the ratio of centrifugal acceleration a_c to the earth's gravity g_p. For reference, the centrifugal acceleration a_c can also be replaced with the gravitational acceleration g_m in the centrifuge modeling. The acceleration g_m in the model is:

$$g_m = N \cdot g_p \tag{2-2}$$

where subscript **m** and **p** refer to the model and prototype, respectively.

The scale factor N has an important role in deriving other similitude relationships in centrifuge modeling, such as physical dimension, and pressure, velocity and time.

2.3.3 Premise of similitude relationships

A scaling law for linear dimensions is derived based on the assumptions that the model and prototype have identical stresses (Azizi, 2000):

$$\sigma_m = \sigma_p \tag{2-3}$$

Figure 2-2 illustrates the centrifuge modeling in dynamic motion and compares the vertical stresses in model and prototype. If the gravitational acceleration g_m in the model is N times larger than the earth's gravity g_p, the vertical stress σ_{vm1} at depth h_{m1} of the model with a soil density ρ is determined by:

$$\sigma_{vm1} = \rho \cdot g_m \cdot h_{m1} = \rho \cdot N \cdot g_p \cdot h_{m1} \tag{2-4}$$

In the prototype, the vertical stress can be represented using the same soil density ρ as:

$$\sigma_{vp1} = \rho \cdot g_p \cdot h_{p1} \tag{2-5}$$

Making use of Equation 2-3, Equations 2-4 and 2-5 can be rewritten:

$$\sigma_{vm1} = \rho \cdot N \cdot g_p \cdot h_{m1} = \sigma_{vp1} = \rho \cdot g_p \cdot h_{p1} \tag{2-6}$$

$$N \cdot h_{m1} = h_{p1} \tag{2-7}$$

Consequently, the similitude relationship for linear dimension is $N \cdot h_{m1} = h_{p1}$ as shown in Equation 2-7. In other words, the model length is reduced by the scale factor N. This is represented using dimensional analysis as follows:

$$N \cdot [L_m] = [L_p] \tag{2-8}$$

In addition, the scale factor of mass M is derived from the assumption of identical stress fields in model and prototype:

$$N \cdot g \cdot [M_m] \cdot [L_m]^{-2} = g \cdot [M_p] \cdot [L_p]^{-2} \tag{2-9}$$

Then, making use of Equation 2-8, Equation 2-9 becomes:

$$N \cdot [M_m] \cdot [L_m]^{-2} = [M_p] \cdot N^{-2} \cdot [L_m]^{-2} \tag{2-10}$$

$$N^3 \cdot M_m = M_p \quad \text{, and} \quad M_m = \frac{1}{N^3} \cdot M_p \tag{2-11}$$

2.3.4 Scale conflicts in multi-physics phenomena

2.3.4.1 Time Scale factor in dynamic motion

Based on dimensional analysis, the time scale in the model is reduced by N, comparing to the time scale in the prototype as shown in Equations 2-12 and 2-13 (Taylor, 1995).

$$g_m = [\mathrm{L_m}] \cdot [\mathrm{T_m}]^{-2} \tag{2-12}$$

$$[T_m] = \sqrt{\frac{[L_m]}{g_m}} = \sqrt{\frac{[L_p]/N}{g_p \cdot N}} = \frac{1}{N} \cdot [T_p] \tag{2-13}$$

2.3.4.2 Seepage in centrifuge modeling

Researchers have discussed the characteristics of pore fluid in seepage flow (Azizi, 2000) and consolidation phenomena (Mikasa and Takada, 1973) in terms of viscosity, density, and permeability. The pore fluid is a key factor to understand the compatibility of time scales in multi-physics modeling. For instance, Stewart et al. (1998) discussed the use of methylcellulose as a viscous pore fluid in centrifuge modeling. Allard and Schenkeveld (1994) investigated the characteristics of pore fluids with their chemical and physical properties through different laboratory tests to develop appropriate pore fluid for meaningful dynamic experiments.

While reviewing the time scale factor of seepage flow in centrifuge, it is essential to know basic soil and fluid properties, such as intrinsic permeability K, coefficient of permeability k, density of fluid ρ, and dynamic fluid viscosity μ. The intrinsic

permeability K characterizes the property of porous materials regarding how gas or liquid can pass through it. K is a function of shape, size, and packing of soil particles (Taylor et al., 1987). In other words, when the model and prototype has the same soil and fluid, the intrinsic permeability K_m (model) is the same as K_p (prototype).

$$K_m = K_p. \tag{2-14}$$

The intrinsic permeability is defined in Equation 2-15 (Taylor, 1995):

$$K = \frac{\mu \cdot k}{\rho \cdot g}. \tag{2-15}$$

where the variables of Equation 2-15 can be expressed using dimensional analysis as follows:

$\mu = [M] \cdot [L]^{-1} \cdot [T]^{-1}$; dynamic fluid viscosity

$k = [L] \cdot [T]^{-1}$; coefficient of permeability

$\rho = [M] \cdot [L]^{-3}$; density of the fluid

$g = [L] \cdot [T]^{-2}$; acceleration of gravity

$K = [L]^2$; intrinsic permeability

Using Equation 2-15, the coefficient of permeability k of soil mechanics becomes:

$$k=\frac{\rho \cdot g}{\mu} K \tag{2-16}$$

According to Darcy's law for seepage flow (Whitlow, 2001), the discharge velocity v through soil particles is:

$$v = k \cdot i \tag{2-17}$$

where k is the coefficient of permeability and i is the hydraulic gradient. The hydraulic gradient i is defined as the ratio of a drop in total head of pore fluid Δh_m to the seepage length as shown in Figure 2-3 (Craig, 1997). The head loss (i.e., head drop) Δh_m is defined by the elevation difference of water surfaces. Thus, the hydraulic gradient is dimensionless and does not scale with acceleration. In other words, the model and prototype have the same hydraulic gradients $i_m = i_p$ regardless of similitude relationships.

2.3.4.2.1 Same pore fluid in seepage-flow modeling

When the pore fluid is the same in the model and prototype, the ratio of coefficient of permeability k in model and prototype is:

$$\frac{k_m}{k_p} = \frac{\frac{\rho \cdot N \cdot g}{\mu} K}{\frac{\rho \cdot g}{\mu} K} = N \tag{2-18}$$

Because the model and prototype have same pore fluid and soil, all other parameters except gravitational acceleration remain the same. Using Equations 2-17 and 2-18, the scale factor for seepage velocities is:

$$\frac{v_m}{v_p} = N \tag{2-19}$$

Using Equation 2-19, the time scale factor in seepage flow can be obtained from dimensional expressions:

$$\frac{[L_m][T_m]^{-1}}{[L_p][T_p]^{-1}} = \frac{[L_m][T_m]^{-1}}{N[L_m][T_p]^{-1}} = N \tag{2-20}$$

$$[T_m] = \frac{1}{N^2}[T_p] \tag{2-21}$$

2.3.4.2.2 Viscous pore fluid in seepage-flow modeling

When the pore fluid is N times more viscous in the model than in the prototype, the coefficients of permeability in model and prototype are related through (Stewart et al., 1998):

$$\frac{k_m}{k_p} = \frac{\frac{\rho \cdot N \cdot g}{N \cdot \mu} K}{\frac{\rho \cdot g}{\mu} K} = 1 \tag{2-22}$$

As shown in Equation 2-22, the permeability is identical in both model and prototype, which means that the seepage velocity is also identical:

$$\frac{v_m}{v_p} = 1 \tag{2-23}$$

Based on Equation 2-23, the time scale factor can be expressed as follows:

$$\frac{[L_m][T_m]^{-1}}{[L_p][T_p]^{-1}} = \frac{[L_m][T_m]^{-1}}{N[L_m][T_p]^{-1}} = N \tag{2-24}$$

$$[T_m] = \frac{1}{N}[T_p] \tag{2-25}$$

Equations 2-24 and 2-25 imply that the time scale factor is the same between dynamic and seepage events when the pore fluid is N times more viscous in the model than in the prototype (Azizi, 2000; Dewoolkar et al., 1999).

2.3.4.3 Consolidation in centrifuge modeling

The time scale factor of consolidation events needs to be considered for viscous and non-viscous pore fluid. When a non-viscous fluid like water is used, the time scale factor is $t_p = N^2 t_m$. This time scale conflicts with the dynamic time scale ($t_p = N\, t_m$) (Dewoolkar et al., 1999; Stewart et al., 1998). Mikasa and Takada (1973) demonstrated that the self-weight consolidation of a thick layer of soft clay in the centrifuge had conflicting time scaling factors between consolidation and seepage events when the same pore fluid is used.

Consolidation is related to the water dissipation. The governing equation of consolidation is:

$$\frac{\partial^2 u}{\partial z^2} = \frac{1}{c_v}\frac{\partial u}{\partial t} \tag{2-26}$$

where u represents the excess pore pressure; t is the time; and z is the soil depth (e.g., Bardet, 1997; Azizi, 2000).

The solution to the consolidation equation contains a dimensionless time factor:

$$T_v = \frac{C_v \cdot t}{H^2} \tag{2-27}$$

where C_v is the coefficient of consolidation; t is the time; and H is the drainage distance. Hereafter, we will show how the fluid viscosity renders the time scale factors identical in dynamic and diffusion events.

2.3.4.3.1 No change in viscosity

The time factor T_v needs to be identical in the model and prototype to duplicate consolidation events. The time factor T_v in model and prototype can be written:

$$\frac{C_{vm} \cdot t_m}{H_m^{\,2}} = \frac{C_{vp} \cdot t_p}{H_p^2} \tag{2-28}$$

Through dimensional analysis, Equation 2-28 can be rewritten as follows:

$$\frac{C_{vm}}{C_{vp}} = \frac{[L_m]^2 \cdot [T_m]^{-1}}{[L_p]^2 \cdot [T_p]^{-1}} = \frac{[L_m]^2 \cdot [T_m]^{-1}}{N^2 \cdot [L_m]^2 \cdot [T_p]^{-1}} = \frac{1}{N^2} \cdot \frac{[T_p]}{[T_m]} \tag{2-29}$$

where

$$C_{vm} = [L_m]^2 \cdot [T_m]^{-1}$$

$$C_{vp} = [L_p]^2 \cdot [T_p]^{-1}$$

The coefficient of consolidation C_v is a function of several parameters:

$$C_v = \frac{k}{\gamma_{\text{pore fluid}} \cdot m_v} \tag{2-30}$$

where m_v is the coefficient of volume compressibility; k is the permeability; and γ_w is the unit weight of pore fluid in the prototype (Bardet, 1997; Craig, 1997). When the model and prototype have the same pore fluid and soil material, the coefficients of consolidation C_v become identical, i.e.:

$$\frac{C_{vm}}{C_{vp}} = 1 \tag{2-31}$$

Consequently, the time relationship becomes $[T_p] = N^2[T_m]$, which is incompatible with the time relationship $[T_p] = N\ [T_m]$ in dynamic motion.

2.3.4.3.2 Change in viscosity

Equation 2-31 gives us an idea on how to equate the time scales in the model and prototype. If the coefficient of consolidation in the model is scaled down to

$\frac{C_{vm}}{C_{vp}} = \frac{1}{N}$, the time relationship becomes $[T_p] = N\ [T_m]$ as shown in Equation 2-25 (Stewart et al., 1998). Eventually, the time scaling factor becomes identical in dynamic and consolidation events. Therefore, the coefficients of consolidation in model and prototype can be rewritten as follows to obtain identical time scaling factors:

$$\frac{C_{vm}}{C_{vp}} = \frac{[L_m]^2 \cdot [T_m]^{-1}}{[L_p]^2 \cdot [T_p]^{-1}} = \frac{[L_m]^2 \cdot [T_m]^{-1}}{N^2 \cdot [L_m]^2 \cdot [T_p]^{-1}} = \frac{1}{N^2} \cdot \frac{[T_p]}{[T_m]} = \frac{1}{N} \qquad (2\text{-}32\text{-a})$$

$$[T_p] = N \cdot [T_m] \qquad (2\text{-}32\text{-b})$$

In order to obtain C_{vm} in Equation 2-32-a, the permeability k in the model needs to be increased N times:

$$\frac{C_{vm}}{C_{vp}} = \frac{\dfrac{k_m}{\gamma_{\text{model pore fluid}} \cdot m_{vm}}}{\dfrac{k_p}{\gamma_{\text{prototype pore fluid}} \cdot m_{vp}}} = \frac{k_m}{k_p} = \frac{1}{N} \qquad (2\text{-}33)$$

When the model and prototype have identical soil and pore fluid with the same unit weight $\gamma_{\text{pore fluid}}$, Equation 2-33 shows that the permeability can be used to scale down C_{vm}. Indeed, the permeability k can be written as:

$$k = \frac{\rho \cdot g}{\mu} K . \qquad (2\text{-}34)$$

where K is the intrinsic permeability and μ is a dynamic viscosity of the pore fluid. K is a function of shape, size, and packing of soil particles (Taylor, 1995). Consequently, K is not affected by the properties of pore fluid. The dynamic viscosity μ turns out to be a variable key factor. It is necessary to increase C_{vm} N times in order to increase N times the permeability k. This can be obtained by increasing N times the dynamic viscosity μ.

2.3.5 Scale factor of seepage quantity

Using Darcy's law, the total seepage quantity Q is (Azizi, 2000):

$$Q = A \cdot v \cdot t \tag{2-35}$$

where A is the area of fluid flow; v is the fluid velocity; and t is the time duration of fluid flow. When the model and prototype have the same fluid, the time scale factor in seepage is $t_m = \frac{1}{N^2} t_p$ as shown in Equation 2-21. Thus, the scale factor of the total seepage quantity becomes in terms other scale factors (e.g., A, t, and v) as follows:

$$\frac{Q_m}{Q_p} = \frac{A_m \cdot v_m \cdot t_m}{A_p \cdot v_p \cdot t_p} \frac{A_m \cdot v_m \cdot t_m}{N^2 A_m \cdot N \cdot v_m \cdot N^2 \cdot t_m} = \frac{1}{N^3} \quad \text{and} \quad Q_m = \frac{1}{N^3} Q_p \tag{2-36}$$

2.3.6 Derivation of other scale factors

Based on previous derivations, the scaling factors for area, volume, force, velocity, frequency, and energy are obtained through dimensional analysis.

Area, $$\frac{A_n}{A_p} = \frac{[L_m]^2}{[L_p]^2} = \frac{1}{N^2} \cdot \frac{[L_m]^2}{[L_m]^2} = \frac{1}{N^2} \quad (2\text{-}37)$$

Volume, $$\frac{V_m}{V_p} = \frac{[L_m]^3}{[L_p]^3} = \frac{1}{N^3} \quad (2\text{-}38)$$

Force, $$\frac{F_m}{F_p} = \frac{[M_m] \cdot [a_m]}{[M_p] \cdot [a_p]} = \frac{1}{N^3} \cdot \frac{[M_m]}{[M_m]} \cdot \frac{N \cdot [a_p]}{[a_p]} = \frac{1}{N^2} \quad (2\text{-}39)$$

Velocity, $$\frac{v_m}{v_p} = \frac{[L_m] \cdot [T_m]^{-1}}{[L_p] \cdot [T_p]^{-1}} = \frac{[L]_m}{N \cdot [L_m]} \cdot \frac{[T_m]^{-1}}{N^{-1} \cdot [T_m]^{-1}} = \frac{N}{N} = 1 \quad (2\text{-}40)$$

Frequency, $$\frac{f_m}{f_p} = \frac{[T_m]^{-1}}{[T_p]^{-1}} = \frac{[T_m]^{-1}}{N^{-1} \cdot [T_m]^{-1}} = N \quad (2\text{-}41)$$

Kinetic energy, $$\frac{\frac{1}{2} \cdot [M_m] \cdot [v_m]^2}{\frac{1}{2} \cdot [M_p] \cdot [v_p]^2} = \frac{1}{N^3} \quad (2\text{-}42)$$

As shown in Equations 2-37 through 2-42, the fundamental scaling relations are repeatedly used to derive all similitude relationships. Figure 2-3 shows a schematic diagram of the centrifuge modeling of seepage with the same pore fluid in model and prototype. Figure 2-3 also lists some scale factors obtained for seepage with non-viscous pore fluid. Table * (Ko, 1988) summarizes most of the scaling factors used in centrifuge modeling.

2.4 Limits of centrifuge modeling

As previously mentioned, the main advantage of centrifuge modeling is to carry out experiments on small-scale models, which is more cost effective than performing full-scale experiments. With a moderate amount of labor and cost, centrifuge modeling can replicate and analyze the behaviors of much larger prototypes.

However, centrifuge modeling has limitations. It is rarely possible to replicate all details of the prototype in the field without making some assumptions about particle sizes and construction effects (e.g., Bolton and Lau, 1988; Ko, 1988; McDowell and Bolton, 2000; Whitman and Lambe, 1986). In other words, it is impossible to scale down all the aspects of the prototypes and to preserve all their physical properties through similitude rules.

The acceleration field in the centrifuge model is not completely uniform but varies with the distance to the centrifuge axis. The location where stresses coincide in both model and prototype is a key factor for determining the acceleration during centrifuge modeling. The distance from the center of rotation to that particular location is the radius r that defines the gravitational acceleration in Equation 2-1. The following section describes the scale effects and non-uniform stress fields and makes suggestions to compensate these problems.

2.4.1 Particle size effect

Centrifuge modeling scales down systematically the model dimensions, but rarely the sizes of soil particles; it basically neglects the "particle size effect". If centrifuge

modeling were to scale down the particle sizes by enforcing the similitude relationships, it would have to replace sand with silts. This substitution of a coarse material by a finer one would likely affect the stress-strain curve of the prototype because silts usually do not exhibit the same stress-strain response as sands.

Several researchers have investigated the effects of particle size in centrifuge modeling. Bolton and Lau (1988) discussed the particle size effect in regard to bearing capacity of granular soils. Ovesen (1979) provided some guidelines on the selection of a critical ratio of particle sizes to circular foundations to avoid "particle size effect." Particle size effects may be important in some applications, such as pile and foundation problems, and further research is certainly warranted to assess its importance in centrifuge modeling.

2.4.2 Non-uniform acceleration field

Centrifuges generate a non-linear acceleration field along the model depth. Since the acceleration field depends on the radial distance between the center of rotation and the soil model, the initial acceleration can be represented as $\omega^2 r$ where ω is the angular rotational speed, and r is the radial distance to a point within the model. The vertical stress within the model is calculated as follows (Taylor, 1995):

$$\sigma_{vm} = \int_0^z \rho\omega^2 (R_t + z)dz = \rho\omega^2 z\left(R_t + \frac{z}{2}\right) \tag{2-43}$$

where R_t is the radius to the top of the soil model as shown in Figure 2-4. The vertical stress is expressed by $\sigma_v = \rho \cdot g \cdot h$ where ρ is the soil density, g is the earth gravity, and h is the depth of soil model. Meanwhile, for most engineering applications, the earth's gravity is uniform in prototypes. The vertical stress in the prototype at depth $h_p = N \cdot h_m$ is:

$$\sigma_{vp} = \rho \cdot g \cdot N \cdot h_m \tag{2-44}$$

where N is the scale factor for linear dimension, and h_m is the depth of soil model. Thus the vertical stress in the prototype varies linearly with depth z.

The scale factor N in Equation 2-44 is determined based on an effective centrifuge radius R_e so that:

$$Ng = \omega^2 R_e \tag{2-45}$$

If the vertical stress in model and prototype are identical ($\sigma_{vm} = \sigma_{vp}$) at some unknown depth $z = h_{me}$, the prototype stress becomes $\sigma_{vpe} = \rho \cdot g \cdot N \cdot h_{me}$ and the effective radius R_e can be determined using Equations 2-43, 2-44, and 2-45:

$$\{\sigma_{vpe} = h_{me} \cdot \rho \cdot g \cdot N\} = \{\sigma_{vme} = \rho \frac{N \cdot g}{R_e} h_{me}(R_t + \frac{h_{me}}{2})\} \tag{2-46}$$

$$R_e = R_t + 0.5 h_{me} \tag{2-47}$$

The difference in vertical stress in Equations 2-43 and 2-47 can be expressed using the relative magnitudes of under-stress and over-stress (Taylor, 1995). Figure 2-5 shows the linear stress in the prototype and the non-linear stress in the model. With respect to the model, the under-stress means that the stress in the prototype is larger than the stress in the model. Likewise, the over-stress implies that the stress in the prototype is smaller than the stress in the model.

The flow chart of Figure 2-6 lists the steps to find the depth where the vertical stress becomes identical in model and prototype according to Taylor (1995). The maximum under-stress is found at depth $0.5\,h_i$ where the vertical stress in the model has lower maximum value. Meanwhile, the maximum over-stress at depth h_m represents higher maximum vertical stress in the model. Those stress differences are:

$$\text{Maximum under-stress} = 0.5h_i\rho gN - 0.5h_i\rho\omega^2\left(R_t + \frac{0.5h_i}{2}\right) \tag{2-48}$$

$$\text{Maximum over-stress} = h_m\rho\omega^2\left(R_t + \frac{h_m}{2}\right) - h_m\rho gN \tag{2-49}$$

The ratio r_{under} of the maximum under-stress to the prototype stress is:

$$r_{under} = \frac{\text{Maximum under-stress}}{\text{Prototype stress}} = \frac{0.5h_i\rho gN - 0.5h_i\rho\omega^2\left(R_t + \frac{0.5h_i}{2}\right)}{0.5h_i\rho gN} \tag{2-50}$$

After using Equation 2-45 and 2-47, r_{under} becomes

$$r_{under} = \frac{h_i}{4R_e} \tag{2-48}$$

Similarly, the ratio r_{over} of the maximum over-stress to the prototype stress at that depth h_m is defined as:

$$r_{over} = \frac{h_m \rho \omega^2 \left(R_t + \frac{h_m}{2} \right) - h_m \rho g N}{h_m \rho g N} = \frac{h_m - h_i}{2R_e} \tag{2-49}$$

Now, the depth h_i can de determined by equating the two ratios of r_{over} and r_{under} as:

$$r_{under} = r_{over} \tag{2-50}$$

$$\frac{h_i}{4R_e} = \frac{h_m - h_i}{2R_e} \quad \text{and} \quad h_i = \frac{2}{3} h_m \tag{2-51}$$

Eventually, the vertical stresses in model and prototype are identical at depth $h_i = \frac{2}{3}(h_m)$ as depicted in Figure 2-5. The radius corresponding to that depth can be used to calculate the centrifugal acceleration in the centrifuge model.

2.4.3 Construction effects

The construction of a centrifuge model is a delicate and labor-consuming task; it requires a careful control of the model properties, such as soil density, water content, etc. Researchers have devises several techniques and devices (e.g., hopper and robots) to construct soil layers and build model structures. Nowadays robots are

capable of constructing centrifuge models in flight in a more realistic manner without having to stop the centrifuge. Taylor (1995) and Ko (1988) described the operations performed by the robots including in-flight sand and clay model construction; ground excavation; injection of contaminants or chemical stabilizers into the groundwater; and placement of soil reinforcement in clay slopes

2.5 Summary

Chapter 2 has reviewed the principles and assumptions of centrifuge modeling and derived the similitude relationships between model and prototype. The centrifuge applies an increased "gravitational" acceleration to the physical model and produces the self-weight stress as in the prototype. The centrifugal acceleration is $a_{\omega} = r \times \omega^2$ (angular rotational speed ω and the radius r), and becomes the gravitational acceleration applied to the centrifuge model.

Centrifuge modeling assumes that prototype and model have identical stress fields and soil densities. Based on these assumptions, the similitude relationships have been derived and verified by means of dimensional analyses and governing equations.

The ratio of the centrifugal acceleration to the earth's gravity is the scale factor to adjust the size of centrifuge model. When the centrifugal acceleration of the model is N times larger than the earth's gravity, the linear dimensional length of the model is scaled down by N.

The time scaling factor has been reviewed for a multi-physics environment where dynamic and water diffusion events occur simultaneously. Examples of such multi-physics phenomena include consolidation during dynamic events. The pore fluid has to be N times more viscous in the model than in the prototype to reconcile the time conflicts in similitude relationships.

In addition, the limitations of centrifuge modeling have been discussed with respect to scale effects, non-uniform stress fields, and construction effects. Centrifuge modeling cannot realistically replicate every detail of the prototype. It is, however, a powerful tool for analyzing nonlinear phenomena in geotechnical engineering if its limitations are recognized.

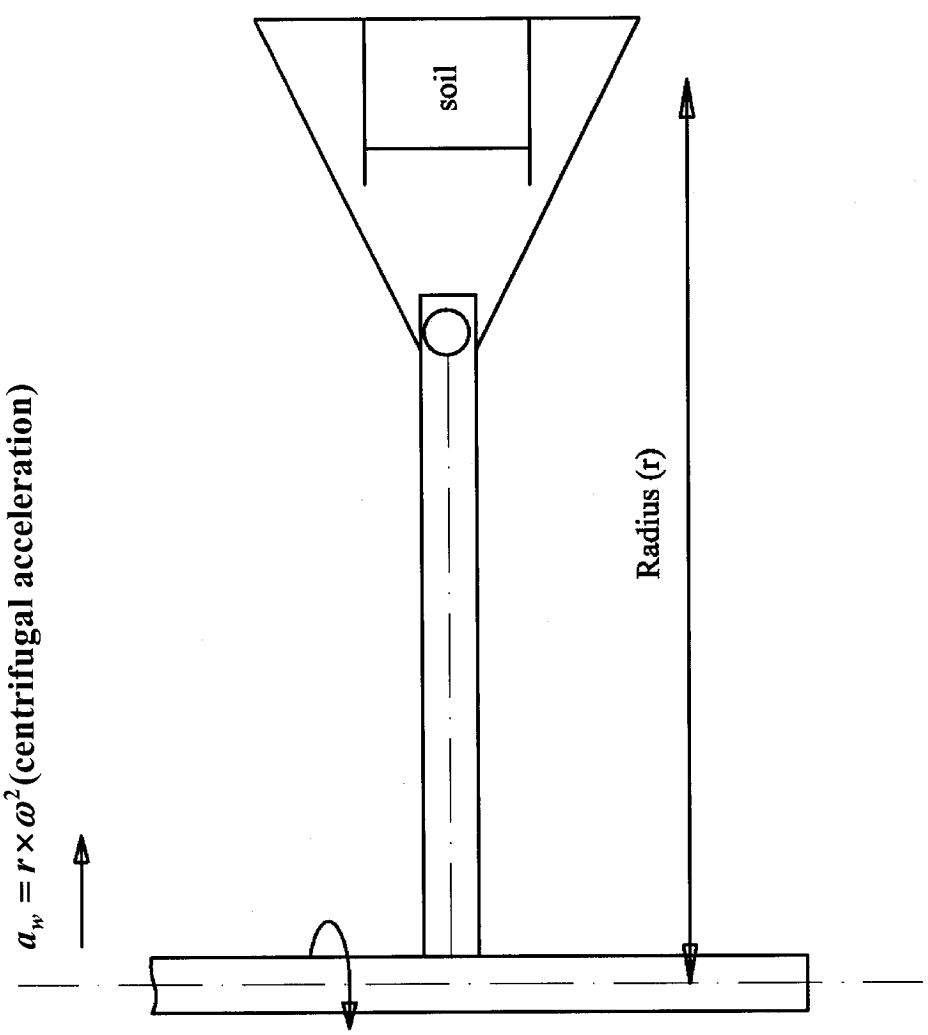

Figure 2-1. Centrifugal acceleration generated during centrifuge flight.

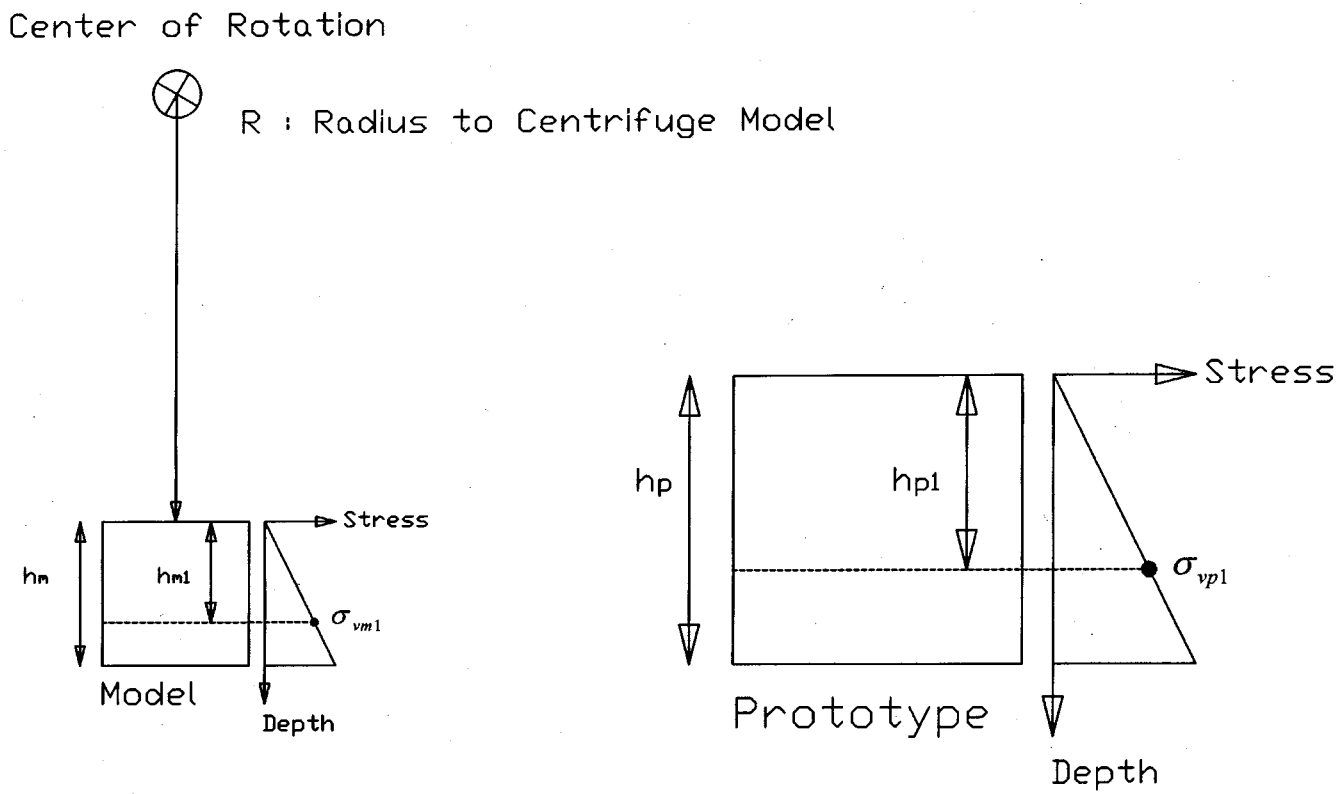

$$\sigma_{vm1} = \rho g_m h_{m1} = \rho N g h_{m1} = \rho g N h_{m1} = \rho g h_{p1} = \sigma_{vp1}$$

$$\sigma_{vp1} = \rho g h_{p1}$$

Figure 2-2. Vertical stress fields inside prototype and model.

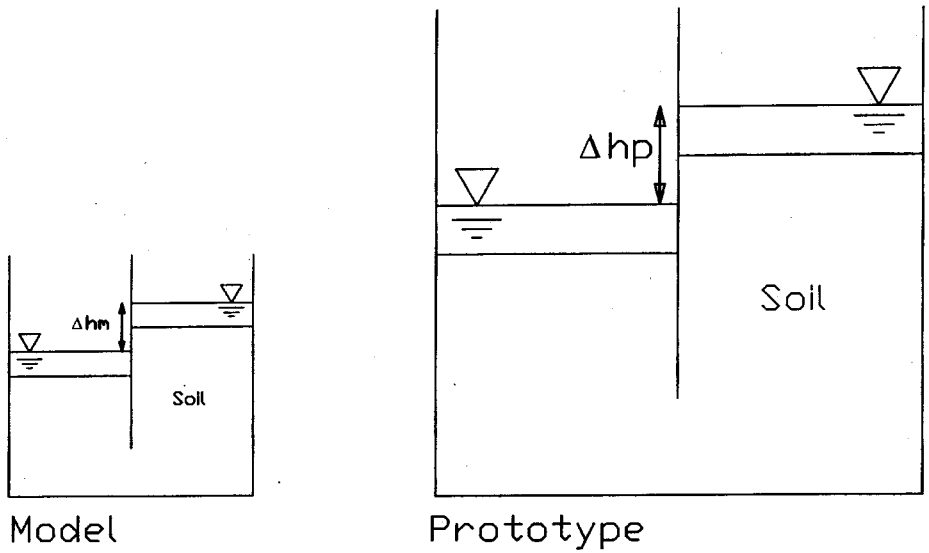

Scale Factors in seepage modeling

	Model	Prototype
Permeability	**1**	**N^{-1}**
Fluid Velocity(v)	**1**	**N^{-1}**
Fluid Quantity(Q)	**1**	**N^{3}**

* Same pore fluid between model and prototype

Figure 2-3. Seepage model with hydraulic scale factors.

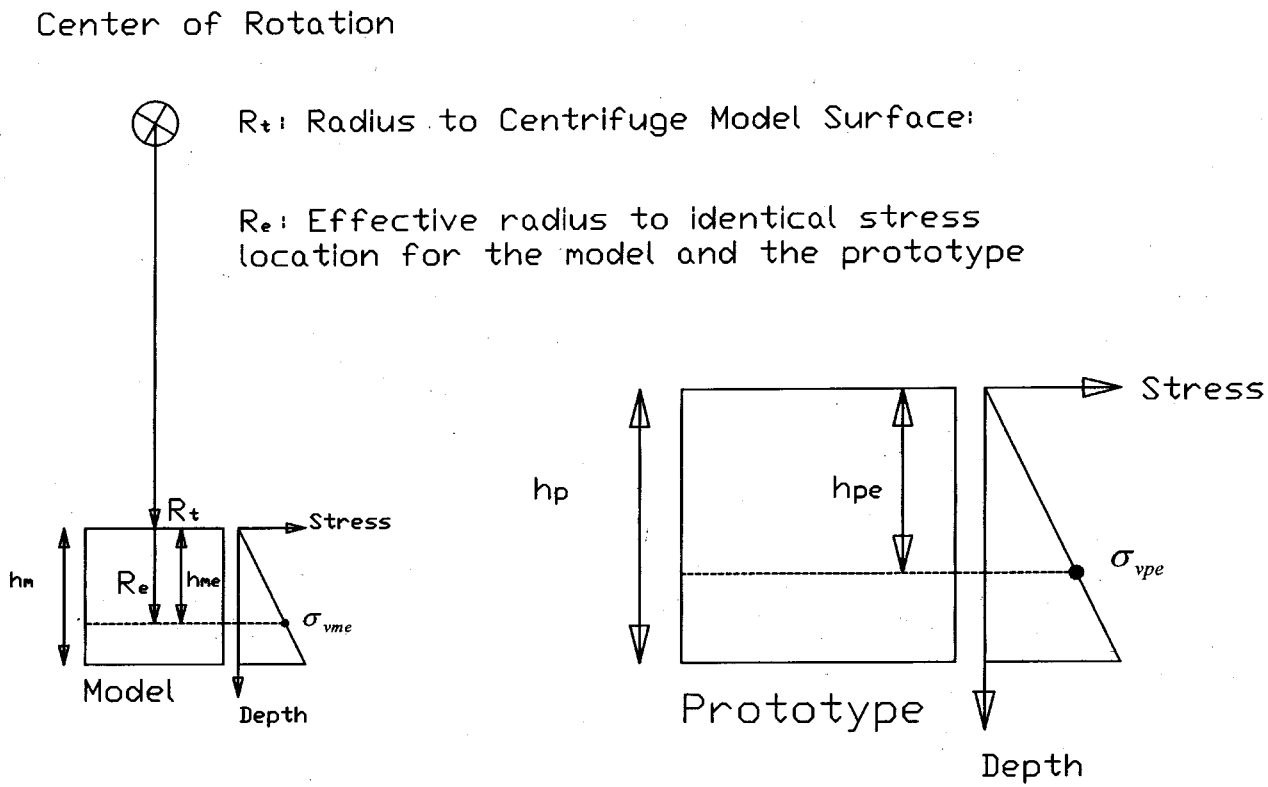

$$\sigma_{vme=}\rho g_m h_{me} = \rho N g h_{me} = \rho g N h_{me} = \rho g h_{pe} = \sigma_{vpe}$$

$$\sigma_{vme} = \sigma_{vpe}$$

Figure 2-4. Identical stress location between model and prototype.

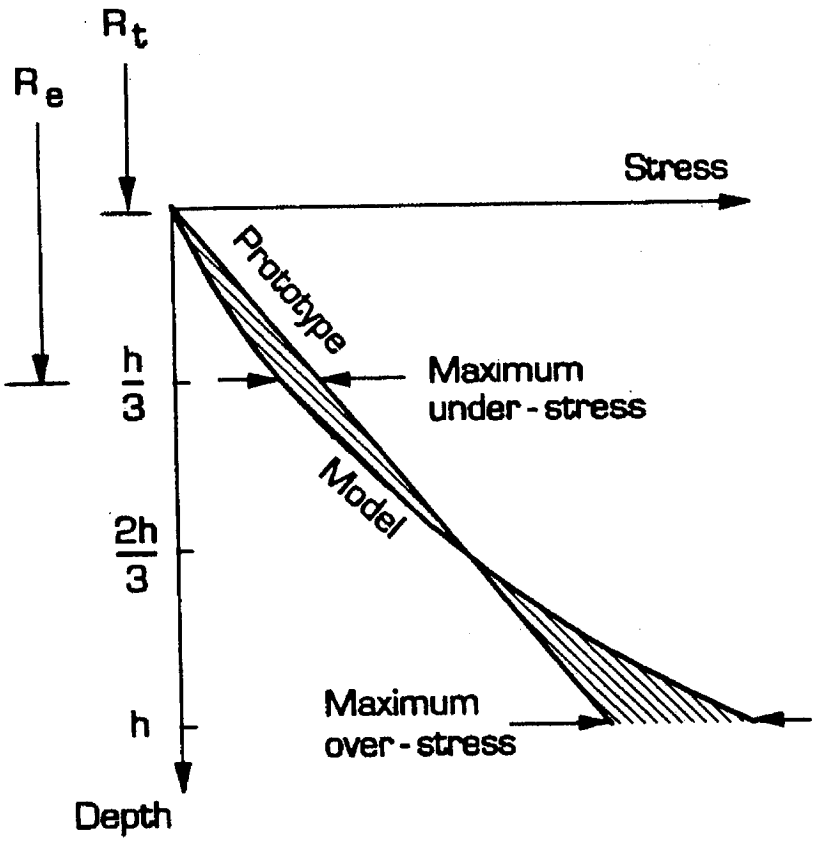

Figure 2-5. Stress variation with depth in a centrifuge model and its prototype (Taylor, 1995).

Table 2-1. Scale factors used in centrifuge modeling (Ko, 1988).

QUANTITY	PROTOTYPE	MODEL
Length	N	1
Area	N^2	1
Volume	N^3	1
Velocity	1	1
Acceleration	1	N
Mass	N^3	1
Force	N^2	1
Energy	N^3	1
Stress	1	1
Strain	1	1
Mass Density	1	1
Energy Density	1	1
Time (Dynamic)	N	1
Time (Diffusion)	N^2	1
Time (Creep)	1	1
Frequency	1	N

3 Review of USC centrifuge

3.1 Introduction

The centrifuge, which is hereafter referred to the USC centrifuge, has been functioning for more than two decades at the California Institute of Technology (Caltech). It was used to study static and dynamic problems in pile-soil interaction, dam, and ground deformation tests (e.g., Scott, 1975; Scott, 1989; Scott et al., 1982). To our knowledge, it is the first centrifuge that utilized a hydraulic loading system to generate the earthquake motion during centrifuge flight.

The USC centrifuge system is made of several components, e.g., hydraulic, electric, and mechanical apparatus, which work together to carry out data recording and processing, hydraulic control of earthquake motion, and centrifuge rotation.

The following sections present the main characteristics of the USC centrifuge and its peripheral facilities especially (1) hydraulic, electric, and mechanical systems to generate earthquake motion; (2) data acquisition system (DAQ) in terms of hardware and software; and (3) the calibration of instrumentation, e.g., transducers and signal conditioners.

Figure 3-1 summarizes the organization of chapter 3, which has five major sections: (1) presentation of the USC centrifuge; (2) equipment; (3) data acquisition system; (4) instrumentation; and (5) calibration of instrumentation.

3.2 General presentation of the USC centrifuge

3.2.1 Specification and capacity of the USC centrifuge

The USC centrifuge (Genisco Model A1030) consists of an 80-inch diameter aluminum-alloy arm (1-meter radius) and is rated at 10,000 g-pounds payload capacity (Allard, 1983). At each end of the centrifuge arm is an 18 inch x 22 inch magnesium-mounting frame located. It is capable of carrying a 200-pound payload to 50 g or 60 pounds to 175g during a centrifuge flight.

As for the dimension and weight of the USC centrifuge, they are:

- Height: 116 inches to the top of slip-rings
- Width: 106 inches.
- Weight: approximately 2,500 pounds

The USC centrifuge is housed in an aluminum enclosure for safety purpose and monitored through wireless cameras. Figure 3-2 shows the schematic USC centrifuge in 3-D view with and without the aluminum enclosure, and Figure 3-3 illustrates the centrifuge with physical dimensions in front view.

3.2.2 Centrifuge dismantlement and transportation

The centrifuge was transported to the University of Southern California (USC) from the California Institute of Technology (Caltech) after having been completely dismantled. During the centrifuge transportation, the inner components of the

centrifuge drive system, such as the drive shaft and bearings were inspected and replaced when necessary. Figure 3-4 shows the dimensions of the central shaft that rotates the centrifuge. In addition, Figure 3-5 shows the dismantled centrifuge during centrifuge transportation from Caltech to USC, and Figure 3-6 shows the dismantled centrifuge with its mechanical and hydraulic core parts, such as the central shaft, electric drive, and rotary unit. Two flexible hoses in Figure 3-6 supply high-pressurized oil (3000 psi) from a hydraulic pump to the centrifuge shake table; they pass through the central shaft.

3.2.3 Soil container

3.2.3.1 Laminar Box

A ring-shearing box, called laminar box, was upgraded from the initial designs created by the centrifuge labs at Cambridge University (Lambe, 1981) and the University of California, Davis (Arulanandan et al., 1983) and the laminar box designed at Caltech (Hushmand et al., 1988). Hushmand et al. (1988) introduced the idea to increase the length-to-depth ratio (2:1 ratio) of the laminar box and shape it as a box rectangular to reduce the possible cantilever deformations and enhance the one-dimensional response.

Bearings, locating between the rectangular rings, are made of steel and have cylindrical shapes. A number of grooves are machined inside each aluminum ring to a depth that is slightly smaller than the radius of bearing. These grooves are to allow the rings to sit on the top of bearings. The bearing is 0.25 inch in diameter as the

thickness of the ring is 0.5 inch. Figure 3-7 shows the laminar box that reduces friction resistance between the adjacent rings. The laminar box has been used for geotechnical problems, such as land deformation, soil-structure response, and liquefaction phenomenon with the earthquake motion. The USC laminar box gives a maximum horizontal displacement of 3.5 inches at the top of 20 rings if all the rings undergo an extreme excursion in one direction from the initially centered position (Hushmand et al., 1988).

The USC laminar box has the following characteristics:

- Inner Dimensions : Length (14 inches), Width (7 inches), and Height (10 inches)
- Number of Rings: 20 rings
- Material: Aluminum alloy

3.2.3.2 Other containers

Besides the laminar box, the USC centrifuge comes equipped with other soil containers, such as rigid rectangular container and cylindrical container. For example, a long cylindrical bucket with triangular supportive arms (see Fig 3-7), 22 inches in height and 6 inches in inside diameter, is used for pile tests because it is deep enough to embed model piles. Other soil containers are (Allard, 1983):

- A cylindrical bucket with a horizontal upper ring: 12 inches in height and 12 inches diameter

- A cylindrical bucket with two handles: 12.75 inches in height and 11.75 inches in diameter (see Figure 3-9)

- A rectangular container: 14.5 inches in length, 11.5 inches in width, and 10 inches in height

- Two cylindrical vessels: 10 inches in height and 10 inches in diameter

3.3 Equipment of the USC centrifuge

The USC centrifuge consists of five major systems to drive the centrifuge: (1) hydro-electric earthquake loading system; (2) signal communication system; (3) electric system; (4) mechanical system; and (5) data acquisition system. Each system has been upgraded and evaluated to improve centrifuge performance regarding the reduced noises on test output signals and stable centrifuge operation at high acceleration.

3.3.1 Hydro-electric loading system

3.3.1.1 General

The hydro-electric loading system of the USC centrifuge is composed of a shake table, a MTS controller, a hydraulic pump, a servo valve, and a rotary unit. The shake table is a platform where the test model and container locate and produces 1-D horizontal dynamic motion. The shake table is composed of the servo valve and actuator that moves the table according to the signal of the MTS controller.

The shake table, shown in Figure 3-10, was custom built by laboratory engineers at Geomatic, which was a division of Dames & Moore (presently URS). The shake table has an allowable moving distance of 0.193 inch for both directions from the center position of the centrifuge magnesium frame (Aboim et al., 1986).

The servo valve (see Figure 3-10) is a flow control device, following the signal of the MTS controller, opening and closing the flow of highly pressurized oil, which is reserved in two 1-gallon accumulators and one 5-gallon accumulator. Figure 3-11 shows the 1-gallon accumulators mounted under then centrifuge arm, and Figure 3-12 shows the 5-gallon accumulator, locating outside the centrifuge. The servo valve, Moog model A076-264C (serial number: 312) has a nominal working range of 3000 psi. The servo valve has a flow rate of 15 gallon per minute (gpm) at 1000 psi valve drop (Lee, 2004).

3.3.1.2 MTS 406 controller

The MTS Model 406.11 controller (see Figure 3-13) has functions of servo-valve controller, transducer conditioner, limit detector, and feedback selector for a closed-loop system. A Schaevitz 100HR LVDT is used as a feedback to the closed-loop system and generates the output signal according to the movement of shake table.

The feedback LVDT works with an AC LVDT conditioner inside the MTS controller, which amplifies the feedback LVDT signal in accordance with a "calibration factor" setup. The internal AC transducer conditioner supplies an AC excitation power (10 kHz, 20 V peak to peak amplitude) to the Schaevitz 100HR

model (AC-operated LVDT) and demodulates the transducer output to ±10 VDC for a full scale output.

Figure 3-14 shows a schematic diagram of the MTS 406.11 controller, and illustrates the control flow of the earthquake simulation. The hydro-electric loading system of the USC centrifuge is a closed-loop system, which compares the displacement feedback to the earthquake motion from the MTS controller.

The "program" port of the MTS 406 controller is the inlet of earthquake simulation signal that is supplied from an external source, such as a signal generator and a computer through a digital-to-analog converter (DAC). The input signal of the "program" port has a range of ± 2~± 10 V. The input signal has a range of ± 2 V according to the "calibration factor" adjustment. The preparation of input signal is described in Chapter 4.

The "span" is a ten-turn control that is used for attenuating precisely the input signal, and determining the dynamic amplitude of the composite command signal. Alteration on the input signal with the "span" and "set point" controls yields the composite command signal. The "span" has a range of 0 to 1000 that corresponds to 0 to 100% of the system operating range. For example, for centrifuge test at 50g and oil pressure of 3000 psi, the value of the "span" was set between 900 and 1000 to achieve the peak amplitude of horizontal acceleration. The response of the shake table depends on several variables, such as oil pressure, centrifugal acceleration, and input motion.

The "set point" is a ten-turn control to provide a precise static offset to establish the mean level of the composite command signal. In other words, the "set point" is used to reposition the shake table to the center position on the centrifuge magnesium frame.

The subsequent sections explain some major functions of the MTS controller, especially how to adjust "calibration factor" and "limit detect" controls. Other details about the MTS 406 can be found in the manual (Allard, 1983).

3.3.1.2.1 MTS 406 controller: "calibration factor" adjustment

The "calibration factor" relates to the feedback LVDT signal, amplifying the initial output voltage of the feedback LVDT. The servo controller compares the signal supplied to the input signal. If there is a difference between the input signal and the response of the shake table, the servo controller assigns an error signal to the "program input" to match the response of the shake table. The "calibration factor" is a value of 288 when the Schaevitz 100HR feedback LVDT works with the input signal of± 2 V range.

The "calibration factor" is set up using the following procedure:

1. Position the calibration-range switch to 100 mV/V ~1100 mV/V range on the conditioner rear panel.
2. Connect the signal generator, which is ready to send sine waves with 10Hz and 2V p-p amplitude to the "program" connector of the MTS controller

3. Turn on the MTS controller.

4. Turn on the hydraulic pump and increase oil pressure by 1000 psi.

5. Turn on the function generator to send sine waves to the MTS controller.

6. Adjust the "calibration factor" (see Figure 3-13) to make the shake table travel the maximum distance from the center position in both directions, stopping just before hitting the metallic stoppers located at both side of the centrifuge frame.

3.3.1.2.2 MTS 406 controller: "limit detect" adjustment

The upper and lower "limit detect" controllers (Figure 3-13) have a function of limiting the movement of the shake table. This control prevents damage to the test model and the shaking system. The "limit detect" has an option to interlock the hydraulic loading system or to light warning indicators if the shake table moves over the limits. The upper and lower "limit detect" are set to -854 and 848 for lower and upper limits respectively.

3.3.1.3 Hydraulic accumulator, pump, and rotary unit

3.3.1.3.1 Accumulator

The hydraulic working pressure is monitored by a pressure gauge installed on the centrifuge conduit as shown in Figure 3-15. The pressure gauge helps to figure out the actual pressure inside hydraulic conduit instead of depending on the hydraulic pump-pressure. When the pump pressure is set to 3000 psi, the working pressure

shows 2800 psi, which is still an adequate amount of oil to move violently the shake table (Aboim et al., 1986). The pump pressure is usually set to 3000 psi because the rotary unit has a pressure limit up to 3000 psi. The pre-charge pressure of 1-gallon accumulators needs to be 1500 psi to swiftly supply the oil to the servo valve during the test to obtain the desired peak acceleration of earthquake motion (Lee, 2004).

To generate the earthquake shaking, the hydraulic piston has to move vigorously with shift oil supply at around 3000 psi. There is no way the pump by itself can deliver 30 gallons a minute (gpm). A source of hydraulic pressure is, therefore, needed as close to the servo valve as possible. Two 1-gallon accumulators, manufactured by Greer Hydraulics, are located under the centrifuge arm and plumbed together with pipes containing highly pressurized oil.

The USC centrifuge has several accumulators as listed below:

- Two 1-gallon accumulators, manufactured by Geer Hydraulics (Figure 3-11), located under the centrifuge arm and used as oil storage to supply swiftly plenty of oil to the servo valve
- One 5-gallon accumulator, manufactured by Parker Hydraulics (Figure 3-12), located outside the centrifuge enclosure to supply the high pressurized oil to the 1-gallon accumulators
- One 1-gallon accumulator next to 5-gallon accumulator used as the reservoir of returning oil from the centrifuge to the hydraulic pump

Figure 3-16 shows a schematic diagram of the hydraulic flow among the hydraulic equipment, and Figure 3-17 shows a drawing that presents the hydraulic conduit system inside the centrifuge arm with a 3-D view.

3.3.1.3.2 Hydraulic Pump

The hydraulic pump (Figure 3-18), HPS6A model manufactured by Team Corporation, is used to supply high pressure oil (3000 psi). The pump (HPS-6A) is driven by a single electric motor that has 5 HP power and requires electric power of 440 VAC with 3 phases. The pump is rated at 1.9 gpm (gallons per minute) when it runs at 1800 rpm with a pressure of 3,000 psi. The pump uses fine and pure oil like MOBIL DTE-26 oil because the servo valve works best with the type of clean and low viscous oil. The procedures of initial pump setting and control are described in the manual (Team Corporation, 1994)

3.3.1.3.3 Rotary unit

The rotary unit (Figure 3-19), model A-7234 manufactured by Talco, is used to supply and return highly pressurized oil between the external pump and the centrifuge. The rotary unit was custom built for the USC centrifuge with non-standard threads, i.e. 3/4²-12 JIC (Wenk, 2003). Figure 3-20 shows the four passages of the rotary unit that allocates two passages for supplying and returning the oil during centrifuge modeling.

The rotary unit will break down if it spins dry without oil supply; the O-rings inside the unit will fail due to the high temperature induced by friction between O-rings and

housings. This results in serious oil leakage during the centrifuge rotation at high speed and high pressure. In case of the oil leakage, the rotary unit can be repaired with Talco 7234 seal kit. The following procedures are used to replace the O-rings (Wenk, 2003):

1. Remove retaining ring (U shaped ring)
2. Press shaft out from housing
3. Remove bolts to dissemble upper cap from the union
4. Remove old seals (Teflon ring & o-ring)
5. Install new seals (o-ring then Teflon ring)
6. Bolt the housing back together loosely (so they can self-align on the shaft)
7. Lubricate the seals & shaft and press shaft into housing assembly.
8. Tighten bolts & install retaining ring.

The centrifuge rotates in a clockwise direction not to twist flexible oil hoses, which might result in serious damage. In addition, a slow oil-pressure change is important to prevent the oil leakage through weep holes that are located on the side of rotary unit.

3.3.2 Signal communication system

3.3.2.1 Slip-ring communication

Before the installation of a wireless network, electrical signals were transferred through a slip-ring stack. Figure 3-21 shows the slip rings that transfer test data, supply 110 VAC power, and upload the earthquake signal to the electro-hydraulic

loading system. The slip ring stack has 44 electrical channels; 40 slip rings were previously allocated to data acquisition and transfer; and 4 other slip rings to supply 110 VAC (10 to 30 amp range) power and earthquake motion signal (Allard, 1983).

3.3.2.2 Wireless network communication

A new wireless network is now replacing the slip-rings to transfer test data and control data. This wireless network eliminates the long cables used between centrifuge and laboratory. It is a unique methodology that eliminates noisy test data and revolutionizes geotechnical centrifuge testing. The wireless network enables us to trigger the data acquisition software (DasyLab) to monitor and record test data before, during, and after earthquake shaking.

Figure 3-22 shows a schematic diagram of the wireless network, including equipment and data flow among DAQ systems. The wireless router, personal computers with wireless network cards, and wireless camera is used to monitor and record the responses of test model and centrifuge itself. The DAQ system is controlled remotely using the "Remote Desktop Connection" of Microsoft Windows XP operating system. This "Remote Desktop Connection" enables computers to communicate with each other through a wireless network and to control from the laboratory the DAQ software running on the centrifuge laptop computer. The set up of the wireless network and "Remote Desktop Connection" are explained in Microsoft Help and Support (Microsoft, 2005; Simmons and Causey, 2003).

3.3.2.2.1 Wireless network components

The wireless network has the following specifications and capabilities.

- ⊙ Linksys wireless router: model wireless-G broadband router V3.0
  - 4-port switch and wireless-G (802.11g) Access Point
  - Wireless data rates up to 54Mbps
- ⊙ Linksys wireless network card: model wireless-G Notebook Adapter V2.0
  - High-speed wireless (802.11g) networking for a notebook computer
  - Data rates up to 54Mbps
- ⊙ Wireless Camera: D-LinkAir DCS-1000W
  - Wireless Internet camera with VGA quality resolution
  - 802.11b wireless networking

3.3.3 Electric system of the USC centrifuge

The USC centrifuge is driven by a Sabina Electric and Engineering motor and controller (model RG2600) that have a single phase and static D.C. drive with a 5 HP and maximum 1725 RPM (Revolutions per Minute) capacity. The motor uses 230 V, and 3-phase power (SGC, 2006). The speed of centrifuge rotation is determined accurately through a 600-tooth gear wheel is located on the main drive shaft, which produces 600 pulses per revolution via a magnetic pickoff. The pulse is converted

and displayed on the LED display of RPM controller shown in Figure 3-23. The RPM controller has an accuracy of 0.1 RPM.

3.3.3.1 Electric powers and grounds of the USC centrifuge

The Sabina Electric and Engineering Type RG 2600 - single phase full wave regenerative static D.C. drive- runs with a 5 HP, 1725 rpm, 230V, 3-phase, constant torque, double-ended electric drive motor (Figure 3-24). Electric power and drive panel (Figure 3-25) are mounted on the wall of centrifuge room to supply electric powers for both Sabina motor and Team pump (HPS6A).

3.3.3.1.1 Power Converters

Three power converters convert 120 VAC power to ±15 VDC, and ± 5 VDC powers for the electric instrumentation on the centrifuge arm, such as accelerometers, porepressure sensors, and signal conditioners. A power converter, SOLA Heavy-Duty SDP2-24-100, produces 24 to 28 VDC with 2.1 Amp by converting 110-240 VAC. The converter has 2 power outlets and uses wires between 20 and 12 AWG for input and output power ports. The model SDP2-24-100 is used for six LVDT demodulators that are installed for AC LVDT transducers.

Another power converter, SOLA Heavy-Duty SCP30T515-DN, converts the 110 VAC to different output types, e.g. ±15 VDC and +5 VDC. This converter supplies the DC voltage powers to transducers such as Druck PDCR81 (pore pressure transducer) and Schaevitz DC LVDT transducers.

The other power converter, manufactured by Power-One (model HCAA-60W-A), were previously used on the centrifuge before installing the converters above. It yields ±15 VDC, and +5 VDC powers for old signal conditioners and has a potentiometer to adjust the range of output voltages. The ground port of the converter was used as a common ground point for all electric equipment for the centrifuge system.

3.3.3.1.2 Power connection panel

As shown in Figure 3-26, an electric power of 110 VAC comes through the slip rings to the power panel on the centrifuge arm where green and red knobs are used as AC power terminals. The hot and neutral power lines are available without a ground line; currently, the hot line is connected to the green knob and the neutral one is connected to the red knob. The centrifuge body is earthed to the ground of building-power supply; therefore, one of the ports in the power panel is used to drain the electric noises from shield cables.

3.3.3.1.3 Electric grounds: earth ground and common ground

The centrifuge arm and its enclosure are earthed to the ground line which is one of the power lines, supplied for the centrifuge drive motor. The drain wires of the shielded cables are connected to the centrifuge body, and they are eventually grounded to the earth ground at the end via the ground line. It is important to know the ground point to prevent ground loop caused by grounding several points, where

the electric potential energies are different. Figure 3-26 shows the ground knob on the power panel to drain all noise signals as mentioned above.

In addition, there is a common electric ground for some old equipment, like a signal conditioner. The signal conditioner generates the output signals that are based on the common electric ground, and this ground is linked to the ground port of the power converter (Power One HCAA-60W-A model).

3.3.4 Mechanical system of the USC centrifuge

A critical step in centrifuge modeling is to balance the rotating masses and avoid undesirable vibrations.

3.3.4.1 Centrifuge balance

The centrifuge balance is critical as it is closely related to test quality and safety. The centrifuge is balanced manually by adjusting several screws and nuts on the centrifuge arm, as shown in Figure 3-27. These screws release the centrifuge arm to find its balanced position. As shown in Figure 3-27, a horizontal metal rod, which has opposite direction threads at both ends, passes through the centrifuge body. The rod secures and releases the centrifuge body because of its opposite thread directions. As shown in Figure 3-27, the side (A) of the rod has a clockwise thread direction to secure the centrifuge arm. Meanwhile, the side (B) of the rod has a counterclockwise thread direction to secure the arm. Eventually, turning the rod end in side (A) clockwise makes the rod end in side (B) rotate anticlockwise. This mechanism

fastens and releases the centrifuge arm conveniently while the centrifuge is balanced. The side (A) corresponds to the Dytran conditioner side, and side (B) to the other side of the centrifuge.

3.3.4.1.1 Balancing procedures of the USC centrifuge

The centrifuge arm is balanced by adjusting the bolts and nuts as well as the horizontal rod passing through the vertical shaft of the centrifuge. The balancing procedure is as follows:

1. Turn the centrifuge arm to front the side (B).

2. Loosen the arm by turning the rod clockwise.

3. Remove all counterweights and soil from both containers at the end of centrifuge arm.

4. Check the gap between the circular plate (called as cap) and the rectangular plate as shown in Figure 3-27. If the gap is not even around the cap, go to next step.

5. Release all screws (Figure 3-27) on the plates. Place the cap close to the rectangular plate by rotating it smoothly along the rod.

6. Adjust the upper setscrews (B1 and B2 in Figure 3-27) or the lower ones (B3 and B4 in Figure 3-27) relatively to align the cap evenly on the rectangular

plate. Even spacing indicates the rectangular plate is perpendicular to the horizontal rod, which prevents the centrifuge arm from tilting down to one side.

7. Monitor the dial gauge (see Figure 3-28) located on the centrifuge arm to indicate a static balance.

8. Push down one end of the centrifuge arm and record the value of the dial gauge for a maximum displacement.

9. Push down the other end and record the value of the dial gauge for another maximum displacement.

10. Find the middle position from above the maximum movements in step (8) and (9).

11. Add some weights inside the counterweight container to position the centrifuge in the middle position at step 10. Note that the centrifuge arm should move freely with similar amount of movement at the ends of centrifuge arm; otherwise, adjust the upper and lower setscrews of right (B2 and B4 in Figure 3-27) or left (B1 and B3 in Figure 3-27) section.

12. After balancing the centrifuge using the procedures above, fasten all screws (C1, C2, C3, C4, A1, A2, A3, and A4) as shown in Figure 3-27.

13. Lock the centrifuge arm by turning the horizontal rod on the side (B) counterclockwise.

3.3.4.2 Procedures of the USC centrifuge operation

The centrifuge cannot be operated without extreme caution to avoid damages to the test sample and the centrifuge itself. Spinning the centrifuge without powering the hydraulic pump can break down the rotary unit by burning its O-rings. This incident did occur in the past, and were expensive to fix. The O-rings were burned out because the lack of oil lubrication induced high friction resistance and high temperature, and resulted in severe oil leakage. The following procedure must be followed before, during, and after a centrifuge test.

Procedures of centrifuge operation before execution:

1. Turn the centrifuge power on.

2. Turn on the notebook computer on the centrifuge arm, and start the "DasyLab" program to control the DAQ system.

3. Check the communication between the centrifuge and the laboratory through the wireless network.

4. For the MTS 406 controller, set the "set point" to 500 and the "span" to 0.

5. Close the oil release valve on the 5-gallon accumulator

6. Turn on the hydraulic pump, and increase the pump pressure by 1000 psi.

7. Turn on the oil supply switch on the 5-gallon accumulator.

8. Turn on the MTS 406.11 controller

9. Adjust the "set point" to position the shake table at the center position of centrifuge magnesium frame.

10. If the laminar box is used, remove the threaded rods inside the laminar box. The rods hold the laminar box during the test preparation.

11. Make sure not to leave any loose objects, like a tool, inside the centrifuge enclosure.

12. Close the centrifuge enclosure.

In addition, the following procedures should be followed when generating earthquake shaking:

13. Turn on the power of centrifuge motor.

14. Connect the RPM count cable (see Figure 3-29) to the centrifuge.

15. Turn on the RPM meter in the control room.

16. Push the start button of the centrifuge controller (see Figure 3-30).

17. Slowly increase the "RPM" up to 200.

18. Increase the hydraulic pump pressure by 2500 psi.

19. Set "span" of the MTS 406 controller to 940.

20. Adjust the "set point" of the MTS406 controller to locate the shake table to the center position on the centrifuge frame.

21. Increase the hydraulic pump pressure by 3000 psi

22. Increase the "RPM" by a specific value to yield a desired centrifugal acceleration- e.g., the centrifuge at a speed of 220 RPM with36" radius yields an acceleration of 50 g.

23. Start acquiring and saving the data through the DAQ system to the notebook computer.

24. Send the earthquake motion from the remote computer to the servo valve on the centrifuge. The signal passes through the digital to analog converter and the MTS controller.

25. Stop saving data after the earthquake shaking.

26. Decrease the speed of centrifuge rotation by dialing the "RPM" to a value of 0.

27. After the centrifuge stops completely, turn off the power of centrifuge motor.

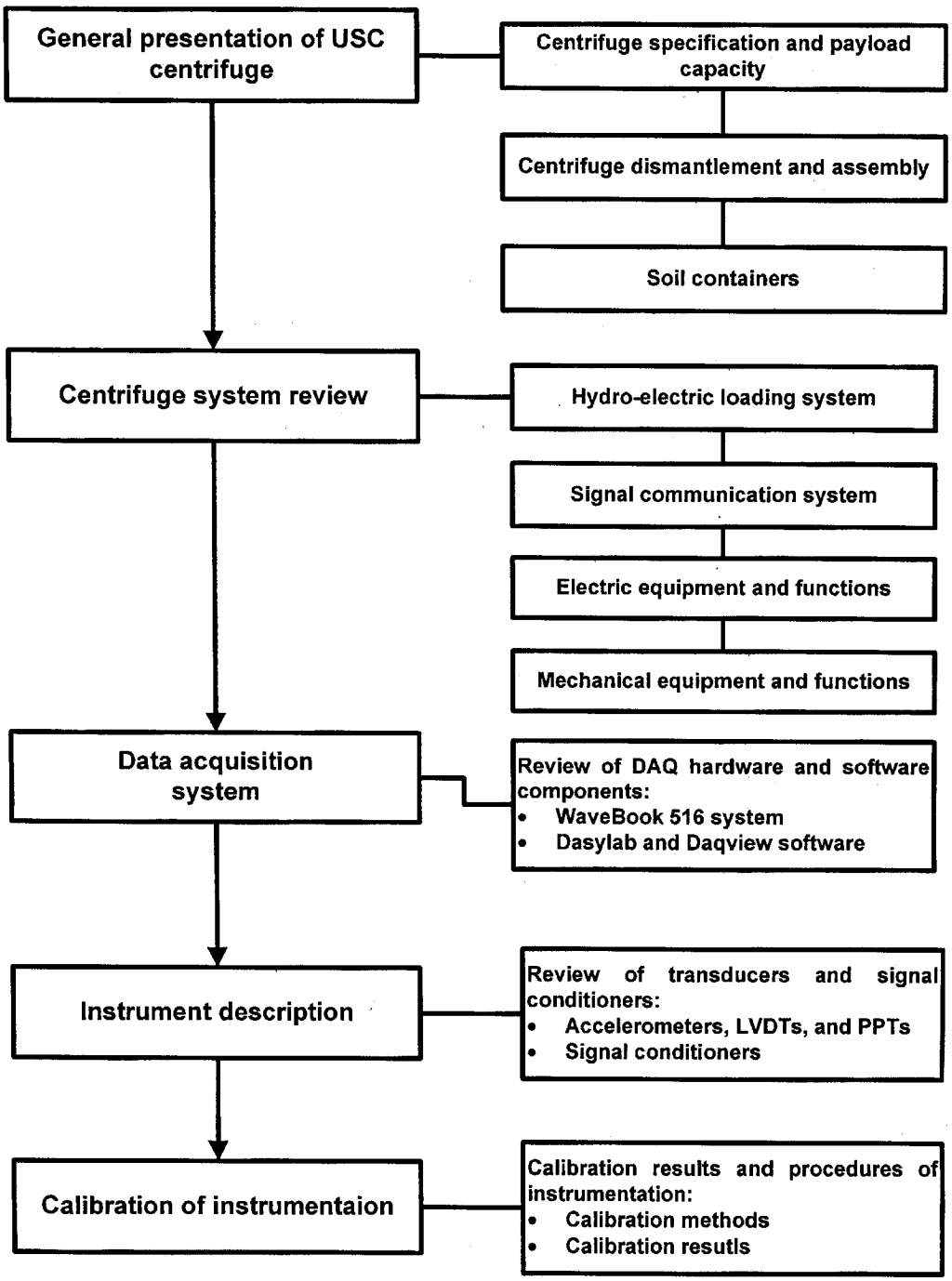

Figure 3-1. Overview of Chapter 3.

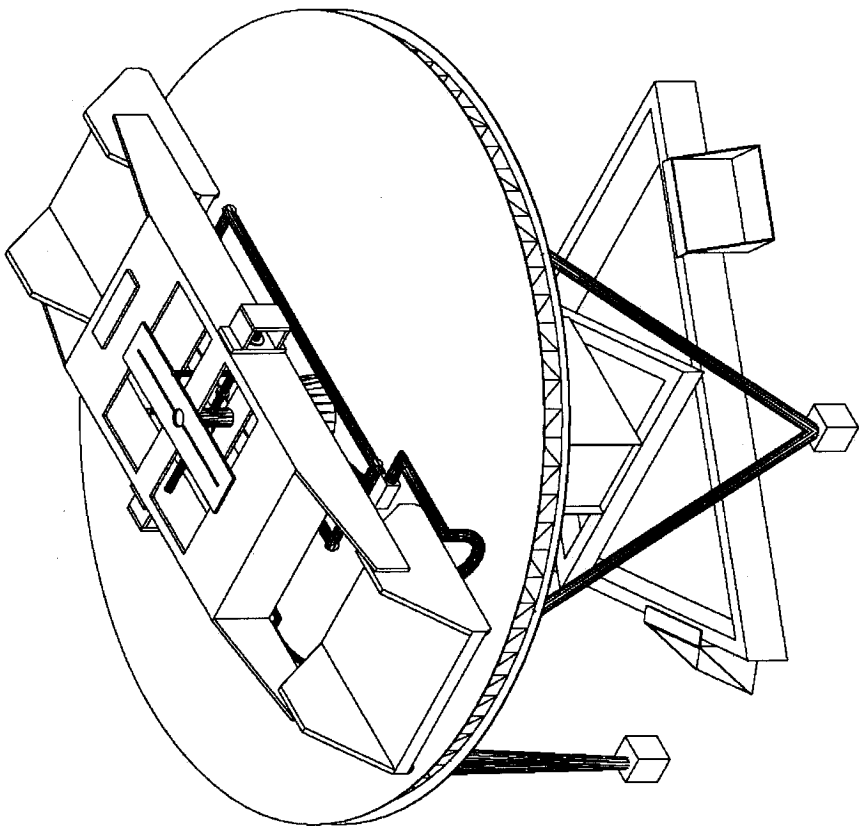

Figure 3-2. 3-D view of the USC centrifuge.

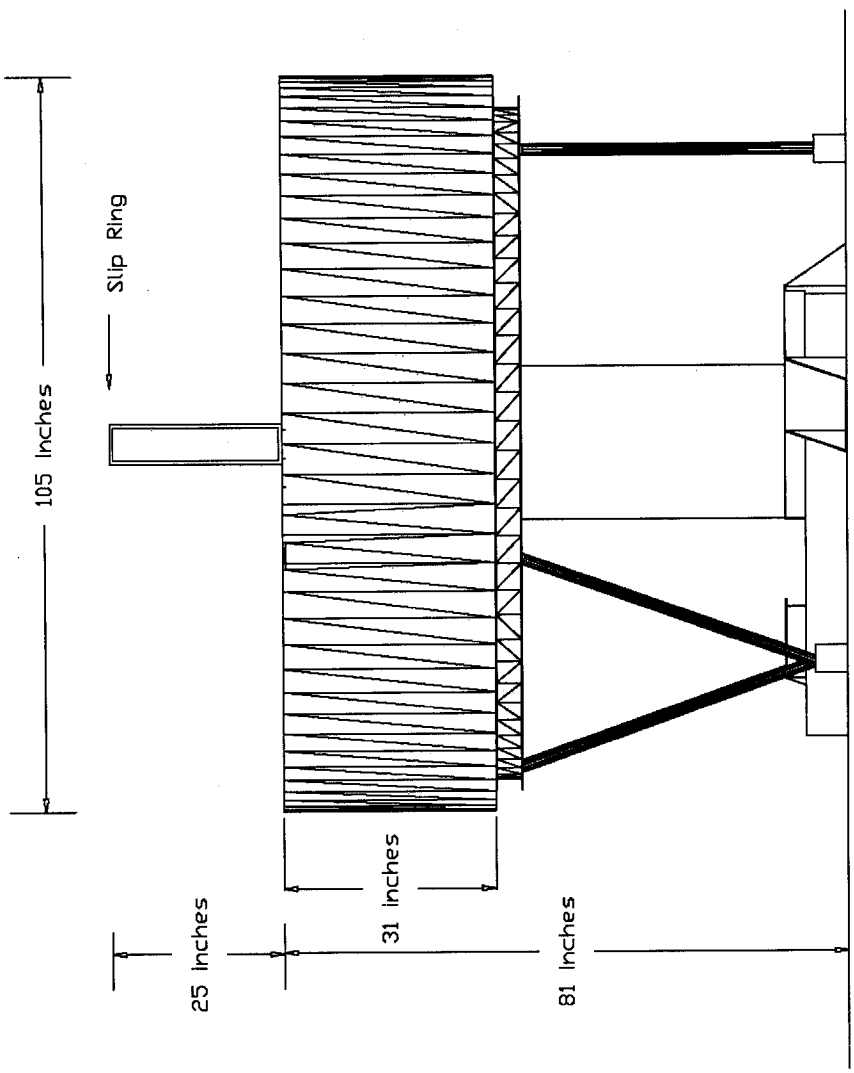

Figure 3-3. Dimensions of the USC centrifuge with its aluminum enclosure.

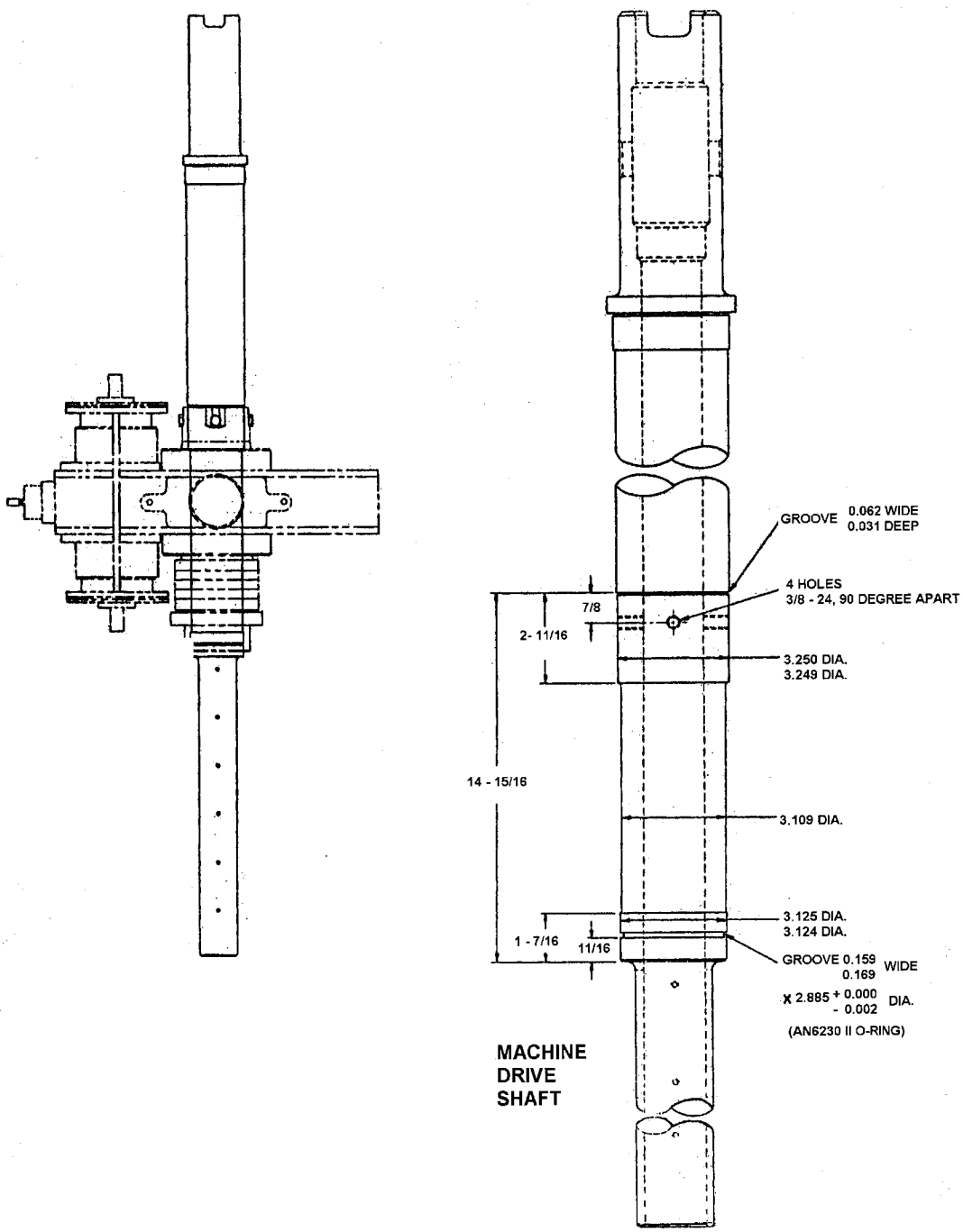

Figure 3-4. Vertical shaft of the USC centrifuge (unit: inch).

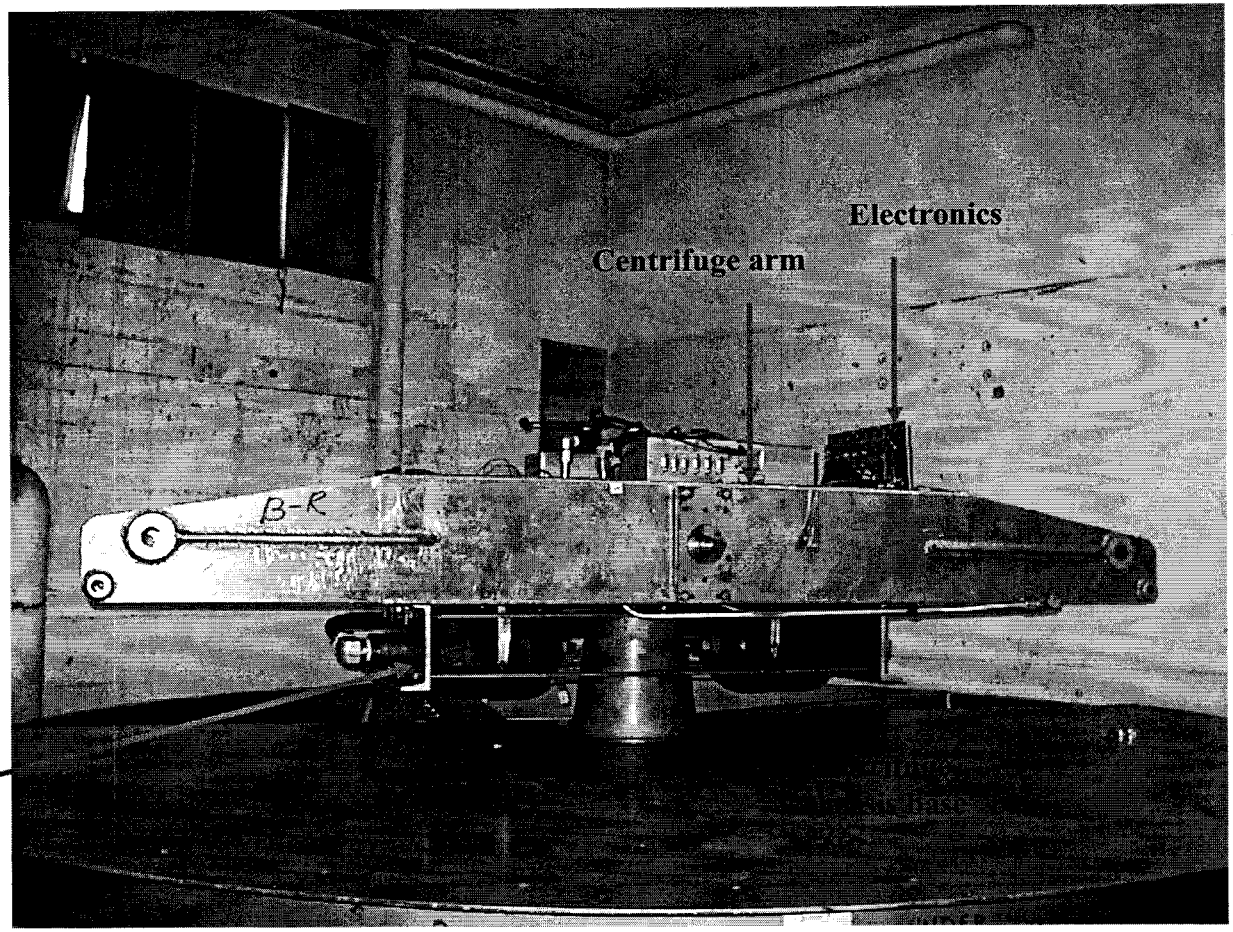

Figure 3-5. Dismantled USC centrifuge without aluminum enclosure.

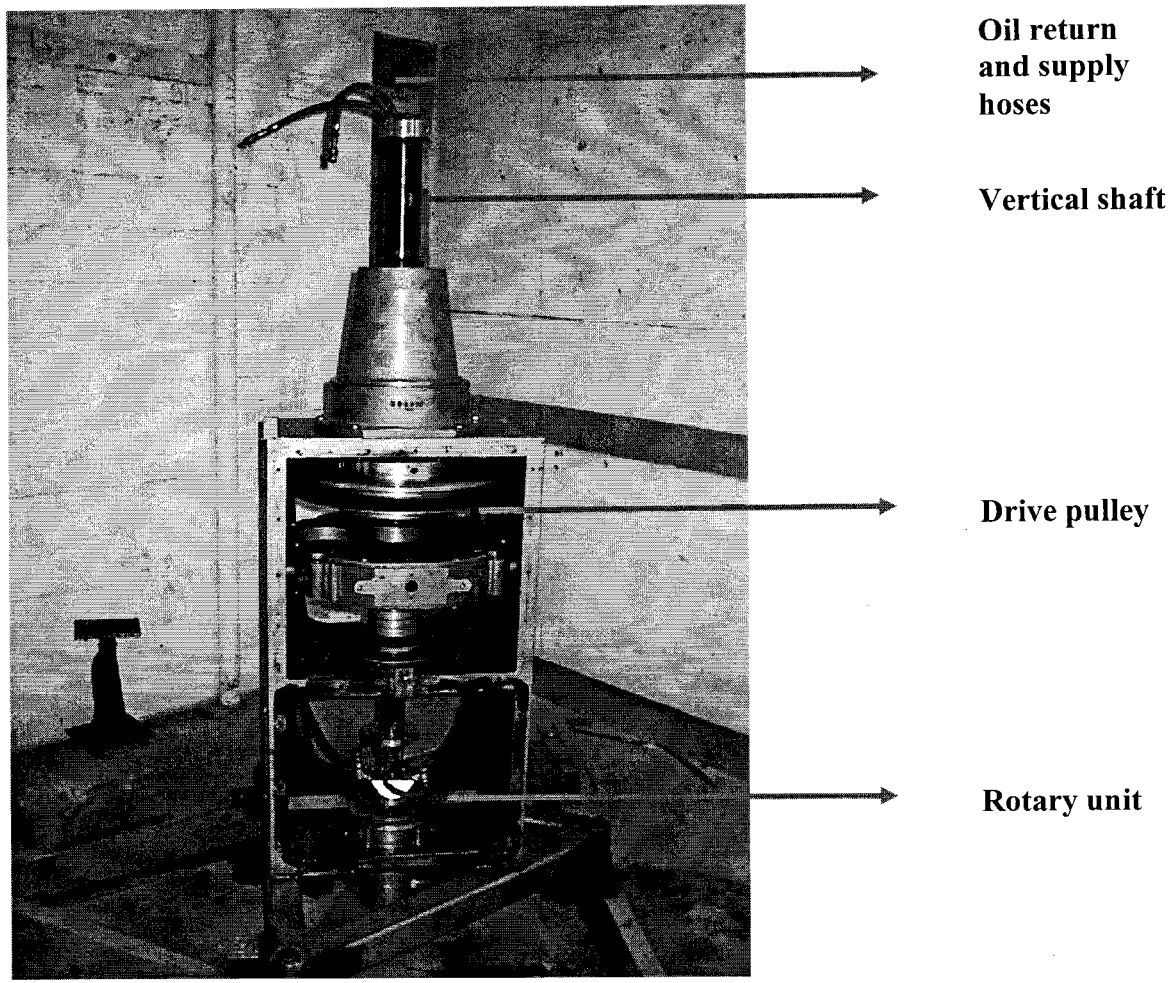

Figure 3-6. Centrifuge core components: drive pulley, rotary unit, and vertical shaft.

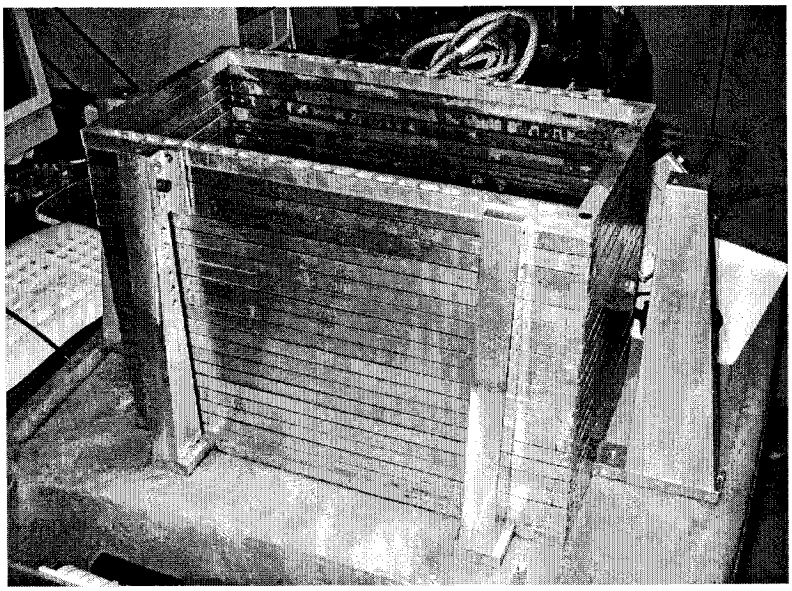

Figure 3-7. USC laminar box.

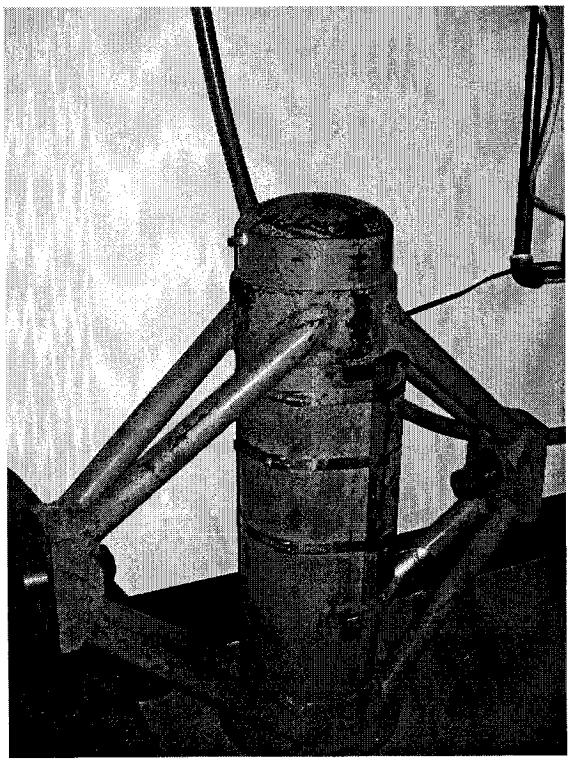

Figure 3-8. Long cylindrical container with triangular supportive arms.

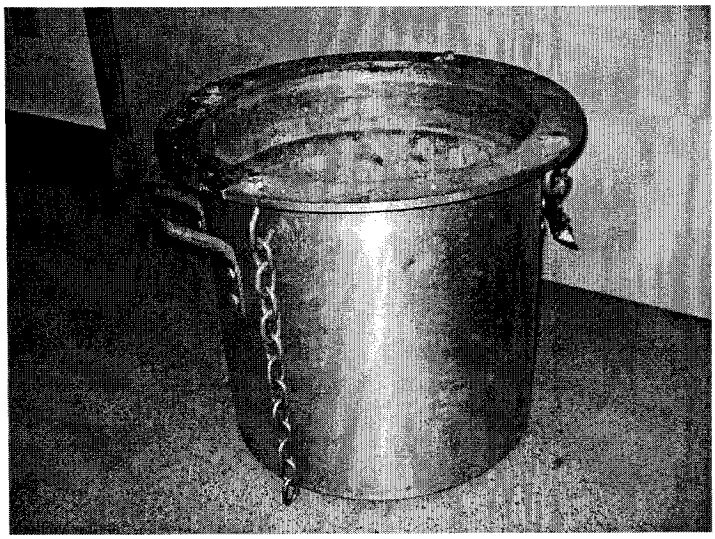

Figure 3-9. Cylindrical bucket used for centrifuge pile tests.

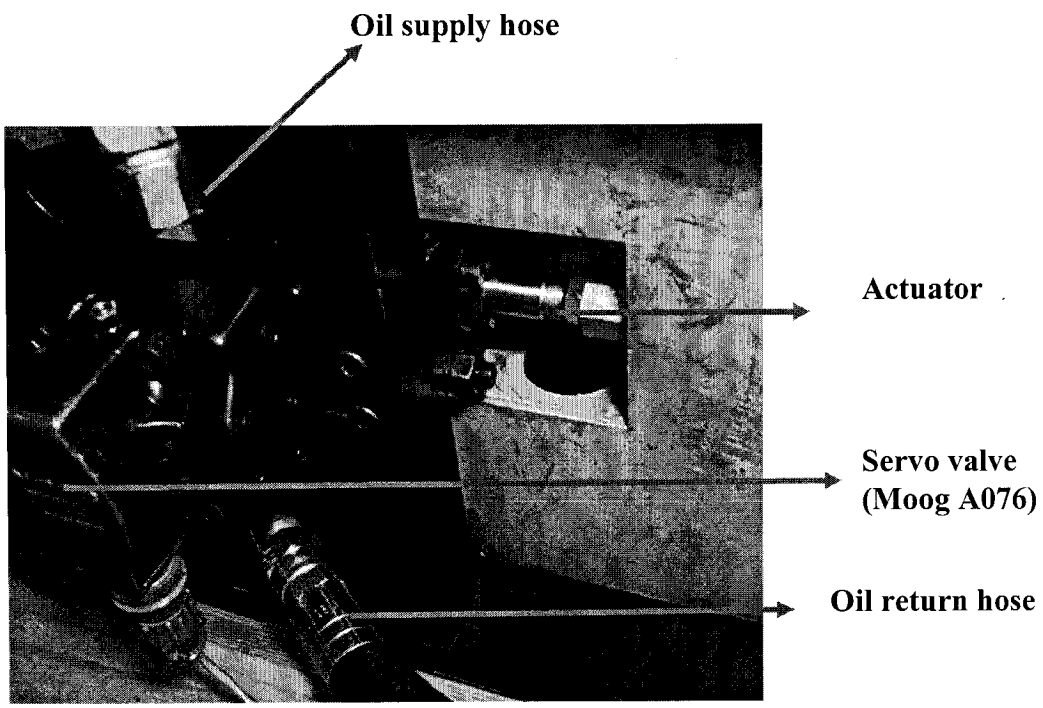

Figure 3-10. Hydro-electric loading system of the USC centrifuge.

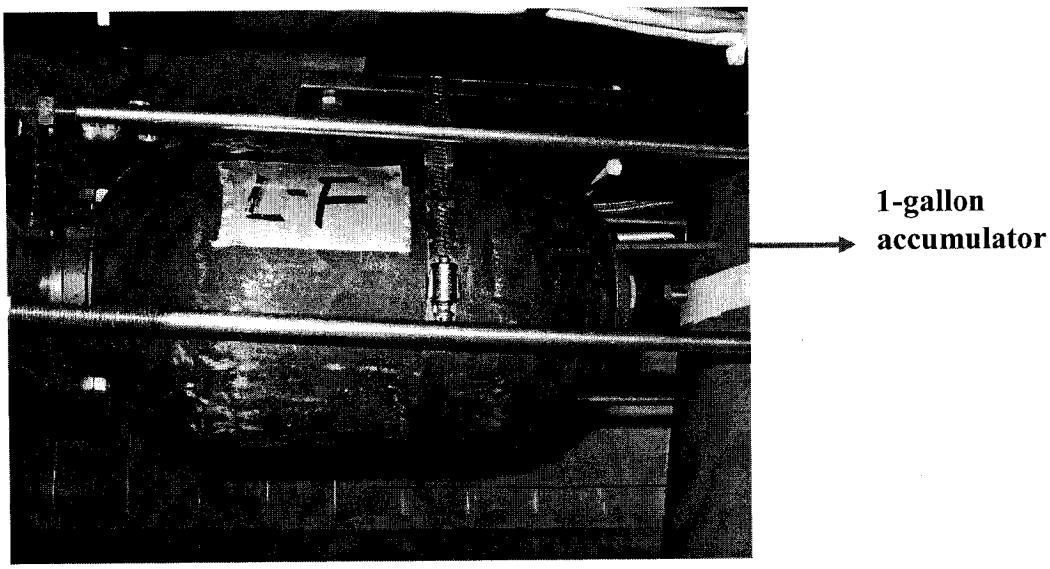

Figure 3-11. 1-Gallon accumulator under the centrifuge arm.

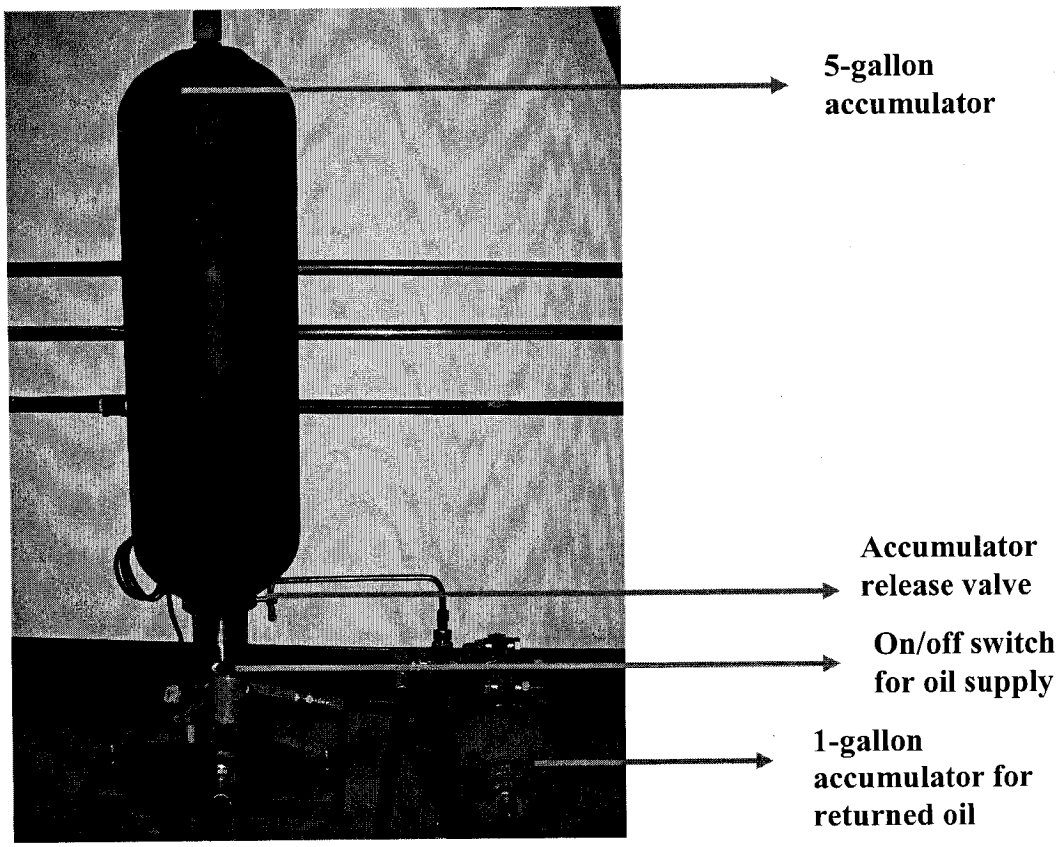

Figure 3-12. Accumulators outside the centrifuge enclosure.

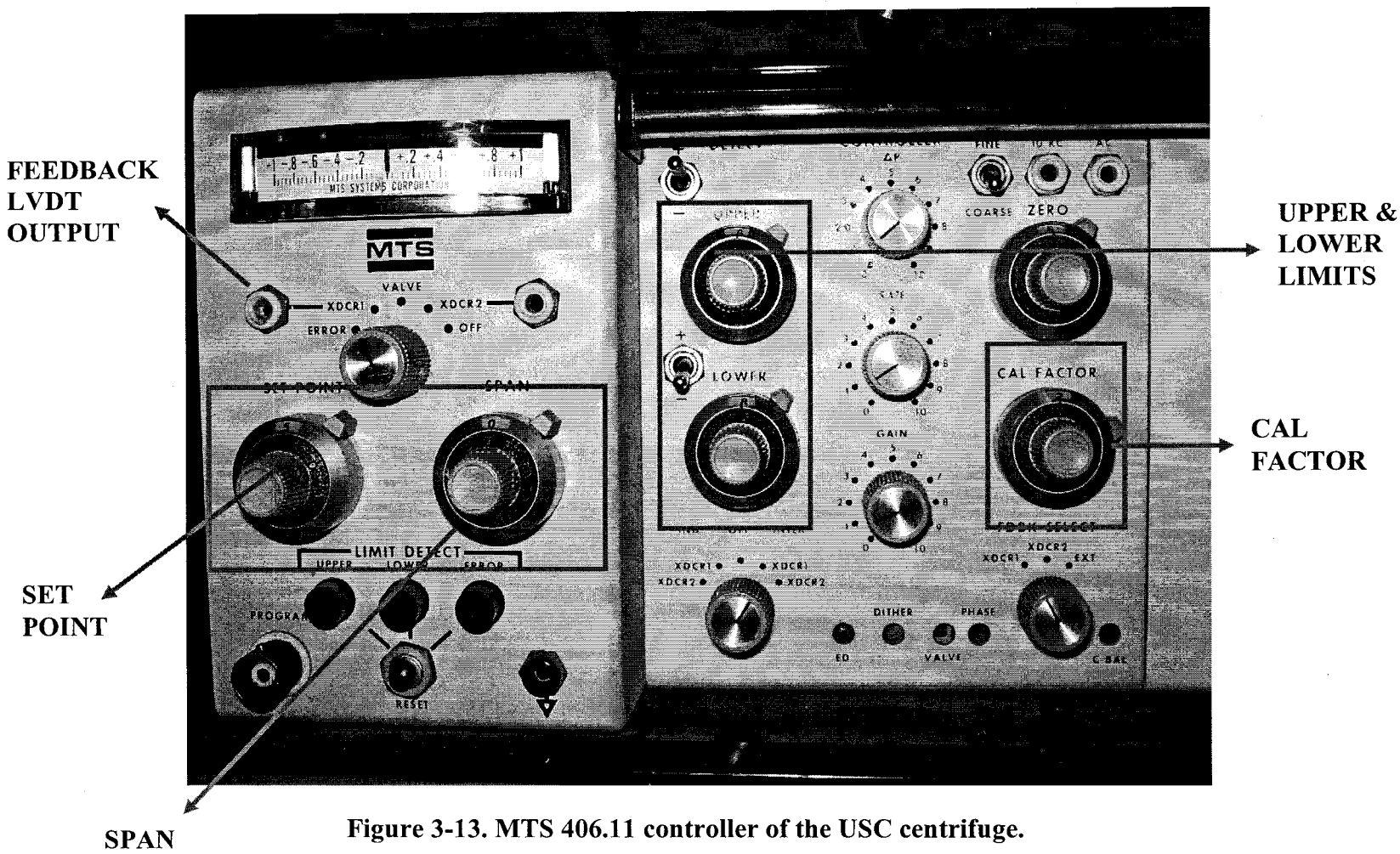

Figure 3-13. MTS 406.11 controller of the USC centrifuge.

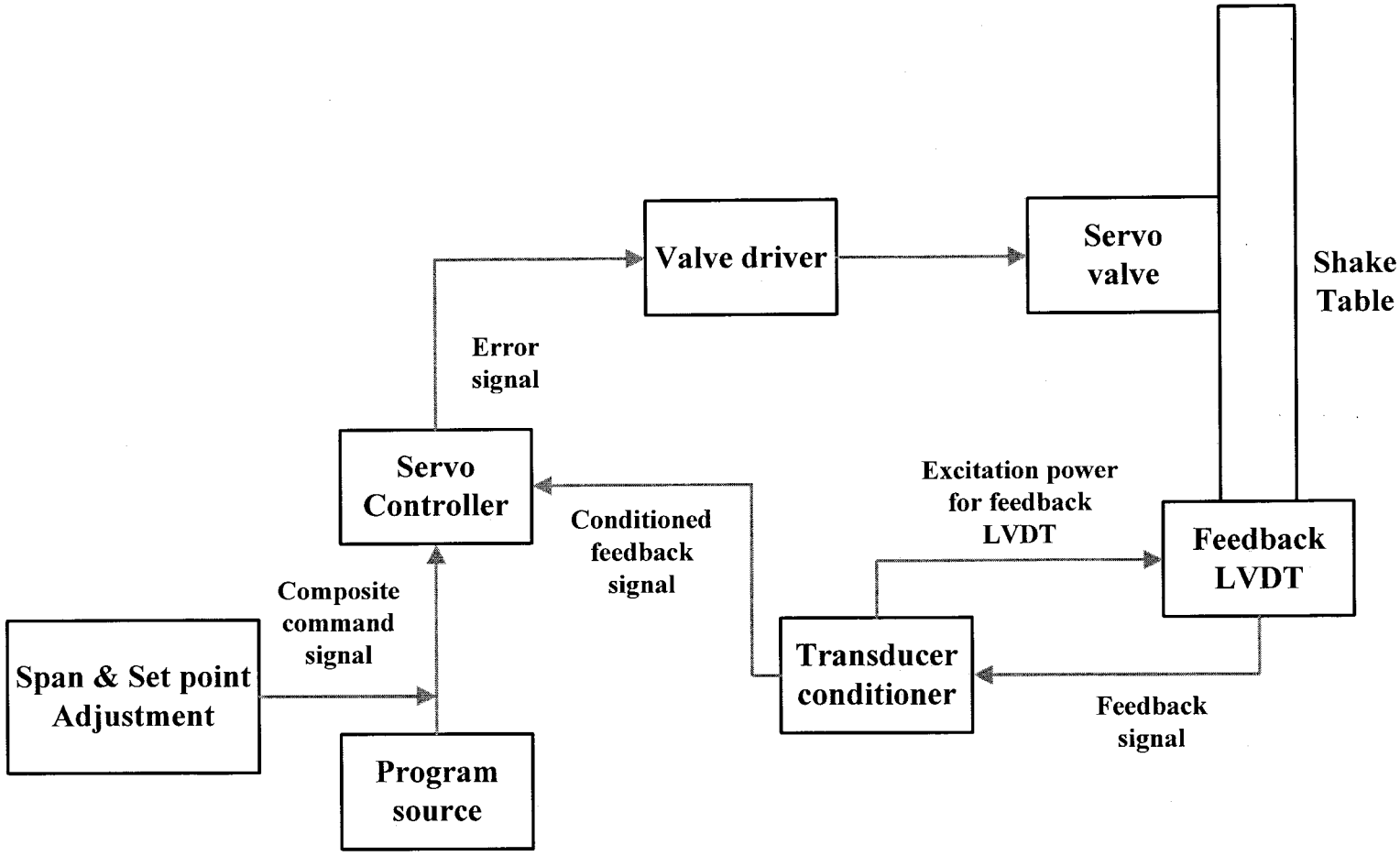

Figure 3-14. Schematic control of earthquake shaking motion.

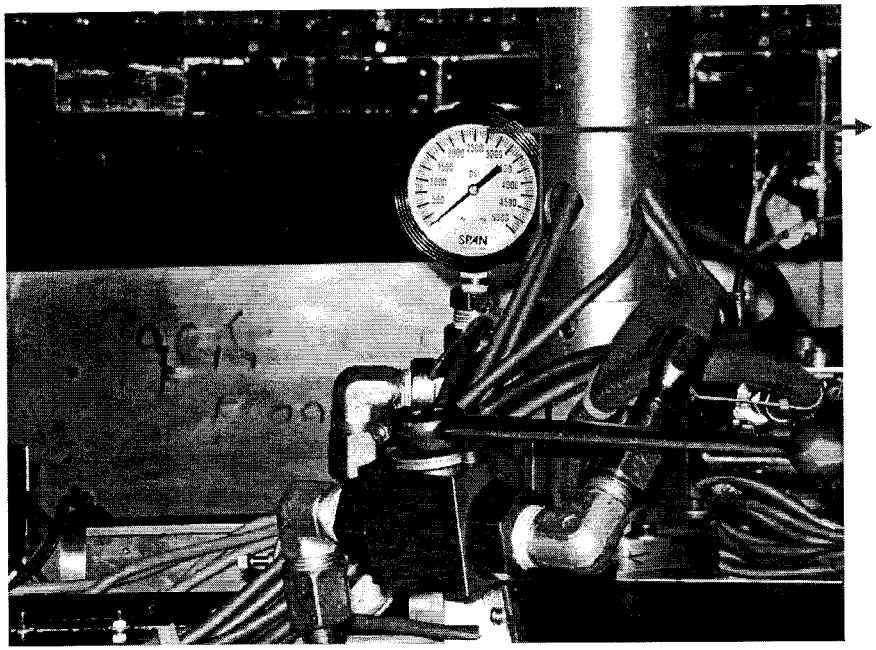

Figure 3-15. Pressure gauge monitoring hydraulic working pressure of centrifuge shaking system.

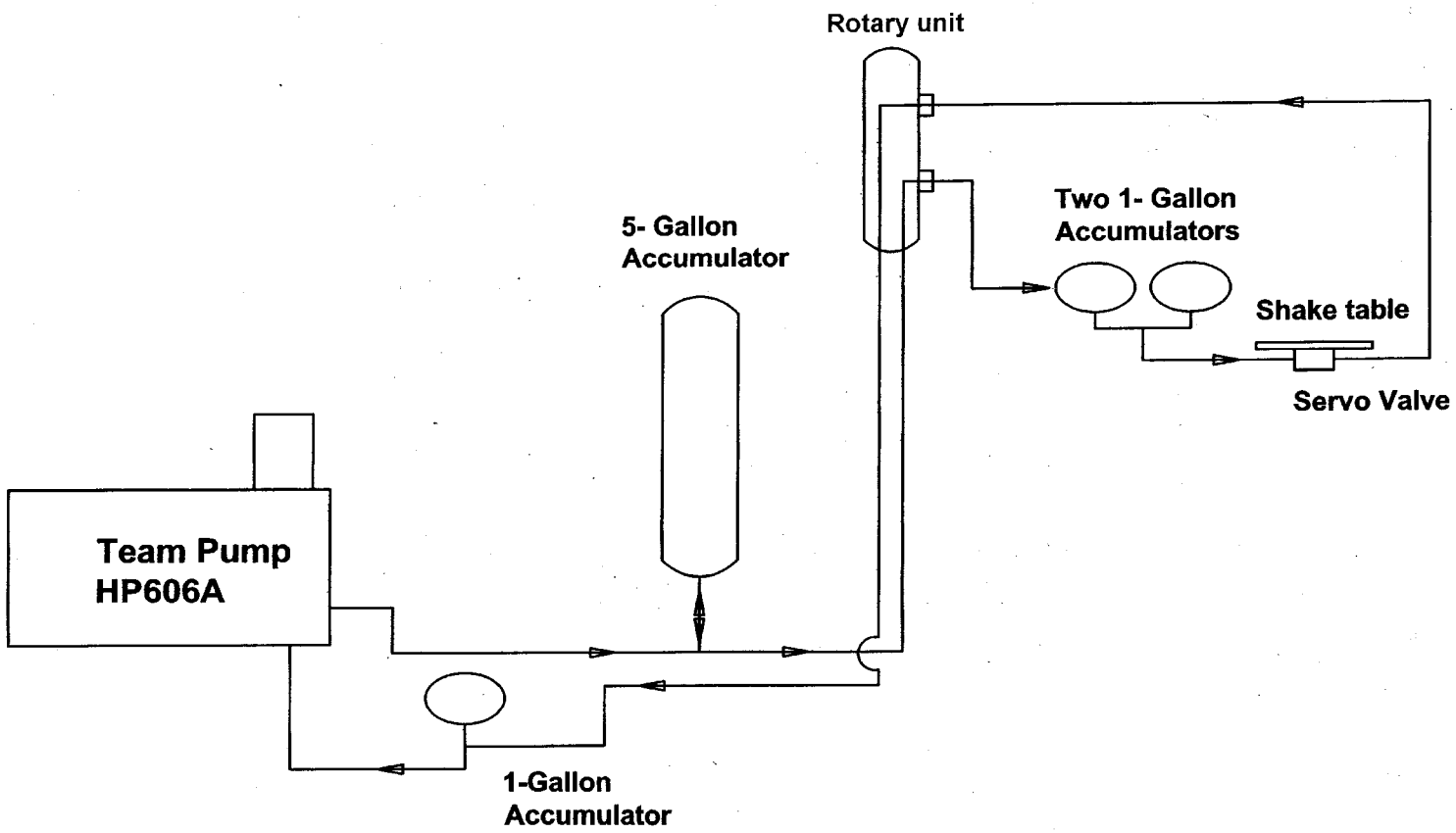

Figure 3-16. Hydraulic oil flow of the USC centrifuge system

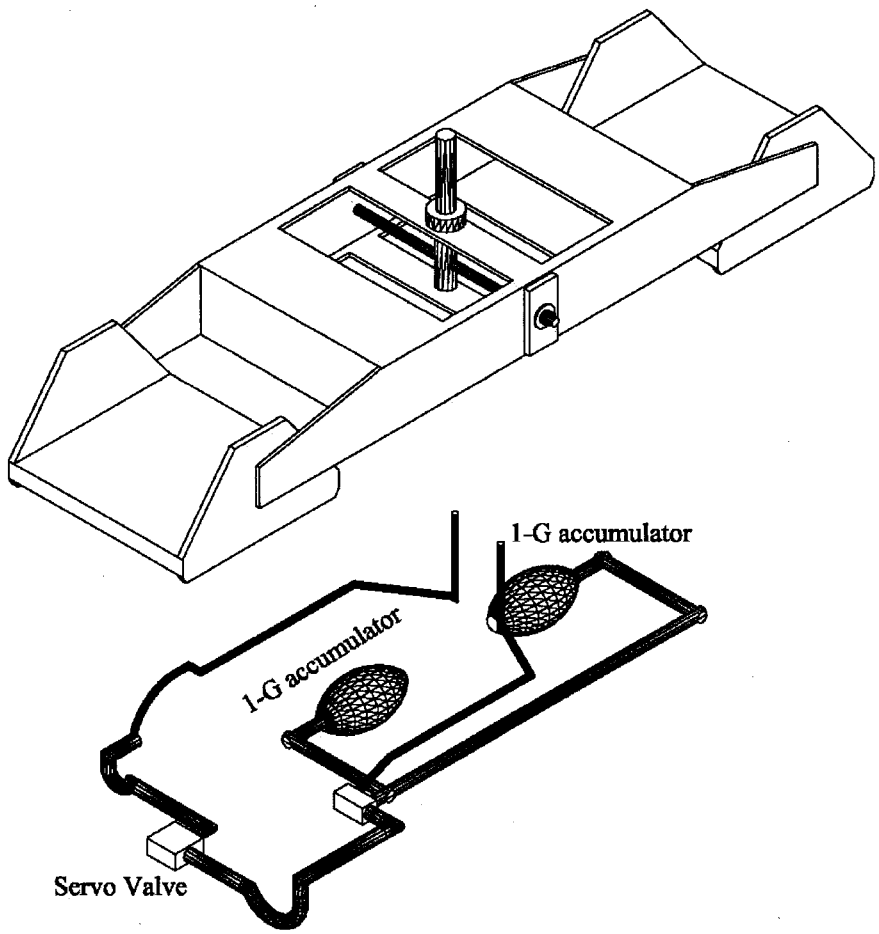

Figure 3-17. Schematic hydraulic conduit of the USC centrifuge.

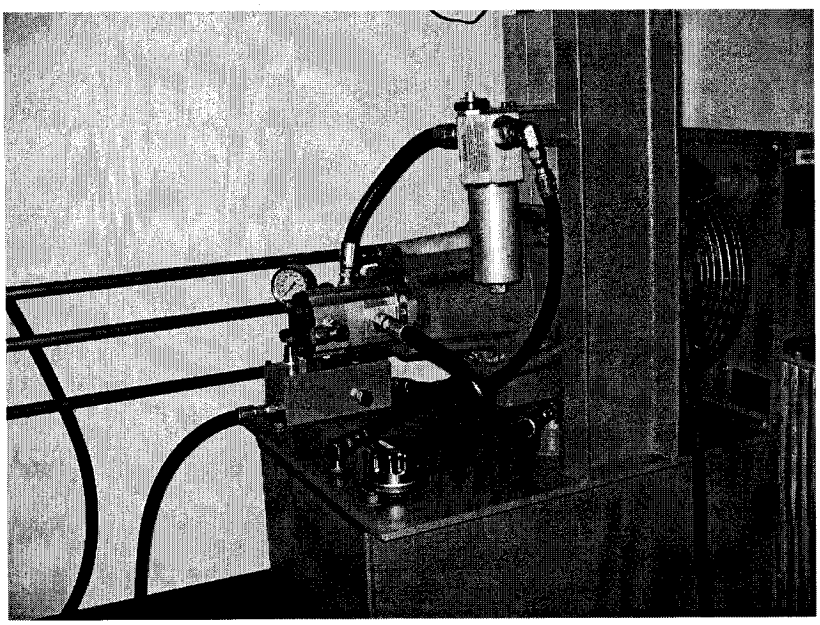

Figure 3-18. Team hydraulic pump: Model HPS 606.

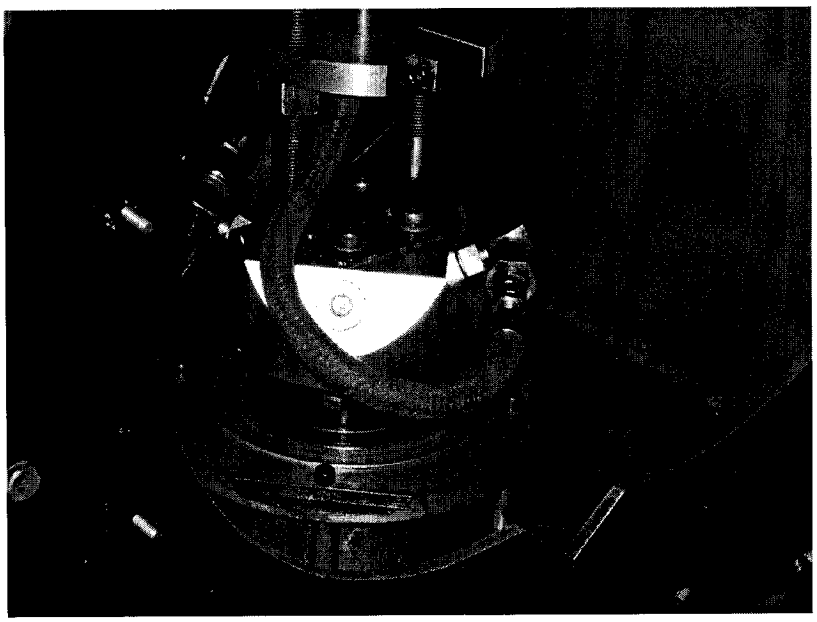

Figure 3-19. Rotary unit to supply and return high-pressured oil during centrifuge flight.

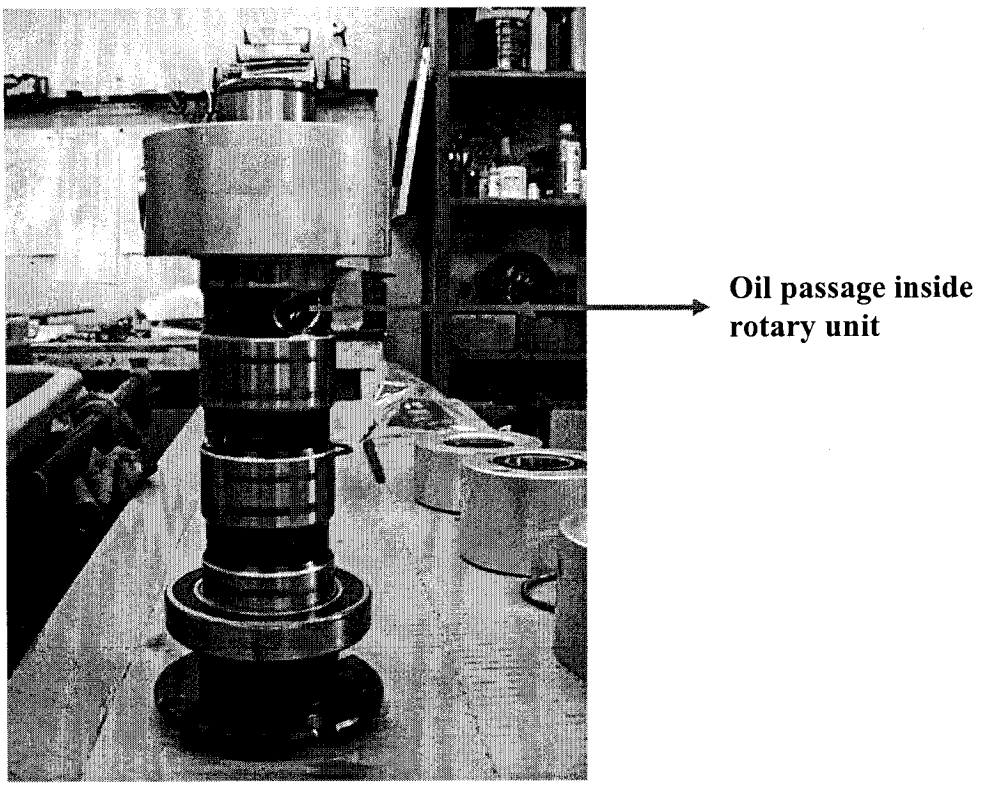

Figure 3-20. Dismantled rotary unit showing oil passages inside

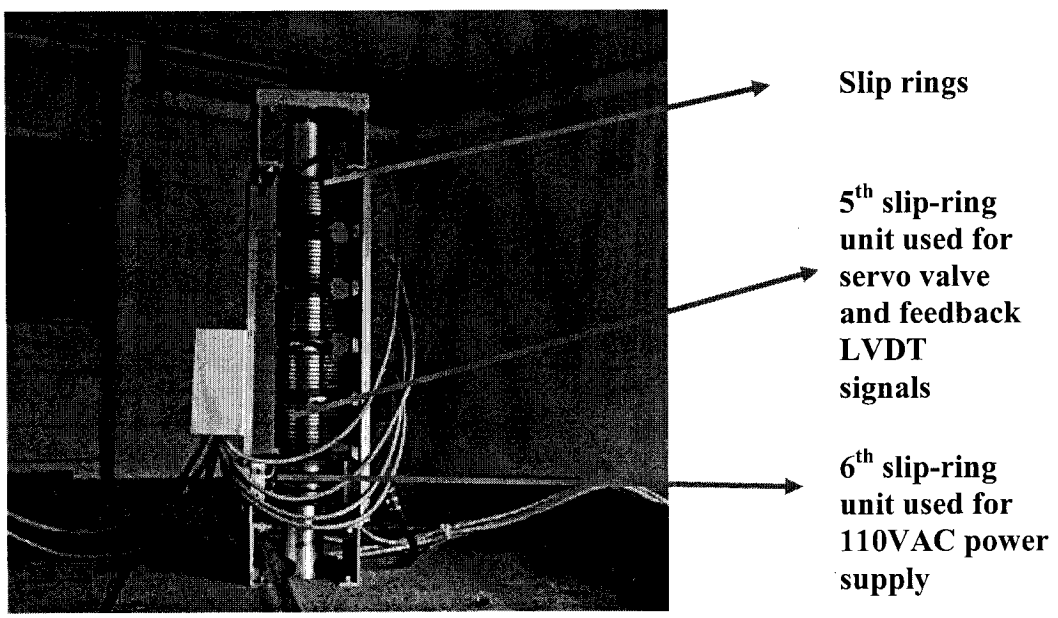

Figure 3-21. Slip rings on the USC centrifuge.

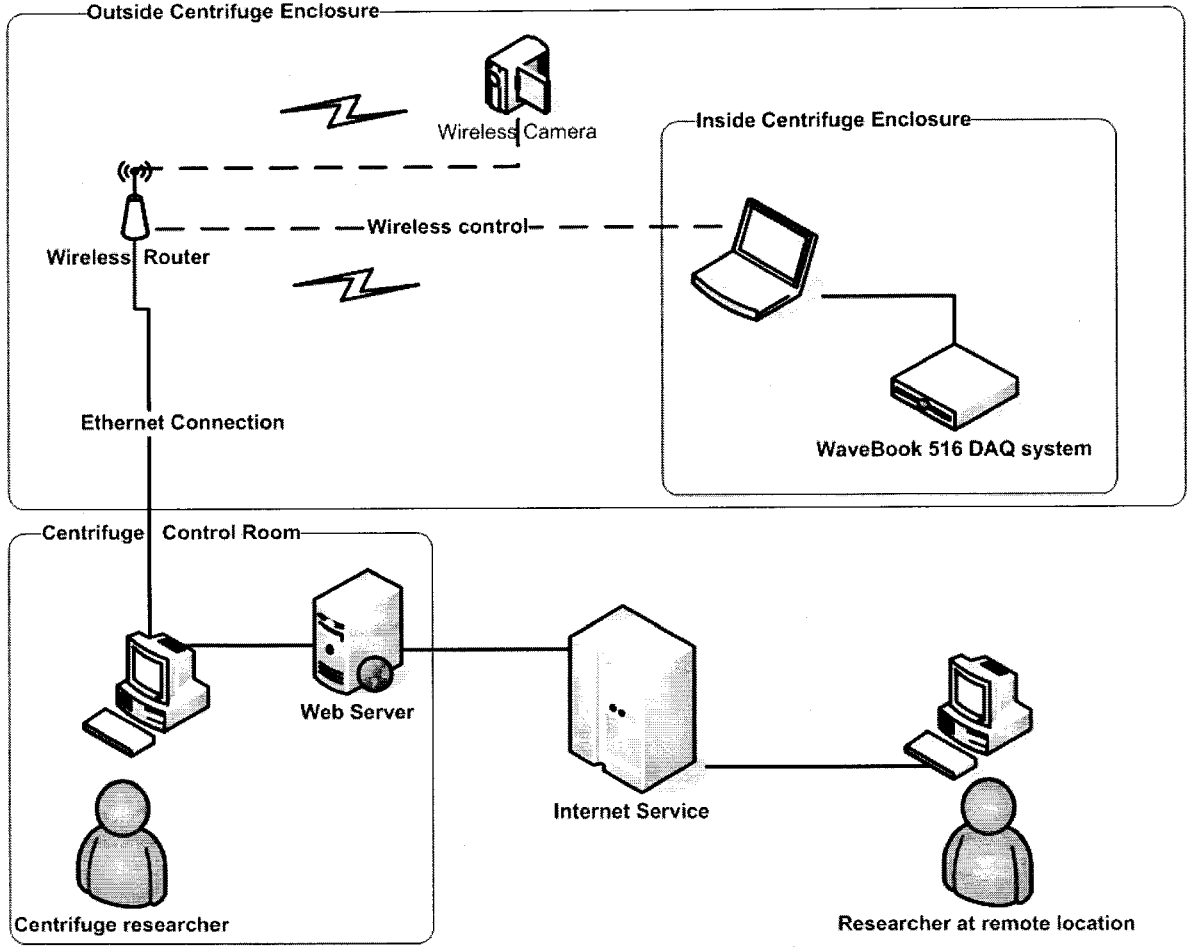

Figure 3-22. Wireless network and remote control of the USC centrifuge.

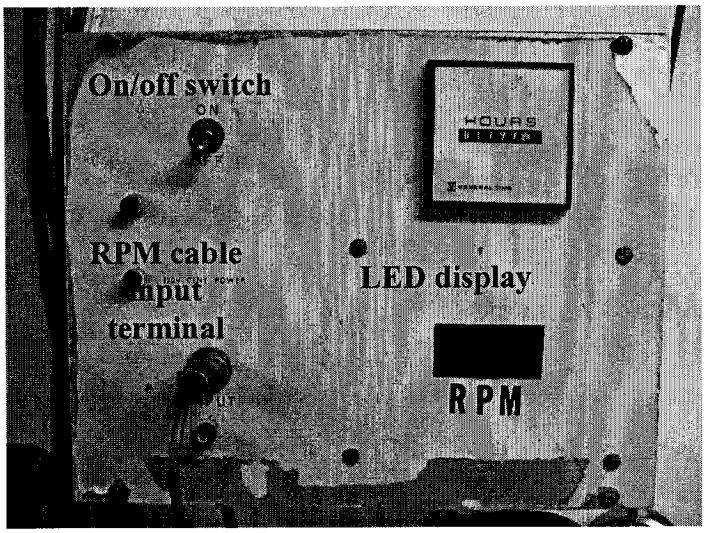

Figure 3-23. Centrifuge speed meter (RPM meter).

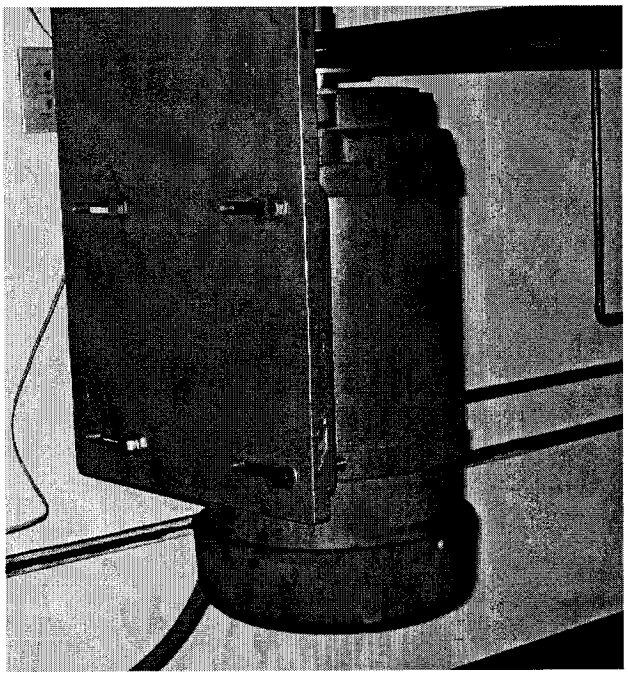

Figure 3-24. Centrifuge motor: Sabina 5 HP motor.

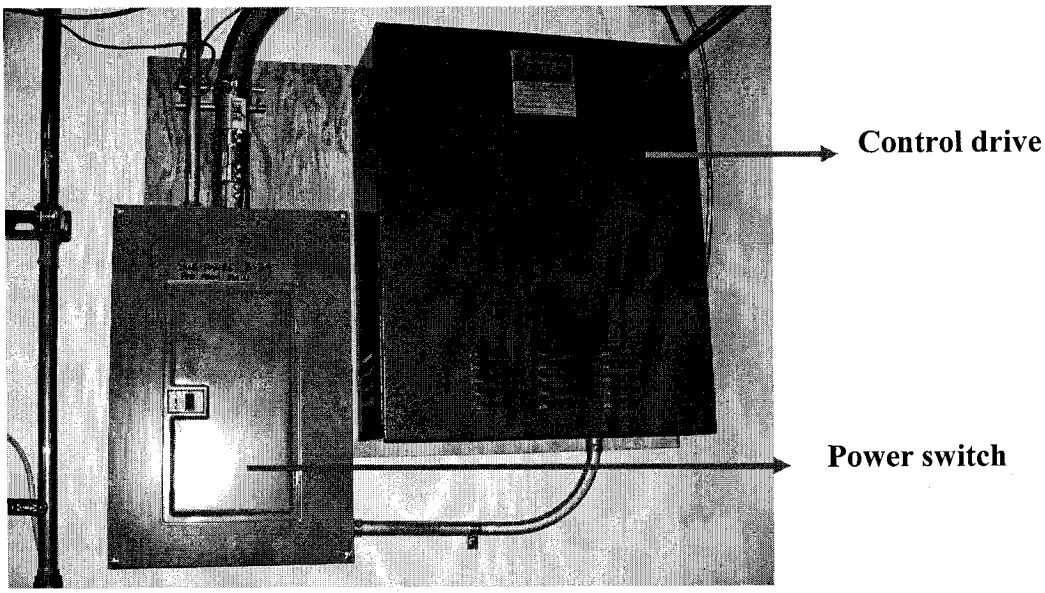

Figure 3-25. Power switch and control drive for the USC centrifuge.

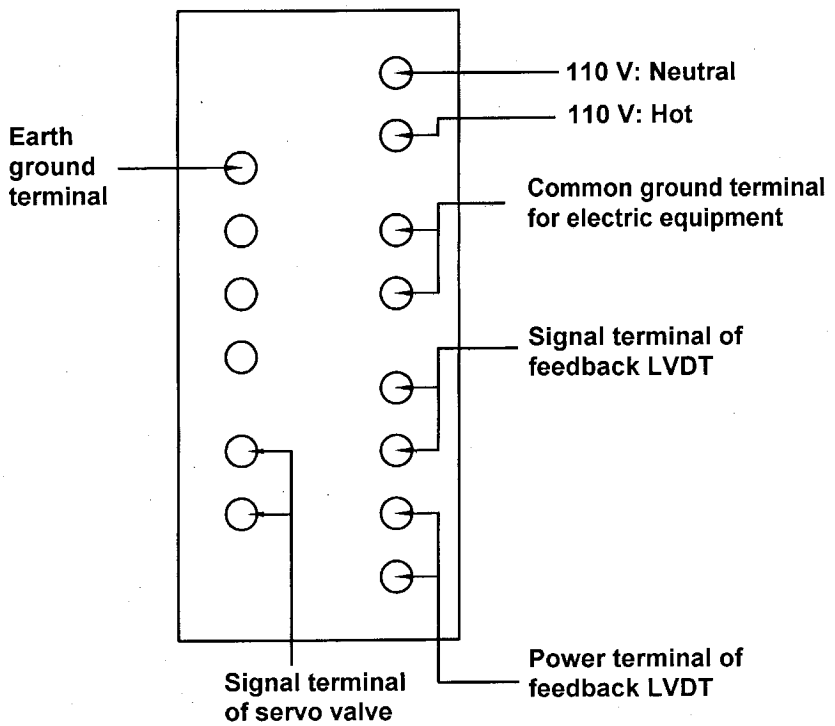

Figure 3-26. Connection panel for 110 VAC power, shake table signals, and ground terminals.

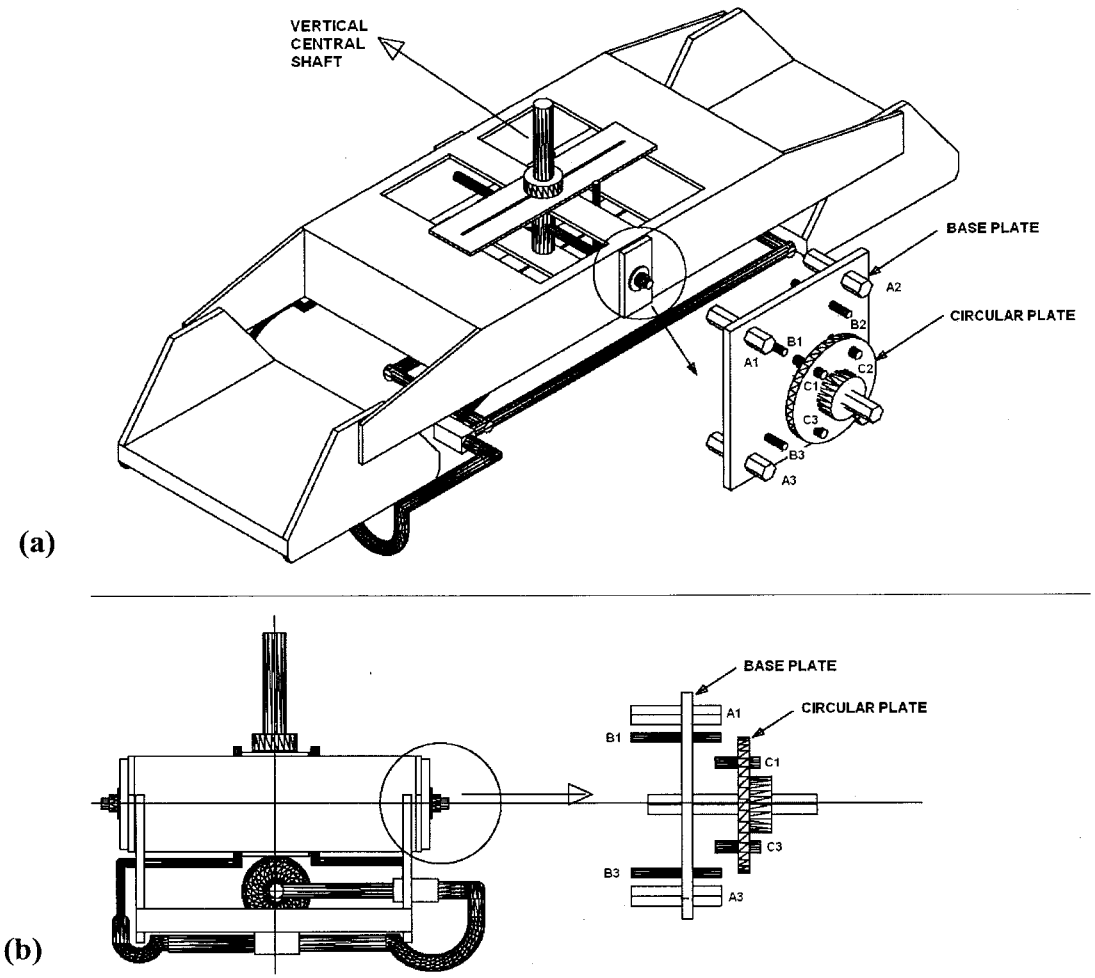

Figure 3-27. Schematic drawing of centrifuge balancing components: (a) 3-D view and (b) side view.

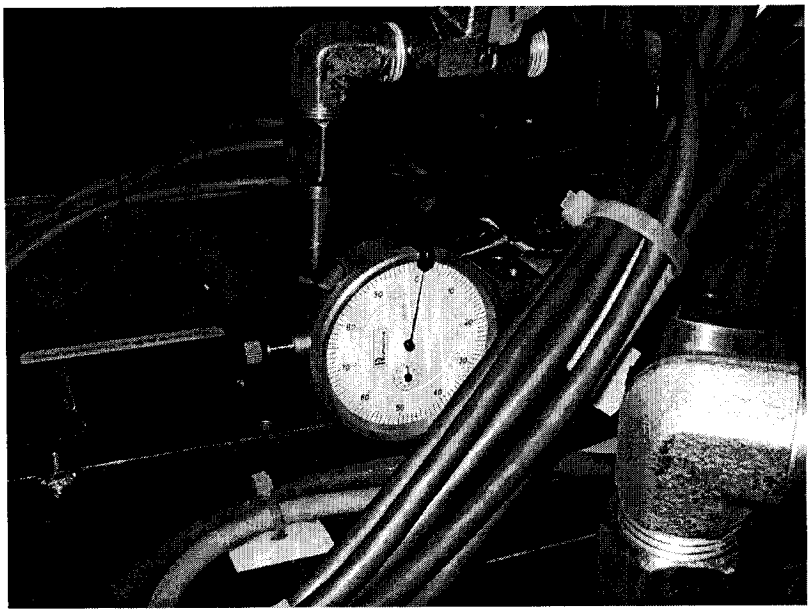

Figure 3-28. Dial gauge monitoring centrifuge balance.

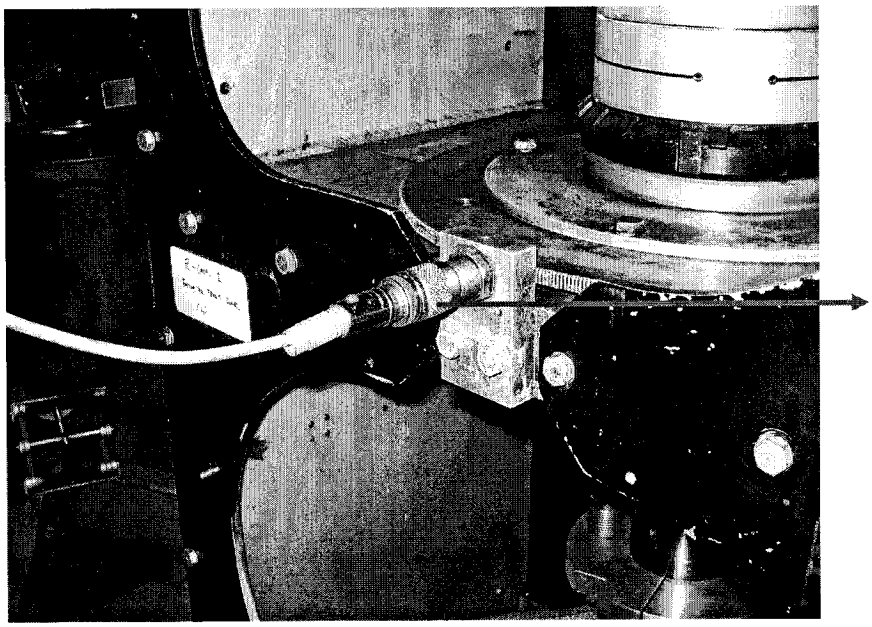

Figure 3-29. Centrifuge RPM connector measuring centrifuge speed.

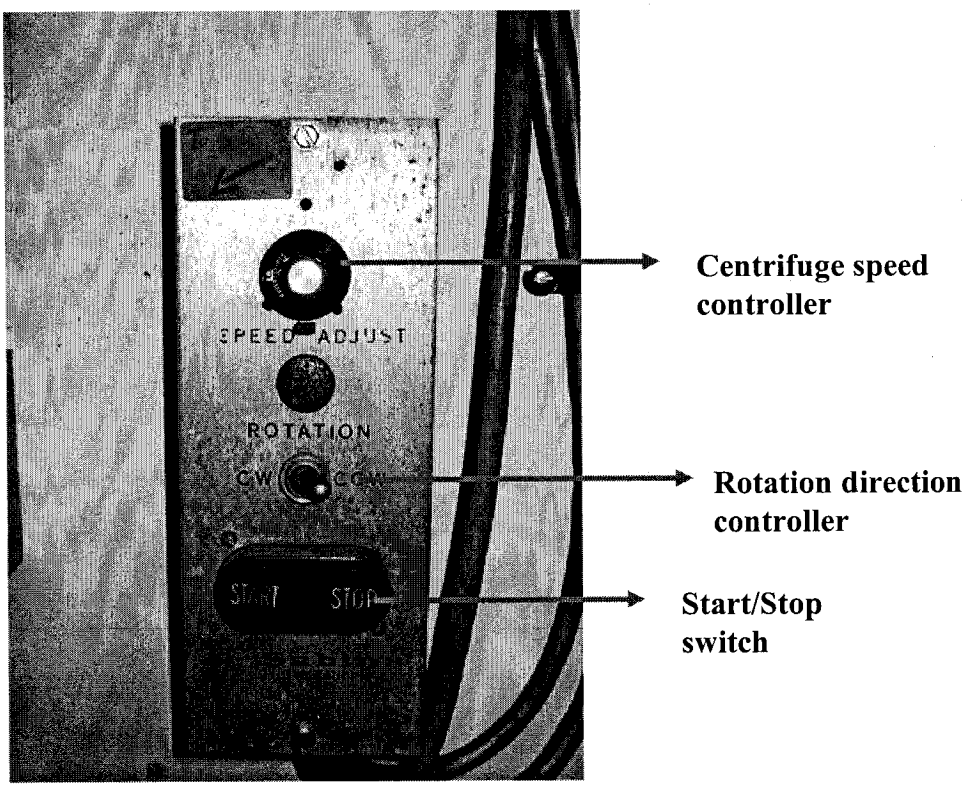

Figure 3-30. Centrifuge speed controller.

3.4 Data Acquisition system

The data acquisition (DAQ) system of the USC centrifuge records the centrifuge test data. The data acquisition system has been upgraded to become more accurate and reliable even at fast sampling rate. The DAQ system consists of following: (1) Analog to Digital Converter (ADC); (2) Digital to Analog Converter (DAC); and (3) computers running the data acquisition programs.

The DAQ system is made of the ADC (WaveBook 516) and DAC (DaqBoard 2001). Driver buffers in hardware and software are presented later to understand the limitations of the DAQ system relative to maximum sampling rate and duration of acquisition.

3.4.1 Hardware of data acquisition system

3.4.1.1 WaveBook 516 system with WBK10A

As shown in Figure 3-31, the WaveBook 516 system with its analog expansion module (called WBK10A) is used as the analog to digital converter. A total of 16 differential channels are available by adding WBK10A expansion module (16 bit resolution) to the WaveBook 516 unit. Figure 3-32 represents the WaveBook 516 system and the notebook computer on the centrifuge arm. The WaveBook system captures the transducer data and passes them to the notebook computer that controls the WaveBook 516 by running DasyLab software. The data are transferred to the laboratory through the wireless network.

The WaveBook 516 system has the following specifications (IOtech, 2005e):

- 1-MHz sampling with 16-bit resolution
- 16 differential inputs, expandable to 72 inputs
- 1-μs channel scanning of any combination of channels
- Up to 1-MHz streaming to RAM, and

The maximum possible sample rate is $\frac{1MHz}{(n+1)}$ when there is a total number n of active channels. For example, if 16 input channels are used (channel number 0 through 15), the WaveBook 516 system has a possible maximum sampling rate for each channel of 625,000 Hz. This is a theoretical value; however, the maximum sampling rate depends on the capacity of the computer memory, computer hard drive, and the number of control modules on the DasyLab software.

3.4.1.2 Additional DAQ options for the WaveBook 516 system

The new ADC system of the USC centrifuge has WBK11 cards in both WaveBook 516 and WBK10A to simultaneously capture the data between the channels through multiplexers for 16 input channels (IOtech, 2005f). This card eliminates channel to channel time skewing. WBK30 is an additional DRAM (Dynamic Random Access Memory) board; it increases the standard buffer of WaveBook 516 system. It works as a FIFO (First in and First Out) memory buffer for the WaveBook 516 and is discussed later with respect to the DAQ capacity.

3.4.1.3 DaqBoard 2001

IOtech DaqBoard 2001 has been used as a DAC system for the USC centrifuge; it transmits the earthquake shaking signal to the MTS controller after converting digital data in the computer to the analog signal. DaqBoard 2001 has a 16 bit resolution and four analog output channels that feature a data upload rate of 100 kHz. In addition, the DaqBoard 2001 has 16 single-ended or 8 differential analog input channels with 200 kHz sampling rate for all input channels (IOtech, 2005b). The output signal from the DAC has a voltage range of $\pm$ 10 V . The update rate of the DaqBoard 2001 can be determined as follows:

1. Determine the centrifugal acceleration for centrifuge modeling.

2. Determine the duration of the earthquake motion in model scale by dividing the prototype duration by the centrifugal acceleration.

3. Based on the duration determined in step 2, determine the update rate of earthquake motion through the number of earthquake data and the centrifugal acceleration. The number of data points divided by the duration of model shaking yields data update rate as shown in Equation 3-1. For example, the update rate is 5000 samples/second (5 kHz) based on 4000 data points and 0.8 second period as shown below.

$$\frac{\text{The number of data points of earthquake motion}}{\text{Shake motion period}} = \text{upload rate} \qquad (3\text{-}1)$$

$$\frac{4000 \text{ data points}}{0.8 \text{ second}} = 5000 \text{ samples/second} = 5 \text{ kHz}$$

3.4.2 Data acquisition program

The data acquisition programs, e.g., DasyLab and DaqView, are used to control the DAQ system to monitor, capture, and save the test data. DasyLab is an interactive program that simplifies PC-based data acquisitions through functional icons. DasyLab offers real-time analysis, control, and the ability to create custom graphical user interfaces (GUIs). In addition, DaqView helps to verify signal connections, acquire and save data to disk, and graphically view real-time data within moments of taking the test data. DaqView is simpler to use but has more limited applications than DasyLab.

3.4.2.1 DasyLab program

One of the advantages of DasyLab is its GUI (**G**raphical **U**ser **I**nterface) that works with the DAQ hardware like the WaveBook 516 system (IOtech, 2005d). Figure 3-33 shows a worksheet containing functional icons, such as ADC, relay, save functions to monitor and capture incoming transducer signals at a sampling rate of 2 kHz per channel. The relay function is used to divide the data acquisition process into two phases: (1) monitoring phase of the transducer signals without saving them to the computer hard drive; and (2) saving phase to record the transducers signals after an interesting point during the centrifuge test. The divided data acquisition process helps to manage efficiently the buffer memory in the DAQ system and the test data without unnecessary using up the PC hard drive.

The chart display and voltmeter icons show the transducer data from the 16 input channels. The voltmeter icon may be selected for numerical display of mean, RMS (Root-Mean-Square), and last values. The chart display shows the time history of the transducer data with functions of zoom, pause, and data selection.

3.4.2.2 DaqView program

DaqView is the DAC control program that loads the earthquake motion data through the DaqBoard 2001. The data has an extension text file format like an ASCII file format. DaqView has controls to adjust the data upload rate and the number of iterations for the earthquake motion. Figure 3-34 shows the interface window of DaqView.

For the liquefaction test of chapter 4, DaqView was setup to upload the earthquake motion to the shake table as follow (IOtech, 2005c):

- Upload rate of earthquake signal: 5000 samples/ sec
- Number of repetition:1
- Number of earthquake data points: 4000 points.

3.4.3 Data acquisition capacity

It is important to understand the capacity of the DAQ system to prevent data loss, aliasing, and worthless data that may overflow the DAQ buffer memory. Aliasing occurs when a maximum frequency of the object signal is more than Nyquist

frequency (Oppenheim and Schafer, 1975). The Nyquist frequency is half of the sampling frequency. The aliasing causes a false lower frequency component to appear in the sampled data (Oppenheim et al., 1999).

This section describes the procedures for transferring data from the DAQ system to the PC hard drive, the data acquisition length with respect to the FIFO (First in and First out) memory buffer in the WaveBook516, and driver buffer memory and functional icons in DasyLab. The following section describes (1) the DAQ hardware components inside the WaveBook system; (2) hardware and software buffers; and (3) the computation method of data acquisition length.

3.4.3.1 FIFO Buffer

Figure 3-35 shows the data flow from the A/D converter (WaveBook516) to the final data storage (PC hard drive). The data transfer rate from the FIFO buffer of the WaveBook 516 to the driver buffer of DasyLab through a parallel port is approximately 380,000 samples per second. The size of the driver buffer depends on the PC memory size.

The FIFO buffer is the first-in first-out memory buffer and has functions, like a shift register where the oldest values come out first. Inside the WaveBook516, the WBK 30 memory card increases the FIFO buffer size by 64MB memory and can store data up to 33.5×10^6 samples (IOtech, 2005f). The major function of FIFO is to keep test data captured at high sampling rate before being transferred to the driver buffer

because of the slow transfer rate through the parallel bus. Hence, the FIFO prevents data loss because the old data are overwritten by new data (IOtech, 2005a)

3.4.3.2 DasyLab Driver Buffer

The internal driver buffer and block size of DasyLab need to be reviewed to understand the data process inside the computer once the data are transferred to the PC. Currently, the driver buffer size is approximately 16MB (maximum 16,384 KB) that is allotted from the PC ram memory.

The driver buffer works as a temporary reservoir that keeps transported data from the FIFO buffer before DasyLab processes the data. Sampling rates faster than the data transfer speed through the parallel bus are possible when the DAQ system has a large FIFO buffer memory. Hence, additional WBK30 memory increases the FIFO buffer size, which acts like a reservoir to receive the data backflow caused by the bottle neck between the FIFO and the driver buffers. Slow data transfer rate through the parallel bus between the buffers causes the bottle neck (IOtech, 2005a).

3.4.3.3 Block Size

The block size in DasyLab has a significant role in processing the data in the driver buffer. The block size defines the number of data that are processed by DasyLab during a single data processing cycle (IOtech, 2005d). An increase in block size increases the speed of data processing by DasyLab. For example, if the block size is too small in comparison with the data sampling rate, data congestion could result

among the functional icons. In general, fast data acquisition operation requires large block sizes, while small block size is adequate for slow data acquisition.

3.4.3.4 Computation of data acquisition duration

This section describes how to compute the duration of data acquisition for the WaveBook 516 system. The data acquisition duration is defined as the duration of data acquisition and computed when the amount of data through the DAQ system exceeds the limit of either the FIFO or the DasyLab driver buffer.

Figure 3-35 describes the procedures to determine the data acquisition length and the number of data until the WaveBook 516 stops because of the data overflow in the buffer memories. The following example represents one input channel with the sampling rate of 1 MHz (IOtech, 2005a).

Step (a): Determine the data acquisition length based on Equation 3-2.

- FIFO size: 64 MB, which holds 33.5×10^6 samples
- Data sampling rate: 1 MHz (1,000,000 samples/sec)
- Data Transfer rate between the WaveBook 516 and the PC through parallel bus: 380,000 samples/sec

$$\text{Time to fullfill FIFO memory} = \frac{\text{FIFO memory size}}{\text{Sampling rate - Transfer rate}}$$

$$= \frac{33{,}500{,}000}{1{,}000{,}000\text{-}380{,}000} = 54 \text{ seconds} \qquad (3\text{-}2)$$

The time duration to fulfill the FIFO buffer limit with 1 MHz sampling rate is 54 seconds, which means that the DAQ system works for 54 seconds until it stops.

Step (b): Calculate the number of transferred data from the FIFO to the driver buffer according to Equation 3-3.

$$\begin{aligned} \text{Transfered data} &= \text{Time to fullfill FIFO} \times \text{transfer rate} \\ &= 54 \text{ seconds} \times 380{,}000 \text{ samples/sec} \\ &= 20.52 \times 10^6 \text{ samples} \end{aligned} \qquad (3\text{-}3)$$

Within 54 seconds obtained from step (a), 20.52×10^6 data points are transferred to the driver buffer through the parallel bus at the rate of 380,000 samples/ second .

Step (c): Determination of the block size

In general, DasyLab automatically determines the block size with half of the sampling rate in format of 2^n. For example, if the sampling rate is 1000 samples/sec, the block size becomes 512 that equals to 2^9. Similarly, if the sampling rate is 2000 samples/sec, the block size becomes 1024.

Step (d): Data transfer rate from the driver buffer to the PC hard drive.

The data transfer rate between the DasyLab driver buffer and the PC hard drive depends on the specifications of the PC, such as the hard drive type, cache size, and buffer size. Therefore, it is difficult to indicate the specific transfer rate at any specific moment. Usually, this speed is too fast to clog the data flow.

After all, the maximum data acquisition length of one channel at the sampling rate of 1 MHz and the data transfer rate of 380 kHz is 54.02×10^6 samples as presented in Equation 3-4.

$$\begin{aligned}\text{Acquisition length} &= \text{Transfered data from the FIFO buffer to the driver buffer} \\ &\quad + \text{the data in the FIFO buffer} \\ &= (20.52\times10^6 + 33.5\times10^6)\ \text{samples} \\ &= 54.02\times10^6\ \text{samples.}\end{aligned} \tag{3-4}$$

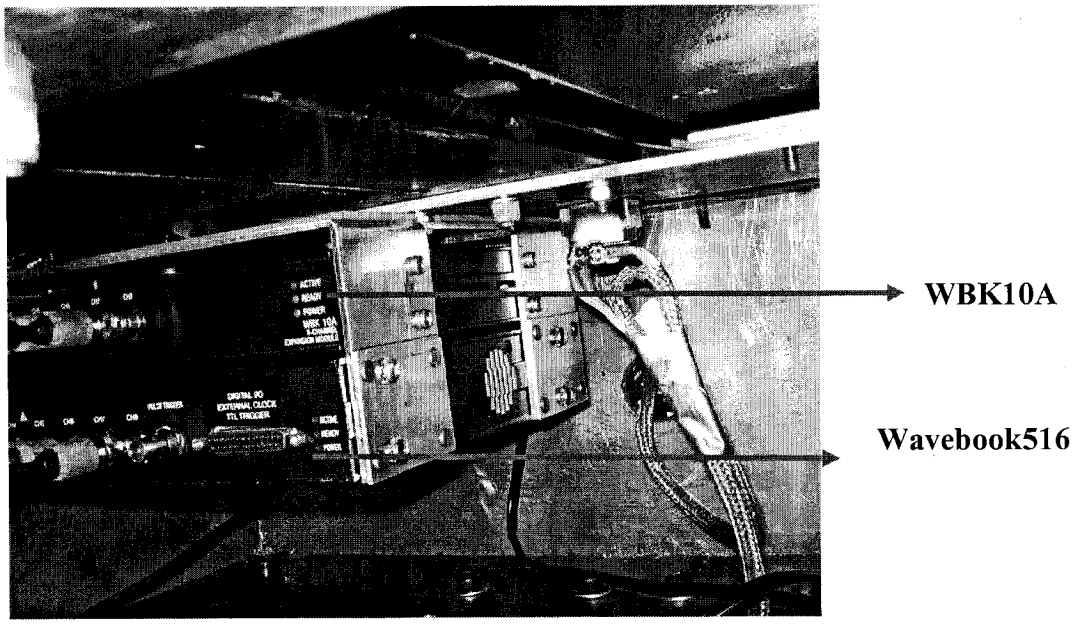

Figure 3-31. USC DAQ system of the USC centrifuge.

Figure 3-32. Portable WaveBook516 system with a notebook computer for centrifuge tests and instrumentation calibration.

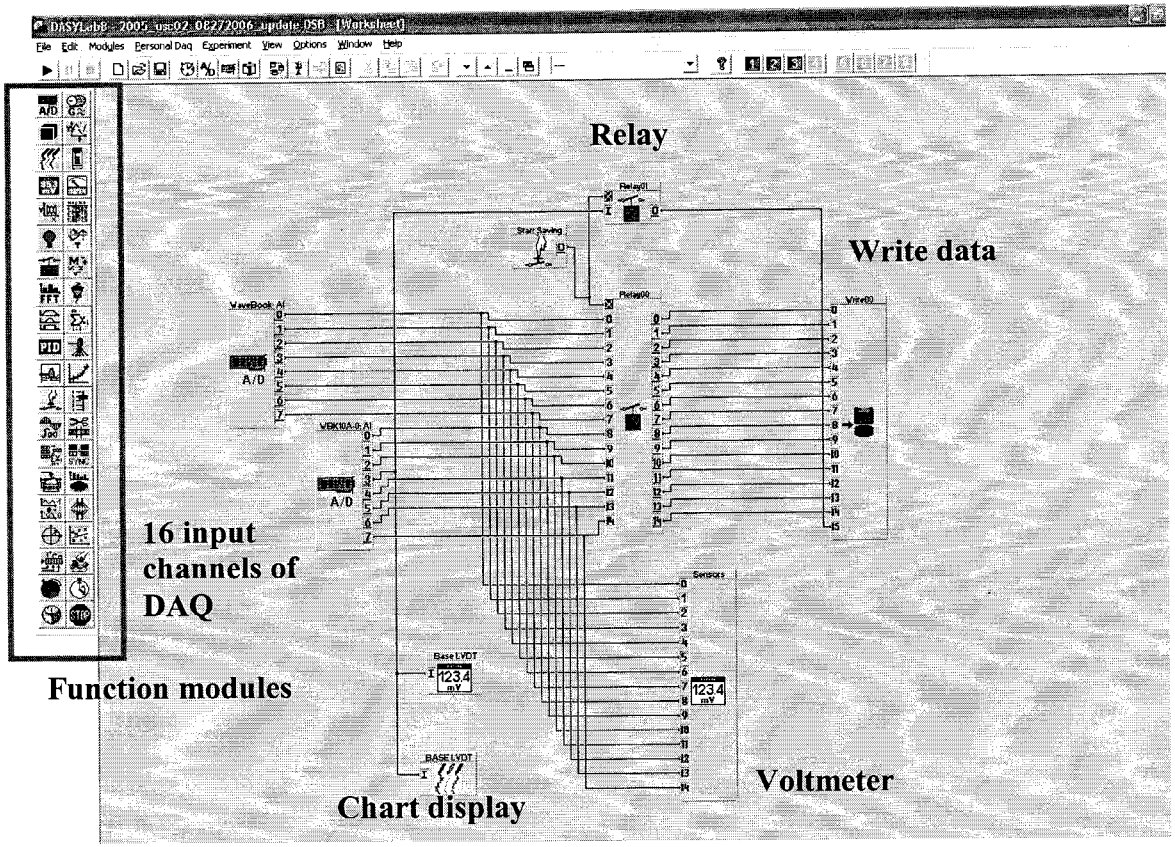

Figure 3-33. Worksheet of DasyLab software designed for the centrifuge USC01 test.

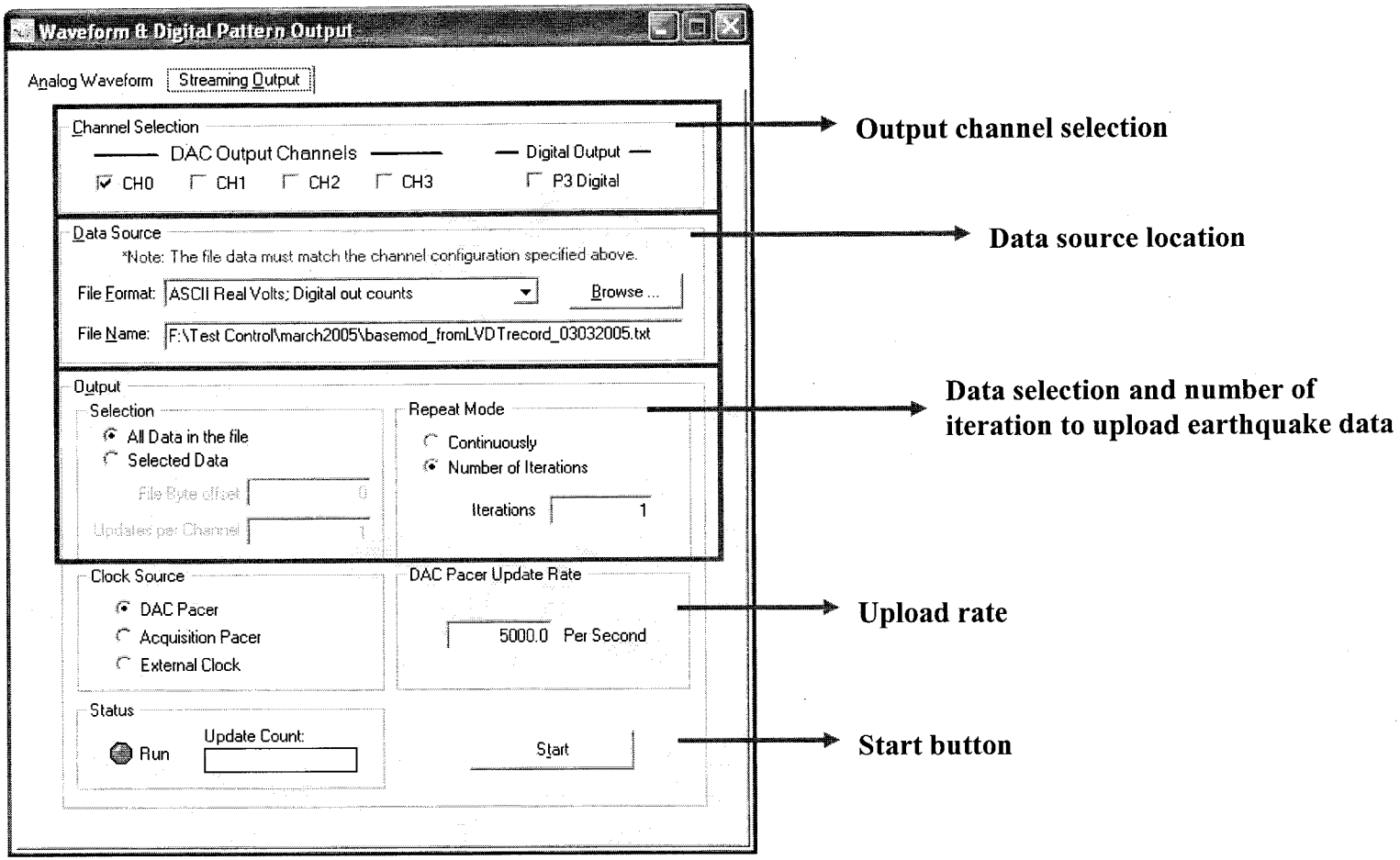

Figure 3-34. Interface of DaqView software designed for the centrifuge USC01 test.

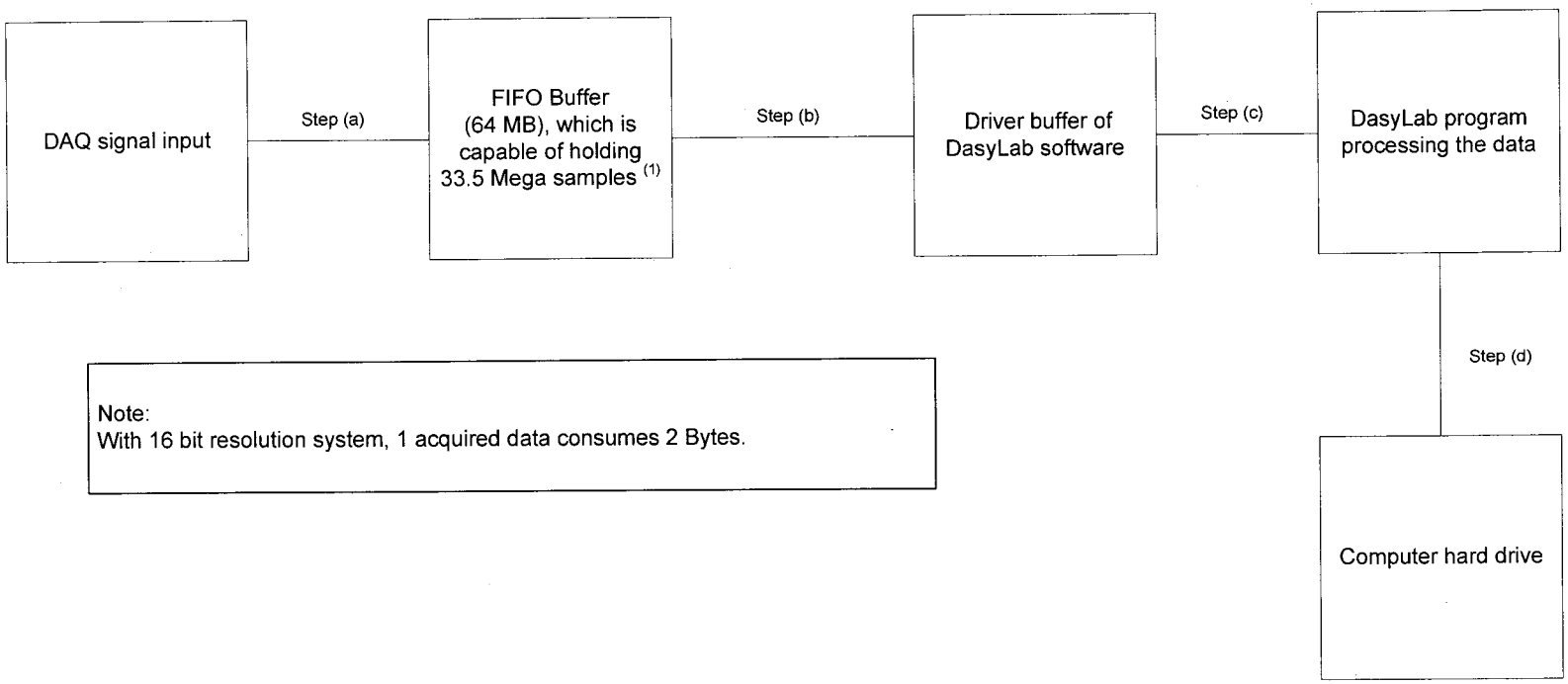

Figure 3-35. Schematic layout of data capacity and data transfer rate for the USC DAQ system.

3.5 Instrumentation

This section describes the instrumentation of the USC centrifuge system, including various types of transducers and signal conditioners. The transducers and signal conditioners are reviewed to understand their usage in specific purposes, such as acceleration, pore pressure, and displacement measurements. Instruments are reviewed in terms of principles and characteristics.

3.5.1 Piezoelectric accelerometer and signal conditioner

3.5.1.1 Piezoelectric accelerometer: Dytran 3145A1

A piezoelectric material is a material that develops an electric charge when subjected to a force. A simple piezoelectric accelerometer consists of a disk-like base of piezoelectric material connected to a proof mass. When the body accelerates, the proof mass exerts a force on the piezoelectric disk and a charge builds up across the electrodes (Gautschi, 2002). Piezoelectric accelerometers are called active devices since they generate their own signals, and theoretically do not need to be powered. Since piezoelectric sensors need dynamic motion to generate the electrical output, they do not respond to steady-state inputs (Dytran, 2003a). Hence, piezoelectric accelerometers are AC-response sensors. Most piezoelectric accelerometers will only operate above a threshold frequency of dynamic motion. Subsequently piezoelectric accelerometers are not ideal for static applications where input acceleration and frequency ranges are both relatively small.

Dytran 3144A and the upgraded model, 3145A1, are used for the dynamic centrifuge tests. The Dytran accelerometers such as 3144A and 3145A1 have miniature sizes as shown in Figure 3-36.

3.5.1.2 Signal conditioner: Dytran 4122B

The Dytran 3145A1 and 3144A accelerometers need Dytran 4122B signal conditioner that supplies excitation power, 2-20 mA constant current with 24 VDC, for those transducers and amplifies an output signal up to $\pm$ 10 V . The Dytran 4122B has six input channels with BNC connectors as shown in Figure 3-37. Table 3-1 lists the specifications and physical dimensions of the Dytran 3145A1.

3.5.2 Displacement transducer and signal demodulator

3.5.2.1 Displacement transducer: Schaevitz 500 MHR and DC-EC 250

LVDT stands for a **L**inear **V**ariable **D**ifferential **T**ransformer. A LVDT measures the distance within a linear range. It consists of three symmetrically spaced coils and a magnetic core to measure the distance by using a variable-reluctance (inductance) principle (Nyce, 2004). The magnetic core moves within the coils and changes the magnetic flux between the primary and the secondary coils. Consequently, it changes the characteristics of the flux path that results in the voltage changes in the circuit.

The USC centrifuge uses Schaevitz 500MHR models for measuring lateral displacements. The Schaevitz 500MHR is an AC-operated LVDT and needs the demodulator to yield DC output in accordance with the core movement of LVDT.

The Schaevitz 500MHR has a lightweight core ideal for application where excessive core weight may affect test results. The Schaevitz 500 MHR has a linear range of±0.5"; its specifications are listed in Table 3-2 (MSI, 2005b).

Schaevitz DC-EC 250 is a DC-operated LVDT transducer to measure the distance within a linear range of ± 0.25 inches . It contains its own signal conditioner to demodulate the signal; it has a scale factor of 40V/inch. In chapter 4, the Schaevitz DC-EC 250 is used to measure vertical displacements. The Schaevitz DC-EC 250 needs an input voltage of ±15 VDC and has an output voltage up to ±10 VDC for full displacement (MSI, 2005a). Table 3-3 lists the specifications of Schaevitz DC-EC 250.

3.5.2.2 Signal conditioner: Honeywell DLD-VH

Honeywell DLD-VH model is a signal conditioner for the Schaevitz 500 MHR featuring an 35mm Din-rail. The Honeywell DLD-VH conditioner has a frequency response of 300 Hz which is approximately the maximum frequency that the DLD-VH can detect. In addition, it needs 18-36 VDC with a 150 mA power for conditioning the Schaevitz 500 MHR model. It supplies the excitation power (AC excitation power of 3 volts RMS with 5 kHz frequency) and amplifies the output signal up to ±5 VDC respectively (Honeywell, 2005a).

Figure 3-38 shows the module in which 6 DLD-VH units and power converter (SOLA Heavy-Duty SDP2-24-100 model) are mounted closely with input and output connectors. Table 3-4 shows the details for the demodulators. Physical wiring

connections between the transducer and signal conditioner will be presented in section 3.6.

Additional capacitors, having a capacitance of 100 MFD, are used to filter out the high frequency noise that occurs on the output signal of DLD-VH models. As one of the solutions to minimize the noise, connecting a 1000μF (microfarad) capacitor directly across the (+) output and the (-) output of the DLD-VH unit definitely brings the noise to a minimum. Figure 3-39 shows a capacitor box where 6 capacitors are installed inside to minimize the noises for 6 DLD-VH units. The capacitor box is equipped with BNC connectors for input and output terminals.

3.5.3 Pore pressure transducer and signal conditioner

3.5.3.1 Pore pressure transducer: Druck PDCR81

Pressure transducers need to be small enough to minimize the interference with the tested model. For the USC centrifuge, Druck PDCR81 transducers are extensively used because of their miniature size. The PDCR 81 transducer is a strain-gauge pressure sensor of the full bridge type. The sensor has red, blue, yellow and green wires for positive power supply, negative power supply, positive output and negative output respectively. The PDCR 81 has a pressure range of 100 psi (Allard, 1983).

3.5.3.2 Signal conditioner: Honeywell DV-05

The Honeywell signal conditioner DV-05 supplies a highly regulated bridge excitation voltage for a strain-gauge transducer like the Druck PDCR81 transducer. DV-05 is used to supply 3 VDC excitation power and amplifies the output signal for

the Druck PDCR81 transducer up to +/- 5 VDC range. Figure 3-40 shows DV-05 composed of the followings: (1) power converter (model SCP 30T515-DN), (2) five Honeywell DV-05 signal conditioners, and (3) input and output connectors. In addition, Table 3-5 presents the specification of DV-05 (Honeywell, 2005b).

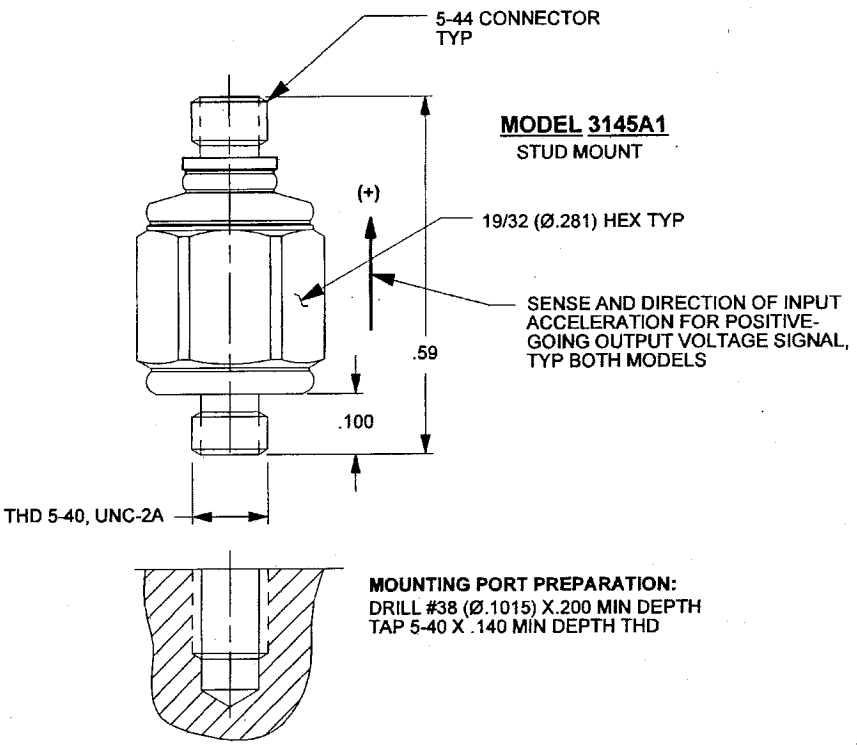

Figure 3-36. Schematic drawing of Dytran 3145A1 accelerometer (Dytran, 2003a).

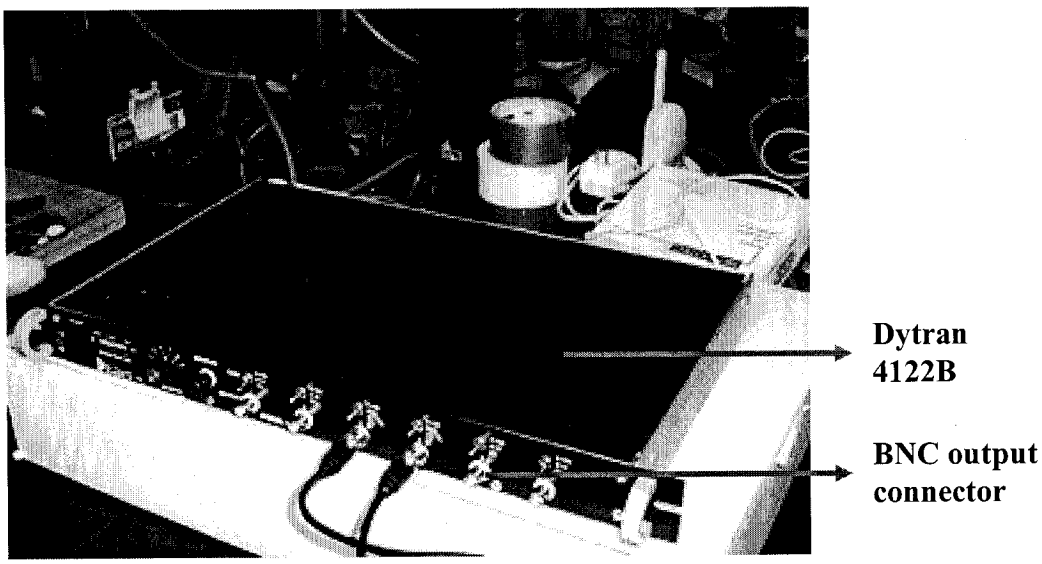

Figure 3-37. Dytran 4122B conditioner.

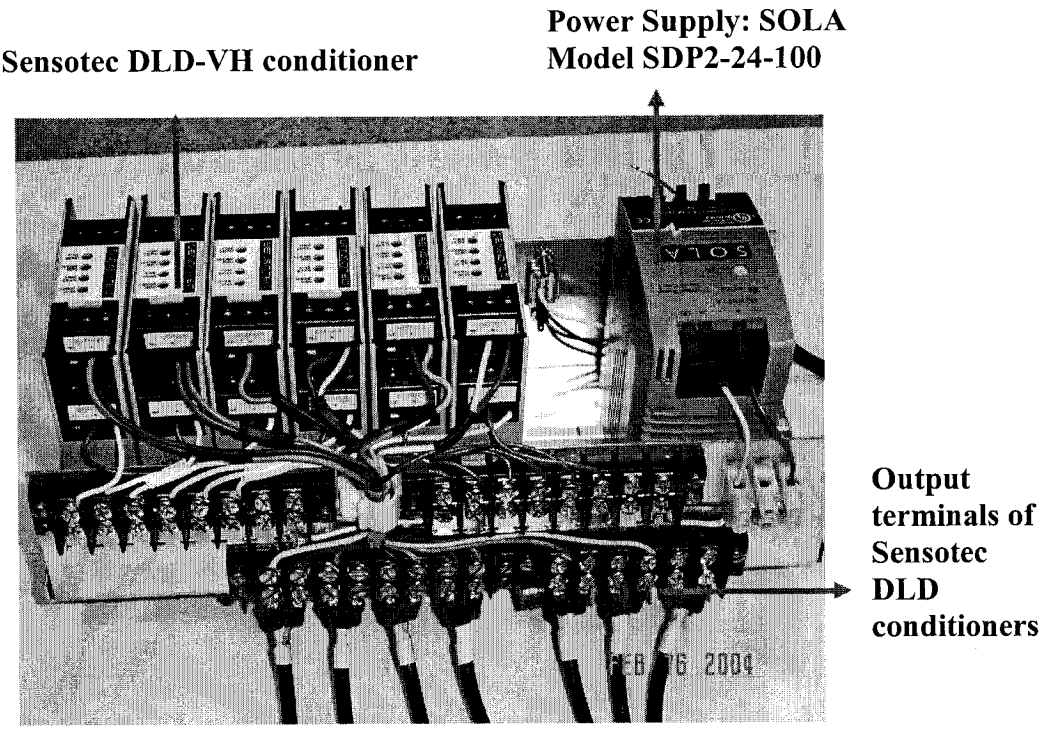

Figure 3-38. Signal conditioning module with Honeywell DLD-VH conditioners and SOLA power converter.

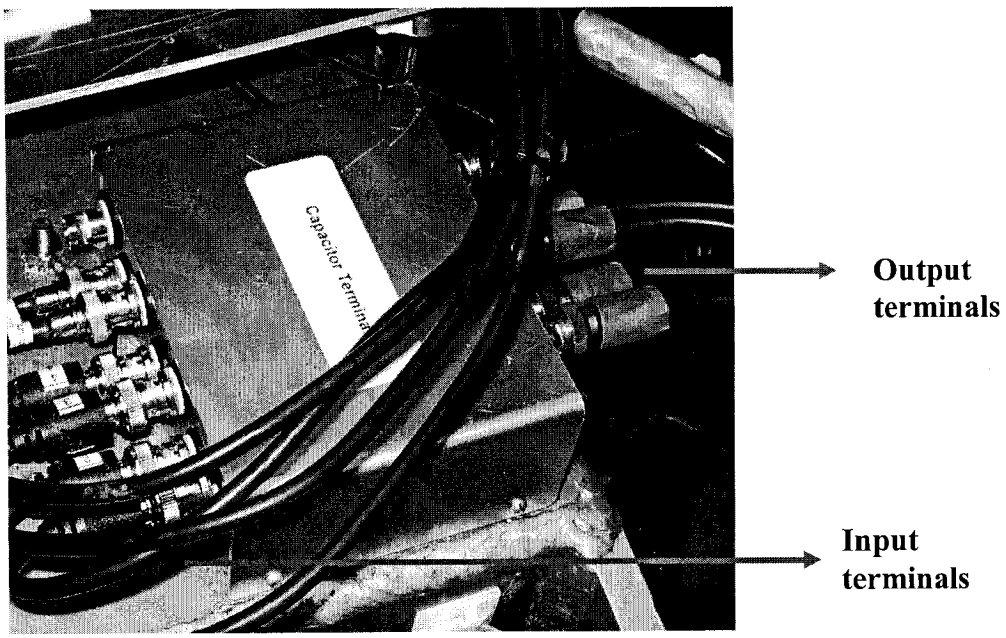

Figure 3-39. Capacitor module reducing high frequency noise from Honeywell DLD-VH conditioner.

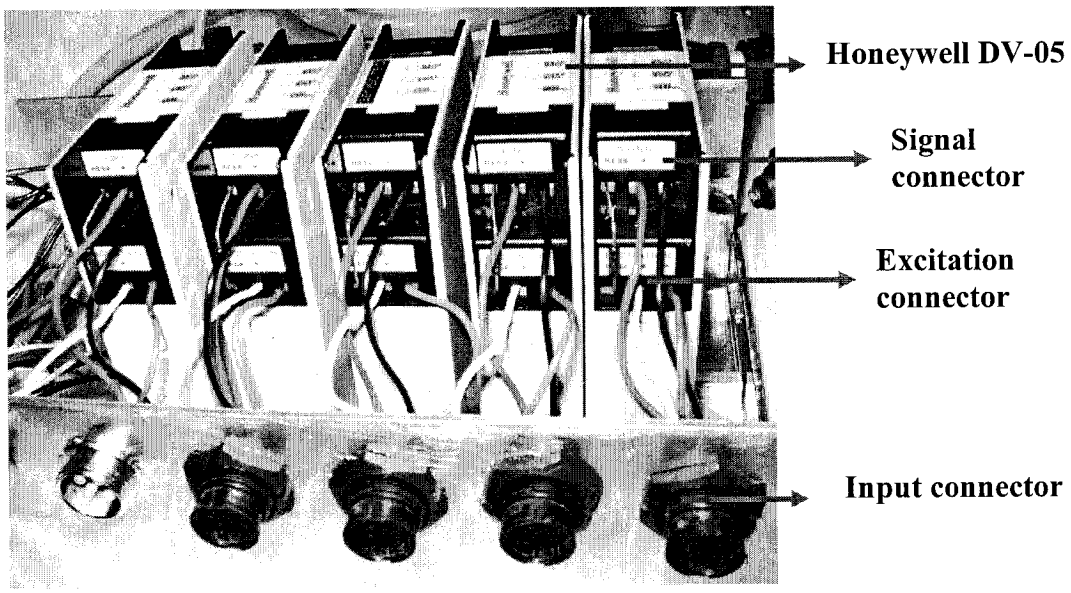

Figure 3-40. Signal conditioning module with Honeywell DV-05 conditioners.

Table 3-1. Specification of Dytran 3145A1 accelerometer.

Physical Dimensions and Weight		
Weight	2.5	grams
Size, Hex ×Height	0.281 × 0.49	inches
Performance		
Sensitivity, ± 10%	10	mV/G
Range	500	G's
Frequency Range	0.5 to 10k	Hz
Resonant frequency (Nominal)	45	kHz
Environmental Specification		
Max. Vibration/Shock	600/3000	G's
Electrical Specification		
Supply current/ Compliance voltage range	2 to 20/ 18 to 30	mA/Volts
Output impediance	100	Ohms
Case ground	Grounded to power ground	

Table 3-2. Specification of Schaevitz 500 MHR model.

Physical Dimensions and Weight	
Weight	Body (17 grams), Core (1.6 grams)
Size, Body/Core	Body (3.3" in Length, 0.375" in Diameter)
	Core (2" in Length, 0.108" in Diameter)
Performance	
Sensitivity	1.60 mV/V/0.001 inch
Output voltage range	+/- 10 V
Frequency range	2 kHz to 20 kHz
Linearity	0.25 % of FSO
Environmental Specification	
Max. Vibration/Shock	20 g up to 2 kHz/ 1000 g for 11 mS
Electrical Specification	
Input voltage	3 V rms @ 2.5 kHz
Impedance (Primary/Secondary)	145 ohm, 445 ohm

Table 3-3. Specification of Schaevitz DC-EC 250.

Physical Dimensions and Weight	
Weight	Body (73 grams), Core (8 grams)
Size, Body/Core	Body (3.8" in Length, 0.75" in Diameter)
	Core (2" in Length, 0.188" in Diameter)
Performance	
Sensitivity	40.0 V/inch
Output voltage range	+/- 10 V
Frequency range at -3 dB	500 Hz
Linearity	0.25 % of FSO
Environmental Specification	
Max. Vibration/Shock	10 g up to 2 kHz/ 250 g for 11 mS
Electrical Specification	
Input voltage	+/- 15 VDC, +/- 25 mA
Ripple	Less than 25 mV rms
Output Impedance	Less than 1 ohm

Table 3-4. Specification of Honeywell DLD-VH conditioner.

Physical Dimensions	
Enclosure style	35 mm din rail
Enclosure size	22.5mm × 75mm × 98.5mm
Performance	
LVDT excitation	3 Volts RMS at 5 kHz
Output voltage range	+/- 5VDC
Frequency response	0 to 300 Hz
Zero adjustment range	+/-100 % coarse, +/- 20% fine adjustment
Gain Adjustment range	Switch selectable (0.1 to 15 VRMS), +/- 10% fine adjustment
Linearity	+/- 0.05% of FSO
Environmental Specification	
Operating temperature	-20 to 140 degrees F
Electrical Specification	
Power requirement	18-36 volts DC @ 150 MA
Power supply isolation	500 V

Table 3-5. Specification of Honeywell DV-05 conditioner.

Physical	
Enclosure style	35 mm din rail
Enclosure size	22.5mm × 75mm × 98.5mm
Performance	
Bridge excitation	5 or 3 volts DC @ 30 mA (user selectable)
Output voltage range	+/- 5VDC
Frequency response	DC - 5000 Hz
Zero adjustment range	+/-60 % coarse, +/- 20% fine adjustment
Gain Adjustment range	Switch selectable (0.5 to 13.3 mV/V), +/- 20% fine adjustment
Electrical Specification	
Power requirement	11 - 28 VDC

3.6 Calibration of transducer and conditioner

Transducers have a tendency to lose their original characteristics, like a scale factor from manufacturers, after they have been used in several tests. Vibrations induced by the spinning of the centrifuge spin and earthquake motions might even change the sensitivities of transducers. Hence, the transducers need to be calibrated periodically to correctly interpret test results. We will now describe the transducer calibrations.

3.6.1 Accelerometer

The Dytran 3145A1 (updated version of the 3144A model) accelerometer works with the Dytran 4122B signal conditioner for centrifuge modeling. The Dytran 3145A1 or 3144A accelerometer responds to dynamic motions above a thread frequency of 0.5 Hz and provides measuring acceleration range of 500 g. To calibrate the Dytran 3144A or 3145A1 accelerometer, two transducers are mounted on a vertical shaker as shown in Figure 3-41 with a target transducer and a reference transducer that is calibrated recently. Both the accelerometers are shaken together and the sensitivity of the target transducer is achieved based on the output of the reference transducer. Figure 3-41 represents the calibration outline of the Dytran accelerometer with the necessary equipment.

A software, called "sinefit.m", is used to compute V_{rms} (root-mean-square voltage) from the target and reference transducers. The frequency of the sinusoidal signal increases with constant amplitude; therefore, the output signals of the accelerometers also increase. Based on the calculated acceleration records from the reference

transducer at each frequency increment, the voltage signals from the target transducer are correlated to determine the sensitivity as a unit of mV/G.

The "sinefit.m" program is a share code program developed by Chen (2003) to achieve the optimal extraction of features such as amplitude, frequency and phase shift in the sample sinusoidal signal. The program codes and operation method are referred to Chen (2003).

3.6.1.1 Calibration equipment

- Reference transducer: Dytran 3100B model
- Target sensor: Dytran 3145A1 or Dytran 3144A model
- Signal generator: Ez sense FG-7602C model
- Vertical shake table
  - Manufacture: Vibrametic Test System
  - Frequency range: 5-20,000 Hz
  - Signal input: max 10 V RMS
  - Shaker displacement: max. +/- 0.5 inch

3.6.1.2 Calibration procedure

1. Mount the Dytran 3145A1 model as a target transducer and the Dytran 3100B model as a reference transducer together on the shaker.

2. Connect the BNC cables from both transducers to the Dytran 4122B conditioner. Set the amplification gains of Dytran 4122B to 10 for both transducers.

3. Connect the signal generator, which is ready to produce sinusoidal waves with the amplitude of +/- 1 V, to the shaker conditioner.

4. Increase the "Amp" dial on the shaker conditioner (see Figure 3-41) by 4 between 0 and 10 values.

5. Connect the outputs of 4122B conditioner to the DAQ system (WaveBook 516 and PC computer).

6. Turn on all the equipment.

7. Increase the sinusoidal wave frequency with 10 Hz increment.

8. Start recording the signals from the reference and target transducers through the WaveBook 516 system.

9. Repeat procedures 7 trough 9 until the final signal frequency reaches 100 Hz.

3.6.1.3 Calibration calculation

This section describes how to compute the scale factor (called sensitivity) of target accelerometer in accordance with the reference accelerometer. The software program "sinefit.m" is used to compute V_{rms} voltage from both the transducer response signals with frequency increment (10 Hz).

1. Compute the acceleration (G_{rms}) from the sinusoidal motion.

    a. The output voltage (V_{rms}) from the reference accelerometer is plugged into the sensitivity ($10.3\, mV_{rms} / G_{rms}$) of the reference transducer, producing the G_{rms} of sinusoidal motion. For example, if the output voltage of reference transducer is $10.3\, V_{rms}$, G_{rms} would be 1.

2. Compute the output voltage (V_{rms}) of the target transducer.

3. Compute the sensitivity of the target transducer by relating V_{rms} in step 2 with G_{rms} from step 1 as in Equation 3-5.

$$\text{Sensitivity of the target transducer} = \frac{\text{V}_{\text{rms}} \text{ of the target transducer}}{\text{G}_{\text{rms}} \text{of the reference transducer}} \qquad (3\text{-}5)$$

The transducer sensitivity is presented as V/G after the subscript RMS terms are cancelled out.

3.6.2 LVDT Calibration

The Schaevitz 500MHR (AC LVDT) and DC-EC250 (DC LVDT) are used for measuring displacements. The Schaevitz 500 MHR uses a signal conditioner (Honeywell DLD-VH) that supplies the excitation power and demodulates the output signal of the transducer. The adjustments of gain and zero controllers of the Honeywell DLD-VH can be found in the user manual (Honeywell). The Schaevitz DC-EC250 model is a DC operated LVDT and has a built-in signal conditioner. Therefore, the DC-EC250 model does not need any signal conditioner for both the excitation power and the signal demodulation.

3.6.2.1 Calibration procedure

The calibration procedures for AC and DC LVDTs are similar with the exception of the following: (1) the DC LVDT (Schaevitz DC-EC 250) does not need a signal conditioner, and (2) the DC-EC 250 has a shorter linear range (± 0.25) than the 500 MHR ($\pm$ 0.5 inches). Figure 3-42 shows the calibration of the 500 MHR model; similarly, the DC-EC 250 can be calibrated without a signal conditioner. Calibration procedures are described below for the Schaevitz 500MHR model:

1. Install the 500MHR model on the calibration stand.
2. Connect the output wires of 500 MHR to the signal-input terminals of DLD-VH module.
3. Connect the output wires from the DLD-VH module to the input channel of WaveBook 516 system.

4. Align the magnetic core with the LVDT body to match the centers of them together.

5. Turn on all the instrumentation and the DAQ system.

6. Move up the magnetic core by using a micrometer showing a movement distance on the LED window.

7. Measure the movement distance by using the WaveBook 516 using DasyLab.

8. Repeat step 6 and 7 until the magnetic core moves to the maximum displacement within the linear range ($\pm$ 0.5 inch).

9. Compute the sensitivity of the LVDT as a unit of V/inch.

3.6.3 Pore-pressure transducer calibration

Druck PDCR 81 and Honeywell DV-05 signal conditioner work together to measure pore-pressure changes inside a soil specimen. The PDCR 81 model is a strain gauge pressure sensor that is a full bridge type. The PDCR 81 needs a signal conditioner to amplify the output signal of the transducer up to +/- 5 VDC.

Figure 3-43 shows the schematic diagram of the calibration setup and equipment of the PDCR81 calibration. To calibrate the PDCR 81, an air-filled chamber was developed after discussions with a technician at GE Druck. The air pressure inside the chamber is controlled by a regulator.

3.6.3.1 PDCR81 Calibration equipment

- PDCR81 pore pressure transducer
- Honeywell DV-05 conditioner
- Air-pressure supply and dial regulator
- Calibration chamber

3.6.3.2 Calibration procedure

1. Connect an air-supply tube to an air inlet of dial-gauge regulator as shown in Figure 3-43.
2. Put the PDCR81 transducer into the chamber sealing the air leakage by using an O-ring.
3. Connect the air tube from the pressure regulator to the chamber.
4. Connect the signal and power connections between the PDCR 81 and the Honeywell DV-05.
5. Connect the output signal of the Honeywell DV-05 unit to the DAQ (WaveBook 516) system.
6. Turn on all the equipment.
7. Supply 2-psi air pressure to the chamber and wait for a few minutes to saturate the chamber evenly.

8. Increase the air pressure by 5 psi.

9. Measure the output signal of the PDCR81 transducer through the Honeywell DV-05 conditioner by means of the DAQ system at a sampling rate of 10Hz.

10. Return to step 8 and repeat the procedures until the air pressure equals to 50 psi.

3.6.4 Calibration results

All transducers are calibrated within a linear range of distance, pressure, and acceleration. Table 3-6 lists the sensitivity values of the transducers used in chapter 4. It also lists additional information about the model numbers, the classification labels, and the serial numbers of the transducers and signal conditioners.

3.7 Summary

Chapter 3 reviewed the specifications and capabilities of the USC centrifuge, the centrifuge-peripheral equipment (e.g., mechanical, electrical, and hydraulic facilities as well as the DAQ system), and the instrumentation (e.g., transducers and signal conditioners). The wireless DAQ system records and transmits efficiently experimental data from the centrifuge to the laboratory. The experiment data, captured and transferred by the wireless DAQ system are of high quality. The DAQ system was set up for optimizing the data flow without clogging the data among the DAQ components. Finally, the various transducers and signal conditioners of the USC centrifuge were described and calibration methods presented.

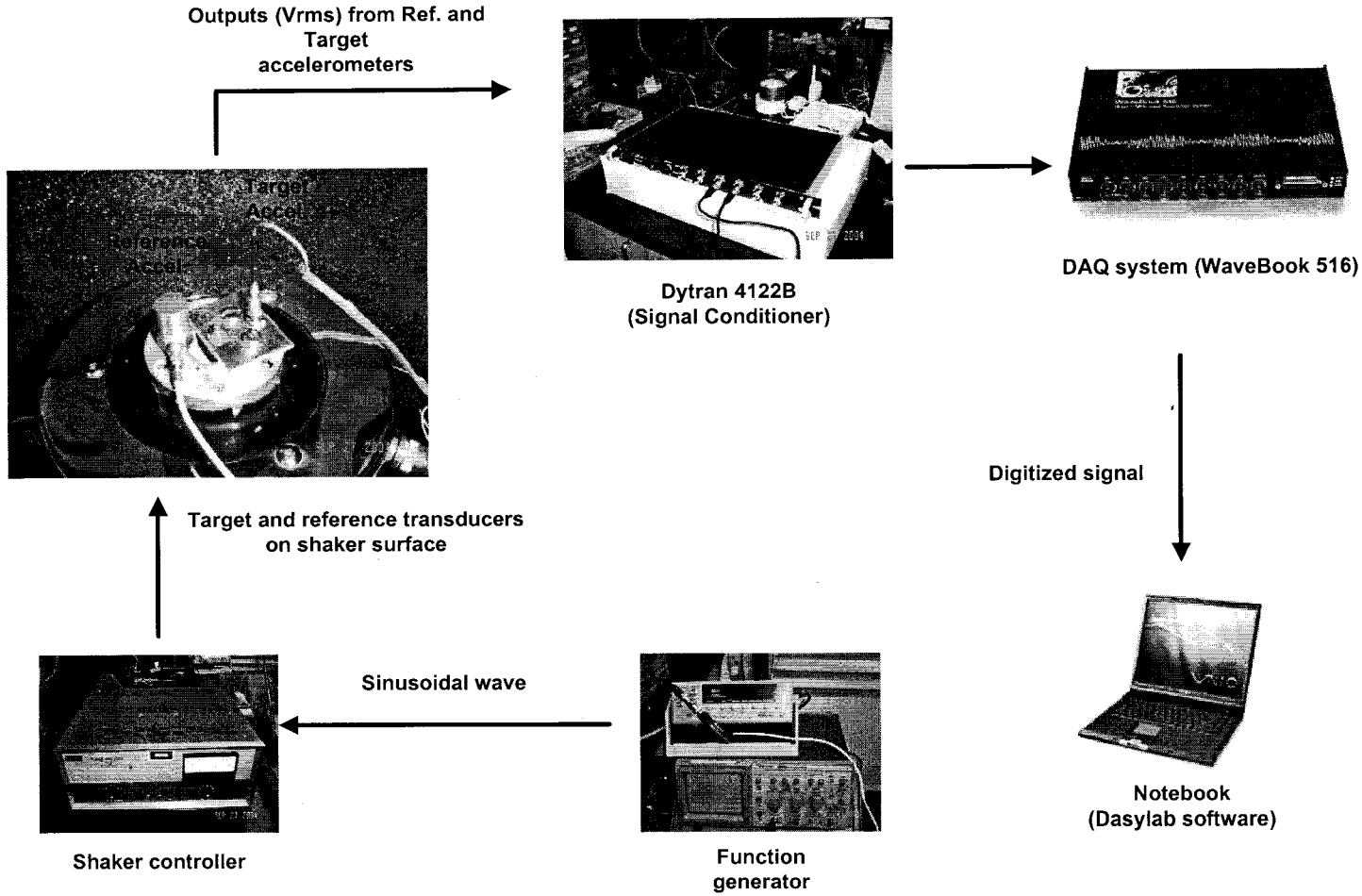

Figure 3-41. Calibration setup of a piezoelectric accelerometer (e.g., Dytran 3145A1 and 31144A models).

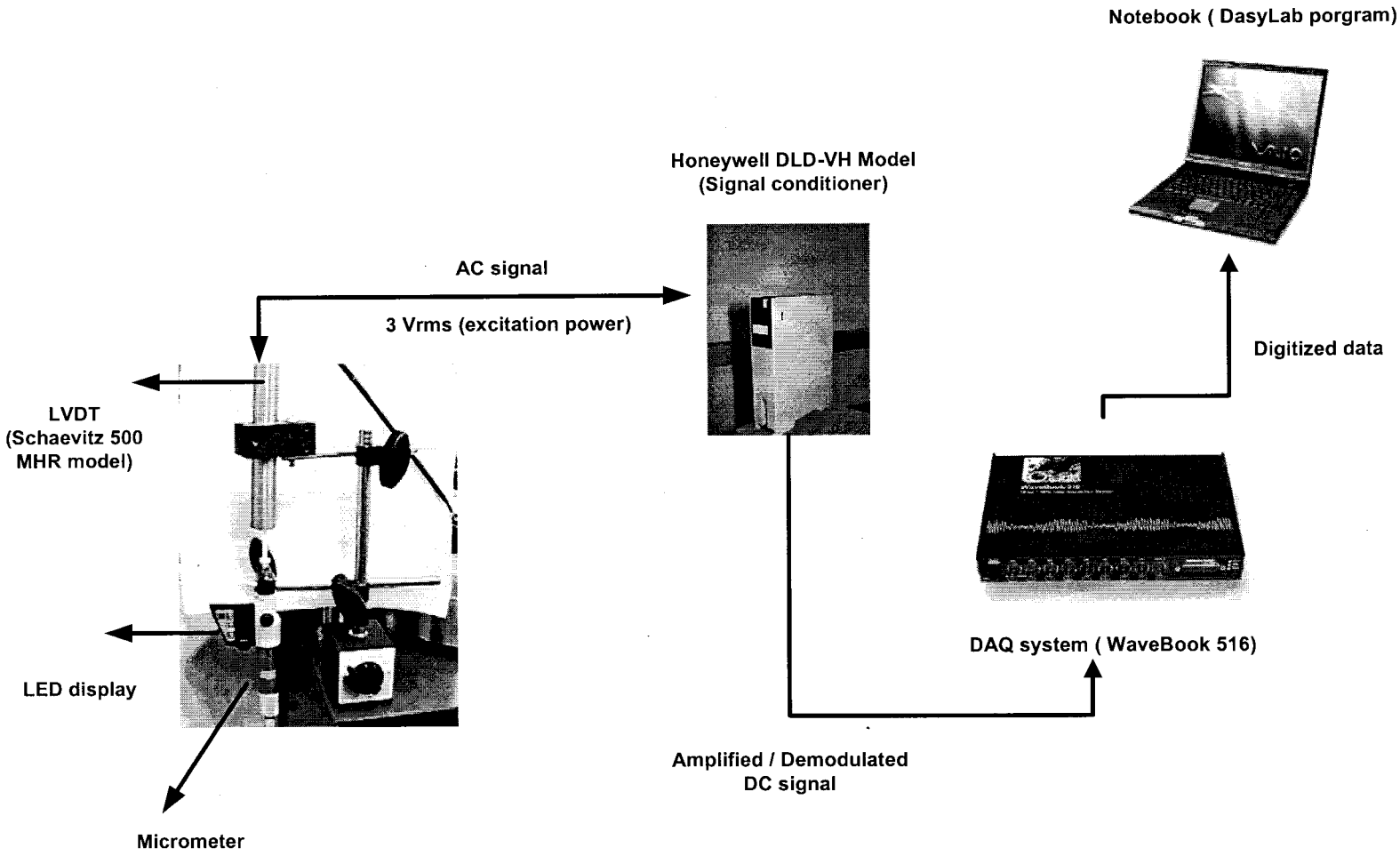

Figure 3-42. Calibration setup of LVDT instrumentation (e.g., Schaevitz 500 MHR and DC-EC 250 models).

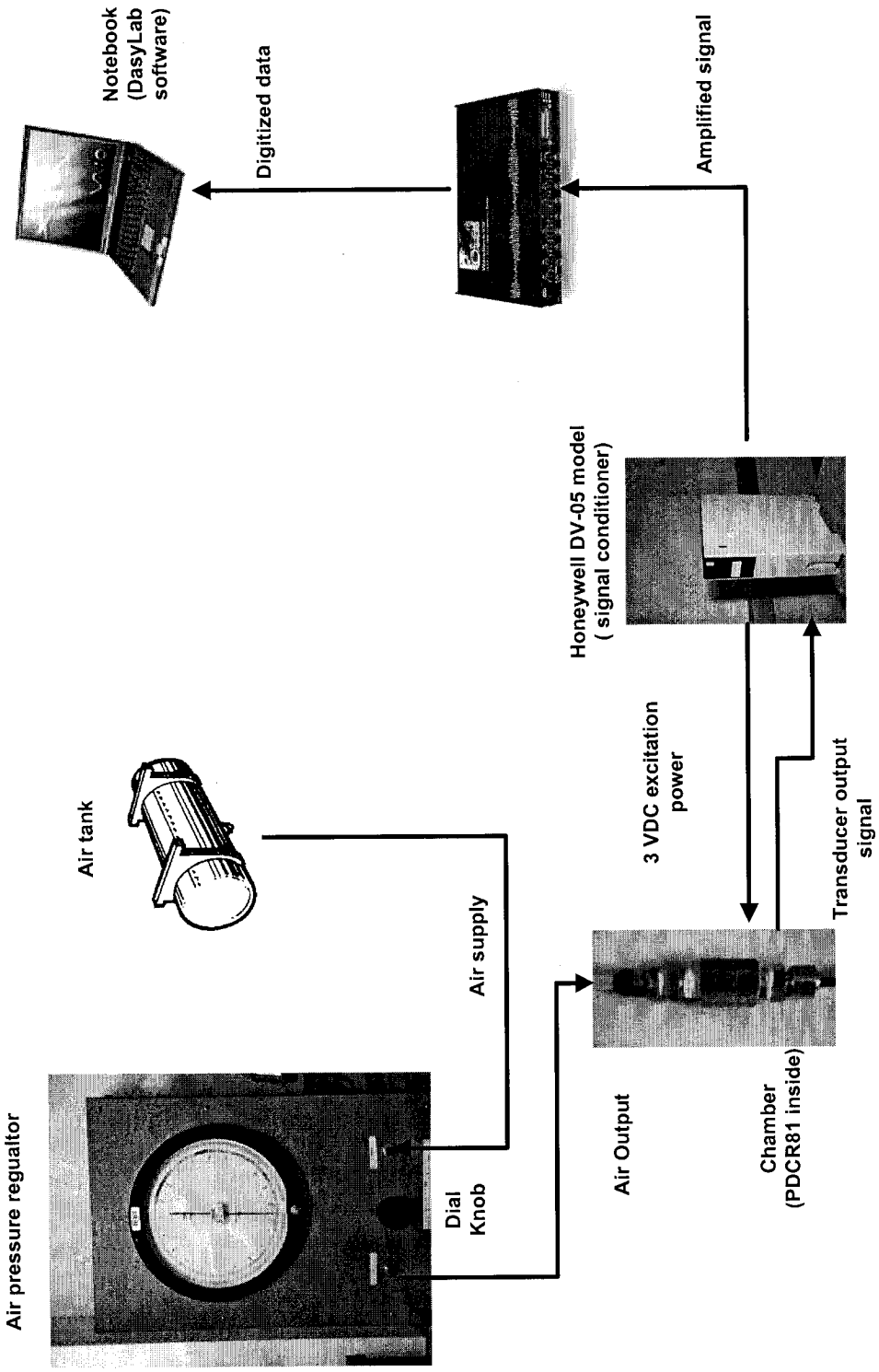

Figure 3-43. Calibration setup of a porepressure transducer (e.g., Druck PDCR 81 model).

Table 3-61. Specification of instrumentation used in centrifuge USC01 modeling.s

Transducer Type	Model	Serial Number	Classification Label	Conditioner Model (CH # or SN)	Sensitivity
Accelerometer	Dytran 3145A1	161	A1	Dytran 4122B CH1	10.3 mV/G
Accelerometer	Dytran 3145A2	162	A2	Dytran 4122B CH2	10.4 mV/G
Accelerometer	Dytran 3145A3	1557	A3	Dytran 4122B CH3	10.82 mV/G
Accelerometer	Dytran 3145A4	1559	A4	Dytran 4122B CH4	11.48 mV/G
Pore Pressure Transducer	Druck PDCR81	3268	P1	Honeywell DV-05 (1023172)	0.058 V/PSI
Pore Pressure Transducer	Druck PDCR82	3269	P2	Honeywell DV-05 (1023160)	0.059 V/PSI
Pore Pressure Transducer	Druck PDCR83	3270	P3	Honeywell DV-05 (1023171)	0.058 V/PSI
Displacement Transducer	Schaevitz 500 MHR	# 2 (1911)	HL1	Honeywell DLD-VH (976734)	10,002 V/inch
Displacement Transducer	Schaevitz 500 MHR	# 3 (1913)	HL2	Honeywell DLD-VH (976705)	9.99 V/inch
Displacement Transducer	Schaevitz 500 MHR	# 6 (1933)	HL3	Honeywell DLD-VH (976733)	10.005 V/inch
Displacement Transducer	Schaevitz 500 MHR	# 5 (1932)	HL4	Honeywell DLD-VH (976738)	9.98 V/inch
Displacement Transducer	Schaevitz DC-EC 250	3707	VL1	N/A	41.4 V/inch
Displacement Transducer	Schaevitz DC-EC 251	3827	VL2	N/A	40.32 V/inch
Displacement Transducer	Schaevitz DC-EC 252	3706	VL3	N/A	40.91V/inch

4 Centrifuge modeling of ground deformation

4.1 Introduction

This chapter presents a centrifuge test on a saturated layer of Nevada sand. Hereafter this test, which is referred to as USC01, investigates the buildup of porepressure induced by an earthquake, which leads to liquefaction, causes permanent deformation and is followed by dissipation of excess pore pressure. The centrifuge test was carried out at 50 g. The model responses were monitored through several transducers to obtain the lateral and vertical displacements, horizontal accelerations, and excess pore pressures. A description of the centrifuge testing and the experimental methodology are referred to Scott (1989), Hushmand et al. (1988) and Allard (1983). Hushmand et al. (1988) conducted liquefaction tests with saturated Nevada sand to investigate land deformations and seismic responses induced by earthquakes.

Figure 4-1 shows the organization of Chapter 4. The main objective of the task reported in this chapter was to evaluate the performance of the USC centrifuge after major revisions and improvements. This chapter describes (1) the preparation of deaired water; (2) equipment and instrumentation used in the centrifuge test; (3) the construction of the centrifuge model; and (4) the centrifuge test results. The test results are reported in terms of lateral and vertical displacements, excess pore pressures, and acceleration data. Various transducers recorded the responses of the soil model while it was shaken by the earthquake motion.

4.1.1 Model description

Figure 4-2 shows a schematic diagram of the laminar box and instrumentation used for the centrifuge test. Table 4-1 lists the locations of the transducers with respect to the reference point along the x, y, and z coordinates on the laminar box. As shown in Figure 4-2, the left lower corner of the laminar box is the origin of the coordinate system. The test model was 10 inches in height, 14 inches in length, and 7 inches in depth. It is made of Nevada No.120 sand with the following characteristics: relative density is 65%; dry unit weight is 16.13 kN/m^3 ; and saturated unit weight is19.9 kN/m^3 . The Nevada sand was saturated with deaired water.

4.1.2 Preparation of earthquake motion

The earthquake shaking motion for the centrifuge test was prepared using the input acceleration data of VELACS (Verification of Liquefaction Analyses by Centrifuge Studies; Arulanandan and Scott, 1993) project model No.3. The earthquake shaking motion was generated as follows:

1. The base acceleration record of VELACS Model #3 was sent to the centrifuge shake table.

2. The displacement of the shake table during the earthquake motion was recorded using a LVDT.

3. The displacement data was made compatible with the MTS 406 controller by scaling the data into the range of within ± 2 V.

4. The converted data was saved in an ASCII file compatible with the DaqBoard system (digital to analog converter).

The MTS controller has a close-loop control with a displacement feedback signal: The earthquake input motion was prepared with the displacement data as described above. The target input motion was satisfactorily duplicated by the shake table; the desired peak acceleration was reached within the centrifuge acceleration by adjusting the uploading rate of input data to the shake table. In other words, the acceleration responses of the shaker were changed by adjusting the time interval Δt of data upload.

Figures 4-3 and 4-4 shows the earthquake acceleration data recorded at the bottom of the laminar box in the time and frequency domains. The maximum and minimum peak accelerations were 0.28 g and -0.3 g at Accelerometer A1 at the model base. The input-motion had a frequency range reaching 300 Hz, which corresponds to 6 Hz in the prototype scale.

4.1.3 Test material preparation

4.1.3.1 Sand preparation

Table 2 lists the main characteristics of the Nevada sand used in the centrifuge test. The sand maximum and minimum dry unit weights are 17.33 kN/m^3 and 13.87 kN/m^3 (Arumoli et al., 1992). The procedures for preparing sand differ depending on the water saturation (i.e., dry versus saturated tests) and soil density (i.e., dense or loose sand). According to the Caltech centrifuge manual (Allard, 1983),

dry sand specimens are prepared by drying them into an oven for 24 hours. Saturated or wet sand specimens are prepared by adding deaired water until the desired water contents is obtained or the water level becomes higher than the soil level.

Figure 4-5 shows the laminar box with a polyethylene bag and plastic cover, which are used to protect the laminar box and prevent the sand and water from penetrating into the gaps between the laminar box rings. Dirt between the rings would cause undesirable friction resistance and impede the free movement of the laminar box.

Loose specimens can be obtained by raining the soil by hand or using a pluviator as shown in Figure 4-6. A pluviator is a tool to pour sand into a test container by controlling the speed and height of falling sand. Dense specimens are obtained by compacting the soil in layers one to two inch thick and using a small taper. The number of blows applied to each layer depends on the desired density (Allard, 1983).

4.1.3.2 Deaired water preparation

Instead of regular tap water, deaired water is used to saturate sand specimens. Deaired water contains much less dissolved air than regular tap water; it is commonly used in soil testing to reach 100% saturation during undrained triaxial tests (Bardet, 1997). The air dissolved in water has to be removed to reach full saturation of the test models and to avoid introducing air bubbles in the voids between soil particles. Deaired water is prepared using the following equipment and procedure:

- A water tank equipped with a vacuum valve and water supply connectors, and water outlet (see Figure 4-7)
- A vacuum pump (e.g., W.M Welch manufacturing corp. model Duo Vacuum Pump, Serial Number 37327-5).
- Additional vacuum pump: USC KAP (Kaprielian Hall) built-in vacuum pump

As shown in Figure 4-7, a water spray nozzle sprays the water into a tank subjected to vacuum. This spraying technique increases the efficiency of the deairing procedure. To expel air as much as possible, it is necessary to keep deairing for approximately 24 hours.

4.1.4 Equipment and instrumentation

The soil container used for the centrifuge test is a laminar box (Figure 3-7), which is 14 inch in length; 7 inches in width; and 10 inches in height. Each ring is made of 0.5-inch aluminum alloy. The maximum horizontal movement at the top of laminar box can reach 3.5 inches, when all the rings are to undergo an extreme movement in one direction without restraint (Hushmand et al., 1988).

The centrifuge test used four types of transducers: (1) Dytran accelerometers; (2) Druck pore-pressure transducers; (3) Schaevitz AC-operated LVDTs for lateral displacement; and (4) Schaevitz DC-operated LVDTs for vertical settlement. Table 4-1 and Figure 4-2 show the locations of transducers relative to the laminar box.

The transducers were mounted so that they can function properly as intended. For instance, a small plate (0.5 inch × 0.5 inch) was attached to the magnetic core of the Schaevitz DC-EC 250 models in order to measure the settlement of soil surface. This plate prevents the magnetic core from sinking into the sand during the test as shown in Figure 4-9. Measuring lateral displacements during the test are depicted in Figure 4-10. The Schaevitz 500 MHR units were attached to specific rings (7^{th}, 13^{th}, and 18^{th} rings) of the laminar box. Similarly, Dytran accelerometers (Figure 4-11) were installed on the opposite side of laminar box to measure the horizontal acceleration. The magnetic cores of LDVT and Dytran transducers, which might become loose during the centrifuge shaking, were secured using a thread locker. In addition, all transducer wires were carefully set up so that there were not pulled or tangled when the soil container swung 90°.

4.1.5 Centrifuge test procedures

The test procedure is divided in (1) model testing and (2) data acquisition. The former covers the procedures of centrifuge model preparation and its operation, whereas the latter describes the specifications and requirements of data sampling.

4.1.5.1 General procedures

The following section describes briefly how to prepare the centrifuge model. Chapter 3 describes how to operate the centrifuge.

1. Select the soil container according to centrifuge test type. There are various soil containers, such as cylindrical bucket, rectangular container, and cylindrical vessels, depending on the test type.

2. Test model needs to be constructed based on the required soil conditions and specifications, such as soil density and water content. These conditions determine which method to use to prepare the model.

3. Transducer cables need to be organized neatly, allowing an extra length of cable from the soil container to the electric equipment attached to the centrifuge arm. This precaution prevents the cables from becoming entangled and stretched when the soil container rotates 90° when the centrifuge rotates.

4. Balance the centrifuge arm by adding weight into the counterweight bucket, which is equal to the weight of the soil and water used for the model construction.

5. Leave the model for approximately 24 hours before starting the centrifuge test to stabilize the test model sufficiently.

6. Using a caliber and/or ruler, measure the model height by averaging, at least, 3 different locations. Turn on the DAQ system before starting the test so that the sensor readings can measure absolute displacements and can be used to calculate the vertical settlement after centrifuge shaking.

7. Start running the centrifuge. Slowly increase the speed of the centrifuge rotation until the speed reaches the desired centrifugal acceleration. For instance, the centrifuge spins at 220 RPM with 36-inch radius from the rotation center to the physical model, which yields 50 g centrifugal acceleration.

8. While monitoring the centrifuge chassis movement, increase slowly the pump pressure by 3000 psi. A rapid change in pump pressure causes the oil to leak through small holes (called "weep holes") on rotary union.

9. After spinning the centrifuge for approximately 10 minutes at constant speed, start data sampling through the DAQ system before applying the earthquake motion.

    a. Idling rotation of the centrifuge stabilizes the test model from sedimentary condition.

    b. Preliminary data sampling before earthquake shaking is required to distinguish the vertical displacements between initial and liquefaction settlements.

10. Apply the earthquake motion to the model.

11. Stop the centrifuge and DAQ operations and transfer the test data from the centrifuge to the remote laboratory via wireless network system.

4.2 Results of centrifuge test

This section presents the experimental results of test USC01, especially: (1) the base input motion in the frequency and time domains; (2) time history of acceleration in the prototype scale recorded by piezoelectric accelerometers (Dytran model 3145A1); (3) time history of pore-pressure recorded inside the test model; and (4) time history of lateral and vertical displacements of test model during and after the earthquake shaking. The vertical displacement of the test model is divided into (1) sedimentation settlement before the beginning of the earthquake motion and (2) porepressure induced settlement after the beginning of the earthquake motion (e.g., Hushmand et al., 1988).

4.2.1 Recorded accelerations

Figure 4-12 shows the horizontal accelerations recorded at various depths of the test model. The maximum acceleration at the ground surface is 0.12 g; which corresponds to a de-amplification of the acceleration due to porepressure buildup; the maximum input acceleration is 0.28 g, at the model base. As shown in Figure 4-12, the high frequency noises in the acceleration record are eliminated using a low pass filter, which is also used for the pore-pressure data, with a cut-off frequency of 200 Hz in the model scale (Oppenheim and Schafer, 1975).

4.2.2 Recorded excess pore pressures

Figure 4-13 shows the time history of excess pore pressures inside the test model at P1, P2, and P3 locations after filtering out high frequency noises with a low pass

filter at cut-off frequency of 4 Hz in the prototype scale (Butterworth Filter with 5^{th} order).

During the test, the pore-pressure changes increases and reaches a plateau. Then the pore-pressure dissipates starting from the bottom as the pore water diffuses toward the ground surface (e.g., Chugh and Vonthun, 1985; Dobry, 1989; Ha et al., 2003). The excess pore pressure builds up to a point that is not sufficient to develop full liquefaction. The P1 transducer recorded that the excess pore pressure reached 34.68 kPa while the confining pressure of soil at same location was 110 kPa. The excess pore pressures and confining pressures at P1, P2, and P3 are shown in Table 4-3.

4.2.3 Recorded lateral displacements

Figure 4-14 shows the lateral displacements measured by the horizontal LVDTs, which were mounted at various heights along the laminar box. The peak transient lateral displacement of ground surface during earthquake shaking at HL4 transducer was approximately 2.25 inches, which corresponded to 0.5 % of the 37.5-foot soil layer thickness. Table 4-4 shows the peak horizontal displacements of LVDTs at various locations, such as HL1, HL2, HL3, and HL4.

4.2.4 Recorded Vertical displacements

Figure 4-15 shows the vertical displacements of the soil surface at 3 different locations. The maximum vertical displacements are approximately 2 inches, 3.7 inches, and 1.5 inches at VL1, VL2, and VL3, respectively. The average permanent

vertical displacement in the prototype is about 2.4 inches, which was about 0.53% of the soil layer thickness.

The vertical displacement is divided into (1) initial settlement and (2) pore-pressure induced settlement (Hushmand et al., 1988). As shown in Figure 4-15, the excess pore pressure reaches a plateau, 20 seconds (prototype scale) after the beginning of the earthquake motion. The total vertical displacement at VL2 is 3.7 inches after combining the settlements of the two phases; the vertical settlement before the earthquake shaking was about 1.8 inches, and the settlement induced by the excess pore-pressures was 1.9 inches. Equation 4-1 shows the formula to compute the total settlement from the two different phases of settlement (Hushmand et al., 1988).

Total settlement = Initial settlement + Liquefaction settlement (4-1)

4.3 Discussion

During the centrifuge test, liquefaction was not fully developed because the excess pore pressures did not reach the confining pressures (Table 4-3). The soil was too dense to be liquefied using the given earthquake motion. The relative density was about 65%, the dry unit weight was16.13 kN/m^3 , and the total unit weight was about 19.9 kN/m^3 at 50 g. The soil might have been not saturated enough to develop enough excess pore-pressures. The model saturation depends on the quality of deaired water and saturation method.

4.4 Summary

A centrifuge test was conducted to evaluate the performance of the USC centrifuge after major improvements of its mechanical, hydraulic, and electrical components. The centrifuge model had a dimension of 9 inch in height, 14 inch in length, and 7 inch in depth. The model used a laminar box filled with Nevada No.120 sand at a relative density of 65%. The test specimen had a dry unit weight of 16.13 kN/m^3 and a total unit weight of19.9 kN/m^3 . The model was saturated with deaired water.

The earthquake motion applied to the model base had a peak horizontal acceleration of .3 g and a frequency of 6 Hz in the prototype scale. The earthquake motion was created from the one used during the VELACS project No. 3 test.

The maximum horizontal acceleration at the top soil surface was 0.12 g through the A4 transducer, which implies that the acceleration was deamplified by porepressure buildup and softening to the soil column. During the test, the excess pore pressure increased and decreased during and after the earthquake shaking. The peak excess pore pressures did not build up enough to reach full liquefaction. At the P1 location, the excess pore pressure reached 34.68 kPa while the confining pressure was initially 110 kPa. The pressure change were however sufficiently to generate permanent ground deformation. The peak lateral displacement at the top of the test model was approximately 2 inches, which corresponded to 0.44% of the 37.5-foot soil layer thickness. The average settlement of the ground surface was about 2.4 inches in the prototype, which corresponded to about 0.53% of the soil layer thickness. The total

settlement was divided into initial settlement and liquefaction settlement. At the VL2 location, the excess pore pressure was observed to reach a plateau, 20 seconds after the beginning of the earthquake motion. The initial settlement and the settlement induced by the excess pore pressures were 1.8 inches and 1.9 inches, respectively.

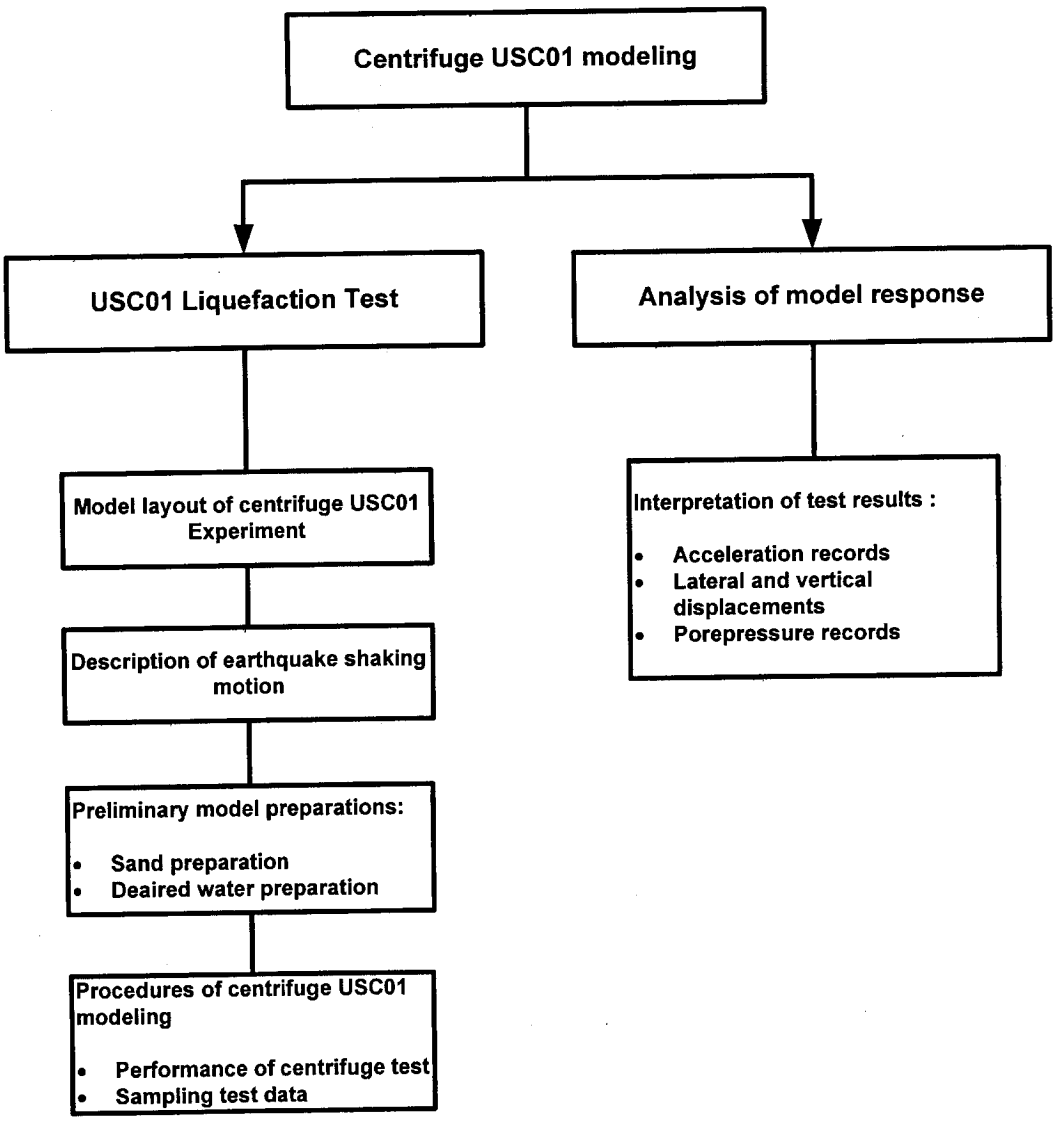

Figure 4-1. Overview of chapter 4.

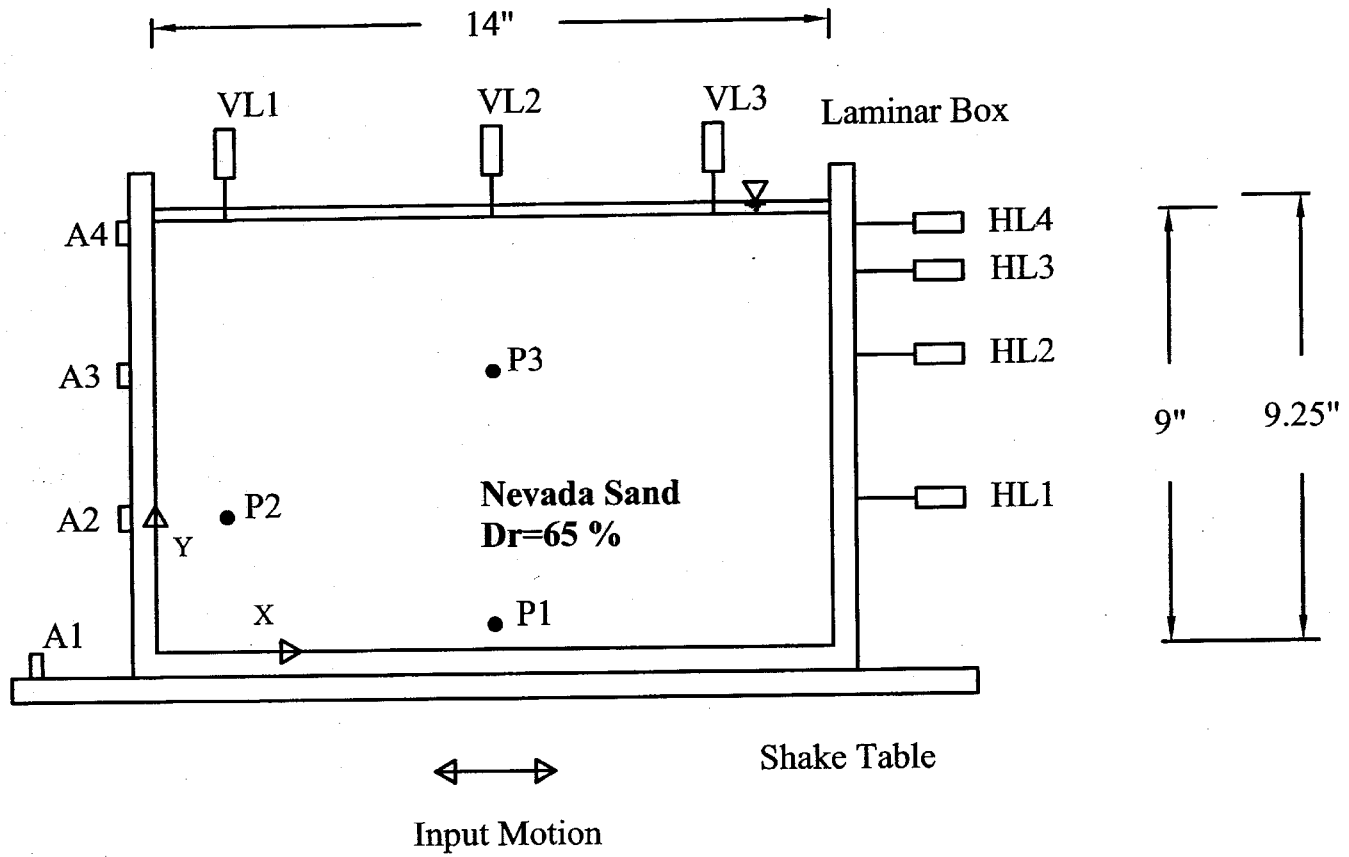

Figure 4-2. Model layout of the centrifuge USC01 test with instrumentation.

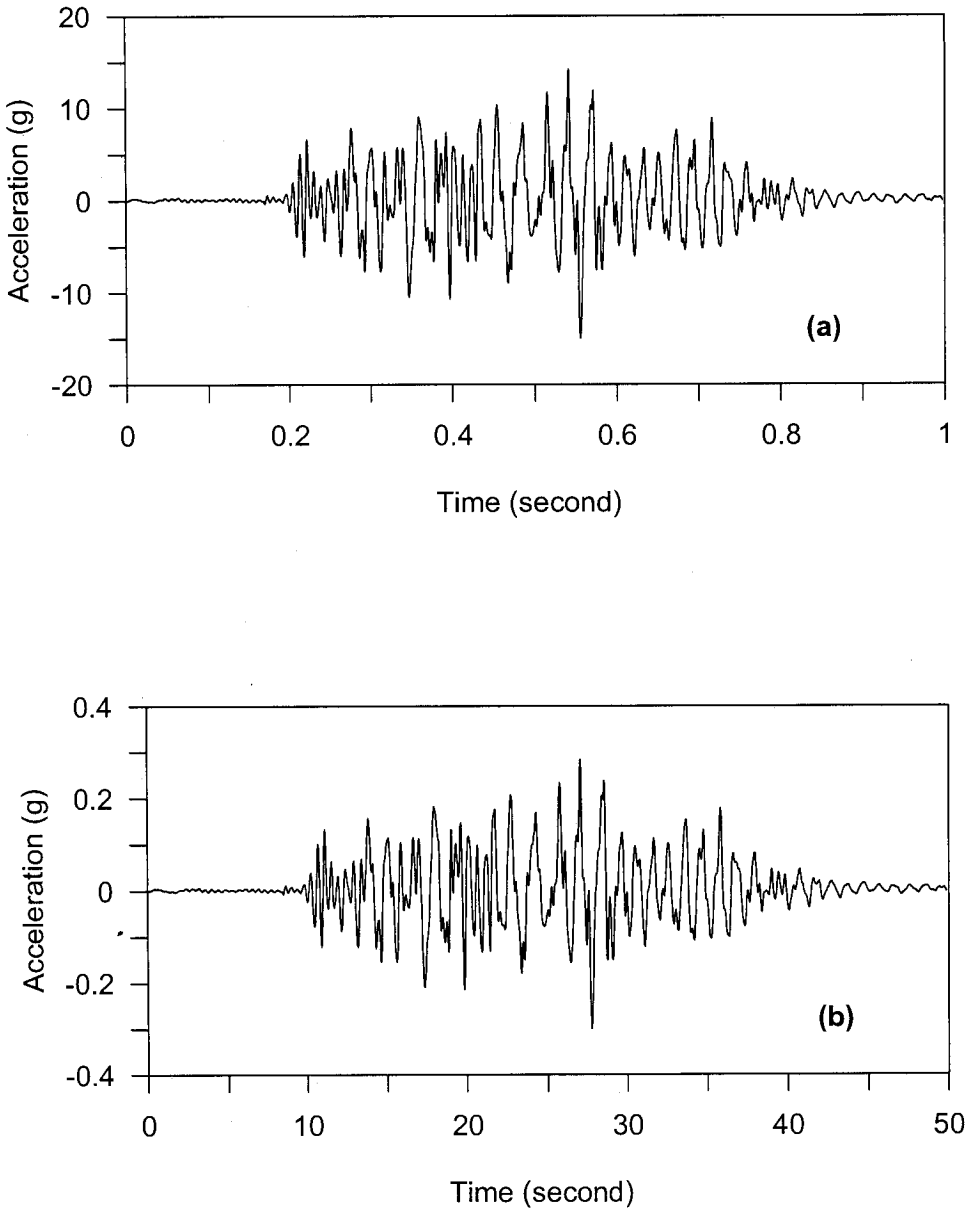

Figure 4-3. Simulated earthquake shaking motion applied to the centrifuge USC01 model: (a) model scale and (b) prototype scale.

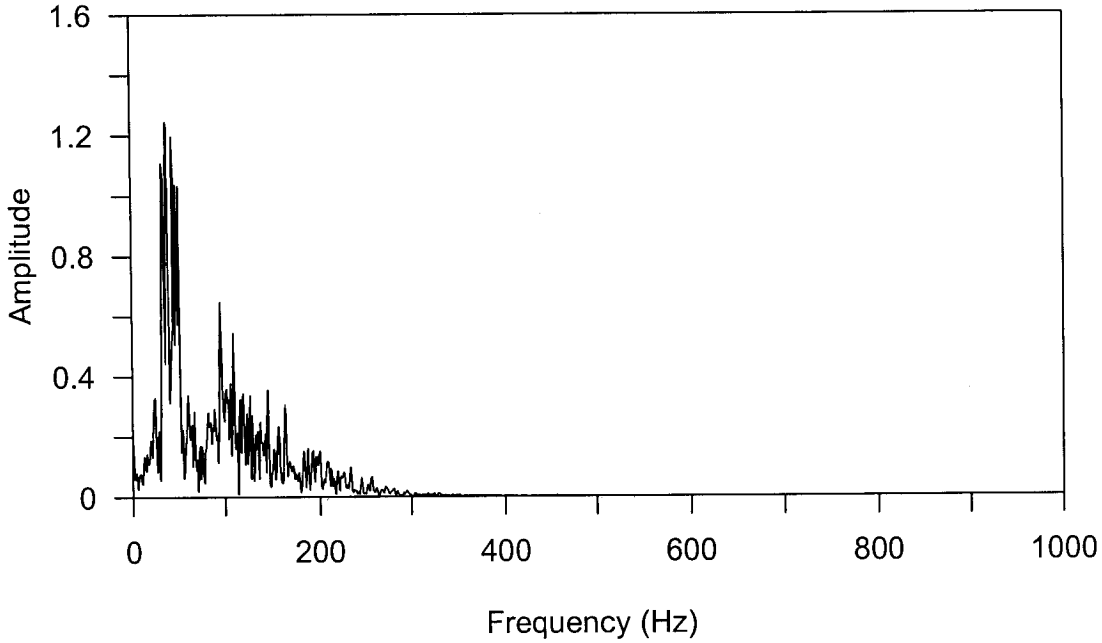

Figure 4-4. Frequency spectrum of simulated earthquake-shaking motion (model scale).

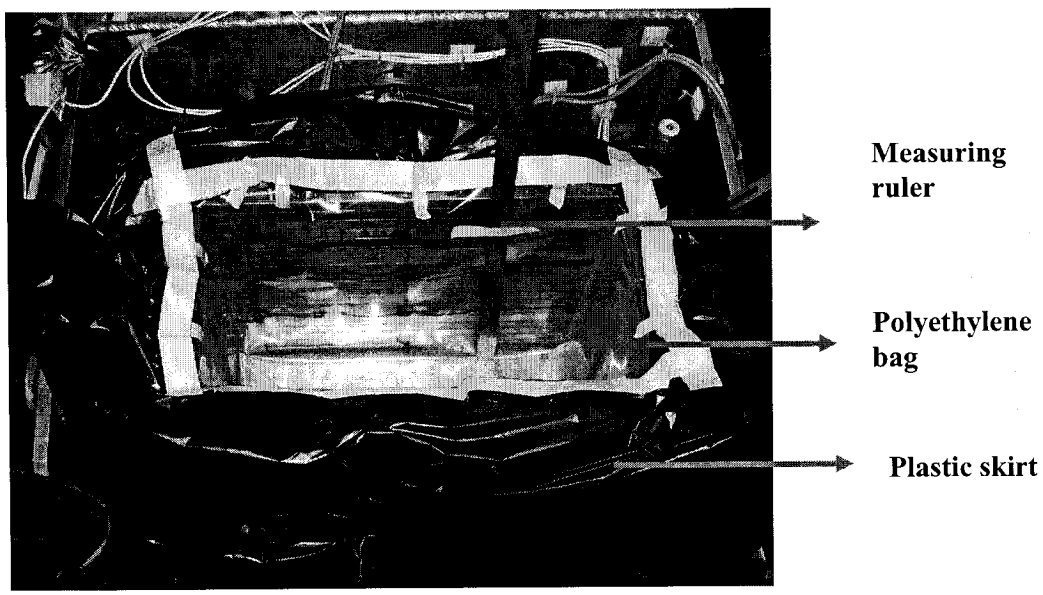

Figure 4-5. Polyethylene bag and plastic skirt protecting the USC laminar box during model construction.

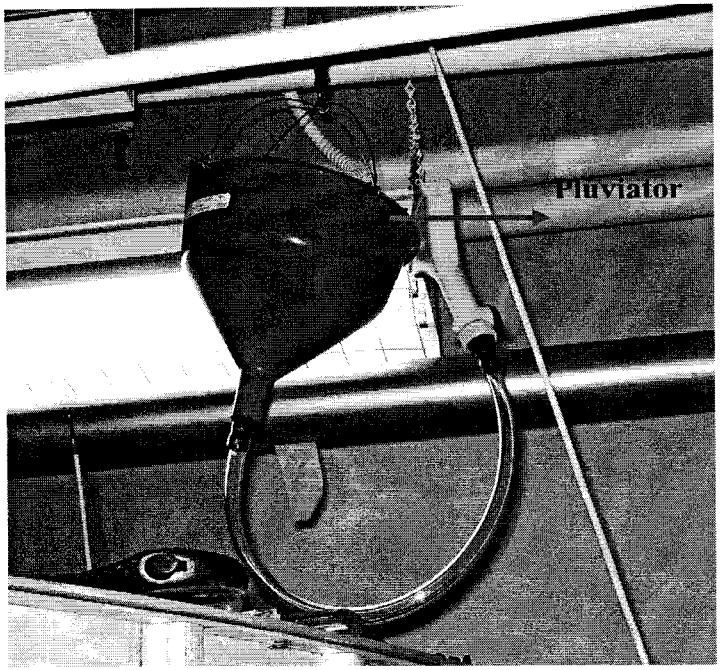

(a)

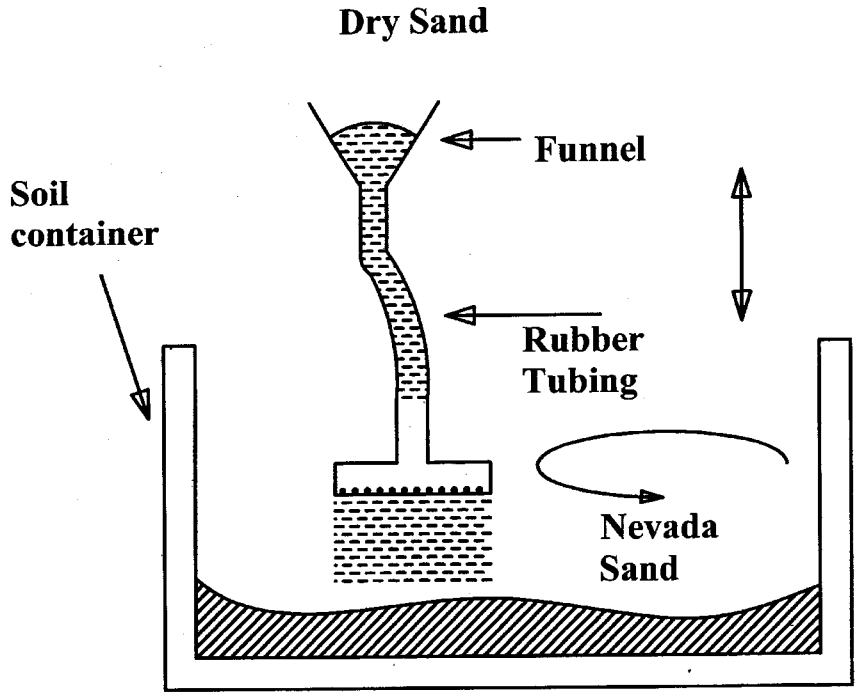

(b)

Figure 4-6. (a) Pluviator used for centrifuge tests; (b) Schematic pluviator used during centrifuge model construction

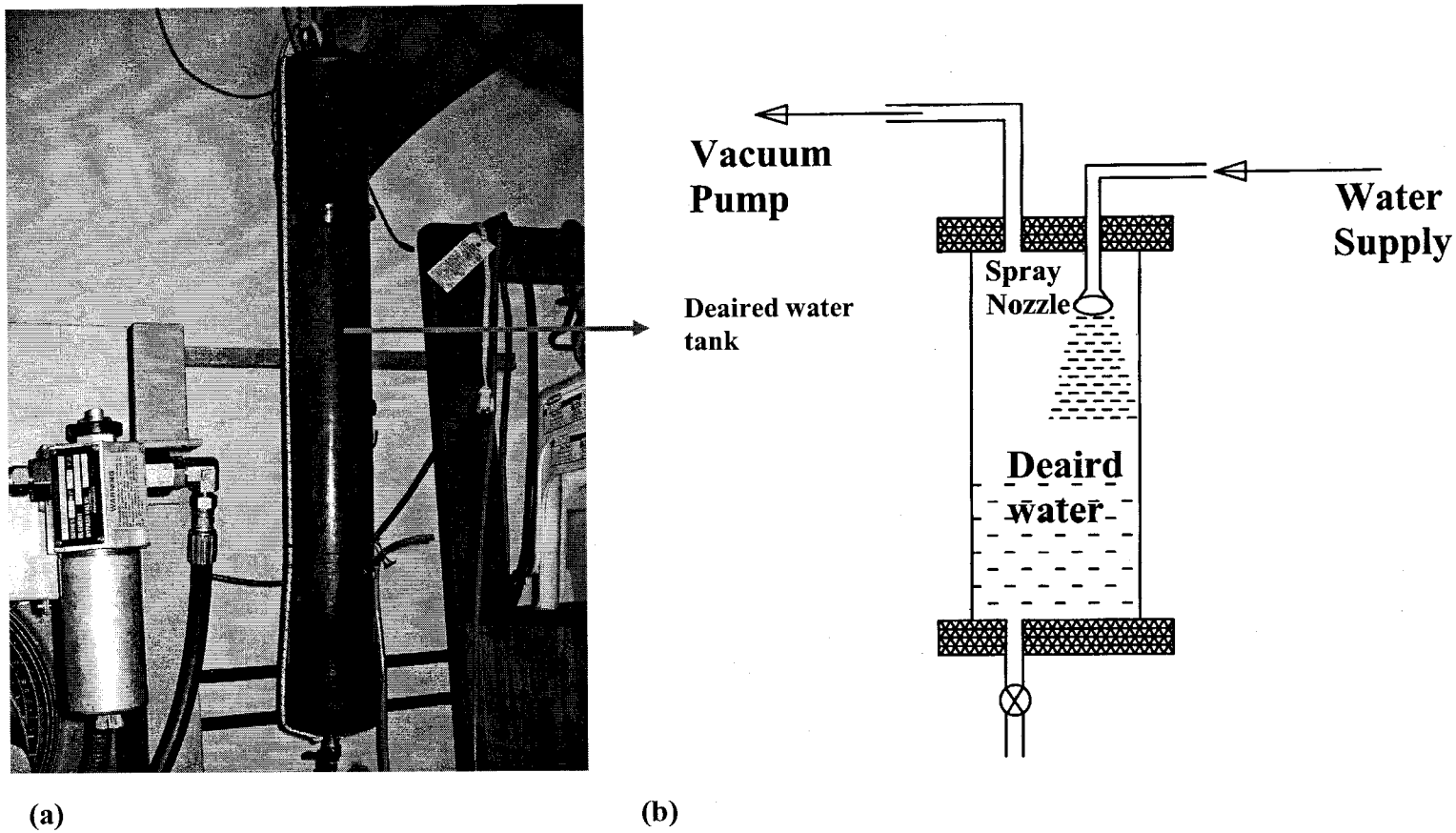

Figure 4-7. (a) Deaired water tank used for centrifuge tests; (b) Schematic diagram of the deairing water tank

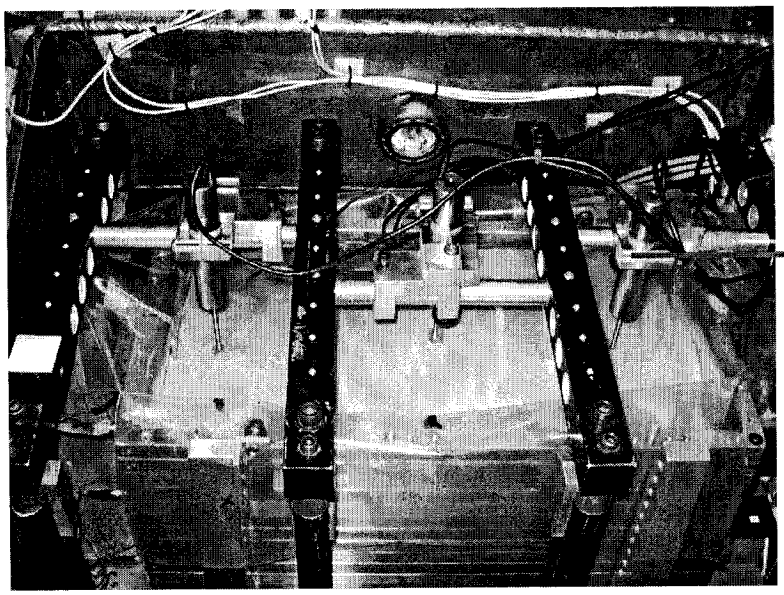

Figure 4-8. Vertical LVDTs installed on the top surface of centrifuge USC01 model.

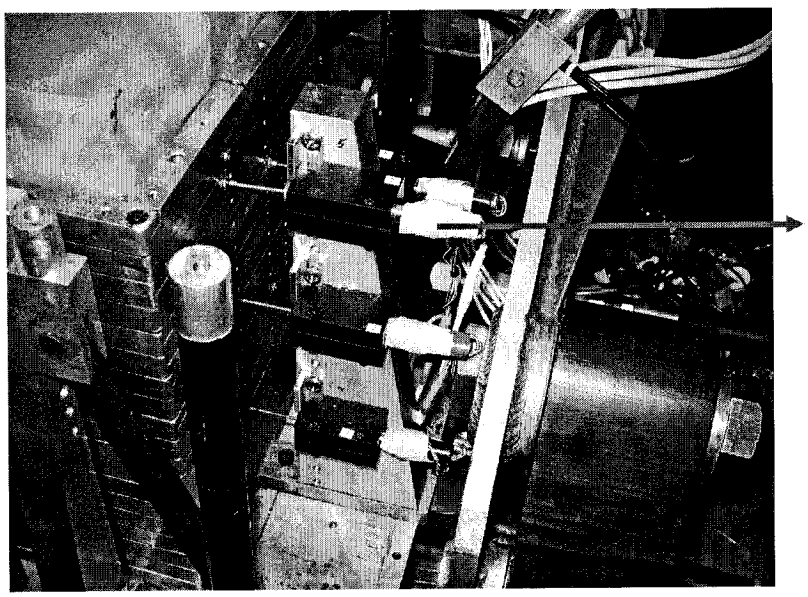

Figure 4-9. Lateral LVDTs mounted on the USC laminar box.

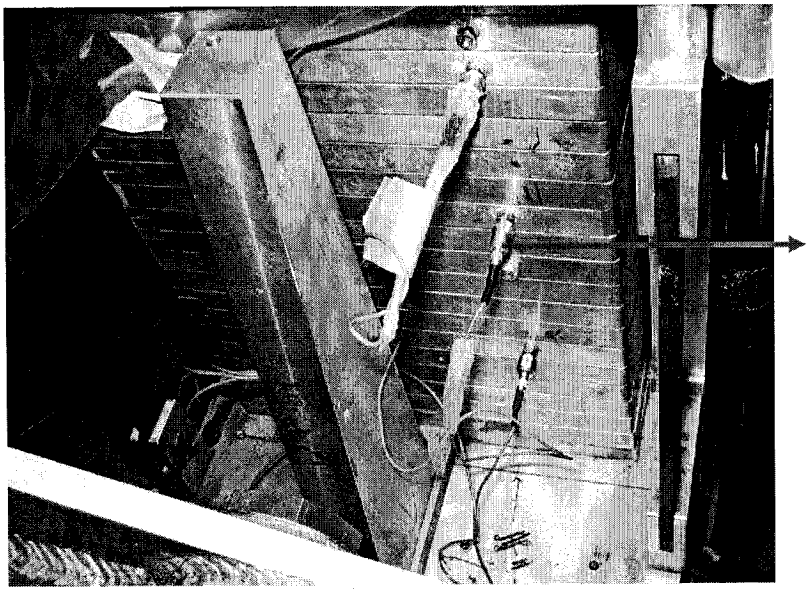

Figure 4-10. Dytran accelerometers mounted on the USC laminar box.

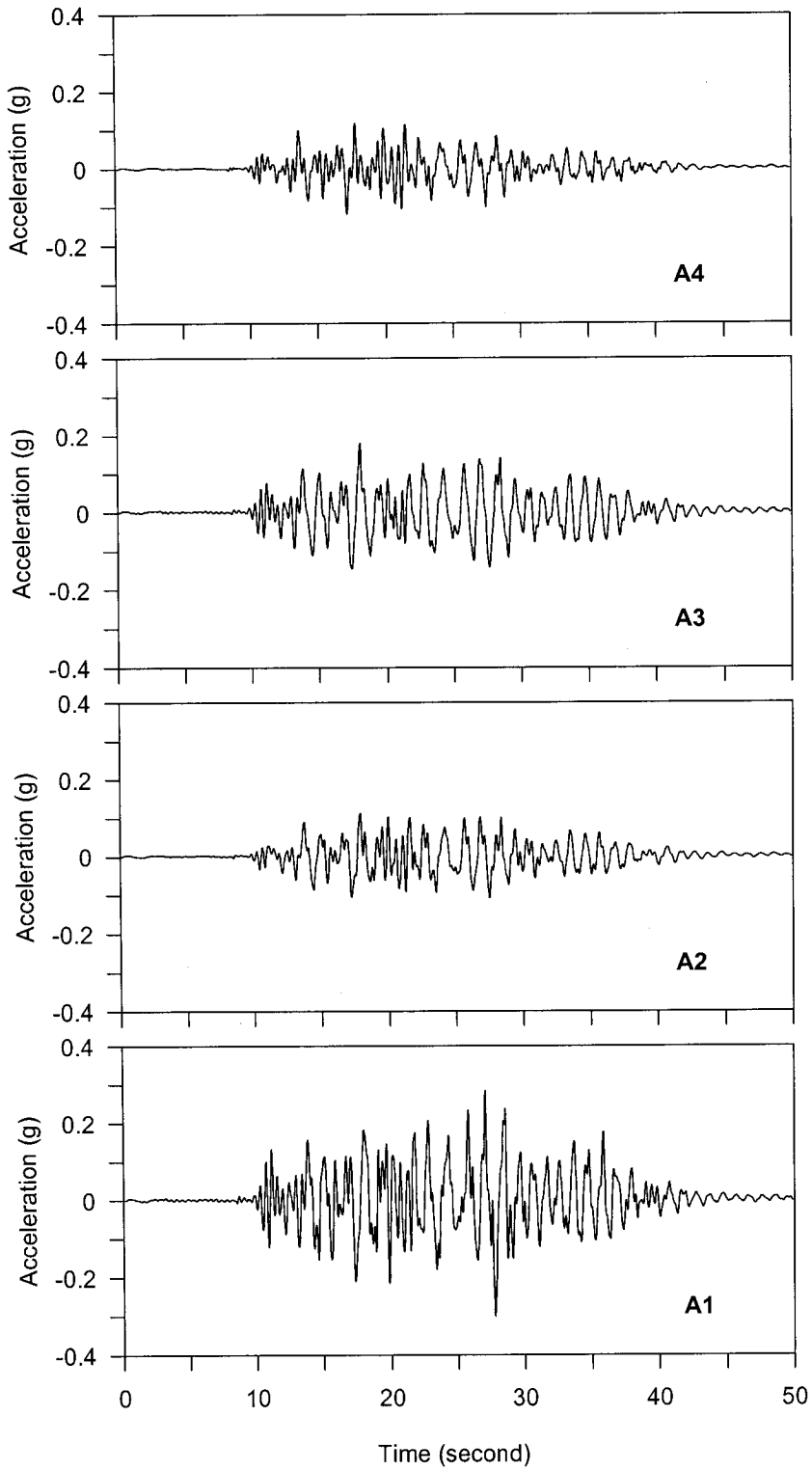

Figure 4-11. Horizontal accelerograms at A1, A2, A3, and A4 locations.

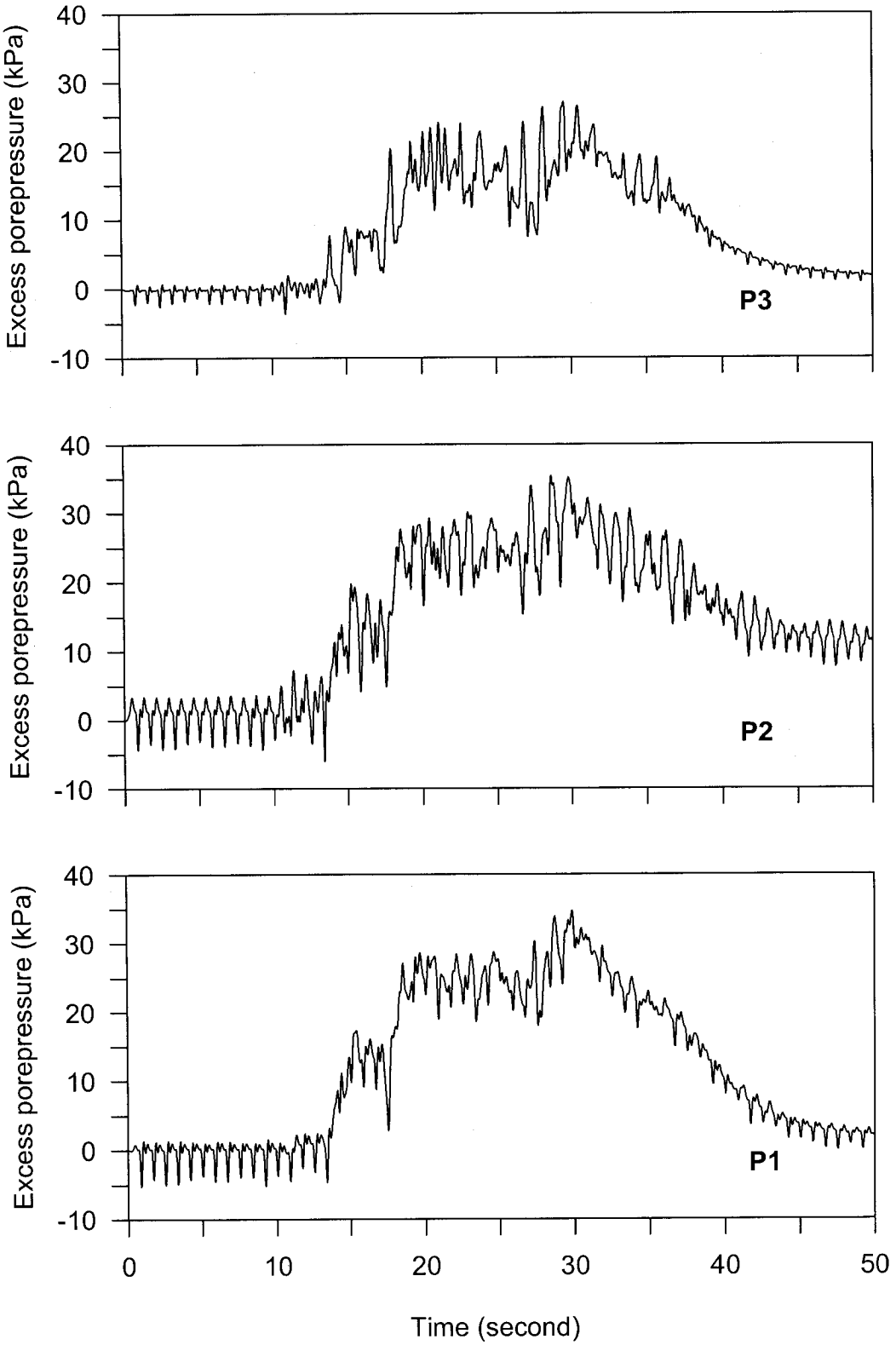

Figure 4-12. Excess porepressures at P1, P2, and P3 locations.

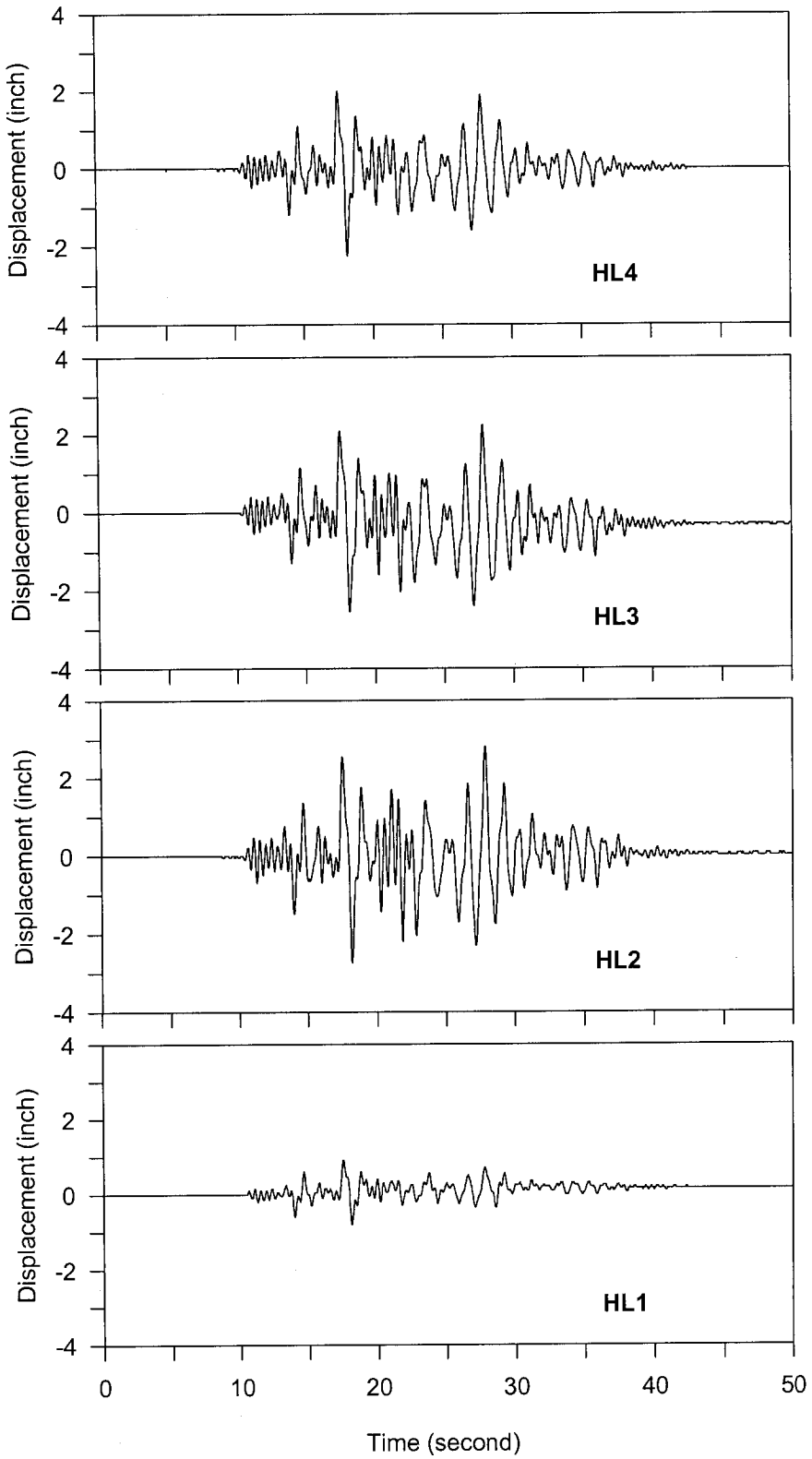

Figure 4-13. Horizontal displacements at HL1, HL2, HL3, and HL4 locations.

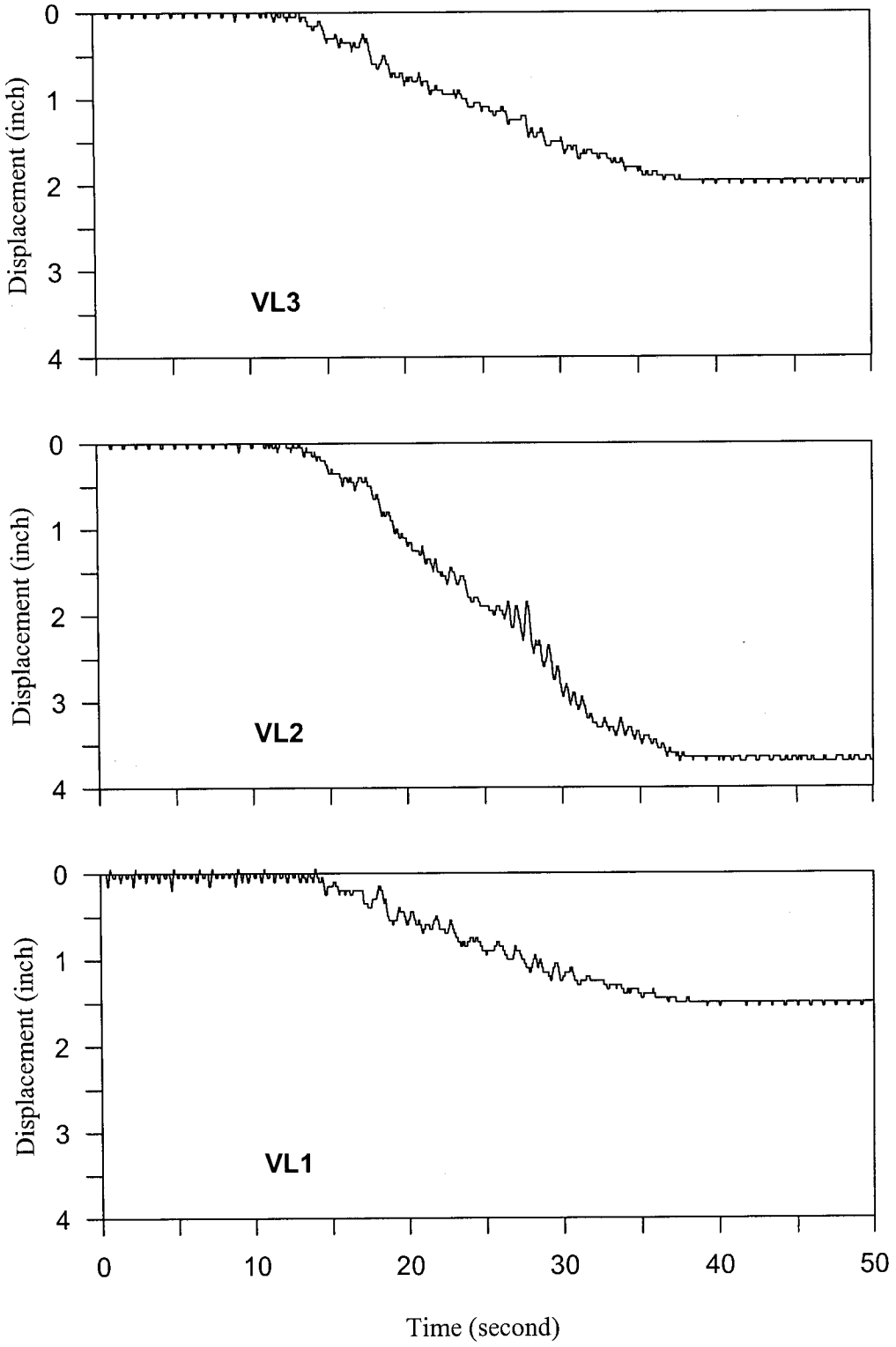

Figure 4-14. Vertical displacements at VL1, VL2, and VL3 locations.

Table 4-1. Transducer locations installed on centrifuge USC01 model.

Transducer	ID	Coordinates (inch)		
		x	y	z
Accelerometer	A1	-2.50	5.00	-0.25
	A2	-0.50	1.00	3.00
	A3	-0.50	1.00	6.00
	A4	-0.50	1.00	8.75
Horizontal LVDT	HL1	14.50	2.50	3.00
	HL2	14.50	2.50	6.00
	HL3	14.50	4.50	7.75
	HL4	14.50	2.50	8.75
Porepressure transducer	P1	7.00	3.50	0.50
	P2	1.50	3.50	2.75
	P3	7.00	3.50	5.75
Vertical LVDT	VL1	1.50	3.80	9.00
	VL2	7.00	3.80	9.00
	VL3	11.60	3.80	9.00

Table 4-2. Properties of Nevada sand.

Property	Value	Unit
Specific Gravity Gs	2.670	
Maxmum dry unit weight	17.330	kN/m^3
Minimum Dry unit weight	13.870	kN/m^3
Maxmum void ratio	0.887	
Minimum void ratio	0.511	
Void ratio at Dr = 40%	0.737	
Void ratio at Dr = 60%	0.661	

Table 4-3. Excess porepressures and soil confining pressures at P1, P2, and P3 locations.

	Max. Excess porepressure	Confining pressure
PPT	(kPa)	(kPa)
P1	34.68	108.93
P2	35.37	80.92
P3	27.05	43.57

Table 4-4. Peak lateral displacements of USC01 model at HL1, HL2, HL3 and HL4 locations.

LVDT	Max. Lateral Displacement (inch)
HL1	0.9
HL2	2.8
HL3	2.25
HL4	2.25

5 Metadata modeling of centrifuge model test

5.1 Introduction

Data modeling in civil engineering had been scarcely used to document experimental data and information until NEES (Network for Earthquake Engineering Simulation). The NEES project was funded by the National Science Foundation (NSF) to share experimental resources among researchers and to enhance the performance of the nation's civil infrastructure (NSF, 2006). Data modeling is defined as the analysis of data objects and the relationships to other data objects (Webopedia, 2006). Metadata modeling was developed to complement data modeling and to provide researchers with data about data, which are necessary to understand how data was obtained (Bardet et al., 2004a~e). The main functions of metadata models are to organize and store the information describing the experimental results, equipment and testing procedures.

The centrifuge metadata model was developed based on the experiences gained during previous data modeling effort. The metadata model uses metadata, defined as information about data, to define data objects and relate them to other data objects. This chapter reviews the structures and functions of the metadata model and illustrates its usage and usefulness with the centrifuge test of Chapter 4. The objectives of Chapter 5 are to explain the concepts and premises of metadata modeling and to apply the metadata model for web reporting and computer visualization.

5.2 Data Modeling Tool: Protégé software

The Protégé software was used to design and develop a metadata model with a graphical user interface (GUI). Protégé is open-source software and has several plug-ins options (Protege, 2005). Figure 5-1 shows the interface window of Protégé software, showing the metadata model of the centrifuge test USC01.

5.3 Premises of the metadata model

The metadata model was developed based on recent developments in computer information and web technologies, and on a previous metadata model proposed by Bardet et al.(2004b; 2004c; 2004d; 2004e), which rejects superfluous details and retained high-level information. Metadata describe other data. For instance, a library catalog contains information (metadata) about publication (data). This example represents the metadata, e.g., author, publisher, year, and key words to understand the publication in a library. Metadata explain the data object with correlated information. The metadata model is constructed by answering the following questions: who, when, where, what, why, and how.

Figure 5-2 shows the concepts of data, metadata, and metadata applications using three separate layers. The bottom layer contains the data stored in files and the middle layer contains metadata about the data. The metadata model glues together the data and metadata to produce a picture of how the data were produced from experiments and simulations (Bardet et al., 2005).

When we take a picture with a digital camera, information such as date, time, and file format are saved beside the picture. That additional information can be defined as metadata. The top layer represents various type of metadata applications where data and metadata are used together to produce comprehensive data reports and computer simulations. These applications help other researchers replicate the same test using the metadata support.

The metadata model organizes and connects data through object-oriented classes. The classes cover File, Person, Organization, Task, and Event. The classes sort and group the data and the metadata through attributes into specific categories (Bardet et al., 2005). The following section describes the metadata classes in detail.

5.4 Metadata modeling

The following section introduces the metadata model, which applies to all centrifuge experiments, and illustrates its application using the centrifuge test of Chapter 4.

5.4.1 Metadata classes

The metadata model is made of 11 classes that fully describe centrifuge tests from the initial test design to the final data processing steps. These classes are: (1) Activity, (2) Organization, (3) Worker, (4) Person (5) File, (6) Publication, (7) Configuration, (8) Equipment, (9) Specimen, (10) Label, and (11) Software. Figure 5-3 shows the relations between the classes. The arrows pointing to the objects are the attributes as shown in Figure 5-3 (Bardet et al., 2005). The metadata model reuses the

information and data of classes through the attributes and eliminates redundant information among classes.

5.4.1.1 Activity class

The Activity class is composed of three subclasses: Project, Task, and Event. The Project class is the highest level of Activity, which organizes all information. Under Project class, the Task class is defined to organize the Event class and can have several Event classes (Bardet et al., 2005). The Task class organizes Event classes in the same way as chapter headings organize paragraphs in a document.

The Event class is an atomic level of activity to construct the project. Table 5-1 and 5-2 list the Task and Event classes for the centrifuge test USC01 with time records. The time records show how much time is required for a specific Event or Task. For test USC01, there are 10 Events grouped into 6 Tasks. Figure 5-4 and Figure 5-5 show the instances of Task and Event classes through Protégé software.

5.4.1.2 Worker, Person and Organization classes

The Organization class presents any group, in which individuals conduct research and/or business. The Organization class might present a school, lab, or any specific organization that conducts, and/or supports the project. Figure 5-6 shows the instances of Organization class for test USC01.

The Person class presents an individual who is related to the project through the Organization, Software, Equipment, Publication, Project and Task classes. Characteristics of the Person class are independent of the Activity class such as the

Event, Task, and Project classes. In other words, when an individual in the Person class plays a role in the Organization class, the individual is related to the project through the Worker class (Bardet et al., 2004e). The Worker class has a new attribute (i.e., role), compared to the Person class. There are many roles such as principal investigator, research assistant, and technician that aid in classifying the individual in the Worker class. Figure 5-7 shows the individuals in the Person class.

5.4.1.3 File class

The File class is composed of various types of files, such as document, drawing, and test data, related to centrifuge test. Figure 5-8 depicts a window of Protégé, listing the instances of File class. EQMotion is a subclass of the File class, introducing additional information on the characteristics of earthquake motion through four additional attributes (Bardet et al., 2004e): maxValue (maximum value of acceleration), scaleFactor (scale factor, N, of the centrifuge model test), samplingRate (a sampling rate through the DAQ system) and uom (unit).

5.4.1.4 Publication class

The Publication class represents technical documents such as manuals, journals, and reports, which are related to the project. For example, the Publication class can be authored by a Person class through the attribute "is_authored_by" as shown in Figure 5-9 (Bardet et al., 2005).

5.4.1.5 Configuration class

The Configuration class does not describe the activity but the state of an object at a given time. The Configuration classes are independently called by related other classes such as Event and Task classes through the attribute "is_configured_by" (Bardet et al., 2005). New Configuration class can be created by adding new information to previous Configuration class. Reconfiguration is useful to avoid repetitive information during consecutive experimental works or parametric studies.

5.4.1.6 Equipment and Software classes

The Equipment class represents all equipment with all parts related to the research, and the Equipment class is organized and stored like a storage inventory. The Equipment class is linked to the Organization class through "is_manufactured_by" and "is_ownded_by" attributes (Bardet et al., 2005).

The Equipment class has a Sensor subclass that has calibration data of the transducers involved in the research. The attributes of the Sensor subclass present the sensor information, such as sensor type, sensor range, and other specifications of the transducers. Additional information for the sensor is referred through the "is_descbribed_in" attribute to another class, like the Publication class (Bardet et al., 2005).

As shown in Figure 5-10, the Software class is configured by the attributes, such as "is_authored_by", "is_described_in", "Homepage", and "Description" (Bardet et al.,

2005). For example, DasyLab and DaqView are software used for in the DAQ system during test USC01.

5.4.1.7 Specimen class

The Specimen class is a generic term representing all the subjects investigated by experiments or computer simulations (Bardet et al., 2005). Therefore, the Specimen class categorizes highly customized objects within the research project. For test USC01, the test model was prepared with Nevada sand, deaired water, and different types of transducers. This test model is classified into the Specimen class with the list of used transducers.

5.4.1.8 Label class

The Label class represents all titles of the objects such as sensors, equipment, and workers that are related to the metadata model. The aim of the Label class is to shorten the full lengthy names of the objects used for the experiment and computer simulation. Note that labels should be short and easy to understand what they stand for at a glance. Figure 5-11 lists instances of the Label class for test USC01.

5.5 Application of metadata model

The applicability and validity of the metadata model can be demonstrated through the following applications: (1) web reports of experiments, and (2) computer simulations (i.e., the model in 3-D visualization).

Web reports can be generated using plug-ins of Protégé (i.e., XML plug-in), which converts OWL metadata into XML metadata, then XML data into HTML files

through a transformation engine coded using Java and XSL languages (e.g., Aiken and Davis, 2000; Harold, 2001; e.g., Knublauch et al., 2004).

A computer simulation, which is referred to as "Shaker", was developed by the Center for Geotechnical Modeling (CGM) at UC Davis to visualize a centrifuge test virtually. The visualization of test USC01 presents the test model with the laminar box in 3-D views with the responses and locations of transducers. The visualization shows the time history of selected transducers, following the earthquake shaking motion (Weber et al., 2003). The metadata model supplies the data required to understand test USC01. It therefore simplifies the preparation of input files for Shaker visualization.

5.5.1 Web reports

Web reports are efficient methods to exchange experimental data and computer simulations over the Internet. One of the benefits of the metadata model is its ability to generate web reports automatically and therefore to update rapidly a centrifuge web site. This approach helps researchers to save time in modifying and replacing information (Bardet et al., 2004c).

The Protégé software has a function to generate XML files for the metadata model (Knublauch et al., 2004). Additional computer codes were developed to transform XML files into HTML files. These codes (e.g., HTMLGenerator.java) use XLS files to design the layout of web report. Figure 5-12 shows how to generate web reports

using the metadata model and Protégé. Details about XML, HTML, and other computer languages can be found in Bardet et al. (2004c).

The web report, which describes test USC01, is shown in Figure5-13. Figure 5-14 shows the inventory page of the website, showing the transducers used in the centrifuge test.

5.5.2 Shaker visualization of the metadata USC01 model

The Shaker software is a tool to visualize the response of a large number of sensors during a centrifuge experiments in 3D views. Shaker represents transducers with different shapes and colors. Using a vector-display method, it shows the dynamic sensor responses and locations (Weber et al., 2003).

5.5.2.1 Input Files of Shaker visualization

The input files for Shaker are separated into two groups: (1) transducer information with location coordinates, and (2) dynamic responses of transducers induced by earthquake shaking motion. The Shaker software needs to load the experimental information file (EXP file), like an usc01.exp file, for displaying the results of test USC01. The experimental information file (i.e., usc01.exp) links all the other required files (Brandenberg, 2004): (1) sensor locations (usc04.IL), (2) earthquake motion data (usc012.EL), (3) channel gain list (usc01.CGL), and (4) container geometric data (containerusc.IV).

5.5.2.1.1 Experiment information file (EXP file)

The experimental information file is a critical file that combines the information of several files such as EL, IL, and IV extension files, loads all necessary information, and starts Shaker. All files should be located within the same folder with the USC01.EXP file. Table 5-3 shows all the linked files to usc01.EXP file that are required to run Shaker.

5.5.2.1.2 Event list file (EL file)

The event list (i.e. usc012.EL) file contains the information about the earthquake motion, e.g., name, time, and date of earthquake event. The event list file contains a channel gain list (usc01.CGL) listing all the transducer labels and the earthquake motion data (usc014.TXT) as shown in Table 5-4. The first two lines of the event list file are reserved for headers. The remainder of the file contains earthquake shake events listed one per line.

5.5.2.1.3 Instrument list file (IL file)

The instrument list (USC04. IL) file presents the sensor locations in the x, y, and z coordinates system, sensor types, sensor labels, and sensor response direction (horizontal or vertical direction). The contents of the USC04.IL file are shown in Table 5-5.

5.5.2.1.4 Container geometry file (IV file)

The container geometry (containerusc.IV) file consists of the geometric coordinates of each ring of the laminar box used for the USC01 test in the VRML file or Open Inventor file format. In addition, the geometry file can define or change the specifications such as the degree of transparency and colors of the test model (Brandenberg, 2004).

5.5.2.1.5 Channel Gain list file: CGL file

The channel gain list (usc01.CGL) file organizes the labels of all transducers used for the test. The first two lines are reserved for headers. The other lines list the labels of sensors used in the centrifuge test.

5.5.2.2 Example of 3-D visualization: USC01 test visualization

This section discusses the output and procedures of SHAKER, using the example of test USC01. Detailed instructions about Shaker and its input files can be found in Webber et al (2003). As shown in Figure 5-15, Shaker has a main window for presenting the test model and its transducers, control buttons to change the views of model, a window showing transducer responses, and control buttons to stop, play, rewind, and forward the simulation process. Shaker is run as follows:

1. When Shaker starts, it loads the experiment information file (EXP files).

2. Next, the user loads the event list file (EL file) that contains the transducer responses.

3. Once the program reads the data from the event list file (EL file), the main viewer displays the test model and the transducers and the response of the selected transducer in main windows.

5.6 Summary

Chapter 5 presents the metadata model and demonstrates its applicability by describing a particular centrifuge model and generating web reports and computer simulations. The metadata model introduces the concept of metadata to describe the data modeling process, which should help researchers to understand better and replicate centrifuge experiments. The metadata required to document a centrifuge test can be generated using the Protégé program. The metadata are organized into classes that characterize different kinds of object, e.g., Organization, File, and Task. The Metadata model is useful to generate web reports and computer visualization; it is a powerful ways to exchange complete information among researchers and engineers, and therefore pave the ways for a better utilization of centrifuges all around the world.

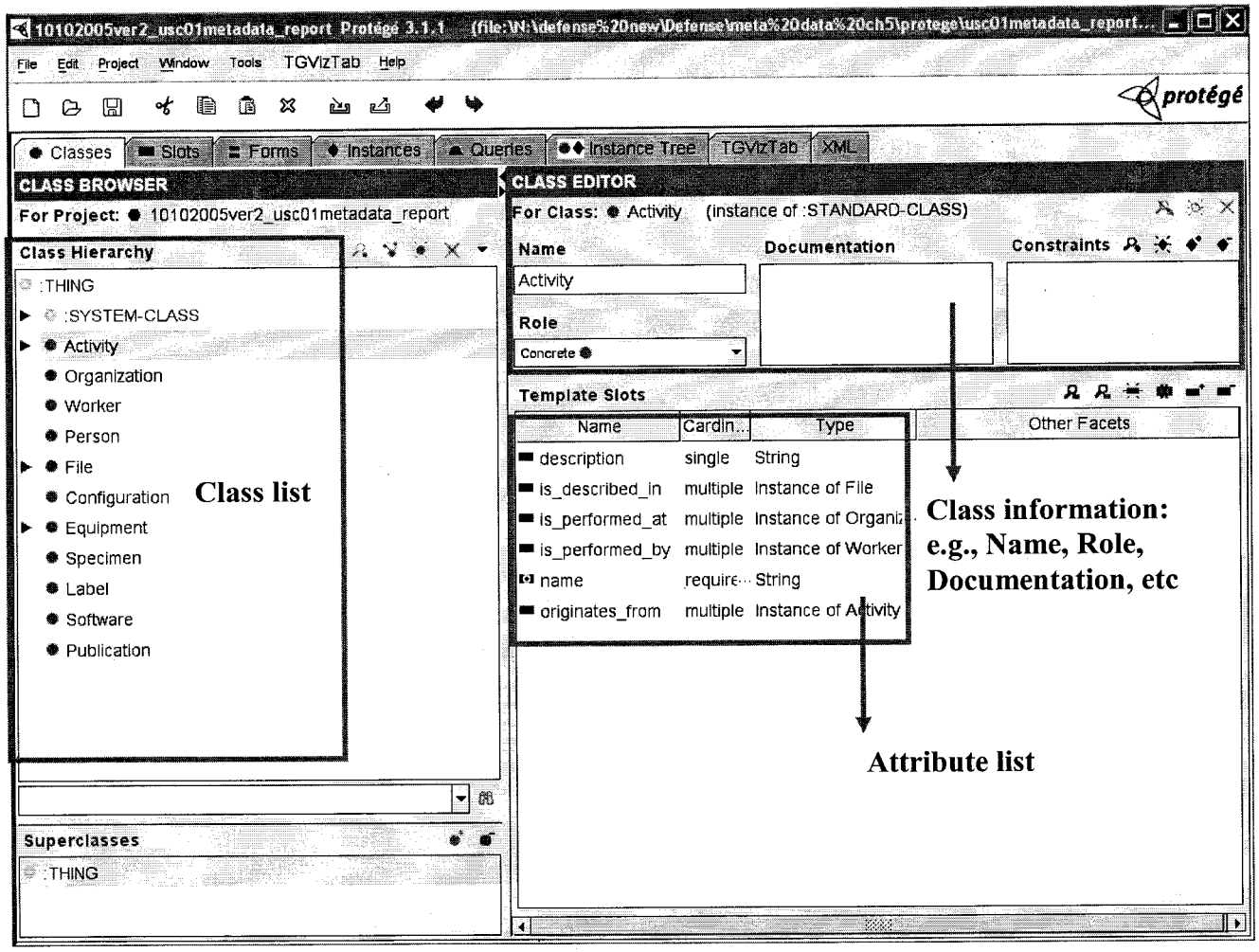

Figure 5-1. Protégé 3.0 display of the centrifuge USC01 experiment.

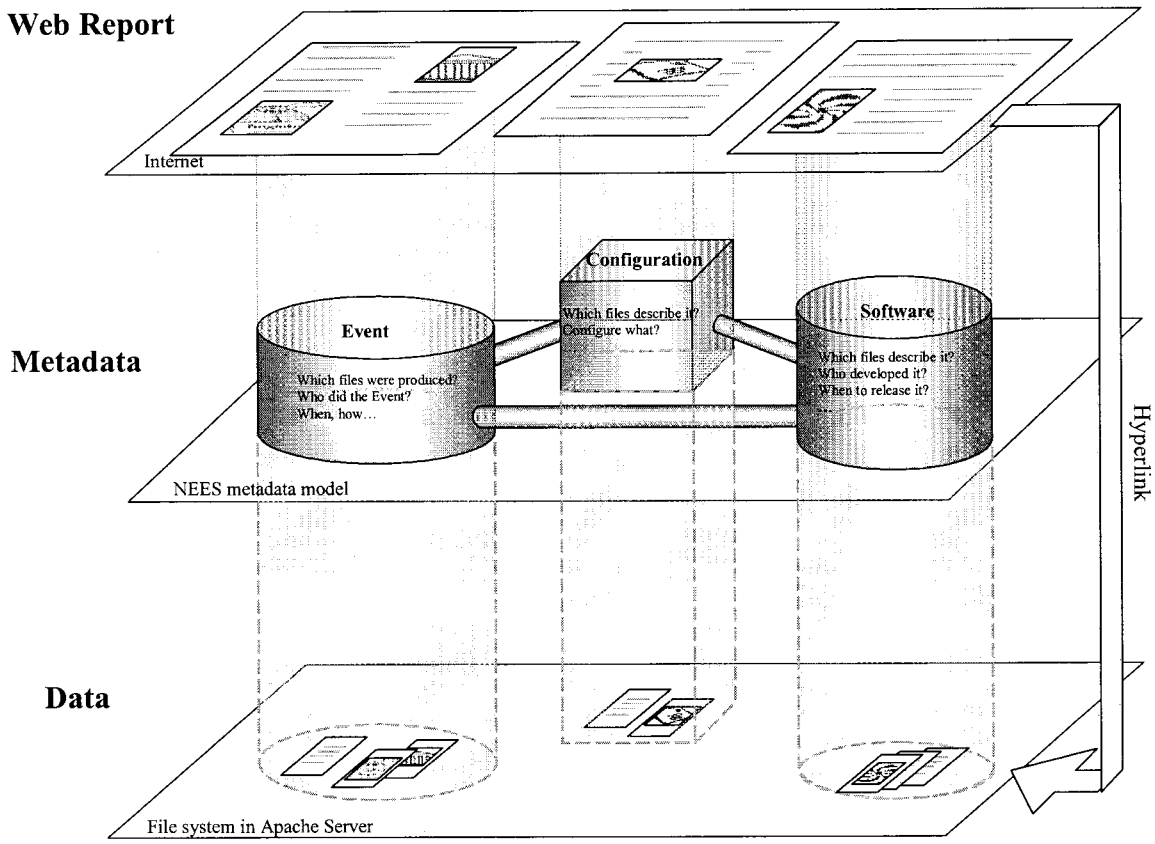

Figure 5-2. Relationship among data, metadata, and metadata application (Bardet et al., 2005).

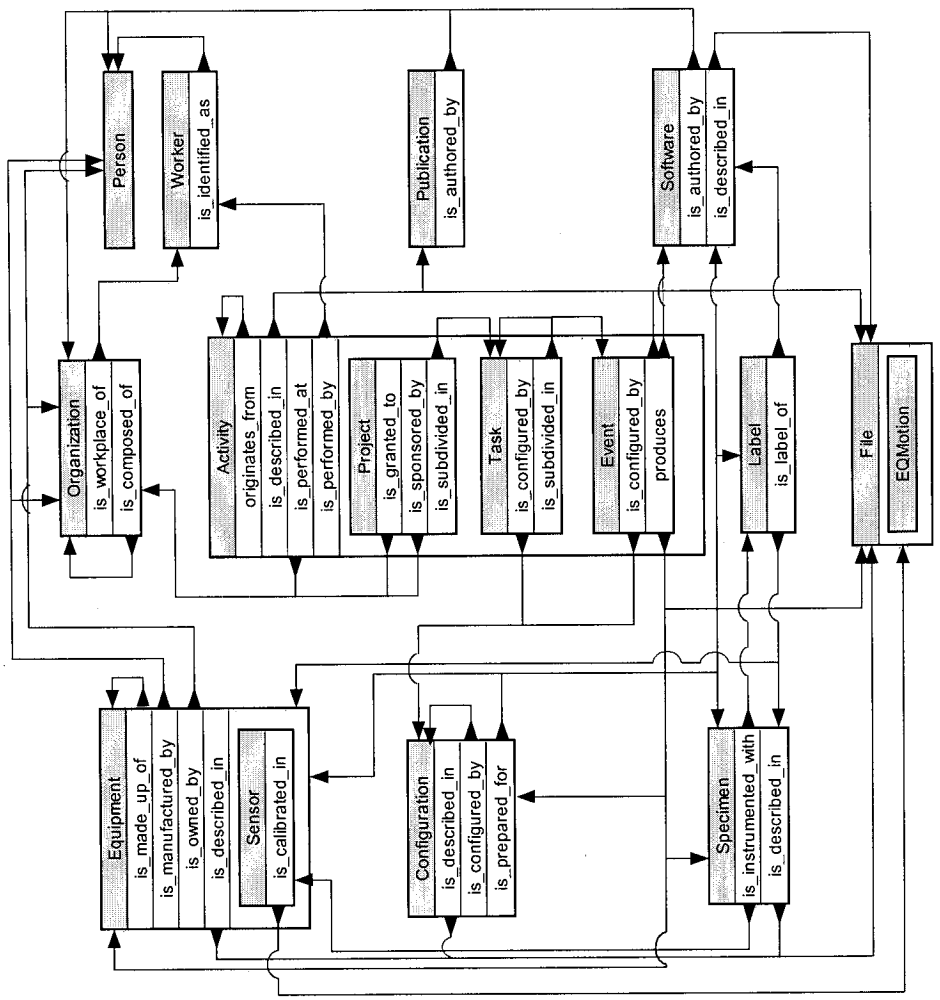

Figure 5-3. Relationships between classes of metadata model (Bardet et al, 2004e).

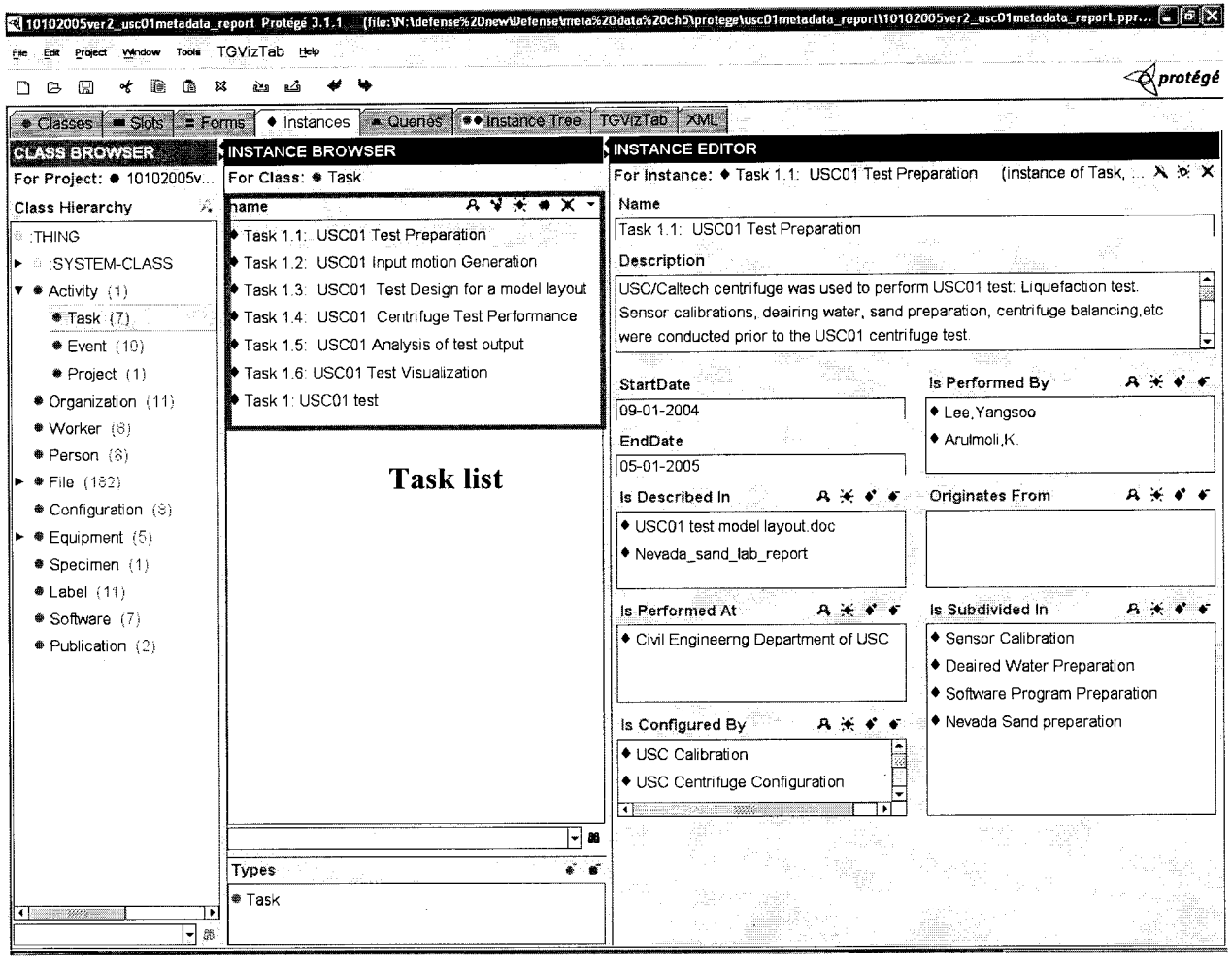

Figure 5-4. Instances of Task class.

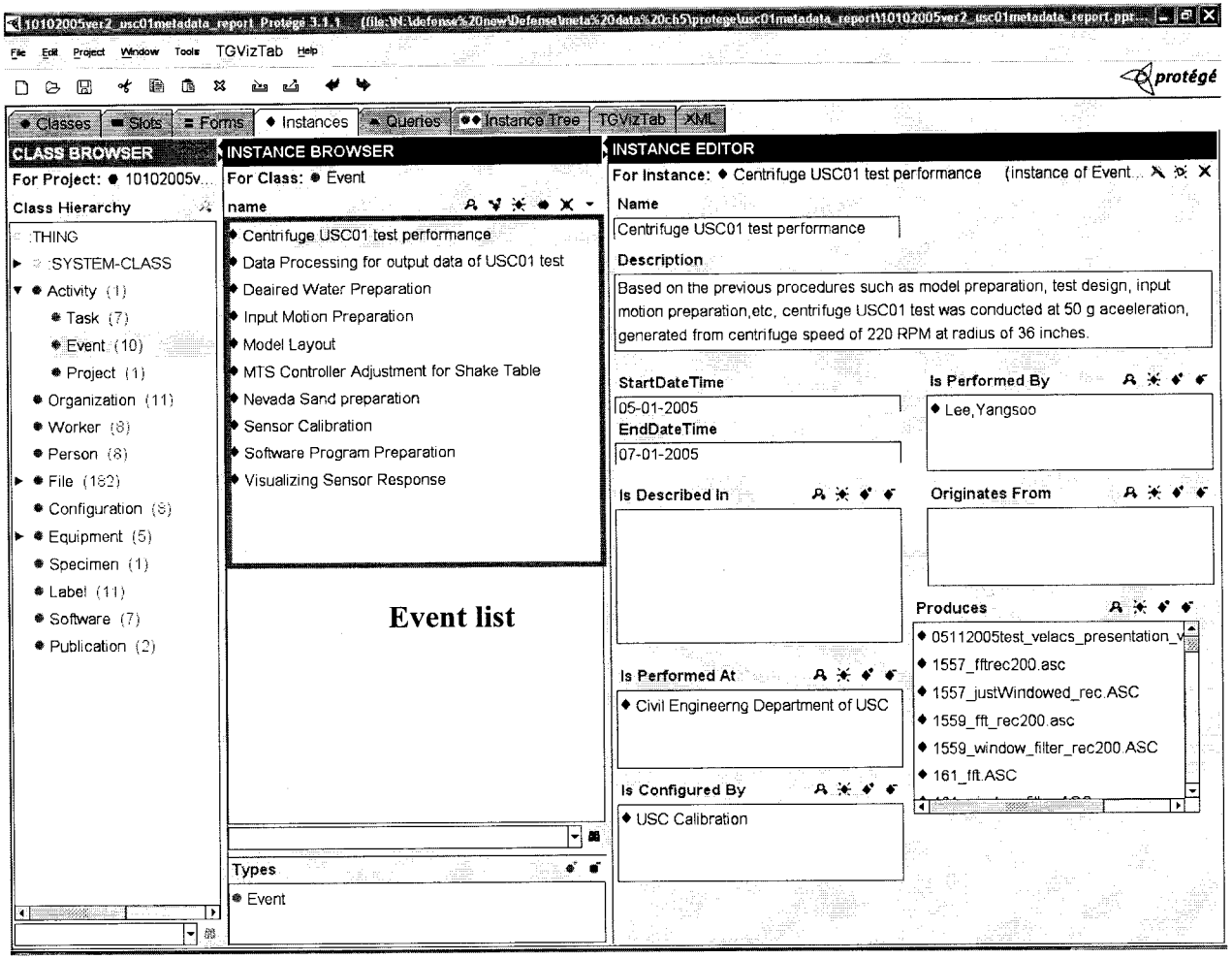

Figure 5-5. Instances of Event class.

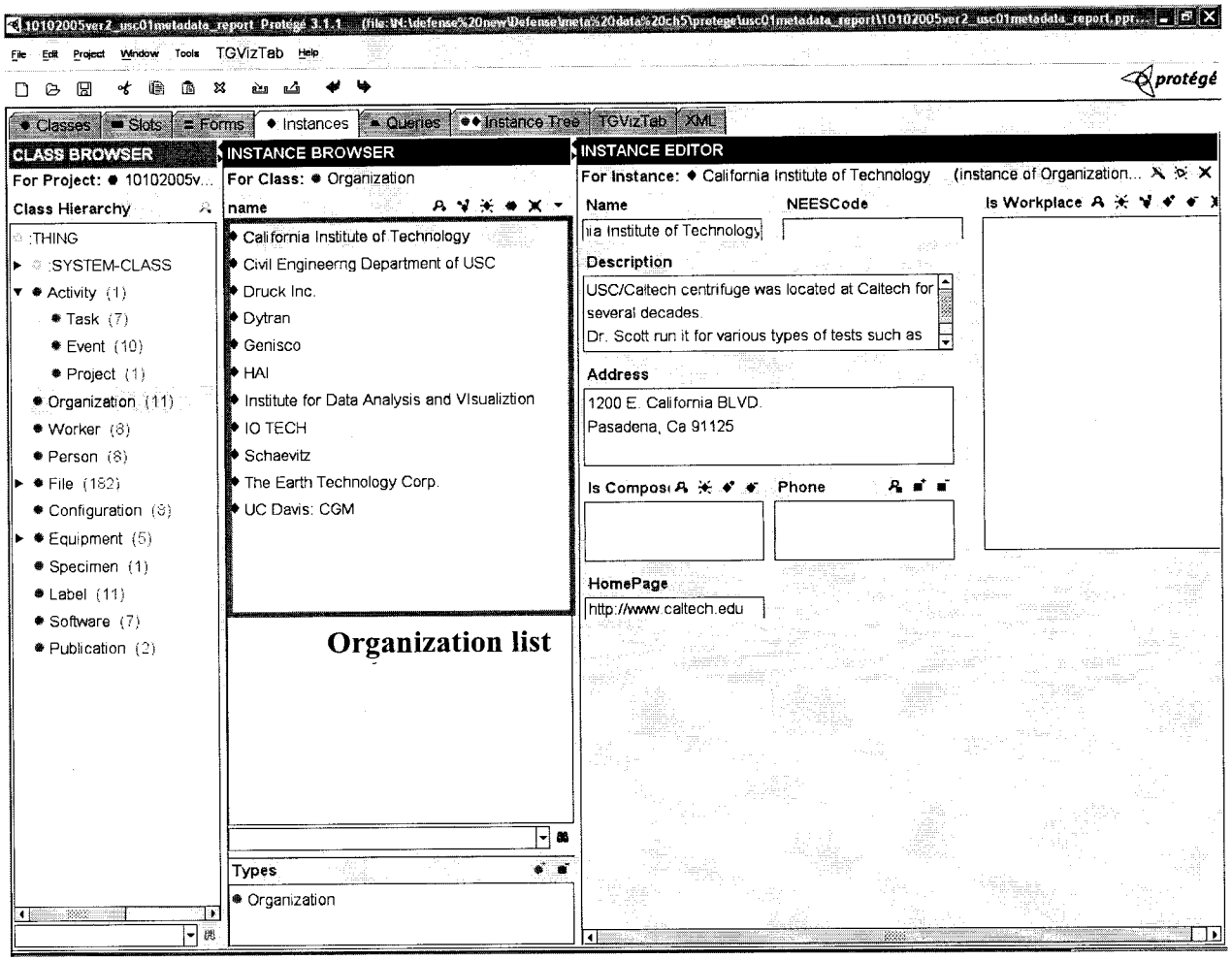

Figure 5-6. Instances of Organization class.

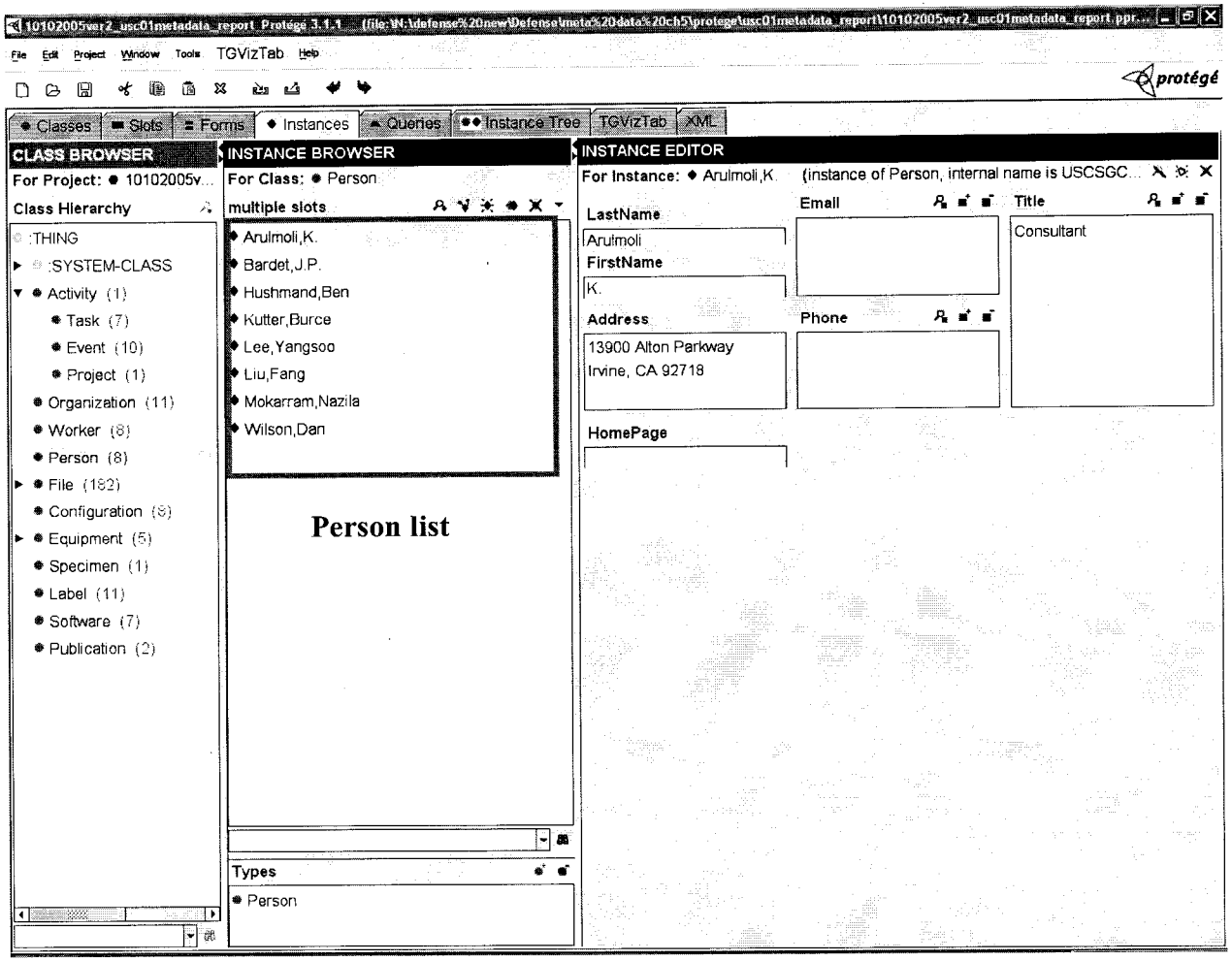

Figure 5-7. Instances of Person class.

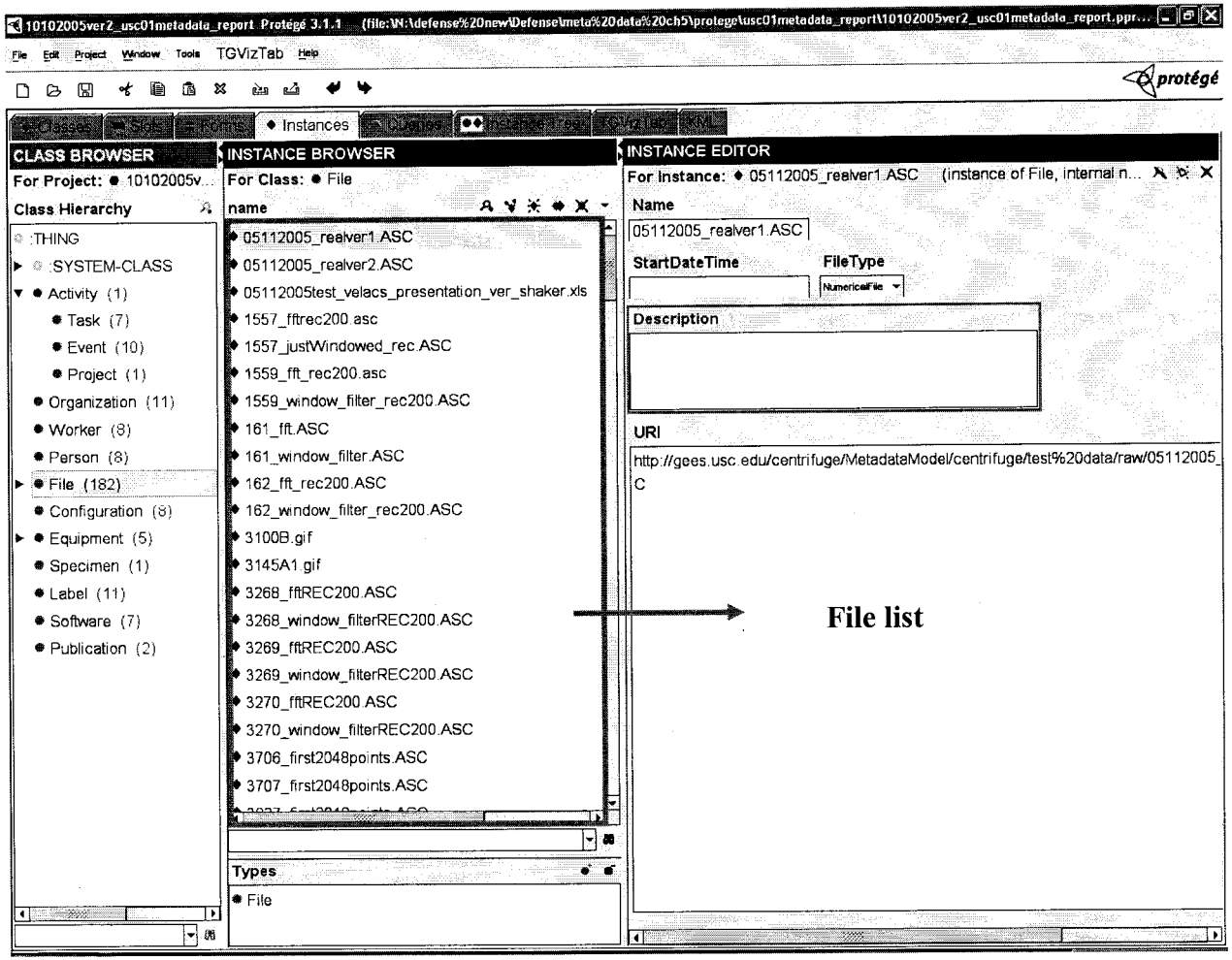

Figure 5-8. Instances of File class.

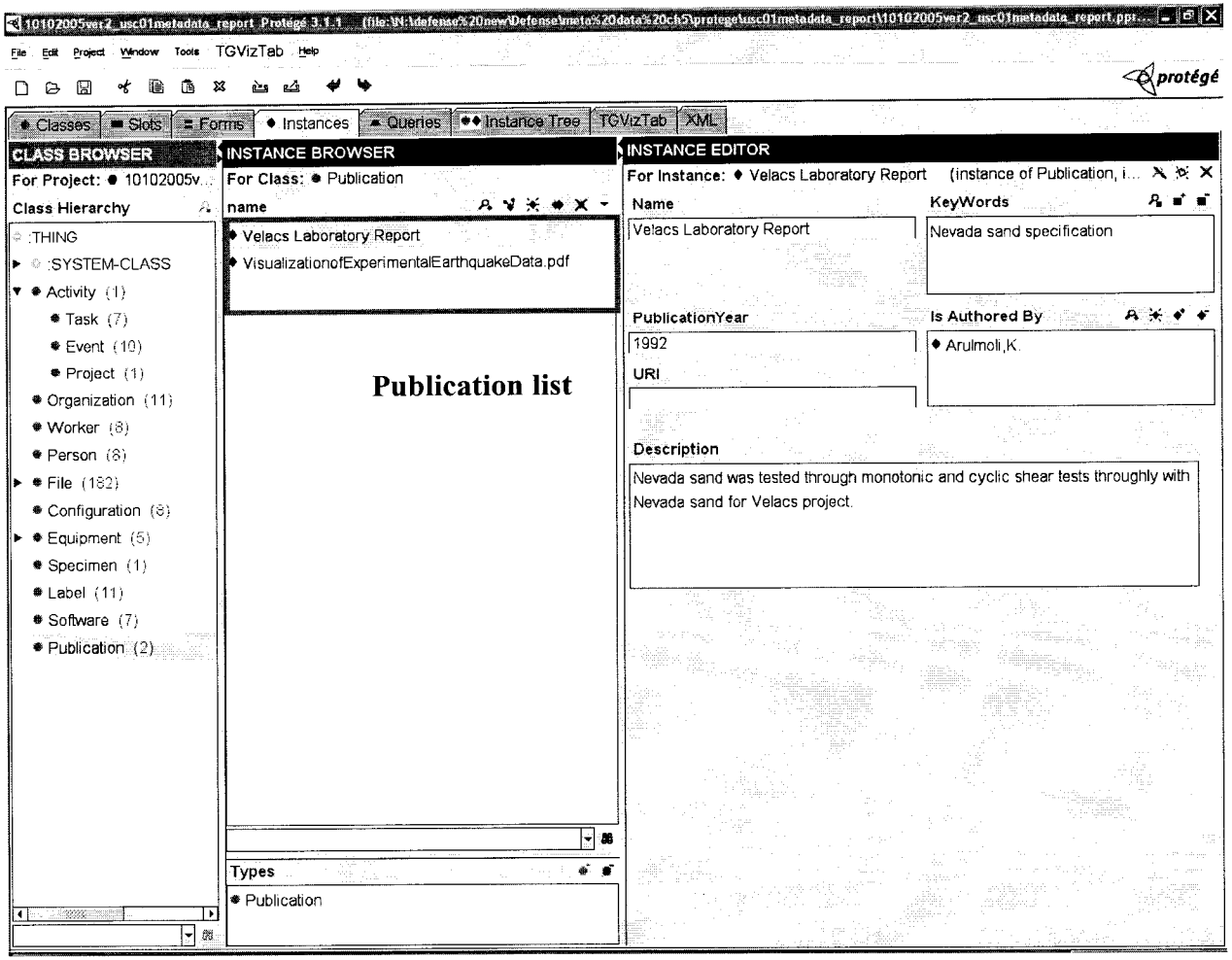

Figure 5-9. Instances of Publication class.

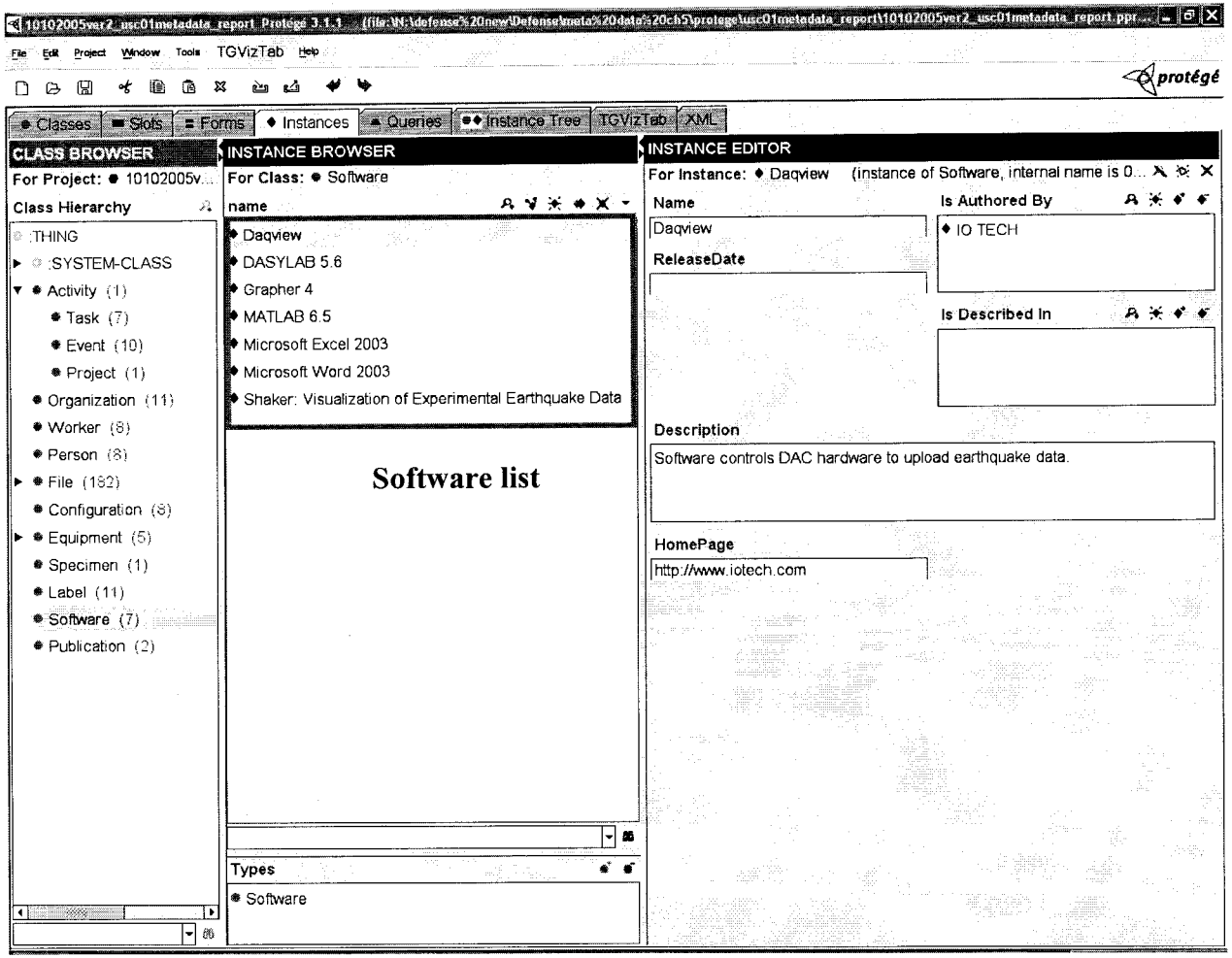

Figure 5-10. Instances of Software class.

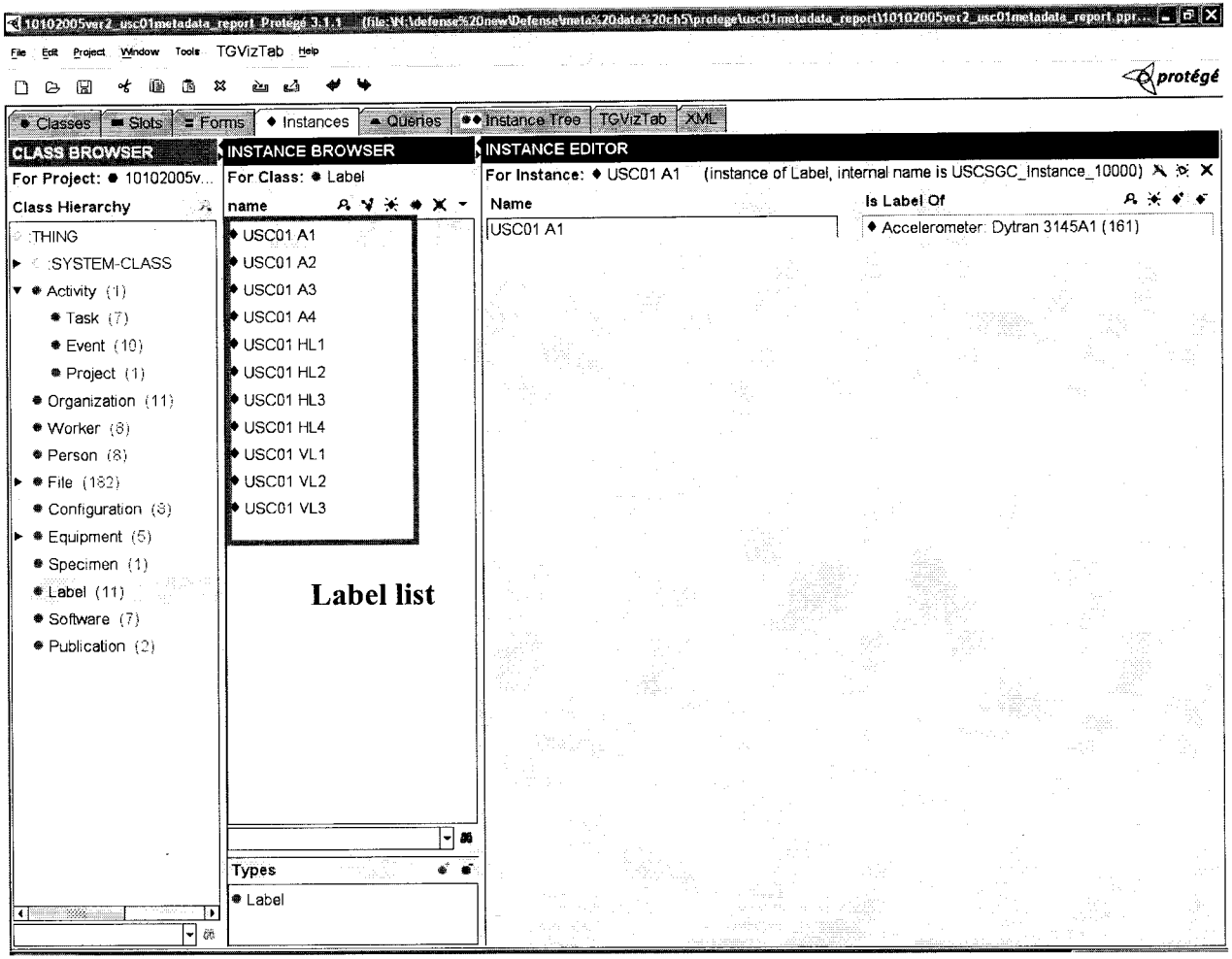

Figure 5-11. Instances of Label class.

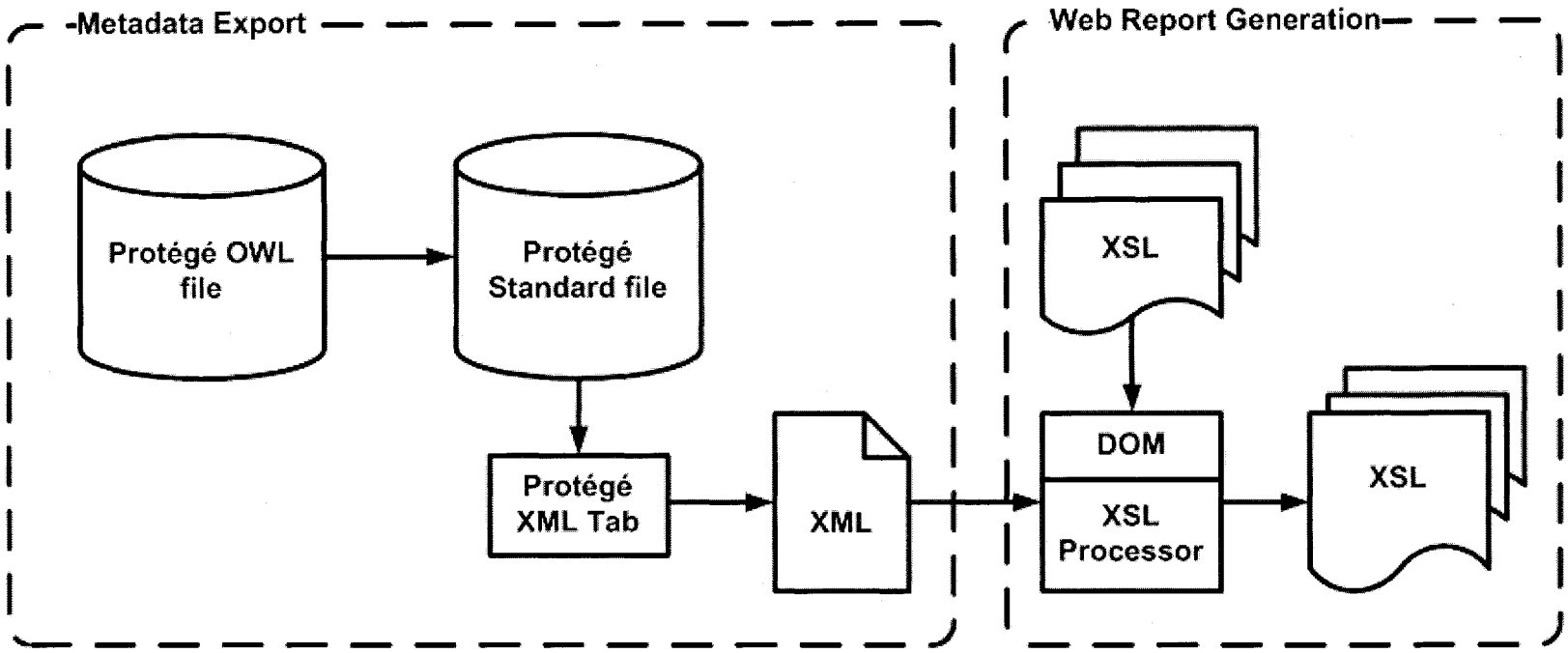

Figure 5-12. Schematic diagram illustrating web report generation (Bardet et al., 2004e).

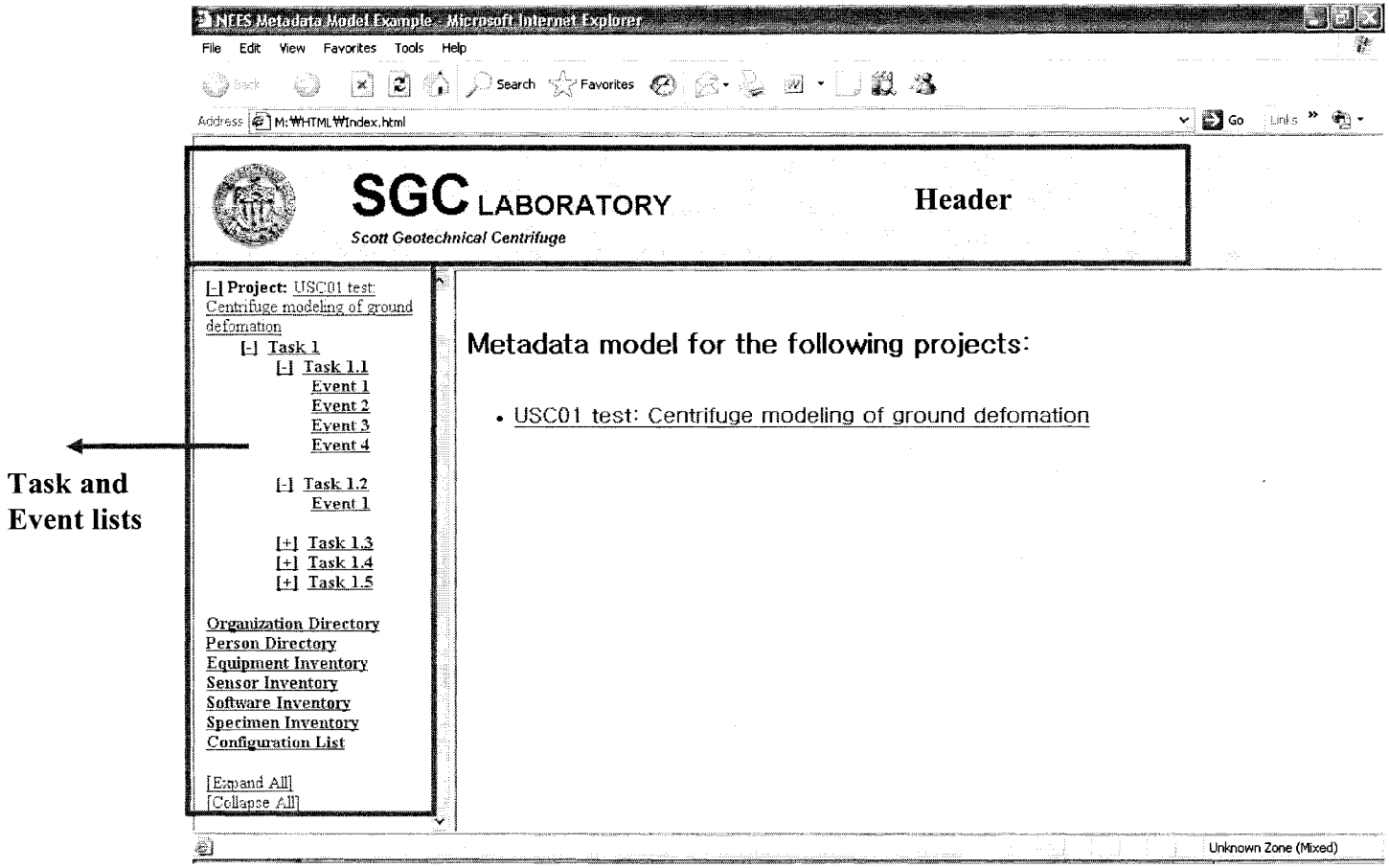

Figure 5-13. Main page of web report on the centrifuge USC01 experiment .

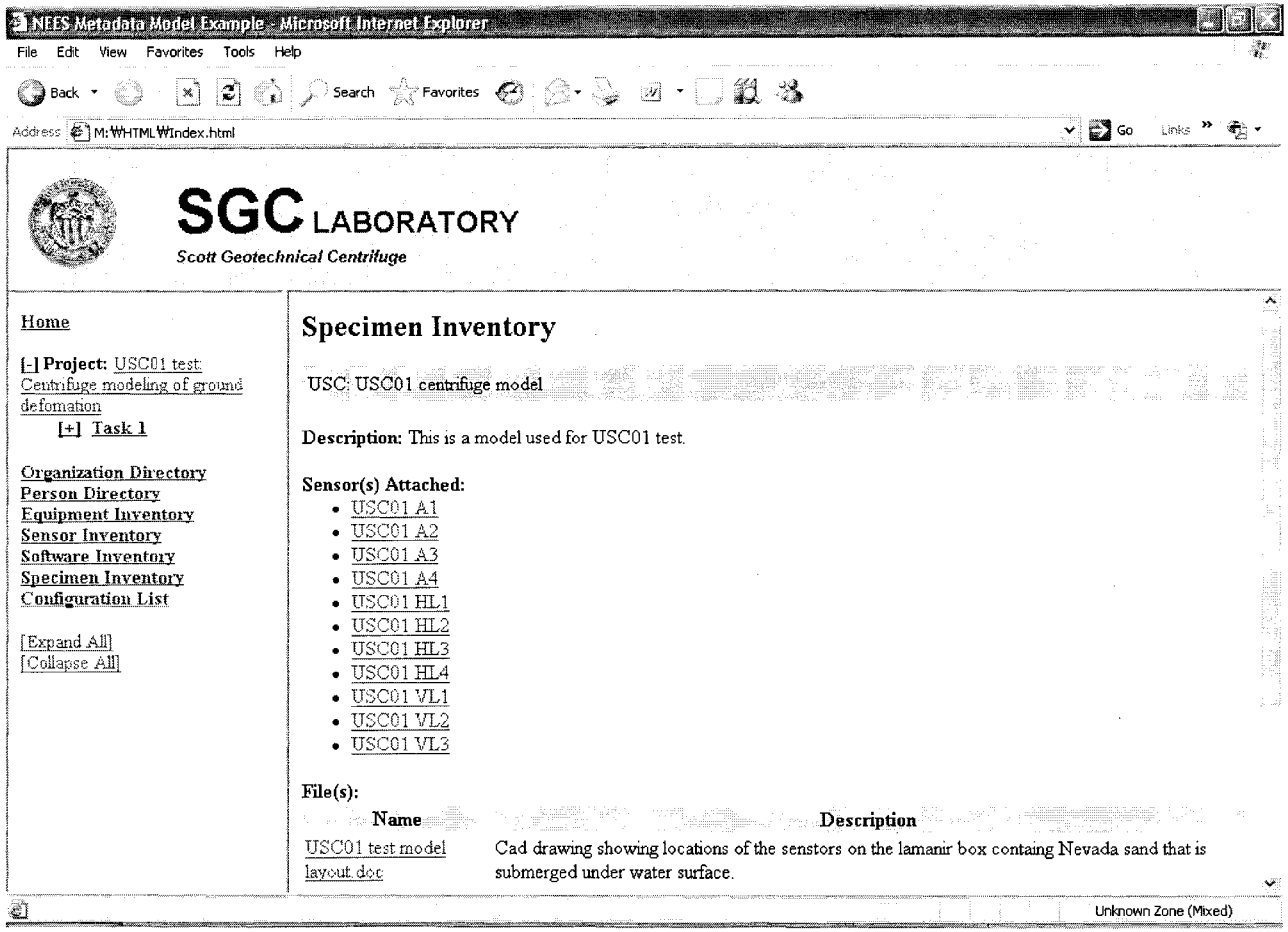

Figure 5-14. Inventory page of web report on the centrifuge USC01 experiment.

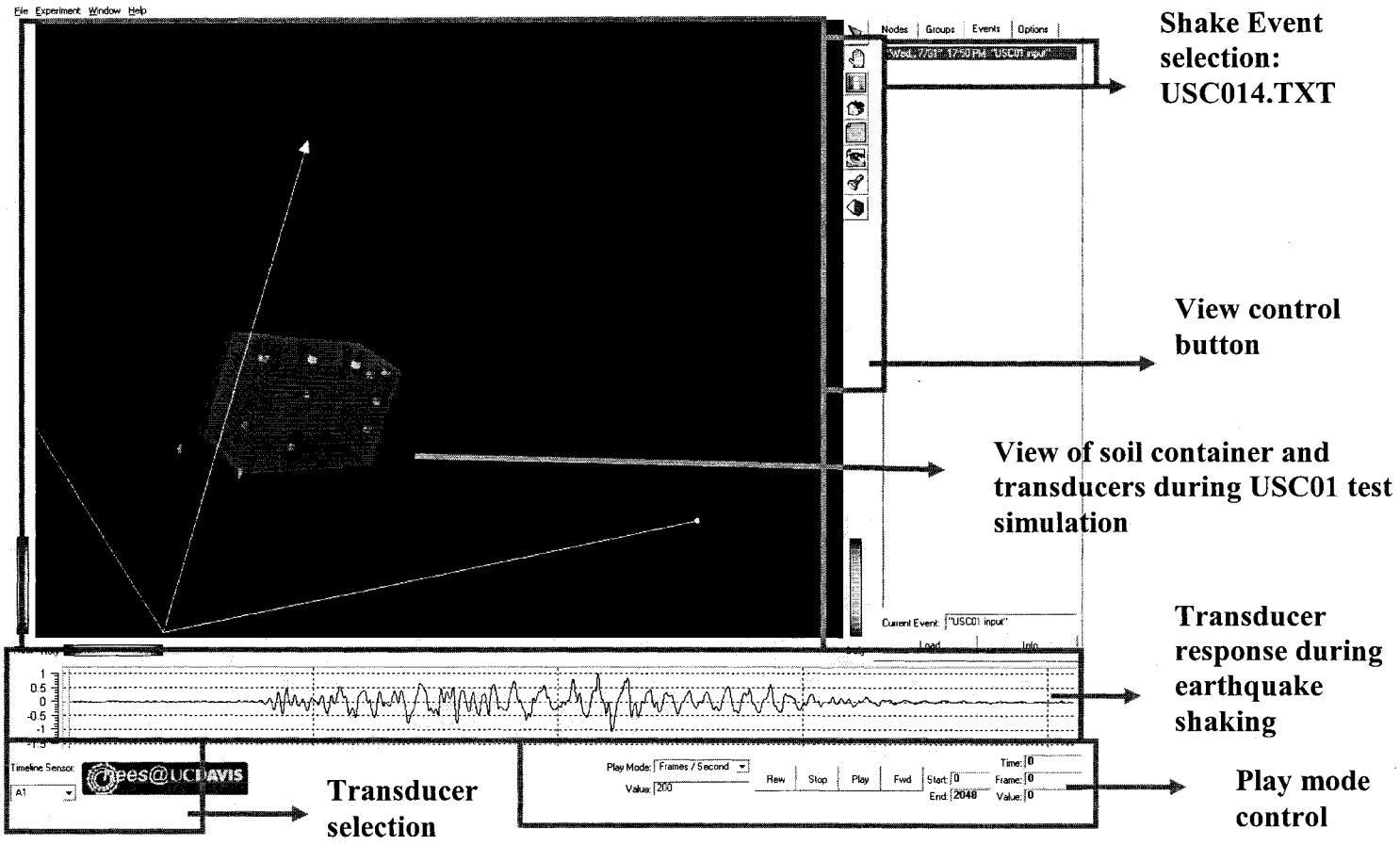

Figure 5-15. SHAKER visualization of the centrifuge USC01 experiment.

Table 5-1. Task classes of the centrifuge USC01 experiment.

ID	Task	Start	Finish
1	Centrifuge test preparation	9/1/2004	4/29/2005
2	Generation of Earthquake shaking motion	3/1/2005	4/1/2005
3	Design of test model	4/1/2005	4/29/2005
4	Performance of centrifuge USC01 test	5/2/2005	6/1/2005
5	Analysis of test result	6/1/2005	7/1/2005
6	Visualization	7/1/2005	8/1/2005

Table 5-2. Event classes of the centrifuge USC01 experiment.

ID	Event	Start	Finish
1	Sensor Calibration	9/1/2004	12/1/2004
2	DAQ software configuration	12/1/2004	2/1/2005
3	Nevada sand preparation	2/1/2005	3/1/2005
4	MTS controller adjustment	3/1/2005	4/1/2005
5	Earthquake motion Adjustment	3/1/2005	4/1/2005
6	Deaired water preparation	4/1/2005	4/29/2005
7	Design of centrifuge test model	4/1/2005	4/29/2005
8	Centrifuge USC01 test	5/2/2005	6/1/2005
9	Interpretation of USC01 test data	6/1/2005	7/1/2005
10	Visualization of centrifuge USC01 model	7/1/2005	8/1/2005

Table 5-3. Experiment information file (USC01.exp) of SHAKER program simulating the centrifuge USC01 experiment

File Content	Example
USC012.EL	Event list file name
USC04.IL	Instrument list file name
Containerusc.IV	Container geometry fine name
0.0 0.0 0.0	Origin if X, Y, and Z
1.0 0.0 0.0	X axis vector
0.0 1.0 0.0	Y axis vector
0.0 0.0 1.0	Z axis vector

Table 5-4. Event list file (USC012.EL) of SHAKER program simulating the centrifuge USC01 experiment

File content	Example
Date	3/10/2005
Time	11:00:00 AM
Event description	USC centrifuge shake motion
Channel gain list (CGL file)	USC01.CGL
Sensor log file name (TXT or PRN file)	USC014.TXT
Comments	USC01 test simulation

Table 5-5. Instrument list file (USC04.IL) of SHAKER program simulating the centrifuge USC01 experiment.

	Instr. Type	Engr. units	Location Description	Position			Direction
				x (mm)	y (mm)	z (mm)	
A1	acc	g's	On the BASE	-63.5	127	-6.35	H
A2	acc	g's	On the RING	-12.7	25.4	69.85	H
A3	acc	g's	On the RING	-12.7	25.4	146.05	H
A4	acc	g's	On the RING	-12.7	25.4	222.25	H
PPT1	ppt	kPa	In the dense sand	177.8	88.9	12.7	
PPT2	ppt	kPa	In the dense sand	38.1	88.9	69.85	
PPT3	ppt	kPa	In the loose sand	177.8	88.9	146.05	
HL1	displ	inch	On the Ring	368.3	63.5	69.85	H
HL2	displ	inch	On the Ring	368.3	63.5	146.05	H
HL3	displ	inch	On the Ring	368.3	114.3	196.85	H
HL4	displ	inch	On the RING	368.3	63.5	222.25	H
VL1	displ	inch	On the soil	38.1	96.52	228.6	V
VL2	displ	inch	On the soil	177.8	109.22	228.6	V
VL3	displ	inch	On the soil	294.64	93.98	228.6	V

6 Conclusion

Centrifuge modeling is now widely used in geotechnical earthquake engineering for simulating various nonlinear phenomena induced by earthquakes. A cost efficient alternative to full-scale testing in the field, centrifuge modeling has been applied to various research subjects in geotechnical earthquake engineering.

Chapter 2 reviews the similitude relationships between centrifuge model and prototype. These similitude relationships rest on the assumptions that centrifuge model and prototype have identical stress field and soil density. The time scale factors in multi-physics phenomenon, where dynamic motion and water diffusion events occur simultaneously, have been examined to resolve conflicts in time scales. When the model and prototype use the same pore fluid, the time scale for the dynamic event is $t_p = N \cdot t_m$, while the time scale for the diffusion event is $t_p = N^2 \cdot t_m$. These conflicting time scales can be reconciled by having models with a pore fluid more viscous than prototypes. The increase in fluid viscosity results in a decrease in fluid velocity in centrifuge models, but the time scales become identical in both dynamic and water diffusion events.

Chapter 3 describes the upgraded USC centrifuge and its ancillary equipment, such as electro-hydraulic earthquake shaking system (e.g., servo valve, controller, pump, and rotary unit), wireless DAQ system, and instrumentation. The USC centrifuge has been completely reassembled and upgraded. The rotary union and servo valve were refurbished to restore their full capabilities, and the DAQ system was replaced with a

newer model having faster speed and larger memory. The USC centrifuge is now equipped with a wireless DAQ system, which eliminate cables between the centrifuge and the control room. The wireless DAQ system results in lesser noise in the experiment data. It was found to increase data quality of centrifuge experiment and improve the frequency response of the DAQ system in dynamic tests.

Chapter 4 demonstrated the performance of the upgraded centrifuge through a particular test in which a saturated sand model was shaken by an earthquake motion. The tested model had a dimension of 9 inch in height, 14 inch in length, and 7 inch in depth. The model used a laminar box filled with Nevada No.120 sand at a relative density of 65%. The earthquake motion had a peak horizontal acceleration at the model base between +0.28 g and -0.3 g and had a frequency of 6 Hz in the prototype scale. The overall performance of the USC centrifuge during this test shows that the USC centrifuge is now fully operational after major improvements of its mechanical, hydraulic, and electrical components.

Chapter 5 presented a new generation of metadata model to document the experimental results and test procedures of centrifuge modeling. The applicability of the metadata model was demonstrated by applying it to the centrifuge experiment of Chapter 4. The metadata model was found useful to document experimental results, data processing and computer simulations. The metadata model introduces the concept of metadata for documenting experimental processes. It helps us understand, organize, and replicate the experimental results from centrifuges. The metadata model was designed to promote the data exchange among researchers. The data

required to the metadata model can be generated using Protégé, a program originally introduced for web semantics. The metadata model was applied to generate web report and computer visualization.

In conclusion, the present work contributes to the advancement of centrifuge modeling by introducing wireless instrumentation and control and promoting a new generation of data models.

References

1. Abdoun, T., Dobry, R., Zimmie, T. F., and Zeghal, M. (2005). "Centrifuge research of countermeasures to protect pile foundations against liquefaction-induced lateral spreading." *Journal Of Earthquake Engineering*, 9, 105-125.

2. Abdoun, T., Dobry, .R. and O'Rourke,T. D. (1997). *Centrifuge and numerical modeling of soil-pile interaction during earthquake induced soil liquefaction and lateral spreading*, American Society of Civil Engineers, New York.

3. Aboim, C., Scott, R. F., Lee, J. R., and Roth, W. H. (1986). "Centrifuge earth dam studies:Earthquake tests and analysis." Grant No. CEE-7926691, National Science Foundation, Washington, DC.

4. Adalier, K., and Elgamal, A. (2005). "Liquefaction of over-consolidated sand: A centrifuge investigation." *Journal of Earthquake Engineering*, 9, 127-150.

5. Adalier, K., Elgamal, A. W., and Martin, G. R. (1998). "Foundation liquefaction countermeasures for earth embankments." *Journal Of Geotechnical And Geoenvironmental Engineering*, 124(6), 500-517.

6. Aiken, P., and Davis, K. H. (2000). "Metadata engineering for corporate portals using xml." Conceptual modeling er 2000, proceedings, 572-573.

7. Allard, M. (1983). "Caltech centrifuge manual." California Institute of Technology, Pasadena, California, U.S.A.

8. Allard, M. A., and Schenkeveld, F. M. (1994) "The delft geotechnics model pore fluid for centrifuge tests." *Proceedings., International Conference Centrifuge 1994*, Leung, Singapore, 133-138.

9. Allersma, H. G. B., Brinkgreve, R. B. J., Simon, T., and Kirstein, A. A. (2000). "Centrifuge and numerical modelling of horizontally loaded suction piles." *International Journal of Offshore And Polar Engineering*, 10(3), 222-228.

10. Arlow, J. and Neustadt, I. (2001). UML *and the unified process: Practical object-oriented analysis and design*, Addison-Wesley Pub Co, Boston, M.A., U.S.A.

11. Arulanandan, K., Anandarajah, A., and Abghari, A. (1983). "Centrifugal modeling of soil liquefaction susceptibility." *Journal of Geotechnical Engineering-ASCE*, 109(3), 281-300.

12. Arulanandan, K., Anandarajah, A., Li, X. S., and American Society of Civil Engineers. Geo-Institute. (2000). *Computer simulation of earthquake effects : Proceedings of sessions of geo-Denver 2000*, American Society of Civil Engineers, Reston, VA.

13. Arulanandan, K., and Scott, R. F. (1993a). "Project VELACS - control test-results." *Journal of Geotechnical Engineering-ASCE*, 119(8), 1276-1292.

14. Arulanandan, K., and Scott, R. F. (1993b) "Verification of numerical procedures for the analysis of soil liquefaction problems." *Proceedings of the International Conference on the Verification of Numerical Procedures for the Analysis of Soil Liquefaction Problems*, Rotterdam, Netherlands.

15. Arulanandan, K., Yogachandran, C., Muraleetharan, K. K., Kutter, B. L., and Chang, G. S. (1988). "Seismically induced flow slide on centrifuge." *Journal of Geotechnical Engineering-ASCE*, 114(12), 1442-1449.

16. Arumoli, K., Mauraleetharan, K., Hossain, M., and Fruth, L. (1992). "VELACS: Verification of liquefaction analysis by centrifuge studies. Laboratory testing program. Soil data report." The Earth Technology Corporation, Long Beach, California.

17. Astaneh, S. M. F. (1993). "Effects of earthquake on saturated soil embankments," Ph.D. Dissertation, University of Colorado, Boulder.

18. Atkinson, M., Bancilhon, F., DeWitt, D., Dittrich, K., Maier, D., and Zdonik, S. (1989) "The object-oriented database system manifesto." *Proc. 1rst Int. Conference on Deductive and Object-Oriented Databases*, Kyoto, Japan.

19. Aydingun, O., and Adalier, K. (2003). "Numerical analysis of seismically induced liquefaction in earth embankment foundations. Part i. Benchmark model." *Canadian Geotechnical Journal*, 40(4), 753-765.

20. Azizi, F. (2000). *Applied analysis in geotechnics*, E&FN Spon, New York, NY.

21. Balakrishnan, A., and Kutter, B. L. (1999). "Settlement, sliding, and liquefaction remediation of layered soil." *Journal of Geotechnical and Geoenvironmental Engr.*, 125(11), 968-978.

22. Balakrishnan, A., Kutter, B. L., and Idriss, I. M. (1998). "Centrifuge testing of remediation of liquefaction at bridge sites." Liquefaction, differential settlement, and foundation engineering, 26-37.

23. Balassanian, S., Cisternas, A., and Melkumyan, M. (2000). *Earthquake hazard and seismic risk reduction*, Kluwer Academic Publishers, Dordrecht ; Boston.

24. Bancilhon, F. (1994). "Object database-systems - the ODMG standard." Information processing '94, vol ii, 123-130.

25. Bardet, J.P. (1997). *Experimental soil mechanics*, Prentice Hall, Upper Saddle River, N.J.

26. Bardet, J. P., and Davis, C. A. (1996). "Performance of San Fernando dams during 1994 northridge earthquake." *Journal of Geotechnical Engineering-Asce*, 122(7), 554-564.

27. Bardet, J. P., and Davis, C. A. (1998). "Deformation of embankments due to liquefaction during 1994 northridge earthquake." Liquefaction, differential settlement, and foundation engineering, 9-18.

28. Bardet, J. P., and Kapuskar, M. (1993). "Liquefaction sand boils in san-francisco during 1989 Loma-Prieta earthquake." *Journal of Geotechnical Engineering-Asce*, 119(3), 543-562.

29. Bardet, J. P., Liu, F., and Mokarram, N. (2005) "Data and metadata modeling for the george e.Brown jr. Network for earthquake engineering simulation." *Eurodyne 2005*, Paris, France, 1467-1472.

30. Bardet, J. P., Liu, F., and Mokkaram, N. (2004a). "Illustration of the NEES metadata model using the minimost experiment." Report of Civil Engineering Dept, University of Southern California, Los Angeles.

31. Bardet, J. P., Liu, F., and Mokkaram, N. (2004b). "A metadata model for the george e. Brown jr. Network for earthquake engineering simulation." Report of Civil Engineering Dept., University of Southern California, Los Angeles.

32. Bardet, J. P., Liu, F., and Mokkaram, N. (2004c). "Report and exchange of nees data sets using metadata models." Report of Civil Engineering Dept, University of Southern California, Los Angeles.

33. Bardet, J. P., Liu, F., Mokkaram, N., Brandenberg, S., Kutter, B., and Wilson, D. (2004d). "Application of the nees metadata model to centrifuge modeling" Submitted

34. Bardet, J. P., Peng, J., Law, K., and Swift, J. (2004e) "Overview of the nees data/metadata model." *Proc. 13th World Conference in Earthquake Engineering*, Vancouver, Canada.

35. Barry, D. A., Lisle, I. G., Li, L., Prommer, H., Parlange, J. Y., Sander, G. C., and Griffioen, J. W. (2001). "Similitude applied to centrifugal scaling of unsaturated flow." *Water Resources Research*, 37(10), 2471-2479.

36. Bolin, R. C., and Stanford, L. (1998). *The northridge earthquake : Vulnerability and disaster*, Routledge, London ; New York.

37. Bolton, M. D., and Lau, C. K. (1988). "Scale effects arising from particle size." Centrifuge 88, J. F. Corte, ed., A.A.Balkema, Rotterdam, 127-134.

38. Bommer, J. J., and Rodriguez, C. E. (2002). "Earthquake-induced landslides in central America." *Engineering Geology*, 63(3-4), 189-220.

39. Brandenberg, S. J. (2004). Personal Communication, November, 2004, Davis, California.

40. Brandenberg, S. J., Boulanger, R. W., Kutter, B. L., and Chang, D. D. (2005). "Behavior of pile foundations in laterally spreading ground during centrifuge tests." *Journal Of Geotechnical And Geoenvironmental Engineering*, 131(11), 1378-1391.

41. Brown, E. C. (1996). "Centrifuge modeling of surface foundations subject to dynamic loads," Thesis M.S., University of Colorado, Boulder.

42. Bucky, P. B. (1931). "Use of models for the study of mining problems" *Am. Inst. Mining and Metallurgical Engineers*, 3-28.

43. Buitelaar, P., Olejnik, D., and Sintek, M. (2004). "A protege plug-in for ontology extraction from text based on linguistic analysis." Semantic web: Research and applications, 31-44.

44. Butterfield, R. (2001). "Dimensional analysis for geotechnical engineers." *Geotechnique*, 51(1), 91-93.

45. Byrne, P. M., Park, S. S., Beaty, M., Sharp, M., Gonzalez, L., and Abdoun, T. (2004). "Numerical modeling of liquefaction and comparison with centrifuge tests." *Canadian Geotechnical Journal*, 41(2), 193-211.

46. Cargill, K. W., and Ko, H. Y. (1983). "Centrifugal modeling of transient water-flow." *Journal Of Geotechnical Engineering-ASCE*, 109(4), 536-555.

47. CGM.(2005). "Principles of centrifuge modeling " Centrifuge Facility (University of California, Davis), <http://cgm.engineering.ucdavis.edu/Facilities/modeling.htm> (January, 2006)

48. Chapuis, R. P., and Aubertin, M. (2003). "On the use of the Kozeny-Carman equation to predict the hydraulic conductivity of soils." *Canadian Geotechnical Journal*, 40(3), 616-628.

49. Chari, T. R. (1979). "Geotechnical aspects of iceberg scours on ocean floors." *Canadian Geotechnical Journal*, 16(2), 379-390.

50. Chen, W. F. (1982). *Soil mechanics, plasticity and landslides*, School of Civil Engineering, Purdue Univ., West Lafayette, Indiana.

51. Chen, Y. (2003). "Optimal features extraction of noisy sinusoidal signals using two-stage linear least squares fitting " <http://www.csois.usu.edu/people/yqchen/sinefit.html> (January, 2004)

52. Chipley, M. T. (1996). "Centrifuge modeling of flow processes," Ph.D. Dissertation, University of Colorado, Boulder.

53. Chugh, A. K., and Vonthun, J. L. (1985). "Pore pressure response analysis for earthquakes." *Canadian Geotechnical Journal*, 22(4), 466-476.

54. Cole, W. F. (1991) "Landslides triggered by the loma prieta earthquake, implications for zonation." *Proceedings of the Fourth International Conference on Seismic Zonation*, Oakland, California, pp.653-660.

55. Corté, J.-F., and International Society of Soil Mechanics and Foundation Engineering. (1988). *Centrifuge 88 : Proceedings of the international conference on geotechnical centrifuge modelling, paris, 25-27 april 1988 = centrifugeuse 88 : Comptes rendus du congrès international sur la modélisation géotechnique en centrifugeuse, paris, 25-27 avril 1988*, A.A. Balkema, Rotterdam, Netherlands ; Brookfield, VT.

56. Craig, R. F. (1997). *Soil mechanics*, E & FN SPON.

57. Craig, W. H. (1985). *Application of centrifuge modelling to geotechnical design : Proceedings of a symposium on the application of centrifuge modelling to geotechnical design, manchester, 16-18 april, 1984*, A.A. Balkema, Rotterdam ; Boston.

58. Craig, W. H. (1988). "Centrifuge models in marine and coastal engineering." Centrifuges in soil mechanics, Balkema, Rotterdam, Netherlands, pp.149-168.

59. Craig, W. H. (1995). "Geotechnical centrifuges: Past, present and future " Geotechnical centrifuge technology, Blackie Academic and Professional, London, U.K., 1-18.

60. Craig, W. H., James, R. G., and Schofield, A. N.(eds). (1988). *Centrifuges in soil mechanics*, Balkema, Rotterdam

61. Culligan, P. J., and Barry, D. A. (1998). "Similitude requirements for modelling napl movement with a geotechnical centrifuge." *Proceedings Of The Institution Of Civil Engineers-Geotechnical Engineering*, 131(3), 180-186.

62. Cyran, T. C. (1990). "Response of piles to impact driving and static load testing in the centrifuge," Thesis M.S., University of Colorado, Boulder.

63. Dakoulas, P., Yegian, M. K., Holtz, R. D., American Society of Civil Engineers. Geo-Institute., and United States. Air Force. Office of Scientific Research. (1998). *Geotechnical earthquake engineering and soil dynamics iii : Proceedings of a specialty conference ; sponsored by geo-institute of the american society of civil engineers ; co-sponsored by us air force office of scientific research ; august 3-6, 1998, university of washington, seattle, washington*, American Society of Civil Engineers, Reston, Va.

64. Das, B. M. (2000). *Fundamentals of geotechnical engineering*, BROOKS/COLE, Pacific Glove, California, U.S.A.

65. Date, C. J. (2004). *An introduction to database systems*, Pearson/Addison Wesley, Boston.

66. De Nicola, A., and Randolph, M. F. (1999). "Centrifuge modelling of pipe piles in sand under axial loads." *Geotechnique*, 49(3), 295-318.

67. Depountis, N., Davies, M. C. R., Harris, C., Burkhart, S., Thorel, L., Rezzoug, A., Konig, D., Merrifield, C., and Craig, W. H. (2001). "Centrifuge modelling of capillary rise." *Engineering Geology*, 60(1-4), 95-106.

68. Dewoolkar, M. M., Goddery, T., and Znidarcic, D. (2003). "Centrifuge modeling for undergraduate geotechnical engineering instruction." *Geotechnical Testing Journal*, 26(2), 201-209.

69. Dewoolkar, M. M., Ko, H. Y., and Pak, R. Y. S. (1999a). "Centrifuge modelling of models of seismic effects on saturated earth structures." *Geotechnique*, 49(2), 247-266.

70. Dewoolkar, M. M., Ko, H. Y., Stadler, A. T., and Astaneh, S. M. F. (1999b). "A substitute pore fluid for seismic centrifuge modeling." *Geotechnical Testing Journal*, 22(3), 196-210.

71. Dobry, R. (1989). "Some basic aspects of soil liquefaction during earthquakes." *Annals Of The New York Academy Of Sciences*, 558, 172-182.

72. Dobry, R., and Abdoun, T. (2001) "Recent studies on seismic centrifuge modeling of liquefaction and its effects on deep foundations." *State-of-the-Art Report (SOAP3), Proc. Fourth International Conference on Recent Advances in Geotechnical Earthquake Engineering and Soil Dynamics*, San Diego, CA.

73. Dobry, R., Abdoun, T., O'Rourke, T. D., and Goh, S. H. (2003). "Single piles in lateral spreads: Field bending moment evaluation." *Journal Of Geotechnical And Geoenvironmental Engineering*, 129(10), 879-889.

74. Dobry, R., and Taboada,V.M. (1996). "Investigation of liquefaction and lateral spreading by centrifuge model tests." California Dept. of Transportation, Sacramento.

75. Duineveld, A. J., Stoter, R., Weiden, M. R., Kenepa, B., and Benjamins, V. R. (2000). "Wondertools? A comparative study of ontological engineering tools." *International Journal Of Human-Computer Studies*, 52(6), 1111-1133.

76. Dytran. (2003a). "Accelerometers -- miniature." <http://www.dytran.com/products/3145A1.pdf> (Nov.1, 2004)

77. Dytran. (2003b). "Electronics -- signal conditioners / vibration meters." <http://www.dytran.com/products/4122B.pdf> (Nov.1, 2004)

78. Elgamal, A.-W. e. a. (1996). "Analysis of site liquefaction and lateral spreading using centrifuge testing records." *Soils and Foundations*, 36(2), 111-121.

79. Elgamal, A., Lu, J. C., and Yang, Z. H. (2005). "Liquefaction-induced settlement of shallow foundations and remediation: 3d numerical simulation." *Journal Of Earthquake Engineering*, 9, 17-45.

80. Ellis, E. A., Soga, K., Bransby, M. F., and Sato, M. (2000). "Resonant column testing of sands with different viscosity pore fluids." *Journal of Geotechnical And Geoenvironmental Engineering*, 126(1), 10-17.

81. Evans, S. G., and DeGraff, J. V. (2002). *Catastrophic landslides : Effects, occurrence, and mechanisms*, Geological Society of America, Boulder, CO.

82. Faccioli, E. (1995) "Induced hazards: Earthquake triggered landslides." *Proceedings of the Fifth International Conference on Seismic Zonation*, Nice, France, pp.1908-1931.

83. Fiegel, G. L., and Kutter, B.L. (1994). "Liquefaction-induced lateral spreading of mildly sloping ground." *Journal of Geotechnical and Geoenvironmental Engr.*, 120(12), 2236-2243.

84. Fiegel, G. L., and Kutter, B. L. (1994a). "Liquefaction-induced lateral spreading of mildly sloping ground." *Journal Of Geotechnical Engineering-ASCE*, 120(12), 2236-2243.

85. Fiegel, G. L., and Kutter, B. L. (1994b). "Liquefaction mechanism for layered soils." *Journal Of Geotechnical Engineering-ASCE*, 120(4), 737-757.

86. Figueroa, J. L., Dief, H., and Dietz, C.P. (1998) "Development of the geotechnical centrifuge at Case Western Reserve University." *International Conference Centrifuge 98 (IS-Tokyo 98)*, Tokyo, Japan.

87. Fong, J., Li, Q., and Huang, S. M. (2003). "Universal data warehousing based on a meta-data modeling approach." *International Journal Of Cooperative Information Systems*, 12(3), 325-363.

88. Fuglsang, L. D., and Ovesen, N. K. (1986). "The applicaition of the theory of modelling to centrifuge studies." Centrifuges in soil mechanics, W. H. Craig, James, R.G., Schofield, A.N., ed., A.A.Balkema, Brookfield, VT., 119-138.

89. Gadre, A., and Dobry, R. (1998). "Lateral cyclic loading centrifuge tests on square embedded footing." *Journal Of Geotechnical And Geoenvironmental Engineering*, 124(11), 1128-1138.

90. Gautschi, G. (2002). *Piezoelectric sensorics : Force, strain, pressure, acceleration and acoustic emission sensors, materials and amplifiers*, Springer, Berlin ; Heidelberg ; New York.

91. Golbreich, C., Dameron, O., Gibaud, B., and Burgun, A. (2003). "Web ontology language requirements w.R.T expressiveness of taxonomy and axioms in medicine." Semantic web - ISWC 2003, 180-194.

92. Green, R. A., and Terri, G. A. (2005). "Number of equivalent cycles concept for liquefaction evaluations - revisited." *Journal Of Geotechnical And Geoenvironmental Engineering*, 131(4), 477-488.

93. Gurumoorthy, C., and Singh, D. N. (2005). "Centrifuge modeling of diffusion through rock mass." *Journal of Testing And Evaluation*, 33(1), 44-50.

94. Ha, I. S., Park, Y. H., and Kim, M. M. (2003). "Dissipation pattern of excess pore pressure after liquefaction in saturated sand deposits." Geology and properties of earth materials 2003, 59-67.

95. Hadush, S., Yashima, A., and Uzuoka, R. (2000). "Importance of viscous fluid characteristics in liquefaction induced lateral spreading analysis." *Computers and Geotechnics*, 27(3), 199-224.

96. Haigh, S. K. e. a. (2001) "Newmarkian analysis of liquefied flow in centrifuge model earthquakes." *Fourth International Conference on Recent Advances in Geotechnical Earthquake Engineering and Soil Dynamics*, Missouri, Paper No. 9.06.

97. Hall, J. F., and Earthquake Engineering Research Institute. (1994). *Northridge earthquake, january 17, 1994 : Preliminary reconnaissance report*, Earthquake Engineering Research Institute, Oakland, Calif.

98. Harold, E. R. (2001). *XML Bible, second edition,* Hungry Minds Inc., New York.

99. He, Y. B., Chua, P. S. K., and Lim, G. H. (2003). "Performance analysis of a two-stage electrohydraulic servo valve in centrifugal force field." *Journal Of Fluids Engineering-Transactions Of The ASME*, 125(1), 166-170.

100. Heaton, T. H., and Hartzell, S. H. (1988). "Earthquake ground motions." *Annual Review Of Earth And Planetary Sciences*, 16, 121-145.

101. Heuze, F., Archuleta, R., Bonilla, F., Day, S., Doroudian, M., Elgamal, A., Gonzales, S., Hoehler, M., Lai, T., Lavallee, D., Lawrence, B., Liu, P. C., Martin, A., Matesic, L., Minster, B., Mellors, R., Oglesby, D., Park, S., Riemer, M., Steidl, J., Vernon, F., Vucetic, M., Wagoner, J., and Yang, Z. (2004). "Estimating site-specific strong earthquake motions." *Soil Dynamics And Earthquake Engineering*, 24(3), 199-223.

102. Holzer, T. L., Bennett, M. J., Ponti, D. J., and Tinsley, J. C. (1999). "Liquefaction and soil failure during 1994 Northridge earthquake." *Journal of Geotechnical And Geoenvironmental Engineering*, 125(6), 438-452.

103. Honeywell.(2005a). "Instrumentation:DLD-VH model." <http://www.sensotec.com/pdf/008-0532-00.pdf> (October, 2005)

104. Honeywell.(2005b). "Instrumentation:DV-05 model." <http://www.sensotec.com/pdf/008-0534-00.pdf> (October, 2005)

105. Hushmand, B. (2004). Personal Communication, November 2004, Tustin, California.

106. Hushmand, B., Scott, R. F., and Crouse, C. B. (1988). "Centrifuge liquefaction tests in a laminar box." *Geotechnique*, 38(2), 253-262.

107. Iai, S., Tobita, T., and Nakahara, T. (2005). "Generalized scaling relations for dynamic centrifuge tests." *Geotechnique*, 55(5), 355-362.

108. Ibraim, I., and Anderson, M. G. (2003). "A new approach to soil characterisation for hydrology-stability analysis models." *Geomorphology*, 49(3-4), 269-279.

109. IOtech.(2005a). "DAQ program manual." <ftp://ftp.iotech.com/pub/iotech/outgoing/Manuals/ProgrammersManual.pdf > (October, 2005)

110. IOtech.(2005b). "DaqBoard 2001." <ftp://ftp.iotech.com/pub/iotech/outgoing/Manuals/DaqBoard%201000%20and%202000%20Series.pdf> (September, 2005)

111. IOtech.(2005c). "DaqView manual." <ftp://ftp.iotech.com/pub/iotech/outgoing/Manuals/DaqView.pdf> (October, 2005)

112. IOtech.(2005d). "Dasylab guide." <ftp://ftp.iotech.com/pub/iotech/outgoing/Manuals/DASYLab%20Guide.pdf > (September, 2005)

113. IOtech.(2005e). "WaveBook 516 manual." <ftp://ftp.iotech.com/pub/iotech/outgoing/Manuals/WaveBook_512A_516_Series.pdf> (August, 2005)

114. IOtech. (2005f). "WBK options." <ftp://ftp.iotech.com/pub/iotech/outgoing/Manuals/WBK%20Options.pdf> (August, 2005)

115. Ishihara, K. (1996). *Soil behaviour in earthquake geotechnics*, Oxford University Press, Oxford.

116. Ishihara, K., and Cubrinovski, S. (2005). "Characteristics of ground motion in liquefied deposits during earthquakes." *Journal of Earthquake Engineering*, 9, 1-15.

117. Ishihara, K., and JGS. (1995). *Earthquake geotechnical engineering : Proceedings of is-tokyo '95/the first international conference on earthquake geotechnical engineering, Tokyo, 14-16 November, 1995*, A.A. Balkema, Rotterdam.

118. Jelali, M., and Kroll, A. (2003). *Hydraulic servo-systems: Modelling, identification, and control*, Springer, London; New York.

119. JGS. (1996). *Special issue on geotechnical aspects of the january 17 1995 hyogoken-nambu earthquake*, Japanese Geotechnical Society, Tokyo, Japan.

120. JGS. (1998). *Remedial measures against soil liquefaction : From investigation and design to implementation*, A.A. Balkema, Rotterdam ; Brookfield, VT.

121. Keefer, D. K. (1984). "Landslides caused by earthquakes." *Geological Society of America Bulletin*, 95(4), 406-421.

122. Kimura, T. (1988). "Centrifuge research activities in japan." Centrifuges in sol mechanics, W. H. Craig, James, R.G., Schofield, A.N., ed., Bakema, Brookfield, VT., 119-138.

123. Kimura, T., Kusakbe, O., and Takemura, J.(eds). (1998). *Centrifuge 98*, Balkema, Rotterdam

124. Knublauch, H., Fergerson, R. W., Noy, N. F., and Musen, M. A. (2004). "The protege owl plugin: An open development environment for semantic web applications." Semantic web - iswc 2004, proceedings, 229-243.

125. Ko, H. Y. (1988). "Summary of the state-of-the-art in centrifuge modeling testing." Centrifuges in soil mechanics, W. H. Craig, James, R.G., Schofield, A.N., ed., A.A.Balkema, Brookfield, VT., 11-18.

126. Ko, H. Y. (1994) "Modeling seismic problems in centrifuges." *Pro., Int. Conf. Centrifuge '94*, Leung, Singapore, 3-12.

127. Koh, S. L. (1980). "Mechanics of landslides and slope stability." *Engineering Geology*, 16(1/2), 1-150.

128. Kramer, S., Siddharthan, R., and American Society of Civil Engineers. Geotechnical Engineering Division. Soil Dynamics Committee. (1995). *Earthquake-induced movements and seismic remediation of existing foundations and abutments : Proceedings of sessions sponsored by the soil dynamics committee of the geotechnical engineering division of the American society of civil engineers in conjunction with the ASCE convention in San Diego, California, October 23-27, 1995*, The Society, New York, N.Y.

129. Kramer, S. L. (1996). *Geotechnical earthquake engineering*, Prentice Hall, Upper Saddle River, N.J.

130. Kutter, B. L. (1984). "Earthquake deformation of centrifuge model banks." *Journal Of Geotechnical Engineering-ASCE*, 110(12), 1697-1714.

131. Kutter, B. L. (1988). "Liquefaction evaluation procedure - discussion." *Journal Of Geotechnical Engineering-ASCE*, 114(2), 243-246.

132. Kutter, B. L. (1995) "Recent advances in centrifuge modeling of seismic shaking." *PRoc., 3rd Int. Conf. on Recent Advances in Geotech. Earthquake Engrg. andSoil Dyan.*, University of Missouri-Rolla, Mo., 927-942.

133. Kutter, B. L., and Balakrishnan, A. (1999) "Visualization of soil behavior from dynamic centrifuge model tests." *Earthquake Geotechnical Engineering, Proceedings of the Second International Conference on*, Rotterdam, pp. 857-862.

134. Kutter, B. L., Idriss, I. M., Khonke, T., Lakeland, J., Li, X. S., Sluis, W., and Zeng, X. (1994) "Design of a large earthquake simulator at UC Davis." *Proc.,Int. Conf. Centrifuge 1994*, Leung, Singapore, 169-175.

135. Kutter, B. L., and James, R. G. (1989). "Dynamic centrifuge model tests on clay embankments." *Geotechnique*, 39(1), 91-106.

136. Lambe, P. C. (1981). "Dynamic centrifugal modelling of a horizontal sand stratum," Thesis Sc.D. --Massachusetts Institute of Technology Dept. of Civil Engineering 1982., Massachusetts Institute of Technology. Dept. of Civil Engineering.,.

137. Lassila, O. (2000). "The resource description framework." *IEEE Intelligent Systems & Their Applications*, 15(6), 67-69.

138. Lawless, B. (1997). *Fundamental analog electronics*, Prentice Hall, London ; New York.

139. Lee, J. (2004). Personal Communication, October 2004, Palo Alto, California.

140. Leung, C. G., Lee, F. H., and Tan, T. S.(eds). (1994). *Centrifuge 94*, Balkema, Rotterdam

141. Lin, J.-S., and Massachusetts Institute of Technology. Dept. of Civil Engineering. (1980). "Attenuation relations for effective peak acceleration as related to liquefaction," Thesis M S --Massachusetts Institute of Technology Dept of Civil Engineering 1980.

142. Ling, H. I., Mohri, Y., Kawabata, T., Liu, H. B., Burke, C., and Sun, L. X. (2003). "Centrifugal modeling of seismic behavior of large-diameter pipe in liquefiable soil." *Journal Of Geotechnical And Geoenvironmental Engineering*, 129(12), 1092-1101.

143. Liu, H. P., Hagman, R. L., and Scott, R. F. (1978). "Centrifuge modeling of earthquakes." *Geophysical Research Letters*, 5(5), 333-336.

144. Liyanapathirana, D. S., and Poulos, H. G. (2004). "Assessment of soil liquefaction incorporating earthquake characteristics." *Soil Dynamics And Earthquake Engineering*, 24(11), 867-875.

145. Lord, A. E. (1999). "Capillary flow in the geotechnical centrifuge." *Geotechnical Testing Journal*, 22(4), 292-300.

146. Madabhushi, S. P. G. (2004). "Modelling of earthquake damage using geotechnical centrifuges." *Current Science*, 87(10), 1405-1416.

147. Mathews, W. H. (1979). "Landslides of central Vancouver island and the 1946 earthquake." *Bulletin of the Seismological Society of America*, 69(2), 445-450.

148. McDowell, G. R., and Bolton, M. D. (2000). "Effect of particle size distribution on pile tip resistance in calcareous sand in the geotechnical centrifuge." *Granular Matter*, 2(4), 179-187.

149. McLean, F. G., Ko, H.-Y., and International Society of Soil Mechanics and Foundation Engineering. (1991). *Centrifuge 91 : Proceedings of the international conference centrifuge 1991, boulder, Colorado, 13-14 June 1991*, A.A. Balkema, Rotterdam, Netherlands ; Brookfield, VT.

150. Mehle, J. S. (1989). "Centrifuge modeling of pile driving," Thesis M.S., University of Colorado, Boulder.

151. Microsoft. (2005). "How to use the remote desktop feature of windows xp professional." <http://support.microsoft.com/kb/315328/en-us> (January, 2006)

152. Mikami, A., and Sawada, T. (2005). "Simultaneous identification of time and space variant dynamic soil properties during the 1995 Hyogoken-nanbu earthquake." *Soil Dynamics and Earthquake Engineering*, 25(1), 69-77.

153. Mikasa, M., and Takada, N. (1973) "Significance of centrifuge model test in soil mechanics." *Proc. 8th Int. Conf. Soil Mech. and Found. Eng.*, 272-278.

154. Mitchell, R. J. (1991). "Centrifuge modeling as a consulting tool." *Canadian Geotechnical Journal*, 28(1), 162-167.

155. Modaressi, H. e. a. (1995) "Numerical modelling approaches for the analysis of earthquake triggered landslides." *Third International Conference on Recent Advances in Geotechnical Earthquake Engineering and Soil Dynamics*, Rolla, Missouri, pp.833-843.

156. Mokwa, R. L., and Duncan, J. M. (2001). "Experimental evaluation of lateral-load resistance of pile caps." *Journal Of Geotechnical And Geoenvironmental Engineering*, 127(2), 185-192.

157. Morris, D. V. (1981). "Dynamic soil-structure interaction modeled experimentally on a geotechnical centrifuge." *Canadian Geotechnical Journal*, 18(1), 40-51.

158. MSI.(2005a). "Position sensor types: DC LVDT." <http://www.meas-spec.com/mymsi/sensors/pdf/lvdt/dc-ec_accusens.pdf> (January, 2006)

159. MSI.(2005b). "Position sensor types:AC LVDT." <http://www.meas-spec.com/mymsi/sensors/pdf/lvdt/mhr-series.pdf > (January, 2006)

160. Mulilis, J. P., Seed, H. B., Chan, C. K., Mitchell, J. K., and Arulanandan, K. (1977). "Effects of sample preparation on sand liquefaction." *Journal Of The Geotechnical Engineering Division-ASCE*, 103(2), 91-108.

161. Muraleetharan, K. K., and Granger, K. K. (1999). "The use of miniature pore pressure transducers in measuring matric suction in unsaturated soils." *Geotechnical Testing Journal*, 22(3), 226-234.

162. Murf, J. D. (1996) "The geotechnical centrifuge in offshore engineering." *Proceddings of offshore technology*, Huston, Texas.

163. Musen, M. A. (1998). "Domain ontologies in software engineering: Use of protege with the eon architecture." *Methods of Information In Medicine*, 37(4-5), 540-550.

164. Musen, M. A., Fergerson, R. W., Noy, N. F., and Crubezy, M. (2001). "Protege-2000: A plug-in architecture to support knowledge acquisition, knowledge visualization, and the semantic web." *Journal of The American Medical Informatics Association*, 1079-1079.

165. Nakajima, H., Hirooka, A., Takemura, J., and Marino, M. A. (1998). "Centrifuge modeling of one-dimensional subsurface contamination." *Journal Of The American Water Resources Association*, 34(6), 1415-1425.

166. Nakata, J. K., and Geological Survey (U.S.). (1999). *The October 17, 1989, Loma Prieta, California, earthquake*

167. National Research Council. (1968). *The great Alaska earthquake of 1964*, U.S. National Academy of Sciences, Washington.

168. National Research Council (U.S.). Committee on Earthquake Engineering Research., and National Science Foundation (U.S.). (1985). *Liquefaction of soils during earthquakes*, National Academy Press: Available from the Committee on Earthquake Engineering, Washington, D.C.

169. Nichols, S. C., and Goodings, D. J. (2000). "Physical model testing of compaction grouting in cohesionless soil." *Journal of Geotechnical And Geoenvironmental Engineering*, 126(9), 848-852.

170. Nova-Roessig, L., and Sitar, N. (1998). *Centrifuge studies of the seismic response of reinforced soil slopes*, ASCE, Reston, Virginia.

171. NRC. (1982). *Centrifuge-soil testing, soil mechanics, and soil properties*, National Academy of Sciences, Washington, D.C.

172. NSF.(2006). "About NEES." <http://www.nees.org/About_NEES/> (January, 2006)

173. Nyce, D. S. (2004). *Linear position sensors: Theory and application*, Wiley-Interscience, Hoboken, NJ.

174. Okamura, M., Abdoun, T. H., Dobry, R., Sharp, M. K., and Taboada, V. M. (2001). "Effects of sand permeability and weak aftershocks on earthquake-induced lateral spreading." *Soils and Foundations*, 41(6), 63-77.

175. Oppenheim, A. V., and Schafer, R. W. (1975). *Digital signal processing*, Prentice-Hall, Englewood Cliffs, N.J..

176. Oppenheim, A. V., Schafer, R. W., and Buck, J. R. (1999). *Discrete-time signal processing*, Prentice Hall, Upper Saddle River, N.J.

177. Orense, R. P. (2005). "Assessment of liquefaction potential based on peak ground motion parameters." *Soil Dynamics And Earthquake Engineering*, 25(3), 225-240.

178. ORST.(2004). "Data model of tsunami experiment databank." Oregon State University, <http://nees.orst.edu/IT/data.model/ > (January, 2006)

179. Ovesen, N. K. (1979) "The scaling law relationship: Panel discussion." *Proceedings of the 7th European Conference on Soil Mechanics and Foundation Engineering*, Brighton, 319-323.

180. Paganelli, F., Khaled, O. A., Pettenati, M. C., and Giuli, D. (2004). "A metadata model for the design and deployment of document management systems." Web engineering, proceedings, 589-590.

181. Pan, S. S., Pu, J. L., Yin, K. T., and Liu, F. D. (1999). "Development of pile driver and load set for pile group in centrifuge." *Geotechnical Testing Journal*, 22(4), 317-323.

182. Parvizi, M., and Merrifield, C. M. (2000). "Mechanical behaviour of a sand bed subjected to low energy dynamic compaction, modelled in a geotechnical centrifuge." *Journal De Physique Iv*, 10(P9), 131-135.

183. Patra, N. R., and Pise, R. J. (2001). "Ultimate lateral resistance of pile groups in sand." *Journal Of Geotechnical And Geoenvironmental Engineering*, 127(6), 481-487.

184. Pilgrim, N. K. (1998). "Earthquake-related deformation beneath gently inclined ground." *Geotechnique*, 48(2), 187-199.

185. Pinto, P. S. e., Portuguese Society for Géotechnique., International Society of Soil Mechanics and Geotechnical Engineering., and Laboratório Nacional de Engenharia Civil (Portugal). (1999). *Earthquake geotechnical engineering : Proceedings of the second international conference on earthquake geotechnical engineering/lisboa/portugal/21-25 june 1999*, A.A. Balkema, Rotterdam.

186. Pokrovsky, G. I., and Fyodorov, I. S. (1936) "Studies of soil pressures and soil deformation by means of a centrifuge." *Proc.1st Int. Conf. Soil Mech.*

187. Pokrovsky, G. I., and Fyodorov, I. S. (1968). *Centrifugal model testing in the construction industry (in Russian)*, Publishing House of Literature for the Construction Industry Moscow.

188. Poorooshasb, F. (1990). "On centrifuge use for ocean research." *Marine Geotechnology*, 9(2), 141-158.

189. Popescu, R. (2002). "Finite element assessment of the effects of seismic loading rate on soil liquefaction." *Canadian Geotechnical Journal*, 39(2), 331-344.

190. Popescu, R., and Prevost, J. H. (1995). "Comparison between velacs numerical class-a predictions and centrifuge experimental soil test-results." *Soil Dynamics and Earthquake Engineering*, 14(2), 79-92.

191. Poulose, A., Nair, S. R., and Singh, D. N. (2000). "Centrifuge modeling of moisture migration in silty soils." *Journal of Geotechnical And Geoenvironmental Engineering*, 126(8), 748-752.

192. Prakash, S., Dakoulas, P., and American Society of Civil Engineers. Geotechnical Engineering Division. (1994). *Ground failures under seismic conitions : Proceedings of the sessions sponsored by the geotechnical engineering division of the American society of civil engineers in conjunction with the ASCE national convention in Atlanta, Georgia, October 9-13, 1994*, ASCE, New York.

193. Protege.(2005). "What is protégé?" Stanford University, <http://protege.stanford.edu/overview/index.html > (January, 2006)

194. Pyke, R. (1988). "Liquefaction evaluation procedure - discussion." *Journal Of Geotechnical Engineering-Asce*, 114(2), 247-250.

195. Resnick, G. S., and Znidarcic, D. (1990). "Centrifugal modeling of drains for slope stabilization." *Journal Of Geotechnical Engineering-Asce*, 116(11), 1607-1624.

196. Rezzoug, A., Konig, D., and Triantafyllidis, T. (2004). "Scaling laws for centrifuge modeling of capillary rise in sandy soils." *Journal of Geotechnical And Geoenvironmental Engineering*, 130(6), 615-620.

197. Richards, D. J., Powrie, W., and Page, J. R. T. (1998). "Investigation of retaining wall installation and performance using centrifuge modelling techniques." *Proceedings Of The Institution Of Civil Engineers-Geotechnical Engineering*, 131(3), 163-170.

198. Richart, F. E., Hall, J. R. J., and Woods, R. D. (1970). *Vibrations of soils and foundations*, Prentice-Hall, Inc., Englewood Cliffs, NJ.

199. Rocha, M. (1957) "The possibility of solving soil mechanics problems by the use of modles." *Proc. of the 4th International Conf. on Soil Mechanics and Foundation, 183*-188.

200. Rodriguez, C. E., Bommer, J.J., and Chandler, R. J. (1999). "Earthquake-induced landslides: 1980-1997." *Soil Dynamics and Earthquake Engineering*, 18(5), 325-346.

201. Roscoe, K. H. (1968). "Soils and model tests." *Proc. of Inst. of Mech. Engineers Journal of Strain Analysis*, 3(1), 57-64.

202. Rothenfluh, T. E., Gennari, J. H., Eriksson, H., Puerta, A. R., Tu, S. W., and Musen, M. A. (1996). "Reusable ontologies, knowledge-acquisition tools, and performance systems: Protege-ii solutions to sisyphus-2." *International Journal Of Human-Computer Studies*, 44(3-4), 303-332.

203. RPI.(1996). "Centrifuge description." Equipment Overview (Rensselaer Polytechnic Institute), <http://www.nees.rpi.edu/article.php3?id_article=39> (May, 2005)

204. Rumbaugh, J. (1991). *Object-oriented modeling and design*, Prentice Hall, Englewood Cliffs, N.J.

205. Sakr, M., and El Naggar, M. H. (2003). "Centrifuge modeling of tapered piles in sand." *Geotechnical Testing Journal*, 26(1), 22-35.

206. Santamaria, J. (2001). *Soils and waves*, John Wiley & Sons Ltd., New York, N.Y., U.S.A.

207. Sassa, K. e. a. (1996). "Geotechnical aspects of the january 17, 1995 hyogoken-nambu earthquake: Earthquake-induced-landslides: Distribution, motion and mechanisms." *Soils and Foundations* (Special Issue), 53-64.

208. Sato, M., Ogasawara, M.,and Tazoh, T. (2001) "Reproduction of lateral ground displacements and lateral-flow earth pressures acting on pile foundations using centrifuge modeling." *Fourth International Conference on Recent Advances in Geotechnical Earthquake Engineering and Soil Dynamics*, Rolla, Missouri, Paper No. 9.33, 6 pages.

209. Savage, J. C., Svarc, J. L., Prescott, W. H., and Gross, W. K. (1998). "Deformation across the rupture zone of the 1964 Alaska earthquake 1993-1997." *Journal Of Geophysical Research-Solid Earth*, 103(B9), 21275-21283.

210. Savvidou, C., and Culligan, P. J. (1998). "The application of centrifuge modelling to geo-environmental problems." *Proceedings of The Institution Of Civil Engineers-Geotechnical Engineering*, 131(3), 152-162.

211. Schofield, A. N. (1980). "Cambridge geotechnical centrifuge operations." *Geotechnique*, 30(3), 227-268.

212. Schofield, A. N. (1981) "Dynamic and earthquake geotechnical centrifuge modeling." *Proc. Int. Conf. Recent Advances in Geotech. Eng. and Soil Dynamics*, St. Louis, Missouri, 1-18.

213. Schofield, A. N. (1988). "An introduction to centrifuge modelling." Centrifuges in soil mechanics, W. H. Craig, James, R.G., Schofield, A.N., ed., A.A. Balkema, Brookfield, VT., 1-10.

214. Scott, R. F. (1963). *Principles of soil mechanics*, Addison-Wesley Pub. Co., Reading, Mass.,.

215. Scott, R. F. (1975). "The centrifugal technique in geotechnology, selected papers." California Institute of Technology, Pasadena, California.

216. Scott, R. F. (1977). "Feasibility and desirability of constructing a very large centrifuge for geotechnical studies." US National Science Foundation.

217. Scott, R. F. (1989). "Centrifuge and modeling technology: A survey " *Rev.Franc.Geotech.*, 48, 15-34.

218. Scott, R. F. (1993). "Lessons learned from velacs project." Velifications of numerical procedures for the analysis of soil liquefaction problems, K. Arulanandan and R. F. Scott, eds., A.A.Balkema, Brookfield, 1773-1784.

219. Scott, R. F., and Hushmand, B. (1995). "Piezometer performance at wildlife liquefaction site, California - discussion." *Journal of Geotechnical Engineering-Asce*, 121(12), 912-919.

220. Scott, R. F., and Schoustra, J. J. (1968). *Soil: Mechanics and engineering*, McGraw-Hill, New York,.

221. Scott, R. F., Ting, J. M., and Lee, J. (1982) "Comparison of centrifuge and full scale dynamic pile tests." *Int. Conf. on Soil Dynamics and Earthq. Engrg.* , Southampton, UK.

222. Sedran, G., Stolle, D. F. E., and Horvath, R. G. (2001). "An investigation of scaling and dimensional analysis of axially loaded piles." *Canadian Geotechnical Journal*, 38(3), 530-541.

223. Seed, H. B., and Idriss, I. M. (1982). *Ground motions and soil liquefaction during earthquakes*, Earthquake Engineering Research Institute, Berkeley, Calif.

224. SGC.(2006). "The caltech centrifuge facility " <http://gees.usc.edu/centrifuge/> (March, 2006)

225. Sharp, M. K., Dobry, R., and Abdoun, T. (2003). "Liquefaction centrifuge modeling of sands of different permeability." *Journal of Geotechnical And Geoenvironmental Engineering*, 129(12), 1083-1091.

226. Siddharthan, R. V., Kutter, B. L., El-Desouky, M., and Whitman, R. V. (2004). "Seismic deformation of bar mat mechanically stabilized earth walls. I: Centrifuge tests." *Journal of Geotechnical And Geoenvironmental Engineering*, 130(1), 14-25.

227. Simmons, C., and Causey, J. F. (2003). *Microsoft windows xp networking inside out*, Microsoft Press, Redmond, Wash.

228. Simunek, J., and Nimmo, J. R. (2005). "Estimating soil hydraulic parameters from transient flow experiments in a centrifuge using parameter optimization technique." *Water Resources Research*, 41(4).

229. Singh, D. N., and Gupta, A. K. (2000). "Modelling hydraulic conductivity in a small centrifuge." *Canadian Geotechnical Journal*, 37(5), 1150-1155.

230. Singh, D. N., and Gupta, A. K. (2001). "Falling head hydraulic conductivity tests in a geotechnical centrifuge." *Journal Of Testing And Evaluation*, 29(3), 258-263.

231. Singh, D. N., and Kuriyan, S. J. (2002). "Estimation of hydraulic conductivity of unsaturated soils using a geotechnical centrifuge." *Canadian Geotechnical Journal*, 39(3), 684-694.

232. Singh, D. N., Kuriyan, S. J., and Madhuri, V. (2001). "Application of a geotechnical centrifuge for estimation of unsaturated soil hydraulic conductivity." *Journal of Testing And Evaluation*, 29(6), 556-562.

233. Sitar, N., and Baldwin, J. E. (1991). *Loma prieta earthquake : Engineering geologic perspectives*, Association of Engineering Geologists, Sudbury, MA.

234. Society for Experimental Mechanics (U.S.). (1984). "Strain-gage and transducer techniques." Society for Experimental Mechanics, Brookfield Center, Conn., v.

235. Sonmez, H., and Gokceoglu, C. (2005). "A liquefaction severity index suggested for engineering practice." *Environmental Geology*, 48(1), 81-91.

236. Stearns, M. Q., Price, C., Spackman, K. A., and Wang, A. Y. (2001). "Snomed clinical terms: Overview of the development process and project status." *Journal of The American Medical Informatics Association*, 662-666.

237. Stewart, D. P., Chen, Y. R., and Kutter, B. L. (1998). "Experience with the use of methylcellulose as a viscous pore fluid in centrifuge models." *Geotechnical Testing Journal*, 21(4), 365-369.

238. Sutherland, H. J., and Rechard, R. P. (1984). "Centrifuge simulations of stable tailings dam." *Journal of Geotechnical Engineering-Asce*, 110(3), 390-402.

239. Swift, J., Eng, J., Bardet, J.P., Liu, F., Mokarram, N. and Pekcan, G. . (2004). "Using the NEES reference data model and the nees metadata browser for centrifuge experiments version 1.1." Report of Civil Engineering Dept, University of Southern California, Los Angeles.

240. Taboada-Urtuzuastegui, V. M., and Dobry, R. (1998). "Centrifuge modeling of earthquake-induced lateral spreading in sand." *Journal Of Geotechnical And Geoenvironmental Engineering*, 124(12), 1195-1206.

241. Taboada-Urtuzuastegui, V. M., Martinez-Ramirez, G., and Abdoun, T. (2002). "Centrifuge modeling of seismic behavior of a slope in liquefiable soil." *Soil Dynamics and Earthquake Engineering*, 22(9-12), 1043-1049.

242. Taboada, M., Martinez, D., and Mira, J. (2005). "Experiences in reusing knowledge sources using Protege and prompt." *International Journal Of Human-Computer Studies*, 62(5), 597-618.

243. Taboada, V. M. (1995). "Centrifug modeling of earthquake-induced lateral spreading in sand using laminar box," PhD Dissertation, Rensselaer Polytechnic Institute, Troy, n.Y.

244. Taboada, V. M., Abdoun, T., and Dobry, R. (1996) "Prediction of liquefaction-induced lateral spreading by dilatant sliding block model calibrated by centrifuge tests." *Eleventh World Conference on Earthquake Engineering [Proceedings*, Pergamon, Paper No. 376.

245. Taboada, V. M., and Dobry, R. (1998). "Centrifuge modeling of earthquake-induced lateral spreading in sand." *Journal of Geotechnical and Geoenvironmental Engineering*, 124(12), 1195-1206.

246. Taboada, V. M. e. a. (2002). "Centrifuge modeling of seismic behavior of a slope in liquefiable soil." *Soil Dynamics and Earthquake Engineering*, 9(12), 1043-1049.

247. Tan, T. S. (1985). "Two phase soil study: A. Finite strain consolidation & b. Centrifuge scaling considerations," California Institute of Technology, Pasadena, California, U.S.A.

248. Tan, T. S., and Scott, R. F. (1985). "Centrifuge scaling considerations for fluid-particle systems." *Geotechnique*, 35(4), 461-470.

249. Taylor, R. N. (1995). "Centrifuges in modelling: Principles and scale effects." Geotechnical centrifuge technology, Blackie Academic and Professional, London, U.K., 19-33.

250. Taylor, R. N., Tan, T. S., and Scott, R. F. (1987). "Centrifuge scaling considerations for fluid particle-systems - discussion." *lamGeotechnique*, 37(1), 131-133.

251. Team Corporation. (1994). "Hydraulic power supply HPS 6A." Team Corporation, Burlington, WA.

252. Teymur, B., and Madabhushi, S. P. G. (2003). "Experimental study of boundary effects in dynamic centrifuge modelling." *Geotechnique*, 53(7), 655-663.

253. Tika, T., and Pitilakis, K. (1995) "The evaluation of earthquake induced displacements of landslides for seismic zonation." *Proceedings of the Fifth International Conference on Seismic Zonation*, Nice, France, 1691-1698.

254. Tokimatsu, K., and Seed, H. B. (1987). "Evaluation of settlements in sands due to earthquake shaking." *Journal of Geotechnical Engineering-ASCE*, 113(8), 861-878.

255. Triantafyllidis, T. (2004). *Cyclic behaviour of soils and liquefaction phenomena : Proceedings of the international conference on cyclic behaviour of soils and liquefaction phenomena, 31 march-02 april 2004, bochum, germany*, A.A. Balkema Publishers, Leiden ; New York.

256. Turner, J. P., American Society of Civil Engineers. Committee on Deep Foundations., and American Society of Civil Engineers. Geotechnical Engineering Division. Soil Properties Committee. (1995). *Performance of deep foundations under seismic loading : Proceedings of sessions sponsored by the deep foundations and soil properties committees of the geotechnical engineering division of the american society of civil engineers in conjunction with the asce convention in san diego, california, october 22-26, 1995*, The Society, New York.

257. UCB. (2001). "400 g-ton centrifuge." Centrifuge facility (University of Colorado, Boulder), <http://civil.colorado.edu/web/grad/geotech/faci/centrifuge/bigcentrifuge.html> (October, 2004)

258. Uschold, M., and Gruninger, M. (1996). "Ontologies: Principles, methods and applications." *Knowledge Engineering Review*, 11(2), 93-136.

259. Vankov, D. A., and Sassa, K. (1999). "Mechanism of earthquake-induced landslides on almost flat slopes studied with a ring shear apparatus." *Journal of Natural Disaster Science*, 21(1), 23-35.

260. Veder, C. (1981). *Landslides and their stabilization*, Springer-Verlag, New York.

261. Vessely, D. A., and Cornforth, D. H. (1998). "Estimating seismic displacements of marginally stable landslides using newmark approach." Geotechnical special publication 75, geotechnical earthquake engineering and soil dynamics iii, American Society of Civil Engineers, Reston, Virginia, pp.800-811.

262. Viswanadham, B. V. S., and Mahesh, K. V. (2002). "Modeling deformation behaviour of clay liners in a small centrifuge." *Canadian Geotechnical Journal*, 39(6), 1406-1418.

263. Von Thun, J. L., American Society of Civil Engineers. Geotechnical Engineering Division., and Association of Engineering Geologists. (1988). *Earthquake engineering and soil dynamics ii : Recent advances in ground-motion evaluation : Proceedings of the specialty conference*, The Society, New York, N.Y.

264. Vulliet, L. (1995) "Predicting large displacements of landslides." *Fifth International Symposium on Numerical Models in Geomechanics*, pp.527-532.

265. Weber, G. H., Schneider, M., D.W., W., Hagen, H., Hamann, B., and Kutter, B. L. (2003). "Visualization of experimental earthquake data." *Proceedings of SPIE*, 5009, 268-276.

266. Webopedia.(2006). "Data modeling." <http://www.webopedia.com/TERM/D/data_modeling.html> (January, 2006)

267. Wenk, R. (2003). "Talco rotary union." Personal Communication, April, 2003.

268. Whitlow, R. (2001). *Basic soil mechanics* Prentice Hall.

269. Whitman, R. V., and Lambe, P. C. (1986). "Effect of bondary conditions upon centrifuge experiments ground motion simulation " *Geotech. Testing Journal*, 9(2).

270. Wikipedia.(2006). "Similitude (model)." <http://en.wikipedia.org/wiki/Similitude_%28model%29> (Feb., 2006)

271. Wilson, D. W., Boulanger, R. W., and Kutter, B. L. (2000). "Observed seismic lateral resistance of liquefying sand." *Journal Of Geotechnical And Geoenvironmental Engineering*, 126(10), 898-906.

272. Wolf, H., Konig, D., and Triantafyllidis, T. (2005). "Centrifuge model tests on sand specimen under extensional load." *International Journal For Numerical And Analytical Methods In Geomechanics*, 29(1), 25-47.

273. Wu, G. X. (2001). "Earthquake-induced deformation analyses of the upper san fernando dam under the 1971 san fernando earthquake." *Canadian Geotechnical Journal*, 38(1), 1-15.

274. Youd, T. L., and Garris, C. T. (1995). "Liquefaction-induced ground-surface disruption." *Journal Of Geotechnical Engineering-Asce*, 121(11), 805-809.

275. Youd, T. L., and Holzer, T. L. (1994). "Piezometer performance at wildlife liquefaction site, california." *Journal Of Geotechnical Engineering-Asce*, 120(6), 975-995.

276. Youd, T. L., and Idriss, I. M. (2001). "Liquefaction resistance of soils: Summary report from the 1996 nceer and 1998 nceer/nsf workshops on evaluation of liquefaction resistance of soils." *Journal of Geotechnical And Geoenvironmental Engineering*, 127(4), 297-313.

277. Zeghal, M., and Elgamal, A. W. (1994). "Analysis of site liquefaction using earthquake records." *Journal Of Geotechnical Engineering-Asce*, 120(6), 996-1017.

278. Zeghal, M., Elgamal, A. W., Zeng, X. W., and Arulmoli, K. (1999). "Mechanism of liquefaction response in sand-silt dynamic centrifuge tests." *Soil Dynamics And Earthquake Engineering*, 18(1), 71-85.

279. Zeng, X. (1996). "A simple procedure to calculate the fundamental frequency of horizontal soil layers." *Geotechnique*, 46(4), 757-760.

280. Zeng, X., and Arulanandan, K. (1995). "Modeling the lateral sliding of a slope due to liquefaction of a sand layer." *Journal of Geotechnical Engineering*, 125(11), 814-817.

281. Zeng, X., and Schofield, A. N. (1996). "Design and performance of an equivalent-shear-beam container for earthquake centrifuge modelling." *Geotechnique*, 46(1), 83-102.

282. Zeng, X., and Steedman, R. S. (1998). "Bearing capacity failure of shallow foundations in earthquakes." *Geotechnique*, 48(2), 235-256.

283. Zeng, X. W., and Lim, S. L. (2002). "The influence of variation of centrifugal acceleration and model container size on accuracy of centrifuge test." *Geotechnical Testing Journal*, 25(1), 24-43.

284. Zeng, X. W., Wu, J., and Young, B. A. (1998). "Influence of viscous fluids on properties of sand." *Geotechnical Testing Journal*, 21(1), 45-51.

285. Zhang, D. (1996). "A study of the mechanism of loess landslides induced by earthquakes." *Journal of Natural Disaster Science*, 18(1), 27-41.

286. Zhang, J., and Zhao, J. X. (2005). "Empirical models for estimating liquefaction-induced lateral spread displacement." *Soil Dynamics and Earthquake Engineering*, 25(6), 439-450.

287. Zornberg, J. G., Friedrichsen, J., and Dell'Avanzi, E. (2005). "Performance of centrifuge data acquisition systems using wireless transmission." *Geotechnical Testing Journal*, 28(2), 144-150.